

Nicole Ahner

# Wetting Optimized Solutions for Plasma Etch Residue Removal for Application in Interconnect Systems of Integrated Circuits



TECHNISCHE UNIVERSITÄT  
CHEMNITZ

Nicole Ahner

Wetting Optimized Solutions for Plasma Etch Residue Removal  
for Application in Interconnect Systems of Integrated Circuits



Nicole Ahner

**Wetting Optimized Solutions for Plasma Etch  
Residue Removal for Application  
in Interconnect Systems of Integrated Circuits**



**TECHNISCHE UNIVERSITÄT  
CHEMNITZ**

**Universitätsverlag Chemnitz**

2013



## **Impressum**

### **Bibliografische Information der Deutschen Nationalbibliothek**

Die Deutsche Nationalbibliothek verzeichnet diese Publikation in der Deutschen Nationalbibliografie; detaillierte bibliografische Angaben sind im Internet über <http://dnb.d-nb.de> abrufbar.

Zugl.: Chemnitz, Techn. Univ., Diss., 2012

Technische Universität Chemnitz/Universitätsbibliothek

**Universitätsverlag Chemnitz**

09107 Chemnitz

<http://www.bibliothek.tu-chemnitz.de/UniVerlag/>

### **Herstellung und Auslieferung**

Verlagshaus Monsenstein und Vannerdat OHG

Am Hawerkamp 31

48155 Münster

<http://www.mv-verlag.de>

ISBN 978-3-941003-61-3

<http://nbn-resolving.de/urn:nbn:de:bsz:ch1-qucosa-102773>

# **Wetting Optimized Solutions for Plasma Etch Residue Removal for Application in Interconnect Systems of Integrated Circuits**

## **Benetzungsoptimierte Reinigungslösungen für die Entfernung von Plasmaätzresiduen für die Anwendung im Verdrahtungssystem integrierter Schaltungen**

Von der Fakultät für Elektrotechnik und Informationstechnik  
der Technischen Universität Chemnitz  
genehmigte

### **Dissertation**

zur Erlangung des akademischen Grades

### **Doktoringenieur (Dr.-Ing.)**

vorgelegt von: Dipl.-Ing. Nicole Ahner  
geboren am: 23. September 1975  
in: Stollberg / Erzgeb.  
eingereicht am: 27. Mai 2011  
Gutachter: Prof. Dr. Thomas Geßner  
Prof. Dr. Michael Hietschold

Tag der Verleihung: 04. April 2012



## **Bibliographische Beschreibung**

*Wet Chemical Solutions for Plasma Etch Residue Removal with Optimized Wetting Behavior by Addition of Surfactants for Application in Interconnect Systems of Integrated Circuits*

**Ahner, Nicole** – 233 Seiten, 100 Abb., 46 Tab., 112 Lit.

Technische Universität Chemnitz, Fakultät für Elektrotechnik und Informationstechnik

Dissertation (in englischer Sprache), 2012

### **Referat**

In mehrlagigen Kupfer/low-k basierten Metallisierungssystemen hochintegrierter elektronischer Bauelemente kann die Entfernung von Residuen nach der Plasmastrukturierung des Dielektrikums mittels herkömmlicher Plasmareinigungsprozesse zur Schädigung der Isolatorschicht und damit zum Ansteigen der relativen Dielektrizitätszahl sowie der Leckströme führen. Neben der Entwicklung schädigungsarmer Plasmaprozesse stellt der Ersatz dieser Prozesse durch Nassreinigungsschritte zur Ätzresiduenentfernung eine vielversprechende Alternative dar. Mit stetig abnehmenden Strukturabmaßen ist bei der Entwicklung dieser Nassreinigungsprozesse neben der Materialkompatibilität auch das Benetzungsverhalten der Reinigungsflüssigkeit von entscheidender Bedeutung, da die Oberflächenenergie der Reinigungslösung das Eindringen dieser in kleinste Strukturen verhindern und es durch hohe Kapillarkräfte zum Kollaps von Grabenstrukturen im Dielektrikum kommen kann. In der vorliegenden Arbeit wurde zunächst mittels Kontaktwinkelanalyse die Oberflächenenergie verschieden prozessierter low-k Dielektrikaschichten sowie herkömmlicher Lösungen zur Entfernung von Ätzresiduen untersucht, um hinsichtlich ihres Benetzungsverhaltens besonders kritische Materialkombinationen aufzuzeigen. Neben der Bestimmung des Benetzungsverhaltens hat sich die Kontaktwinkelanalyse zur Oberflächenenergieberechnung als schnelle und empfindliche Methode zur Analyse der Auswirkung von Plasmaprozessen auf die Oberfläche von low-k Dielektrika erwiesen. Die Untersuchungen haben gezeigt, dass besonders polymerisierende Plasmaprozesse eine niederenergetische Oberfläche erzeugen, welche von den derzeit in der Halbleiterfertigung bevorzugten hochenergetischen wasserbasierten Reinigungslösungen nur schlecht benetzt wird. Um diesem Effekt entgegenzuwirken wurde in der vorliegenden Arbeit die Senkung der Oberflächenenergie der Reinigungslösungen durch Zugabe

von Tensiden untersucht. Es wurden mehrere Tenside unterschiedlichen Typs den Reinigungsflüssigkeiten zugemischt und die Kompatibilität dieser Lösungen mit low-k Dielektrika, Kupferschichten und Diffusionsbarrieren untersucht sowie ihr dynamisches Verhalten analysiert. Dabei hat sich gezeigt, dass die Auswahl der geeigneten Spüllösung nach dem eigentlichen Reinigungsprozess von entscheidender Bedeutung ist. Optische, elektrische sowie strukturelle Daten deuten darauf hin, dass bei Verwendung einer Spülung mit deionisiertem Wasser in den meisten Fällen Tensidrückstände im porösen Dielektrikum verbleiben. Eine Spülung mit Isopropanol war hingegen in der Lage, einen Großteil dieser Tensidrückstände zu entfernen. Unter Einbeziehung der Daten zur Materialkompatibilität und dem dynamischen Verhalten der Tensidlösungen bei Raumtemperatur und erhöhter Badtemperatur sowie ihrer Langzeitstabilität konnte schließlich eine Prozessempfehlung für die Verwendung der benetzungsoptimierten Reinigungslösungen in der BEOL-Prozessierung gefunden werden.

**Stichworte**

Low-k Dielektrika, Ätzresiduen, Plasmaschädigung, Nassreinigung, Benetzung, Strukturkollaps, Oberflächenenergie, Kontaktwinkel, Tensid, dynamische Oberflächenenergie, ULSI

**Abstract**

In multi-level Co/low-k based interconnect systems of ultralarge-scale integrated electronic devices the removal of plasma etch residues by common plasma cleaning processes has been shown to alter material properties like k-value and leakage current of the low-k dielectric. Besides the development of less damaging plasma processes their substitution by wet cleaning steps is in the focus of research and development. With further decreasing feature dimensions the development of wet cleaning processes has to include wetting issues like the non-wetting of small features due to the surface energy of the liquid or pattern collapse effects of low-k dielectric trenches due to high capillary forces. This work at first focuses on the determination of the surface energetic character of common cleaning solutions for PERR and differently etched or ashed low-k dielectric surfaces by contact angle analysis, to outline which combinations of solid and liquid will be critical regarding their wetting behavior. Besides the determination of the wetting behavior the contact angle analysis turned out to be a fast and sensible analytic tool to understand the surface modifications introduced by different plasma processes and can help to understand the mechanisms of plasma damage of low-k dielectric surfaces. The analysis showed that especially polymerizing plasma etch processes produce a low-energetic low-k dielectric surface with a negligible polar energy

contributions, which inhibits their wetting by high energetic water based cleaning solutions, which actually are favored by semiconductor manufacturers. The strategy to overcome these wetting issues followed in the present work is the reduction of the surface energy of the cleaning liquids by the application of surfactants. Several types of surfactants have been applied to the cleaning liquids and the compatibility of the surfactant solutions to BEOL materials like low-k dielectrics, copper and diffusion barriers as well as their dynamic behavior has been studied. The analysis showed that choosing the appropriate rinsing solution after the cleaning process is essential to ensure its compatibility to porous low-k dielectrics. Optical, electrical and structural data indicated that DIW rinse in most of the cases was not able to remove residual surfactant species within the material, while for an IPA rinse most of the residual surfactants have been removed. Considering the data received for compatibility to low-k materials, copper and barriers, the dynamic behavior of the surfactant solutions as well as influences of increased bath temperature and long term stability a general advice about surfactant selection and processing of surfactant aided solutions within BEOL is given.

**Keywords**

low-k dielectric, plasma etch residue, plasma damage, wet cleaning, wetting, pattern collapse, surface energy, contact angle, surfactant, dynamic surface energy, ULSI



*Sobald man in einer Sache Meister geworden ist,  
soll man in einer neuen Schüler werden.*

*Gerhart Hauptmann*





## Table of Contents

List of Acronyms and Symbols .....	I
Vorwort .....	VIII
<b>1. Introduction</b>	<b>1</b>
1.1. Integration of new materials in FEOL and BEOL processing .....	3
1.2. Overview of the dissertation .....	7
<b>2. Processing and integration of low-k dielectrics in BEOL</b>	<b>11</b>
2.1. General introduction .....	11
2.2. Strategies to decrease the k-value of the insulator .....	14
2.2.1. Decreasing the k-value by reducing the polarizability of the dielectric ..	14
2.2.2. Introduction of porosity to Si-O based low-k dielectrics .....	15
2.3. The dual damascene process .....	19
2.3.1. Trench first – via last and Via first – trench last patterning schemes .....	20
2.3.2. Integration schemes for low-k dielectric materials .....	23
2.4. Patterning of Si-O like low-k dielectrics by dry etching .....	25
2.5. Etch residue composition and cleaning strategies .....	26
2.5.1. Composition and impact of plasma etch residues .....	26
2.5.2. Residue removal by plasma cleaning and its impact on low-k materials.	27
2.5.3. Removal of plasma etch residues by wet chemical processes .....	32
2.5.4. New challenges in wet chemical PERR in 32/22 nm technology .....	36

<b>3.</b>	<b>Wetting and surface energies in wet cleaning processes</b>	<b>39</b>
3.1.	<i>General introduction</i> .....	39
3.2.	<i>The contact angle</i> .....	41
3.2.1.	Thermodynamics – Young’s equation .....	42
3.2.2.	Contact angle hysteresis .....	43
3.3.	<i>The role of surface energies in wetting</i> .....	45
3.3.1.	The origin of surface energies.....	45
3.3.2.	Model considerations concerning surface energies .....	48
3.4.	<i>Wetting concerns in wet chemical PERR for 32/22 nm technology</i> .....	51
3.4.1.	Pattern collapse of low-k dielectric features .....	52
3.4.2.	Non-wetting of small structures .....	54
3.5.	<i>Strategies to optimize the wetting behavior</i> .....	56
<b>4.</b>	<b>Application of surfactants for liquid surface energy decrease</b>	<b>59</b>
4.1.	<i>General introduction</i> .....	59
4.2.	<i>Classification of surfactants by the hydrophilic group</i> .....	61
4.2.1.	Ionic surfactants .....	61
4.2.2.	Amphoteric surfactants .....	61
4.2.3.	Nonionic surfactants .....	61
4.3.	<i>Classification of the surfactants by the hydrophobic group</i> .....	63
4.3.1.	Hydrocarbon surfactants .....	63
4.3.2.	Perfluorinated surfactants .....	63
4.3.3.	Silicon containing surfactants .....	64
4.3.4.	Block-copolymers .....	64
4.4.	<i>Surfactants in aqueous media</i> .....	65

4.4.1. Solubility of surfactants .....	65
4.4.2. Surface activity at liquid/vapor interface .....	67
4.4.3. Interfaces between liquids and solids .....	69
4.5. <i>Surfactants in nonaqueous media</i> .....	70
4.5.1. Surfactants in polar solvents .....	70
4.5.2. Surfactants in nonpolar solvents .....	70
4.6. <i>Dynamic behavior of surfactant molecules – diffusion and adsorption</i> .....	71
4.7. <i>Surfactants in PERR</i> .....	72
<b>5. Analytical methods</b> .....	<b>75</b>
5.1. <i>Determination of surface energies and wetting behavior</i> .....	75
5.1.1. The surface energy of the solid .....	75
5.1.2. The surface energy of the liquid .....	78
5.2. <i>Experimental setup</i> .....	82
5.3. <i>Dynamic surface energy of surfactant solutions</i> .....	83
5.4. <i>Analytics for material compatibility</i> .....	85
5.4.1. Spectral ellipsometry .....	85
5.4.2. CV – measurement .....	85
5.4.3. FTIR .....	86
5.4.4. Sheet resistance .....	88
<b>6. Experimental determination of surface energies and wetting behavior</b> .....	<b>89</b>
6.1. <i>Sample and process description</i> .....	89

6.1.1.	Description of the solid samples .....	89
6.1.2.	Description of plasma processes .....	91
6.1.3.	Description of the liquid samples.....	94
6.2.	<i>Surface energies of the solid samples</i> .....	94
6.2.1.	Low-k and ultra low-k dielectrics after etching processes.....	94
6.2.2.	Surfaces after polymerizing processes .....	98
6.2.3.	Ultra low-k dielectrics after stripping processes.....	99
6.2.4.	Metallic surfaces and barriers .....	100
6.2.5.	Polished and hardmask surfaces .....	102
6.3.	<i>Surface energies of the cleaning solutions</i> .....	104
6.4.	<i>Contact angle analysis</i> .....	105
6.5.	<i>Finding the appropriate cleaning solution with sufficient wetting behavior without additional contact angle measurements</i> .....	107
6.6.	<i>Selection of cleaning solution to be optimized in their wetting behavior</i> .....	108
<b>7.</b>	<b>Optimized wetting of cleaning solutions by application of surfactants</b>	<b>111</b>
7.1.	<i>Process and sample description</i> .....	111
7.1.1.	Selection of surfactants .....	111
7.1.2.	Processes for material compatibility study .....	114
7.2.	<i>Dynamic surface energy of DIW-mixed surfactants</i> .....	115
7.3.	<i>Dynamic surface energy of surfactants mixed in cleaning solutions</i> .....	117
7.3.1.	Analysis at room temperature .....	117
7.3.2.	Impact of surfactant addition on the static surface energy of the cleaning solutions .....	120
7.3.3.	Analysis at increased bath temperature.....	121
7.3.4.	Long term stability of surfactant solutions .....	123

7.4. Compatibility of surfactant solutions to a porous low-k dielectric .....	126
7.4.1. Surfactants mixed in DIW .....	126
7.4.2. Surfactants mixed in cleaning solutions at room temperature.....	132
7.4.3. Surfactants mixed in cleaning solutions at elevated bath temperature...	137
7.5. Compatibility to metals and barrier materials .....	140
7.5.1. Influence on sheet resistance .....	140
7.5.2. Surface condition after rinsing.....	141
7.6. Influence of surfactant addition on the wetting behavior of the cleaning solutions and on pattern collaps forces .....	144
7.6.1. Wetting behavior of surfactant solutions on low-energetic solid surfaces .....	144
7.6.2. Influence of wetting optimized cleaning solutions on pattern collaps forces .....	147
7.7. Process advice for a wetting optimized and material compatible wet cleaning process for PERR.....	148

## **8. Summary and Outlook**

**153**

## **Appendix**

A	Surface energy values of the studied solid surfaces and cleaning liquids.....	161
B	Contact angle values and comparison of the energetic character of solids and liquids.....	163
C	Surface energy calculation of the PTFE substrate.....	168
D	Compatibility study of the solutions B1, B2 and C1 to a porous low-k dielectric and copper.....	169
E	Dynamic surface energy values of the studied surfactants mixed in DIW	171
F	Dynamic surface energy values and long term stability of the studied surfactants mixed in cleaning solutions.....	182

G	Compatibility study of the surfactant solutions to copper and diffusion barrier materials.....	187
H	Compatibility study of the surfactant solutions to a porous low-k dielectric - FTIR data.....	188
I	Rating of the surfactant aided solutions regarding wetting behavior and material compatibility.....	205
	References.....	207
	List of Figures.....	213
	List of Tables.....	219
	List of Equations.....	223
	Theses.....	225
	Curriculum Vitae.....	229
	Own Publications and Conference Contributions.....	231

## **Inhaltsverzeichnis**

Liste der Abkürzungen und Symbole.....	I
Vorwort .....	VIII
<b>1. Einleitung</b>	<b>1</b>
1.1. <i>Integration neuer Materialien in FEOL und BEOL</i> .....	3
1.2. <i>Überblick über die Dissertation</i> .....	7
<b>2. Prozesse und Integration von low-k Dielektrika im BEOL</b>	<b>11</b>
2.1. <i>Allgemeines</i> .....	11
2.2. <i>Strategien zur Reduzierung des k-Wertes des Isolatormaterials</i> .....	14
2.2.1. Verringerung der Polarisierbarkeit des Dielektrikums .....	14
2.2.2. Erzeugung von Porosität in Si-O basierten low-k Dielektrika .....	15
2.3. <i>Der Dual Damascene Prozess</i> .....	19
2.3.1. Die Strukturierungsschemata "Trench first - via last" und "Via first - trench last" .....	20
2.3.2. Integrationsschemata für die Integration von low-k Materialien .....	23
2.4. <i>Strukturierung von Si-O basierten low-k Dielektrika durch Trockenätzen</i> .....	25
2.5. <i>Zusammensetzung von Plasmaätzresiduen und ihre Entfernung</i> .....	26
2.5.1. Zusammensetzung und Einfluss von Plasmaätzresiduen .....	26
2.5.2. Entfernung von Ätzresiduen durch Plasmareinigung und deren Auswirkung auf low-k Dielektrika .....	27
2.5.3. Nasschemische Entfernung von Plasmaätzresiduen .....	32
2.5.4. Neue Herausforderungen für nasschemische Residuenentfernung in der 32 nm und 22 nm Technologie.....	36



---

### **3. Benetzungsverhalten und Oberflächenenergien in Nassreinigungsprozessen** **39**

3.1. Allgemeines .....	39
3.2. Der Kontaktwinkel .....	41
3.2.1. Thermodynamische Betrachtung - Die Young'sche Gleichung.....	42
3.2.2. Kontaktwinkelhysterese .....	43
3.3. Bedeutung von Oberflächenenergien für die Benetzung .....	45
3.3.1. Ursprung von Oberflächenenergien .....	45
3.3.2. Modelle für die Berechnung von Oberflächenenergien .....	48
3.4. Benetzungseffekte der nasschemischen Ätzresiduenentfernung in der 32 nm und 22 nm Technologie .....	51
3.4.1. Strukturkollaps von Strukturen aus low-k Materialien .....	52
3.4.2. Nichtbenetzung kleinster Strukturen .....	54
3.5. Strategien zur Optimierung des Benetzungsverhaltens .....	56

### **4. Verringerung der Oberflächenenergie einer Flüssigkeit durch Tensidzugabe** **59**

4.1. Allgemeines .....	59
4.2. Klassifikation von Tensiden nach ihrer hydrophilen Gruppe .....	61
4.2.1. Ionische Tenside .....	61
4.2.2. Amphotere Tenside .....	61
4.2.3. Nichtionische Tenside .....	61
4.3. Klassifikation von Tensiden nach ihrer hydrophoben Gruppe .....	63
4.3.1. Kohlenwasserstofftenside .....	63
4.3.2. Fluorhaltige Tenside .....	63
4.3.3. Siliziumhaltige Tenside .....	64

4.3.4. Block-Copolymer-Tenside .....	64
4.4. <i>Tenside in wässrigen Lösungen</i> .....	65
4.4.1. Löslichkeit von Tensiden.....	65
4.4.2. Oberflächenaktivität an der Grenzfläche flüssig/fest .....	67
4.4.3. Grenzflächen von Flüssigkeiten und Festkörpern .....	69
4.5. <i>Tenside in nichtwässrigen Lösungen</i> .....	70
4.5.1. Tenside in polaren Lösungsmitteln.....	70
4.5.2. Tenside in nichtpolaren Lösungsmitteln.....	70
4.6. <i>Dynamisches Verhalten von Tensidmolekülen - Diffusion und Adsorption</i> ....	71
4.7. <i>Verwendung von Tensiden bei der Entfernung von Plasmaätzresiduen</i> .....	72

## **5. Analytische Methoden** **75**

5.1. <i>Berechnung von Oberflächenenergien und Bestimmung des Benetzungsverhaltens</i> .....	75
5.1.1. Oberflächenenergie des Festkörpers.....	75
5.1.2. Oberflächenenergie der Flüssigkeit .....	78
5.2. <i>Experimenteller Aufbau</i> .....	82
5.3. <i>Bestimmung der dynamischen Oberflächenenergie von Tensidlösungen</i> .....	83
5.4. <i>Analyse der Materialkompatibilität</i> .....	85
5.4.1. Spektralellipsometrie .....	85
5.4.2. CV-Messungen .....	85
5.4.3. FTIR.....	86
5.4.4. Bestimmung des Schichtwiderstandes.....	88

## **6. Experimentelle Bestimmung der Oberflächenenergien und es Benetzungsverhaltens** **89**

<i>6.1. Proben- und Prozessbeschreibung .....</i>	<i>89</i>
6.1.1. Beschreibung der untersuchten Festkörperproben .....	89
6.1.2. Beschreibung der verwendeten Plasmaprozesse .....	91
6.1.3. Beschreibung der untersuchten Flüssigkeiten .....	94
<i>6.2. Oberflächenenergien der Festkörperproben .....</i>	<i>94</i>
6.2.1. Low-k und Ultra low-k Proben nach Ätzprozessen .....	94
6.2.2. Proben nach polymerisierenden Prozessen .....	98
6.2.3. Ultra low-k Proben nach Strippprozessen .....	99
6.2.4. Metallische Proben und Diffusionsbarrieren .....	100
6.2.5. Polierte Proben und Hartmaskenoberflächen .....	102
<i>6.3. Oberflächenenergien der Flüssigkeiten .....</i>	<i>104</i>
<i>6.4. Kontaktwinkelanalyse .....</i>	<i>105</i>
<i>6.5. Bestimmung der Kombination von Flüssigkeit und fester Oberfläche mit geeignetem Benetzungsverhalten ohne zusätzliche Benetzungstests .....</i>	<i>107</i>
<i>6.6. Auswahl der Reinigungsflüssigkeiten für die Optimierung der Benetzung ...</i>	<i>108</i>

## **7. Optimierte Benetzungsverhalten von Reinigungsflüssigkeiten durch Zugabe von Tenside** **111**

<i>7.1. Prozess- und Probenbeschreibung .....</i>	<i>111</i>
7.1.1. Auswahl der Tenside .....	111
7.1.2. Prozesse für die Untersuchung der Materialkompatibilität .....	114
<i>7.2. Dynamische Oberflächenenergie von Tensiden in deionisiertem Wasser .....</i>	<i>115</i>
<i>7.3. Dynamische Oberflächenenergie von Tensiden in Reinigungslösungen .....</i>	<i>117</i>
7.3.1. Analyse bei Raumtemperatur .....	117

7.3.2.	Einfluss der Tensidzugabe auf die statische Oberflächenenergie .....	120
7.3.3.	Analyse bei erhöhter Badtemperatur .....	121
7.3.4.	Langzeitstabilität der Tensidlösungen .....	123
7.4.	<i>Kompatibilität der Tensidlösungen zu einem porösen low-k Material .....</i>	<i>126</i>
7.4.1.	Tenside in deionisiertem Wasser .....	126
7.4.2.	Tenside in Reinigungslösungen bei Raumtemperatur .....	132
7.4.3.	Tenside in Reinigungslösungen bei erhöhter Badtemperatur .....	137
7.5.	<i>Kompatibilität zu metallischen Proben und Diffusionsbarrieren .....</i>	<i>140</i>
7.5.1.	Einfluss auf den Schichtwiderstand der Proben .....	140
7.5.2.	Oberflächenzustand der Proben nach der Spülung .....	141
7.6.	<i>Einfluss der Tensidzugabe auf das Benetzungsverhalten der Reinigungslösungen auf die Kräfte beim Strukturkollaps .....</i>	<i>144</i>
7.6.1.	Benetzungsverhalten der Tensidlösungen auf niederenergetischen Oberflächen .....	144
7.6.2.	Einfluss des optimierten Benetzungsverhaltens auf beim Strukturkollaps wirkende Kräfte .....	147
7.7.	<i>Empfehlung für einen benetzungsoptimierten Prozess zur nasschemischen Entfernung von Ätzresiduen.....</i>	<i>148</i>

## **8. Zusammenfassung und Ausblick 153**

### **Anhang**

A	Oberflächenenergiewerte der untersuchten festen und flüssigen Proben .	161
B	Kontaktwinkeldaten und Vergleich der energetischen Charaktere der untersuchten Flüssigkeiten und Festkörper.....	163
C	Berechnung der Oberflächenenergie des PTFE-Substrats.....	168
D	Kompatibilitätsuntersuchung der Lösungen B1, B2 und C1 zu einem	169

porösen low-k Dielektrikum und Kupfer.....	
E     Dynamische Oberflächenenergie der DIW-Tensidlösungen.....	171
F     Dynamische Oberflächenenergie und Langzeitstabilität der tensidversetzten Reinigungslösungen.....	182
G     Kompatibilitätsstudie der Tensidlösungen zu Kupfer und Diffusionsbarrieren.....	187
H     Kompatibilitätsstudie der Tensidlösungen zu einem porösen low-k Dielektrikum .....	188
I     Bewertung der Tensidlösungen hinsichtlich ihres Benetzungsverhaltens und ihrer Materialkompatibilität.....	205
 Referenzen.....	 207
Abbildungsverzeichnis.....	213
Tabellenverzeichnis.....	219
Verzeichnis der verwendeten Gleichungen.....	223
Thesen.....	225
Curriculum Vitae.....	229
Eigene Publikationen und Konferenzbeiträge.....	231

**List of Acronyms and Symbols**

BEOL	.....	Back End of Line
CCD	.....	Charged coupled device
Cmc	.....	Critical micelle concentration
CMOS	.....	Complementary metal oxide semiconductor
CMP	.....	Chemical mechanical planarization
CV	.....	Capacitance voltage (measurement)
CVD	.....	Chemical vapor deposition
FEOL	.....	Front End of Line
FTIR	.....	Fourier Transform Infrared Spectroscopy
HLB	.....	Hydrophilic lipophilic balance
IC	.....	Integrated circuit
ITRS	.....	International Technology Roadmap for Semiconductors
MIR	.....	Mid infrared
MOSFET	.....	Metal oxide semiconductor fieldeffect transistor
MSE	.....	Mean square error
NDA	.....	Non disclosure agreement

OWRK	.....	Method of Owens, Wendt, Rabel and Kaelble
PECVD	.....	Plasma enhanced chemical vapor deposition
PERR	.....	Plasma etch residue removal
RCA clean	.....	Cleaning process developed by Werner Kern at Radio Corporation of America
SAC	.....	Semi aqueous chemistry
SC1	.....	Standard clean 1
SC2	.....	Standard clean 2
SCCO <sub>2</sub>	.....	Supercritical carbon dioxide
TFVL	.....	Trench first – via last
UV	.....	Ultra violet
VFTL	.....	Via first – trench last
ZfM	.....	Center for Microtechnologies at the Chemnitz University of Technology

### **Symbols and physical units**

$\alpha$	.....	Polarizability
$\alpha_d$	.....	Distortion polarizability
$\alpha_e$	.....	Electronic polarizability
$\sigma$	.....	Surface energy

$\sigma^-$	.....	Basic surface energy part
$\sigma^+$	.....	Acid surface energy part
$\sigma^D$	.....	Dispersive surface energy part
$\sigma^D_S$	.....	Dispersive surface energy part of the solid
$\sigma^H$	.....	Surface energy part resulting from hydrogen bonds
$\sigma_i, \sigma_j, \sigma_1, \sigma_2$	.....	Surface energy of two different surfaces within a system
$\sigma^P$	.....	Polar surface energy part
$\sigma^P_L$	.....	Polar surface energy part of the liquid
$\sigma^P_S$	.....	Polar surface energy part of the solid
$\gamma$	.....	Interfacial energy
$\gamma_{ij}, \gamma_{12}$	.....	Interfacial energy of two different interfaces within a system
$\gamma_{LV}$	.....	Energy of the interface liquid/vapor
$\gamma_{SL}$	.....	Energy of the interface solid/liquid
$\gamma_{SV}$	.....	Energy of the interface solid/vapor
$\epsilon_0$	.....	Vacuum permittivity
$\epsilon_{rel}$	.....	Relative permittivity
$\theta$	.....	Contact angle



$\theta_0$	.....	Intrinsic contact angle
$\theta_A$	.....	Advancing contact angle
$\theta_R$	.....	Receding contact angle
$\tau$	.....	Signal delay of an interconnect system
A	.....	Area
C	.....	Electrical capacitance
D	.....	Distance
F	.....	Force
f	.....	Frequency
h	.....	Height
J	.....	Leakage current density
k	.....	Permittivity
l	.....	Wetted length
n	.....	Refractive index
N	.....	Number of atoms or molecules
p	.....	Pressure
P	.....	Power consumption
psi	.....	Pounds per square inch

---

Q	.....	Area fraction of a heterogeneous surface
R	.....	Radius
r	.....	Roughness factor
$R_{el}$	.....	Electrical resistivity
sccm	.....	Standard cubic centimeters
V	.....	Voltage
w	.....	Width
$W_{ii}$	.....	Work of cohesion within a homogeneous material
$W_{ij}, W_{12}$	.....	Work of cohesion between two phases
<b>Materials</b>		
3MS	.....	Trimethylsilane
4MS	.....	Tetramethylsilane
CoWP	.....	Cobalt Tungsten Phosphide
CTAB	.....	Cetyl trimethylammonium bromide
DIW	.....	Deionized water
FSG	.....	Fluoro silicate glass
HDA	.....	Hydroxileamine

---

HSQ	.....	Hydrogen silsesquioxane
ILD	.....	Interlayer dielectric
IPA	.....	Isopropyl alcohol
low-k	.....	Dielectric material with a permittivity lower than SiO <sub>2</sub>
MSQ	.....	Methyl silsesquioxane
OMCTS	.....	Octamethylcyclotetrasiloxane
p-DEMS	.....	Porous dielectric fabricated using Diethoxymethylsilane precursor
PFBE	.....	Perfluorobutylethylene
PTFE	.....	Polytetrafluoroethylene
SiCOH	.....	Hybrid dielectric material consisting of Si, C, O and H
SiO <sub>2</sub>	.....	Silicon dioxide
SSQ	.....	Silsequioxane
TaN	.....	Tantalum nitride
TiN	.....	Titanium nitride
TMCTS	.....	Tetramethylcyclotetrasiloxane
TMDD	.....	2,4,7,9-Tetramethyldec-5-yne-4,7-diol
Ultra low-k	.....	Dielectric materials with a permittivity lower than 2.4

## **Vorwort**

Die vorliegende Arbeit entstand während meiner Zeit als Doktorandin im Rahmen des Internationalen Graduiertenkollegs 1215 "Materials and Concepts for Advanced Interconnects and Nanosystems" sowie meiner Zeit als wissenschaftliche Mitarbeiterin am Zentrum für Mikrotechnologien der TU Chemnitz und am Fraunhofer ENAS. Ich möchte allen Mitarbeitern des ZfM und des Fraunhofer ENAS danken, die mich während dieses Abschnitts begleitet haben, sei es durch Gespräche und ihren Zuspruch oder fachliche Unterstützung und Hilfestellung.

*Besonderer Dank gilt: / Special thanks go to:*

Herrn Prof. Dr. Thomas Gessner und Herrn Prof. Dr. Stefan E. Schulz dafür, dass sie mir die Möglichkeit gaben, diese Arbeit zu schreiben, die fruchtbaren Diskussionen und für die eingeräumten Freiheiten während der Bearbeitung des Themas;

Herrn Prof. Dr. Michael Hietschold für seine Bereitschaft, diese Arbeit zu begutachten;

Herrn Prof. Dr. Stefan E. Schulz für die Unterstützung bei der Abfassung dieser Arbeit, das entgegengebrachte Vertrauen und Verständnis in der einen oder anderen schwierigen Phase meiner Zeit als Doktorandin;

Herrn Michael Rennau und Frau Manuela Zacher für die Unterstützung bei den umfangreichen elektrischen Messungen und bei der FTIR-Analyse;

Herrn Dr. Sven Zimmermann für die Durchführung der Plasmaprozesse, seine Ratschläge, die gewinnbringenden Diskussionen und vor allem auch für seinen unvergleichlichen Humor, der mein Leben wahrscheinlich um einen nicht zu vernachlässigenden Zeitraum verlängert hat ;- ) Danke Svenni!

Herrn Dr. Frieder Blaschta, der mich nicht nur einmal mit seinem unglaublich umfangreichen Wissen auf die richtige Spur gebracht hat;

Frau Birgit Groth für die Hilfe bei den Nassprozessen und die vielen aufmunternden Gespräche in wirklich schwierigen Zeiten;

den unermüdlichen Mitarbeiterinnen der Universitätsbibliothek der TU Chemnitz, die unzählige Artikel und Magazinbestellungen für mich besorgten oder

bereitstellten und niemals die Geduld verloren, wenn mir dann immer noch etwas fehlte.

Herrn Matthias Schaller und Herrn Thomas Oszinda bei GLOBALFOUNDRIES für die fruchtbaren Diskussionen;

Herrn Eugene Baryschpolec von Air Products für die Organisation und Bereitstellung der Tenside und Reinigungslösungen, für die immer schnelle, freundliche und unbürokratische Hilfestellung und vor allem auch für seinen Zuspruch und seine Anteilnahme während meiner längeren Erkrankung. Danke Eugene! / Mr. Eugene Baryschpolec of Air Products, for organizing and supplying the surfactants and cleaning solutions, his fast, kind and uncomplicated help and especially for his encouragement during a longer phase of illness of mine. Thanks a lot Eugene!

Herrn Veit Leonhardt für die vielen Diskussionen fachlicher und persönlicher Natur, die Korrekturlesung dieser Arbeit und vor allem für seine Freundschaft, die mir nach wie vor unglaublich viel bedeutet.

dem harten Kern meiner Icewars-Jungs, die mich nunmehr schon über fast 10 Jahre kennen mit allen Ticks und Marotten, alle Hochs und Tiefs miterlebt haben und mich auch nach längerer Abwesenheit wieder diskussionslos in ihrer Mitte aufgenommen haben, ob nun virtuell oder im richtigen Leben: Timo (Corum), Rene (Ita), Rene (hulmel), Claus (uaz), Flo (axis), Robin (Spezi), Martin, Stefan (Hau), Micha (Teufelchen) ... vielen Dank! Timo... du warst immer da, wenn ich dich gebraucht hab, ich danke dir für deine Freundschaft!

meiner Mutter, die immer an mich geglaubt und mich unterstützt hat, wo und wie sie nur konnte, die mir in schlimmen Zeiten immer Rückhalt gegeben hat und ohne die ich heute nicht da wäre, wo ich bin. Danke Mutti!

meinem Freund Volker Bendull, der zum Mittelpunkt meines Lebens geworden ist, unermüdlich in seiner Unterstützung, aber auch sofort zur Stelle, wenn ich mal wieder einen Schubbs in die richtige Richtung benötigt habe. Ich danke dir für dein Vertrauen, dein Verständnis und deine Geduld, dafür dass du immer an meine Fähigkeiten geglaubt hast und für deine Wärme und Liebe.

## **1. Introduction**

The progress in development of microelectronic integrated circuits over the last decades enabled rapid advances in nearly every field of our industrialized society. Fabrication automation, telecommunication, medical diagnostics, engineering, natural science, automotives or weather forecasts are only a few branches which strongly profiteer from increasing IC performance. But also in the private sector microelectronics created new digitalized opportunities for everyone, like mobile communication or personal computing.

The demands to become smaller, faster and cheaper made microelectronic devices affordable and are the main drivers of research and development in semiconductor industry. Since the development of the first germanium based solid state transistor by Shockley, Bardeen and Brattain at Bell Labs in 1947 [1, 2], many fundamental discoveries have accompanied research and development. Silicon based IC technology was introduced in 1954 by Teal of Texas Instruments [3]. The first connected or integrated transistor structures have been developed by Noyce and Kilby at Fairchild and Texas Instruments, respectively, in 1958 [4]. In contrast to discrete devices integration rapidly reduced the size of microelectronic devices and enabled the fabrication of more complex features. In 1959 Kilby and Noyce presented the first transistor manufactured in planar technology, followed by the first MOSFET in 1960 (Khang at Bell Labs) [5].

The main advantages of fabricating multiple transistors on one single substrate is the reduction of manufacturing costs, the ability to produce complex, reliable and reproducible integrated circuits, which entered the market in the 1960's. IC speed more and more increased by miniaturization of the transistor structures and rapid increase of the number of transistors on a single chip. In 1965 Gordon Moore stated

[illegible]

Improvements in processing have been able to overcome the limitations of device scaling for more than 40 years, but there has always been the question, how long Moore's Law will keep its validity. Knowledge gaps which have to be focused by research and development are identified by the International Technology Roadmap

for Semiconductors (ITRS), assuming the continuity of Moore's law. Increasing integration density by dimensional scaling ensured higher speed and reduced power consumption of a digital circuit. The digital content of an integrated circuit, along with storage components, is the CMOS transistor, but many microelectronic devices will have analog functionalities like radio frequency devices, sensors, actuators, bio chips or micromechanical systems (MEMS). They represent the interface with the actual environment, which is analog. Both trends, further miniaturization called "More Moore" and functional diversification called "More than Moore", are now implemented into the ITRS.

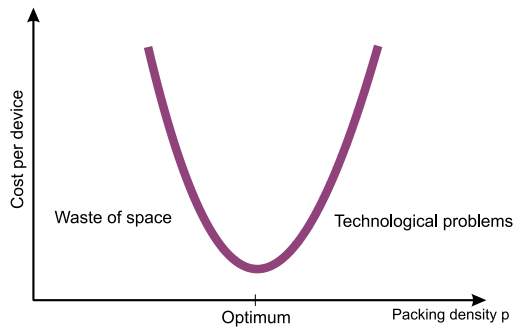


**Figure 1-2:** Packing density of transistors on an IC and production cost per device. Below the optimum point the available space on the chip is wasted while beyond this point production costs are too high due to technological difficulties. Moore's Law refers to the optimum value of packing density and costs per device.

### 1.1. Integration of new materials in FEOL and BEOL processing

With further decreasing feature sizes many of the traditionally applied materials in semiconductor manufacturing do not longer meet the requirements of future technology nodes summarized in the ITRS. This resulted in the development of new material concepts in FEOL and BEOL processing. Prominent examples in



FEOL are the replacement of  $\text{SiO}_2$  as gate insulator by high-k materials or of the poly crystalline Si by metal gate structures and the introduction of stressor materials to increase charge carrier mobility. Since the mid 90's of the last century the number of materials applied in semiconductor technology has more than doubled (see **Figure 1-3**).

**Table 1-1:** Guidelines for interconnect technology actually listed in the ITRS for short and long term development. The red fields mark issues where at present no manufacturable solutions are known.

Year of production	2010	2011	2012	2015	2018	2020
Technology node	32	32	32	22	15	?
MPU/ASIC $\frac{1}{2}$ pitch [nm] metal 1	45	38	32	21	15	11.9
Interlevel metal insulator effective dielectric constant ( $k_{\text{eff}}$ )	2.6-2.9	2.6-2.9	2.6-2.9	2.4-2.8	2.1-2.5	2.0-2.3
Interlevel metal insulator bulk dielectric constant ( $k$ )	2.3-2.5	2.3-2.5	2.3-2.5	2.1-2.3	1.9-2.3	1.7-1.9
Cu diffusion barrier and etch stop bulk dielectric constant ( $k$ )	3.5-4.0	3.5-4.0	3.5-4.0	3.0-3.5	2.6-3.0	2.4-2.6
Conductor effective resistivity [ $\mu\Omega\text{cm}$ ] Cu metal 1	4.08	4.30	4.53	5.58	6.70	8.19
Barrier cladding thickness [nm] metal 1	3.3	2.9	2.6	1.9	1.3	1.1
Manufacturable solutions exist and are being optimized	Manufacturable solutions are known			Manufacturable solutions are not known		

hydrogen 1 H 1.0079																	helium 2 He 4.0026																	
lithium 3 Li 6.941	beryllium 4 Be 9.0122																	boron 5 B 10.811	carbon 6 C 12.011	nitrogen 7 N 14.007	oxygen 8 O 15.999	fluorine 9 F 18.998	neon 10 Ne 20.180											
sodium 11 Na 22.990	magnesium 12 Mg 24.305																	aluminum 13 Al 26.982	silicon 14 Si 28.086	phosphorus 15 P 30.974	sulfur 16 S 32.065	chlorine 17 Cl 35.453	argon 18 Ar 39.948											
potassium 19 K 39.098	calcium 20 Ca 40.078	scandium 21 Sc 44.956	titanium 22 Ti 47.867	vanadium 23 V 50.942	chromium 24 Cr 51.996	manganese 25 Mn 54.938	iron 26 Fe 55.845	cobalt 27 Co 58.933	nickel 28 Ni 58.693	copper 29 Cu 63.546	zinc 30 Zn 65.39	gallium 31 Ga 69.723	germanium 32 Ge 72.61	arsenic 33 As 74.922	selenium 34 Se 78.96	bromine 35 Br 79.904	krypton 36 Kr 83.80																	
rubidium 37 Rb 85.468	strontium 38 Sr 87.62	yttrium 39 Y 88.906	zirconium 40 Zr 91.224	niobium 41 Nb 92.906	molybdenum 42 Mo 95.94	technetium 43 Tc [98]	ruthenium 44 Ru 101.07	rhodium 45 Rh 101.07	palladium 46 Pd 106.42	silver 47 Ag 107.87	cadmium 48 Cd 112.41	indium 49 In 114.82	tin 50 Sn 118.71	antimony 51 Sb 121.76	tellurium 52 Te 127.60	iodine 53 I 126.90	xenon 54 Xe 131.29																	
cesium 55 Cs 132.91	barium 56 Ba 137.33	lanthanum 57 La 138.91	cerium 58 Ce 140.12	praseodymium 59 Pr 140.91	neodymium 60 Nd 144.24	promethium 61 Pm [145]	samarium 62 Sm 150.36	europium 63 Eu 151.96	gadolinium 64 Gd 157.25	terbium 65 Tb 158.93	dysprosium 66 Dy 162.50	holmium 67 Ho 164.93	erbium 68 Er 167.26	thulium 69 Tm 168.93	ytterbium 70 Yb 173.04	lutetium 71 Lu 174.97	hafnium 72 Hf 178.49	tantalum 73 Ta 180.95	niobium 74 Nb 92.906	molybdenum 75 Mo 95.94	technetium 76 Tc [98]	ruthenium 77 Ru 101.07	rhodium 78 Rh 101.07	palladium 79 Pd 106.42	silver 80 Ag 107.87	cadmium 81 Cd 112.41	indium 82 In 114.82	tin 83 Sn 118.71	antimony 84 Sb 121.76	tellurium 85 Te 127.60	iodine 86 I 126.90	xenon 87 Xe 131.29		
francium 87 Fr [223]	radium 88 Ra [226]	actinium 89 Ac [227]	thorium 90 Th 232.04	protactinium 91 Pa 231.04	uranium 92 U 238.03	neptunium 93 Np [237]	plutonium 94 Pu [244]	americium 95 Am [243]	curium 96 Cm [247]	berkelium 97 Bk [247]	californium 98 Cf [251]	einsteinium 99 Es [252]	fermium 100 Fm [257]	mendelevium 101 Md [258]	nobelium 102 No [259]	lawrencium 103 Lr [260]	bohrium 104 Bh [264]	hassium 105 Hs [277]	meitnerium 106 Mt [268]	darmstadtium 107 Ds [271]	roentgenium 108 Rg [272]	copernicium 109 Cn [285]	nihonium 110 Nh [286]	flerovium 111 Fl [289]	tennessine 112 Ts [289]	oganesson 114 Og [289]	unbinilium 115 Uub [289]	ununilium 116 Uuq [289]	unununium 117 Uuu [289]	unununium 118 Uuu [289]	unununium 119 Uuu [289]	unununium 120 Uuu [289]	unununium 121 Uuu [289]	unununium 122 Uuu [289]

Before 90's

Since the 90's

Beyond 2006

\* Lanthanide series

lanthanum 57 La 138.91	cerium 58 Ce 140.12	praseodymium 59 Pr 140.91	neodymium 60 Nd 144.24	promethium 61 Pm [145]	samarium 62 Sm 150.36	europium 63 Eu 151.96	gadolinium 64 Gd 157.25	terbium 65 Tb 158.93	dysprosium 66 Dy 162.50	holmium 67 Ho 164.93	erbium 68 Er 167.26	thulium 69 Tm 168.93	ytterbium 70 Yb 173.04	lutetium 71 Lu 174.97
---------------------------------	------------------------------	------------------------------------	---------------------------------	---------------------------------	--------------------------------	--------------------------------	----------------------------------	-------------------------------	----------------------------------	-------------------------------	------------------------------	-------------------------------	---------------------------------	--------------------------------

\*\* Actinide series

actinium 89 Ac [227]	thorium 90 Th 232.04	protactinium 91 Pa 231.04	uranium 92 U 238.03	neptunium 93 Np [237]	plutonium 94 Pu [244]	americium 95 Am [243]	curium 96 Cm [247]	berkelium 97 Bk [247]	californium 98 Cf [251]	einsteinium 99 Es [252]	fermium 100 Fm [257]	mendelevium 101 Md [258]	nobelium 102 No [259]	lawrencium 103 Lr [260]
-------------------------------	-------------------------------	------------------------------------	------------------------------	--------------------------------	--------------------------------	--------------------------------	-----------------------------	--------------------------------	----------------------------------	----------------------------------	-------------------------------	-----------------------------------	--------------------------------	----------------------------------

**Figure 1-3:** Chemical elements applied in semiconductor technology. Beyond 2006 the number of elements used has more than doubled compared to the 1990's due to the integration of new materials to meet the requirements of the ITRS for future technology nodes.

The speed of integrated circuits has been increased by miniaturization to reduce signal propagation time within the active areas of the transistors, but when technology reached the 250 nm node opposed effects within the interconnect system started dictating IC performance [10]. Due to increasing parasitic capacitances signal delay and crosstalk effects are limiting overall IC speed and SiO<sub>2</sub> as insulating material no longer meets the requirements of future technology nodes due to its high k-value of about 4.0.. The so called RC-product, which is a measure of signal delay within interconnect structures has to be minimized. Besides the replacement of Aluminum by copper for wiring (reduction of R) low dielectric constant materials (low-k) emerged to replace SiO<sub>2</sub> [11, 12].

The integration of low-k materials, which actually contain organic species and are porous to reduce the k-value down to  $< 2.5$ , is challenging and commonly applied processes for patterning, cleaning, CMP etc. have be adjusted to be compatible to the sensible low-k materials. This is especially true for cleaning processes due to the fact that the use of aggressive chemicals can easily alter the properties of a variety of materials like low-k materials, copper or diffusion barriers. Besides the removal of particles and other contaminants, the removal of plasma etch residues is one of the most important cleaning processes and covers up to 30% of all cleaning processes [13]. Commonly applied processes to remove polymeric residues deposited during dielectric etching are no longer compatible to hybrid low-k materials, which actually have a porosity of 20-30%. Especially oxidizing chemistries used in plasma and wet cleaning have to be avoided due to the fact that they strongly degrade the dielectric's electrical parameters [14]. To find alternative and Cu/low-k compatible cleaning processes is one of the main issues in BEOL research and development. But with smaller and smaller structures additional challenges occur, especially in the field of wet chemical PERR, which is a promising alternative to low-k material damaging plasma processes.

In 32 nm and especially in 22 nm technology the focus in developing wet cleaning solutions will no longer be only on compatibility and chemical composition of the cleaner, but has to include the wetting behavior of the system liquid/solid. Due to its surface tension / surface energy the cleaning liquid may not be able to penetrate into very small structures and no residue removal will be possible in those cases. This is especially critical for small via structures. Another issue is the trend of semiconductor manufacturing to prefer water based cleaning liquids which have the advantage of being environmentally friendly, nontoxic and ensure low disposal costs [15]. But such kind of cleaning solutions are high energetic and will show a poor wetting behavior on low-energetic polymeric residue layers. The high surface

energy of the cleaning liquid can also introduce the effect of pattern collapse to interconnect structures, which is actually known in lithography for photoresist structures. High capillary forces are able to deform and even destroy small trench structures. In 32 nm and 22 nm technology porous and mechanically weak low-k patterns will have to face this challenge. This drives the demand of the development of wetting optimized wet cleaning solutions, which enable wetting of small structures and prevent pattern collapse.

## **1.2. Overview of the dissertation**

In this work at first the focus is on the basic determination of the energetic characteristics of wet cleaning solutions commonly used for PERR and of several materials applied in BEOL processing, especially differently etched/ashed low-k dielectrics. The surface energy values gathered are used to determine the wetting behavior of the system solid / liquid and to disclose combinations of cleaning liquid and solid surface where the wetting will be critical. The approach to overcome those kinds of wetting issues followed in this work is the optimization of the wetting behavior of the cleaning liquid. By the application of surfactants the surface energy of the liquids can be decreased to ensure optimal wetting. The compatibility of the surfactant aided solutions to BEOL processing is studied and finally a basic advice for selecting suitable surfactants and processing of wetting optimized surfactant aided wet cleaning solutions will be presented.

The first part of chapter 2 gives an introduction to low-k technology and integration issues. Material concepts and dual damascene integration schemes used to fabricate interconnect wiring systems will be discussed. In the second part the focus will be on plasma etch residue removal strategies. The origin of polymeric residues and their composition as well as commonly applied plasma processes to remove etch

residues are introduced. Low-k material damaging by several plasma processes is described, which gives rise to the strategy to substitute dry cleaning processes by all wet plasma etch residue removal.

Common wet cleaning processes as well as new cleaning strategies like the application of supercritical fluids are discussed. Newly emerging wet cleaning challenges in 32/22 nm technology, which mainly include wetting concerns like nonwetting of small structures or pattern collapse effects and are focused by this work, are briefly introduced. This finally shows the necessity to understand wetting mechanisms and strategies to analyze the wetting behavior of cleaning solutions and solid surfaces to be cleaned.

Chapter 3 will go more into detail on wetting, describing the thermodynamic background and importance and origin of surface energies to understand wetting. Several model considerations to describe surface energies and which allow their experimental determination will be shown. The second part of this chapter focuses on a more detailed description of wetting concerns emerging in PERR like nonwetting of small structures and finally shows several strategies to overcome those issues. One of those strategies is the reduction of the surface energy of the cleaning liquid, which finally stands in the focus of this work. One approach to lower the cleaning liquid's surface energy is the application of surfactants, an approach only rarely studied in the recent years.

Chapter 4 describes the basic mechanisms of a surfactant lowering the surface energy of a liquid medium as well as types and application fields of surfactants and special issues to be analyzed, like the compatibility of surfactant solutions to materials used in BEOL. The determination of the energies of solid and liquid surfaces was done by applying the method of Owens, Wendt, Rabel and Kaelble

(OWRK) and the pendant drop method, both described in chapter 5 as well as the maximum bubble pressure method to analyze the dynamic behavior of the surfactants selected for this work. This chapter also introduces the analytical methods used to determine whether a surfactant solution is compatible to dielectric, metallic and barrier materials, e.g. spectral ellipsometry, FTIR and electrical measurements.

In chapter 6 the results of the surface energy calculations of the solid and liquid samples are shown. The OWRK method turned out to be very useful finding an appropriate combination of liquid and solid for optimal wetting behavior. Additionally the analysis of differently treated dielectric samples by contact angle measurement and surface energy calculation turned out to be not only helpful to determine the wetting behavior of the surfaces but also to evaluate the impact of plasma processes on the surface properties of the low-k dielectric. The values of polar and dispersive energy contribution after plasma treatment give a hint of whether or not a damage of the dielectric surface happened or if a polymer has been deposited. Meanwhile this method has been developed into a standard analytical method to analyze the influence of plasma processes on dielectric samples. The low surface energy of most of the materials analyzed showed the need to optimize the surface energy of the studied water based cleaning liquids, which turned out to have a too high surface energy to ensure good wetting on the studied solid surfaces.

In chapter 7 several types of surfactants are applied to the cleaning liquids to lower their surface energy. The compatibility to BEOL materials and their dynamic behavior has been studied and a general advice about selecting surfactants and processing of surfactant aided solutions within BEOL processing is given.

Chapter 8 finally summarizes the results of this work and gives an overview of future works necessary to further develop wetting optimized cleaning solutions by application of surfactants.

## **2. Processing and integration of low-k dielectrics in BEOL**

In the first part of this chapter the focus is on the factors limiting the signal speed especially within the interconnect system of integrated circuits, their origin and strategies to overcome those issues. The integration of new materials like low-k and ultra low-k dielectrics will be discussed, especially looking on challenges integrating those kinds of materials. The second part of this section will concentrate on the area of plasma etch residue removal in Cu/low-k technology. Here the origin of plasma etch residues, common removal processes and new cleaning strategies will be discussed, which meet the requirements of future technology nodes.

### **2.1. General introduction**

Today's integrated circuits performance is mainly limited by parasitic effects within the interconnect system [16]. Within FEOL the gate delay dominated the IC's performance and could be minimized by decreasing gate lengths and further miniaturization of transistor structures. Until the 250 nm generation emerged the influence of the interconnect system to the overall speed of the IC was rather inessential. With further decreasing feature geometries crosstalk and delay times of the interconnect system gained ascendancy over the delays caused by FEOL features (Figure 2-1) [12, 17].

The main driver of parasitic effects within interconnect structures are parasitic capacitances (Figure 2-2), which occur between wires and between metallization levels [19, 20]. The total delay of the interconnect system can be described by the RC product:



$$\tau = R \cdot C \quad (2-1)$$

where  $R$  is the resistivity of the metal used for wiring and  $C$  are the capacitances between wires or levels.  $R$  could be decreased by replacing aluminum by copper for metallization. Copper has a 30 % lower resistivity than aluminum and additionally shows less electromigration effects [21, 22].

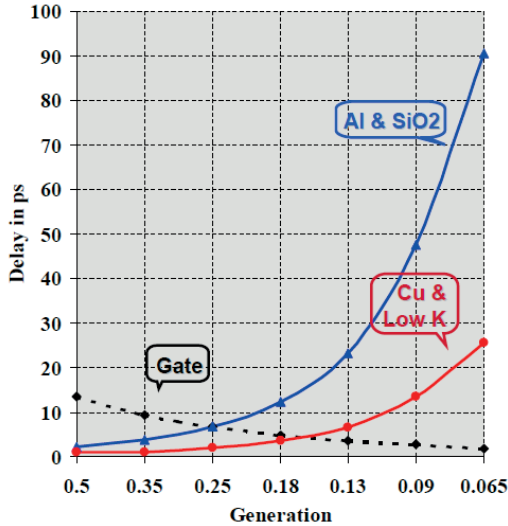


**Figure 2-1:** Expected interconnect delay for copper and low-k devices. Beyond the 250 nm technology node the delay times of the devices are no longer ruled by the transistor itself but by parasitic effects of the global wiring system. [18].

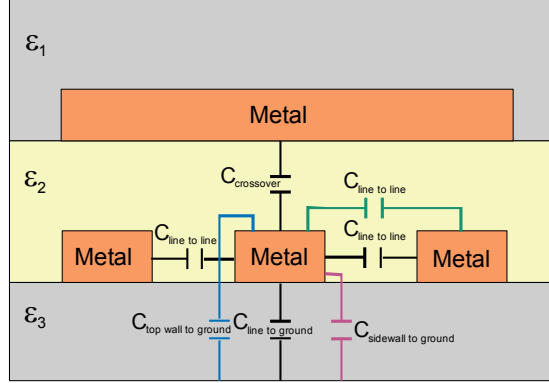


**Figure 2-2:** Parasitic capacitances occurring within the interconnect system of an integrated circuit. With decreasing feature sizes the metal lines become closer to each other and the capacitances increase, leading to a larger RC-product of the interconnect system [19].

To further decrease  $\tau$  the capacitances within the interconnect system have to be minimized. The smaller the distance between two metal lines the bigger is the capacitance (equation 2-2) [12].

$$C = \varepsilon_0 \cdot \varepsilon_{rel} \cdot \frac{A}{d} \quad (2-2)$$

Besides signal delay the power consumption of integrated circuits is challenging. Power consumption strongly increases with higher frequencies and feature density:

$$P = \alpha \cdot C \cdot f \cdot V^2 \quad (2-3)$$

where  $P$  is the power consumption,  $\alpha$  is the wire activity,  $f$  is the frequency and  $V$  is the voltage of the power supply [12]. In addition to this dynamic power consumption leakage currents between wires bring in a static power consumption and should be as low as possible.

The decrease of  $\epsilon_{rel}$  (k-value) of the dielectric insulating material between the wires and metallization levels is a promising approach to overcome those issues. This caused the development of low-k materials with a much lower k-value than the formerly used  $\text{SiO}_2$  ( $k \sim 4$ ). The following section will go more in detail on this.

## 2.2. Strategies to decrease the k-value of the insulator

### 2.2.1. Decreasing the k-value by reducing the polarizability of the dielectric

The k-value represents the polarizability of the dielectric when exposed to an electric field and is defined by the equation of Clausius and Mossotti:

$$\frac{\epsilon_{rel} - 1}{\epsilon_{rel} + 2} = \frac{N}{3 \cdot \epsilon_0} \cdot (\alpha_e + \alpha_d) \quad (2-4)$$

where  $\alpha_e$  is the electronic polarization,  $\alpha_d$  is the distortion polarization and N is the total number of the atoms or molecules [12, 23].

The k-value of a dielectric can be lowered by decreasing its polarizability and density. Polarizability can be reduced by incorporation of less polar groups like carbon or fluorine based species [12, 24]. By this method the k-value of Si-O based dielectrics can be reduced down to 2.6. For further reduction the film density has to be lowered. An important way to reduce film density is the incorporation of air into the material by pores or to form air gaps, which replace the low-k dielectric. In this work the focus will be set on porous materials, but also dense dielectrics are analyzed due to the fact that actual integration schemes include dense dielectrics e.g. to avoid mechanical instabilities [12, 18]. Based on their principal structure low-k dielectrics can be divided into three main groups (see scheme page 13) [12].

### 2.2.2. Introduction of porosity to Si-O based low-k dielectrics

Different techniques have been developed to form porous dielectric materials in the recent years. They include sol-gel processing to form aerogels and xerogels [25], surfactant template self-assembled silica [26], two phase (organic / inorganic) porogen approaches (e.g. MSQ) [27] or nano clustered silica [28], all of them deposited by spin-on. Actually semiconductor manufacturing focuses on SiCOH based dielectrics deposited by PECVD using a two-step porogen approach [29, 30]. At first a codeposition of two precursors is done to form a hybrid material consisting of a SiCOH backbone with inclusions of an organic sacrificial phase called porogen. In a second step the thermally instable porogen is removed by a curing process and pores form. A large number of SiCOH precursors (Figure 2-3 a-d) have been investigated in recent years, including e.g. 3MS ( $\text{Si}(\text{CH}_3)_3\text{H}$ ), 4MS ( $\text{C}_4\text{H}_{12}\text{Si}$ ), OMCTS ( $(\text{CH}_3)_2\text{SiO}$ )<sub>4</sub> or TMCTS ( $\text{Si}_4\text{C}_4\text{H}_{16}\text{O}_4$ ) [18]. As porogen  $\alpha$ -terpinene ( $\text{C}_{10}\text{H}_{16}$ ), limonene ( $\text{C}_{10}\text{H}_{16}$ ) or cyclo hexane ( $\text{C}_6\text{H}_{12}$ ) are some of the most preferred species (Figure 2-3 e-g) [31]. In Figure 2-4 the network structure of a dense TMCTS based SiCOH and the structure of the same material fabricated using a porogen is shown.

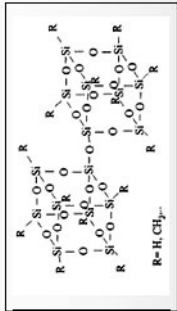
The main principle to further decrease the dielectric constant below 2.6 is the replacement of Si-O bonding by Si-C, the loosening of the network by incorporation of large terminating  $\text{CH}_3$  groups and the incorporation of air filled pores. The porogen included in the hybrid material has to be removed to form porosity. This can be done by thermal annealing, E-Beam curing or UV assisted thermal curing, which is the mostly favored curing method [32]. During curing the porogen is decomposed and driven out, the SiCOH matrix is crosslinking and a stable porous network is formed. To increase the mechanical strength of the porous network some Si-C bondings are broken (e.g. by UV radiation) and are replaced by Si-H. Due to the fact that Si-H is much smaller than Si- $\text{CH}_3$  the network becomes

denser which increases mechanical stability but also leads to a minor increase of the k-value. Actually developed porous SiCOH materials have a porosity of 20-30 % with a pore size of 1 - 2 nm.

# Classification of low-k dielectrics

## Silsequioxanes (SSQ)

**Basic structure:**  $(R-SiO_{3/2})_n$



$R = \text{hydrogen, alkyl, alkenyl, alkoxy, aryl}$

**lower k-value:** Si-R bonding is less polarizable than Si-O

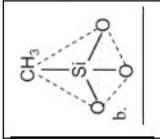
**typical materials:** HSQ ( $k = 3.0 - 3.2$ )  
MSQ ( $k = 2.8$ )

$k$ -value for MSQ is lower because Si-CH<sub>3</sub> is much larger than Si-H

**Deposition:** typically spin-on

## Silica based

**Basic structure:** tetrahedral



**lower k-value:** Si-O bondings are replaced by

Si-F or Si-CH<sub>3</sub>

**typical materials:**

FSG ( $k = 3.4 - 3.6$ )

Carbon doped oxides ( $k = 2.4 - 3.0$ )  
 $k$ -value for carbon doped oxides is lower because Si-CH<sub>3</sub> is larger than Si-F

**Deposition:** spin-on (FSG) or CVD (carbon doped oxide)

## Organic polymers

**Basic structure:** carbon based (C-C)

**lower k-value:** lower polarizability of carbon species compared to Si-O

**typical materials:** nonfluorinated polymers ( $k = 2.5 - 3.5$ )  
fluorinated polymers ( $k = 1.9 - 3.0$ )  
a:CF ( $k = 2.1 - 2.6$ )

**Deposition:** spin-on and CVD

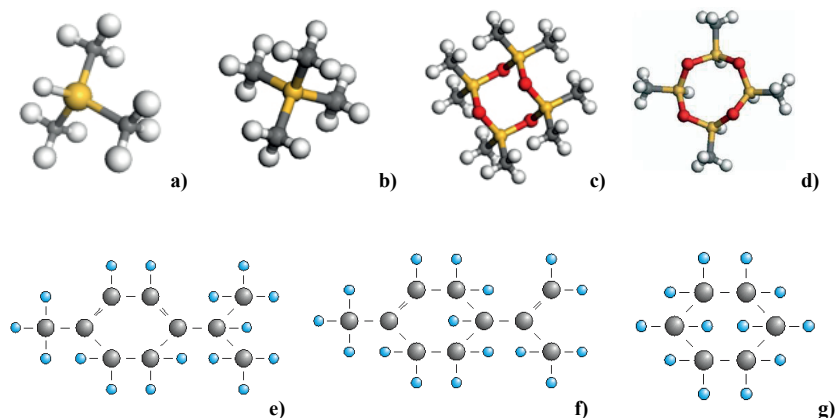


**Figure 2-3:** Typical precursor (a-d) and porogen (e-f) molecules used to fabricate dense and porous low-k dielectrics by PECVD. a) Trimethylsilane (3MS), b) Tetramethylsilane (4MS), c) Octamethylcyclotetrasiloxane (OMCTS), d) Tetramethylcyclotetrasiloxane (TMCTS), e)  $\alpha$ -terpinene, f) limonene, g) cyclohexane [Sources: a-d: Air Liquide S.A., e-f: Fraunhofer ENAS]

To achieve bulk k-values of  $< 2.0$  the integration of air gaps, where a sacrificial phase is removed and large voids are formed between the metal lines, is considered. Air gap structures (Figure 2-5 a and b) may provide a higher mechanical stability than porous low-k dielectrics, but integration schemes include a hybrid construction of low-k dielectrics and air gaps [18, 33].

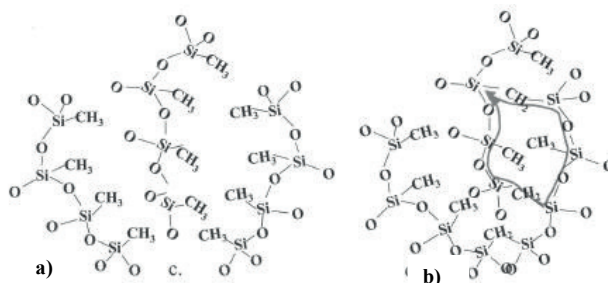


**Figure 2-4:** Network structure of a porous low-k dielectric fabricated with TMCTS precursor without porogen addition (a) and with porogen (b).

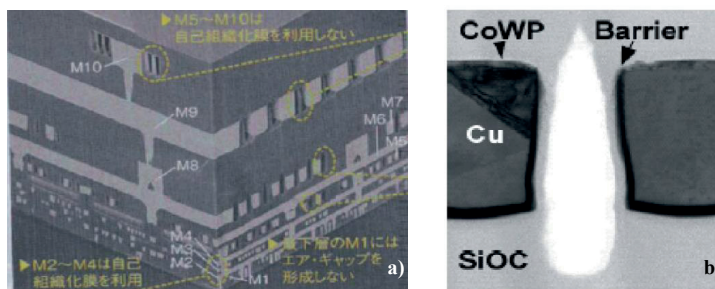


**Figure 2-5:** Air gaps partially replacing low-k dielectrics within the interconnect system. To achieve bulk dielectric constants below 2.0 the hybrid integration of air gaps and low-k materials is a promising approach. Figure 2-4a shows fully integrated air gaps in a multilevel wiring system (IBM) and Figure 2-4b shows a single air gap (Panasonic) [7].

### 2.3. The dual damascene process

As reported before, Aluminum has been replaced by copper for metallization within the interconnect system. It owns a much lower resistivity than Al and shows less electromigration. The common subtractive patterning scheme used in Al technology has been replaced by the damascene process for copper technology. In



this process scheme the dielectric is patterned at first, followed by the electrochemical deposition of the metal. Dual damascene processing is the most common metallization scheme, where via and trench levels are patterned and afterwards filled with copper at once.

### **2.3.1. Trench first – via last and Via first – trench last patterning schemes**

In Dual Damascene processing two patterning sequences can be used: Trench first – via last (TFVL) and via first – trench last (VFTL) [34], both starting with a dielectric stack consisting of an etch stop layer (e.g. SiN) on the bottom, the interlayer dielectric (ILD) for the via structures, an embedded etch stop layer (optional) and the ILD layer for the trench structures. In this section the general processing schemes are described for SiO<sub>2</sub> used as ILD.

The TFVL processing scheme starts with the definition of the trench patterns. After deposition, exposure and patterning of the photoresist the dielectric is etched down to the embedded etch stop layer and the first photoresist is removed. To define the via patterns again photoresist is deposited, exposed and patterned aligned to the trench structures. The dielectric is now etched down to the bottom etch stop layer. During this process the trench structures are protected by the resist from further etching, which is removed after etching.

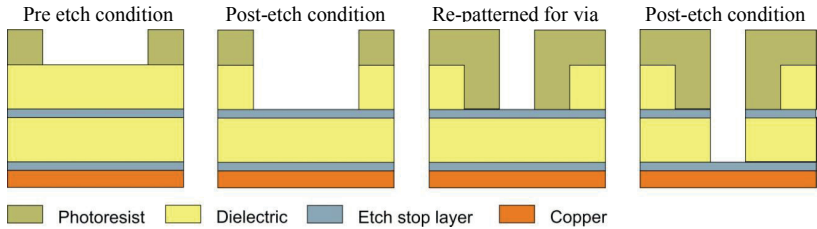


**Figure 2-6:** Trench first – via last processing sequence.

The thick photoresist layer needed for the 2<sup>nd</sup> lithography step is one big disadvantage of the TFVL integration scheme. With decreasing feature sizes very small via structures are difficult to form in thick resist layers and so this scheme is only used for larger structures of the uppermost metallization levels.

The characteristic of VFTL compared to TFVL is that at first the via structures are defined. (Figure 2-7 a and b). After photoresist deposition, exposure and patterning the ILD is etched down to the etch stop layer at the bottom of the dielectric stack and the resist is removed. To define the trench pattern in the ILD and to protect the via structures at the bottom from being etched again photoresist is deposited, exposed and patterned. The ILD is now etched down to the embedded etch stop layer and the trench is formed. Afterwards the photoresist is removed.

Those process steps are followed by the deposition of the diffusion barrier, copper seed layer and copper and the removal of the excess copper by CMP (**Figure 2-8**). .

Especially with decreasing feature sizes and increasing aspect ratios both dielectric patterning schemes show advantages and disadvantages. One of the VFTL scheme's advantages is the direct alignment of subsequent layers, while in TFVL the indirect alignment of trench and via requires stringent overlap rules to avoid

defects. The void free filling of high aspect ratio via features by an organic material is one of the most challenging issues in VFTL processing.

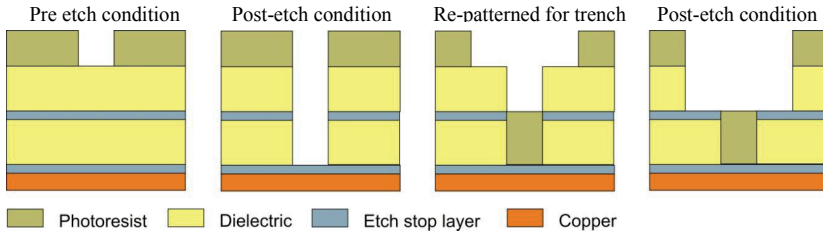


**Figure 2-7:** Via first – trench last processing sequence.

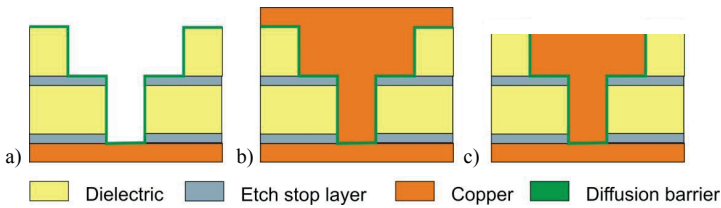


**Figure 2-8:** After patterning trench and via the diffusion barrier is deposited (a), the structure is filled with copper (b) and the excess copper is removed by CMP (c)

Any void in the via fill material can lead to a deformation of the via shape during trench etch process. A smooth and fence-free transition between via and trench, which provides a continuous copper seed layer for the electroplating process is one of the biggest advantages of the TFVL scheme. But with increasing feature sizes the main challenge of TFVL is a non-planar resist surface due to large step heights causing a reduction of the depth of focus in the lithography. Aspect ratios are therefore limiting the decision which approach one could take: TFVL is more

suitable for wide lines with moderate aspect ratios, while VFTL is capable to cover higher aspect ratios, but suffers from the improper transition between trench and via, the so-called fence or shell profile. The introduction of thin hard mask layers (metal or dielectric hardmasks) to avoid large step heights in TFVL processing is a very promising approach to overcome the lithography issues described before. In case of low-k dielectrics even double or triple layer-hardmasks are reported to protect the low-k materials. The advantages of the hard mask approach are the fence-free shape of the dual damascene structure, the elimination of resist poisoning and the lower etch selectivities between the different materials compared to the VFTL scheme.

### **2.3.2. Integration schemes for low-k dielectric materials**

Plasma processes like etching and resist stripping are known to degrade the electrical properties of the dielectric. This is especially true for oxygen based plasma stripping processes. By the introduction of additional mask layers the resist can be removed without exposing the dielectric to the plasma. Due to weak mechanical properties full integration of porous low-k dielectrics is critical. The low-k material has to withstand forces applied by CMP or during packaging and several temperature treatments during the fabrication of subsequent metallization levels without cracking or delamination. Hybrid integration schemes including porous low-k dielectrics as well as dense dielectrics are one approach to overcome stability issues. Further reliability issues include the diffusion of copper into the dielectric. Sidewalls and bottom of the structures are covered by a barrier material which inhibits copper diffusion. At the upper side of the structure the copper can be covered by an etch stop dielectric, whose interface shows less adhesion to the copper than other barrier materials. That is the reason why copper diffusion will

mainly occur at this interface. To prohibit copper diffusion and the formation of voids or other failures within via/wire structures, a cobalt tungsten phosphide film (CoWP) can be selectively deposited on the copper after CMP. This film consists of 90% nano crystalline cobalt, 2% tungsten and 8% phosphorous. The grain boundaries of the cobalt are sealed by tungsten and phosphorous species and a strongly adhering metal/metal interface is formed. This usually 10 – 15 nm thin film also works as an etch stop layer. Every dielectric layer additionally integrated influences the effective k-value of the Cu/low-k structures and has to be designed to have a low dielectric constant on its own or to be as thin as possible. **Figure 2-9** illustrates several typical inter-level dielectric (ILD) architectures used in the creation of interconnect wiring levels.

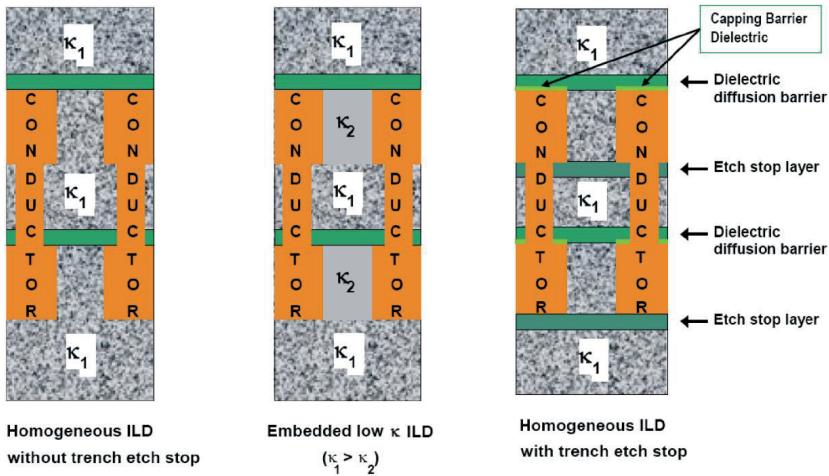


**Figure 2-9:** Copper / low-k integration schemes. Different constructions including embedded low-k, etch stop layers, barrier and capping layers integrated to e.g. overcome copper diffusion, result in varying effective k-values of the wiring system; actually the k-values given in the ITRS are related to the schemes showed above [7].

## 2.4. Patterning of Si-O like low-k dielectrics by dry etching

Due to their chemical composition consisting of a Si-O-Si network with organic CH<sub>3</sub> species silica based low-k materials can be patterned using C-F containing etch gasses, e.g. C<sub>2</sub>F<sub>6</sub>, C<sub>4</sub>F<sub>8</sub>, CF<sub>4</sub> or CHF<sub>3</sub> [35-37]. Fluorine species are reacting with the SiO<sub>2</sub> like species of the dielectric, forming volatile SiF<sub>4</sub> as main reaction product. Ion bombardment as physical component of the etching process is loosening Si-O bond to support the reaction. During etching CF<sub>x</sub> radicals lead to the formation of a C-F containing polymer at the bottom and the sidewalls of the features. Oxygen radicals added to the etching gas or released during SiO<sub>2</sub> etching remove the polymer or decrease its film thickness. These competing reactions make sure the polymer does not become too thick. The sidewall polymer protects the dielectric from being removed by the etching gas and ensures an anisotropic etching process. At the feature bottom the polymer is loosened by ion bombardment so the reactive species of the etching gas can diffuse through this layer and react with the dielectric. A bottom polymer thickness less than 1 nm enables the ions to bombard the underlying surface, break up bonds, increase temperature and finally increase the transport rate of reactive species through the polymer film [38].

Etch profiles, etch rates, selectivities and polymer deposition can be influenced by additives to the etching gas, e.g. Ar, H<sub>2</sub>, N<sub>2</sub>, O<sub>2</sub>, C<sub>4</sub>F<sub>8</sub>. Ion bombardment has no or only a small influence on the sidewall polymer, keeping the layer intact to protect the dielectric from being etched. Due to UV radiation occurring during plasma etching the polymer is crosslinking and forms a dense, chemically inert film. Recent developments lead to the application of more carbon rich etching gasses like cyclic C<sub>4</sub>F<sub>8</sub>, C<sub>4</sub>F<sub>6</sub> or C<sub>3</sub>F<sub>6</sub> [39]. By reducing the fluorine content the etch rate of the dielectric decreases due to the fact that fluorine is the main component to form volatile SiF<sub>4</sub> and the polymer deposition rate increases.

During etching low-k dielectrics containing organic species like  $\text{CH}_3$  additional reaction products like  $\text{CO}$ ,  $\text{CO}_2$ ,  $\text{H}_2\text{O}$  and  $\text{H}_2$  are formed. Methyl containing dielectrics lead to an increased polymer deposition rate due to the fact that they contain less oxygen. For porous dielectrics the etch rates are much higher than for dense material, but stabilizes during the process due to the formation of polymer at the pore walls [40]. The etching process strongly depends on the composition of the dielectric and every variation of the process parameters affects the surface condition of the dielectric. This will especially be important for cleaning processes following the patterning, which have to remove the polymeric residue from feature bottom and sidewalls. In the following chapter common and new processes for plasma etch residue removal will be summarized.

## **2.5. Etch residue composition and cleaning strategies**

### **2.5.1. Composition and impact of plasma etch residues**

Polymeric residues mainly consist of  $\text{CF}$  species in different bonding configurations depending on the etch chemistry used for patterning. Additionally inorganic species like  $\text{Si}$  from the etched dielectric and resputtered  $\text{Cu}$  can be incorporated. If the copper surface is exposed to the reactive species of the etching gas  $\text{CuF}_2$  and  $\text{CuF}$  can form on the copper surface [41-43]. The composition of the residue strongly depends on the process conditions, which makes it difficult to find a universal cleaning strategy. The removal of the residues from bottom and sidewalls of the features is necessary for different reasons:

- Residues at the bottom will increase contact resistivity when contacting the underlying metallization level [44-46].

- With decreasing feature sizes even 3-4 nm thin polymeric residues at the sidewalls cannot be tolerated to keep the critical dimensions.
- Due to their low surface energy the residues can affect the adhesion of subsequent barrier layers [47].
- Copper within the residue may be able to diffuse into the dielectric leading to a degradation of its electrical parameters [48].

Plasma etch residues can be removed by dry plasma processes and by wet cleaning. Due to the fact that inorganic species like copper or silicon do not form volatile reaction products using commonly applied oxidizing or reducing plasmas they cannot be removed by dry processing [38]. A dry cleaning process has always to be followed up by a wet chemical cleaning.

### **2.5.2. Residue removal by plasma cleaning and it's impact on low-k materials**

Low-k dielectrics containing organic species like  $\text{CH}_3$  are known to be altered by plasma processes like cleaning or stripping. This is especially true for porous dielectrics, where the damaged region can reach far into the bulk material. Plasma damage is caused by different mechanisms: ion bombardment, reactive radicals and UV radiation (49, 50). The effects of plasma damage include carbon depletion, densification of the surface near area and hydrophilization of the low-k material's surface. The loss of carbon is due to the destruction of Si-C bonds, which can be caused by high energetic UV radiation and reactive radicals within the plasma [52, 53].

A destruction of chemical bonds in the surface near area of the dielectric can also be caused by ion bombardment, leaving behind dangling Si-bonds, which are easily



saturated by  $\text{-OH}$  groups. All these effects lead to a degradation of the electrical parameters of the low-k material:

- Carbon loss means a decrease in low polarizable bonds and causes an increase of the k-value
- The formation of dangling bonds and their saturation by  $\text{-OH}$  leads to a conversion of the formerly hydrophobic to a hydrophilic character of the dielectric's surface. In the case of porous low-k materials this also occurs at the pore walls inside the dielectric. Hydrophilization leads to moisture uptake, which increases the k-value and leakage current of the material.

Oxidizing plasma chemistries are able to effectively remove  $\text{CF}_x$  species from feature bottom and sidewall. Their ability to especially remove carbon species turned out to be the biggest disadvantage when applied to carbon enriched low-k dielectrics. Recent developments therefore focused on alternative plasma cleaning processes using reducing chemistries to avoid a degradation of the dielectric. The following sections will go more into detail on this topic.

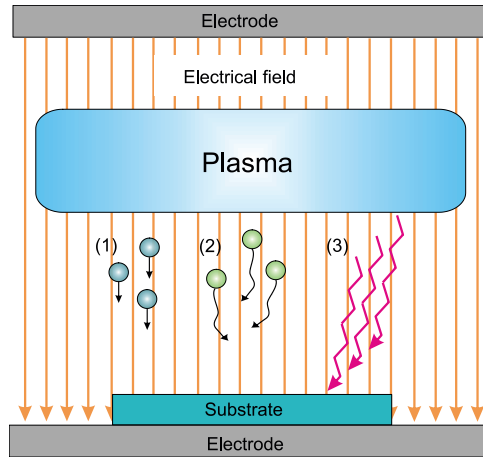


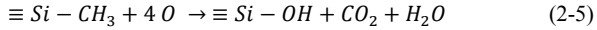
**Figure 2-10:** Low-k damaging species occurring during plasma processing. (1): ion bombardment, (2) reactive radicals, (3) UV radiation

#### 2.5.2.1. Oxidizing plasmas

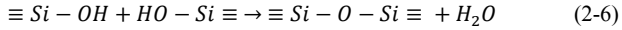
Oxygen based plasma processes are able to completely remove  $\text{CF}_x$  species from bottom and sidewalls of the structure, but  $\text{CuF}_x$  at Cu is not affected. The oxygen plasma is very effective in removing carbon by forming volatile CO and  $\text{CO}_2$ , but has the disadvantage to form copper oxide on copper at the feature bottom [49]. Another, but most crucial drawback is the removal of carbon from dielectrics containing organic species. This effect is known as plasma damage and will be discussed later.

Oxidizing plasmas have been shown to convert the surface near area of a SiCOH dielectric into a hydrophilic  $\text{SiO}_2$ -like material. Porous dielectrics can be altered by oxygen species deep into the bulk of the material because the reactive species are able to diffuse into the porous structure. Oxygen is reacting with the methyl groups

bonded to the Si-O-Si network, the Si-C bond is broken and unsaturated bonding places are formed. Those dangling bonds are in many cases saturated by –OH from surrounding atmosphere. One possible reaction mechanism is shown in equation (2-5) [50, 54-58]:



The highly polar Si-OH species can induce moisture absorption or react to form Si-O-Si compounds (equation 2-6):



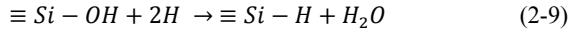
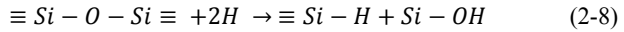
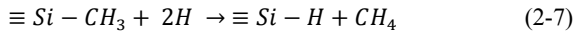
In any case the carbon incorporated into the dielectric to reduce polarizability is removed. The depth of this carbon depleted area is influenced by the plasma process conditions. It increases with the concentration of reactive species and with substrate temperature. Due to the damage effect of oxidizing plasma processes on low-k dielectrics, alternative less damaging processes are in the focus of research and development activities.

#### 2.5.2.2. *Reducing plasmas*

Reducing plasmas, especially hydrogen based plasma chemistries, have gained a lot of interest in the recent years due to reduced damage effects on low-k dielectrics.  $CF_x$  species can be removed effectively by hydrogen plasmas, but fluorine is more easily removed than carbon because the formation of HF is energetically more favored than  $CH_4$  as reaction product. An about 1 nm thin carbon rich layer can remain at the feature sidewalls and has to be removed by an additional cleaning

step. Reducing plasmas are able to remove copper oxide from the feature bottom by forming Cu and H<sub>2</sub>O as reaction products, but cannot remove resputtered copper incorporated into the sidewall residue [50, 51].

Plasma processes using reducing chemistries are widely studied and are one candidate to replace damaging oxygen plasma processes. Especially hydrogen plasmas have been analyzed. It was found that atomic hydrogen in a plasma can also lead to the formation of polar Si-OH and Si-H bonds. Possible reactions can be seen in equations 2-7 – 2-9, where reaction 2-7 and 2-9 are the most probable ones [50, 54, 59, 60].



The film damage was found to be strongly influenced by the substrate temperature and the density of hydrogen species in the plasma: higher substrate temperatures minimized the damage while higher densities increased the damaging effects. Film porosity, actually in the range of 15-30%, also turned out to be an important factor: dielectrics with low porosity only showed carbon depletion on the very top layers while highly porous materials have been damaged down to the bulk. The hydrogen plasma processes have been modified by adding e.g. He or Ar to further increase resist removal rates [61-64]. Although the damage is much smaller than for oxidizing plasmas, at least the very top layers have been modified in any case. Addition of N<sub>2</sub> to the hydrogen plasma leads to the formation of Si-NH<sub>2</sub> and Si-O bonds and supports moisture uptake [54, 65]. The analyzes showed that a completely nondamaging plasma cleaning process has not been found yet. That is why wet chemical removal of plasma etch residues is a promising alternative to

plasma processes. Integration of porous low-k dielectrics and further decrease of feature dimensions at 32 nm technology node and below turns out to be a big challenge for the development of appropriate cleaning processes. In the following section common cleaning processes and new strategies for plasma etch residue removal will be described.

### **2.5.3. Removal of plasma etch residues by wet chemical processes**

With the introduction of copper and low-k materials within the interconnect system, wet cleaning processes for etch residue removal have become challenging. Common wet processes in Aluminum technology using HDA solutions to dissolve etch polymers had to be replaced due to their incompatibility to copper, (corrosion) [66-68]. If low-k dielectrics, especially porous materials, are exposed to the solutions, contaminants can be trapped in the porous structure leading to material degradation and reliability issues. To increase throughput in production, single wafer processes have been introduced with process times of approximately 1 minute per wafer. Remover formulations therefore have to be more aggressive toward the residues to be effective. Cleaning solutions based on organic solvents are more and more replaced by water based cleaners. Those solutions are less toxic and inflammable, disposal costs are reduced and they are more environmentally friendly [66]. With decreasing feature dimensions the turn to water based solutions has raised suppositions about the ability of the liquid to remain effective due to wetting issues and limitations of mass transport, This section describes common processes for PERR with a focus on new developments to meet the requirements of future technology nodes.

#### 2.5.3.1. *RCA cleaning process*

The most common wet cleaning process for silicon wafers in IC industry is the RCA clean [69]. This process consists of SC1 and SC2 and is able to remove both polymers and metallic contaminations. SC1 is a water based mixture of ammonium hydroxide and hydrogen peroxide at approximately 60°C bath temperature. This process is strongly oxidative and removes organic species. SC2 uses a mixture of hydrochloric acid and hydrogen peroxide in water at 60°C. It removes metallic and other ionic contaminations. There have been several investigations to find alternative wet plasma etch residue removers, including nitric, hydrofluoric, sulfuric and chromic acids. The cleaning mechanism is the same as for standard RCA: the residue is undercut and lifted off the dielectric. It was found that most of these processes are too aggressive, especially looking at porous dielectrics, copper at the feature bottom and low tolerance in changing critical dimensions, so new wet cleaning strategies have emerged [66].

#### 2.5.3.2. *Solvent based and semi aqueous fluoride solutions*

This most common type of residue remover in copper damascene technology contains a small amount ( $< 2\%$ ) of HF or  $\text{NH}_4\text{F}$  and up to 30% water mixed in an organic solvent. Fluorine is the chemical reactive species, which etches the underlying  $\text{SiO}_2$ -like layer and lifts off the residue. With the turn to water based solutions fluorine containing cleaners have also been modified and the amount of organic solvents has been reduced, resulting in the development of solutions with more than 80 % water [66].

#### 2.5.3.3. *Solvent – Hydroxylamine solutions*

HDA solutions have been the standard in Al technology, but they are much too aggressive for copper interconnects. There has been a large amount of copper loss and these kinds of cleaners were thought to demise. But it has been possible to mitigate the corrosive behavior of HDA on copper. The formulations have been turned to be compatible to Copper/low-k technology [66].

#### 2.5.3.4. *Advanced aqueous chemistries*

Those solutions are the most challenging ones for development due to the fact that neither photoresist or polymeric residues are water soluble. To mitigate evaporation and increase bath life the operation temperatures should be kept in the range of room temperature. There has to be found a balance between aggressiveness to the residues and benign behavior towards copper and low-k dielectrics. The chemical active compound in these solutions can be fluorine, but there are several new developments, which do not contain fluorine anymore [66].

#### 2.5.3.5. *Radical anion chemistry*

This residue removal strategy is based on reductive naphthalene radical anion chemistry. The solutions are fabricated by electrolysis using platinum electrodes in an electrochemical cell. Radical anions are generated from a reaction of metallic sodium and naphthalene in an appropriate solvent. The solutions causes defluorination of the residue surface, a swelling and finally lift off of the residue [38, 70]. These solutions have passed first compatibility tests to copper and low-k materials, but are still in an experimental state. It is unsure if the use of sodium will

finally be compatible. Additionally an incomplete removal of the swollen residues has been reported, which is caused by the pinning of the polymer on feature edges.

#### 2.5.3.6. *Other oxidizing chemistries*

Mixtures of DIW and ozone have been under investigation. They are especially interesting due to their high removal rates, but have been found to be not compatible to dielectrics which contain organic species. Dilute sulfuric acid mixed with hydrogen peroxide or ammonium hydroxide mixed with hydrogen peroxide has been considered as residue removing solutions. The residue is broken into smaller fragments by those liquids by oxidation, which have to be removed by a subsequent DIW rinse. Besides these processes are not compatible to organic low-k dielectrics, they need a huge amount of DIW and toxic species, which stands in contrast to recent strategies in research and development [38].

#### 2.5.3.7. *Supercritical CO<sub>2</sub> cleaning*

Supercritical fluids, especially supercritical CO<sub>2</sub> (SCCO<sub>2</sub>), are in the focus of research and development due to their environmentally friendly behavior and low surface energy. They are produced by applying pressure and temperature beyond the critical point of CO<sub>2</sub> at 31°C and 1100 psi [71]. Besides the relative cost extensive equipment needed to fabricate the supercritical fluids, its low solvating power is one disadvantage. Nevertheless they are a promising alternative to high surface energy liquids, which can cause pore and pattern collapse or may not be able to penetrate in small features. Additives like co-solvents have to be used to increase solubility, but the effect of them to the cleaning chemistry is not fully understood till now. Additionally the processes using supercritical fluids are not



well standardized to be used in conventional cleaning equipment and do not meet the process time requirements needed for single wafer processing [38].

#### **2.5.4. New challenges in wet chemical PERR in 32/22 nm technology**

Wet cleaning solutions are facing difficult challenges getting applied in 32 and 22 nm technology. Of course they have to meet compatibility requirements to the materials used within the interconnect system and have to be able to remove organic and inorganic residue species without influencing critical dimensions or any other material parameters. With decreasing feature sizes especially the wetting behavior of wet chemical PERR solutions gets into the focus of interest. Most obviously difficult is the wetting of CF-containing polymeric residue surfaces, which own a very low surface energy. This effect is in clear contrast to the efforts to use cleaning solutions mainly based on water. Those solutions are known to have high surface energies and will show a poor wetting behavior on polymeric residues. Additional effects caused by shrinking feature geometries have to be faced.

Especially via structures are critical due to the fact that a high energetic cleaning solution may not be able to enter the feature and no cleaning will occur. This becomes even more difficult if the sidewalls of the via hole are covered by a low-energy polymer. But even if the liquid is able to penetrate into the structure, the cleaning process can suffer from low mass transport rates [72]. In combination with small feature sizes, high aspect ratios and high surface energy cleaning solutions the weak mechanical properties of porous low-k dielectrics can result in pattern collapse during drying after wet cleaning. This effect is well known from high aspect ratio photoresist features in lithography [73].

High capillary forces not only lead to the destruction of trench structures by sticking, but can cause a collapse of the porous network of the dielectric. All those effects are directly connected to the wetting behavior of solid and liquid media and can be described and declared by analyzing the surface energies of both phases. The following chapter will go more into detail on wetting, surface energies and describes the origins of capillarity effects, which may occur using wet cleaning in future technology nodes.



### **3. Wetting and surface energies in wet cleaning processes**

As described in the previous section the wetting behavior of a wet cleaning solution becomes more and more important as feature dimensions are further decreasing. Development of wet cleaning liquids for future technology nodes has therefore not only to consider chemical and compatibility issues, but has to design solutions with optimized wetting properties. Low energetic surfaces and the trend to use water based cleaners are additionally complicating this intention. The key to understanding whether or not a solid surface is wetted by a liquid is the knowledge about the interaction of surface energies of both media and how those energetic characteristics can be influenced. For the liquid phase usually the notation “surface tension” and for the solid “surface energy” is applied, but it has been shown that both physical values are almost equivalent [74-76]. Therefore the term “surface energy” will be used for both media in this work. This chapter describes the main basics of wetting, contact angles and surface energies. The methods of experimental determination of surface energies will be introduced in chapter 5.

#### **3.1. General introduction**

Wetting is important in many processes, both natural and industrial. It is essential looking at any kind of coating processes, e.g. using paint or ink, in pharmacy, personal care, etc. But also in semiconductor industry one can find process steps depending on good wetting, e.g. spin coating, wet etching and of course all wet cleaning applications. An evaluation of wetting for this kind of processes always has to consider equilibrium and dynamic aspects of wetting. Equilibrium effects of wetting are described best by thermodynamics. A drop of a liquid put on a solid surface forms a contact angle  $\theta$  at the wetting perimeter / wetting line (see Figure

3-1) and an equilibrium of the 3 involved phases vapor, liquid and solid is established [77].

The measurement of the contact angle therefore is a method to determine the static wetting behavior of a system liquid/solid. The smaller the contact angle, the better is the wetting.

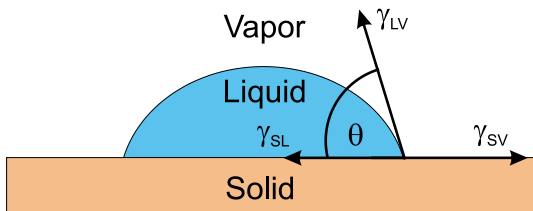


**Figure 3-1:** A liquid drop on a solid substrate forming the contact angle  $\theta$  at the contact point of the phases solid / liquid / vapor. At a thermodynamic equilibrium the interfacial energies can be described by Young's equation.

Dynamic effects are often described in terms of a moving wetting line. This results in changing contact angles depending on the wetting velocity. A full description of the kinetics of dynamic wetting processes has been achieved till now. One applicable concept is that described by Havkens, who introduced a spreading coefficient [78]. This is a measure of the work done in destroying a unit area of the surface of solid/liquid and liquid/vapor to form an area of solid/vapor surface and is determined using the contact angle and the surface energy of the liquid/vapor system  $\gamma_{LV}$ . The spreading coefficient  $S$  is especially important for processes which need a spontaneous wetting, for which  $S$  is zero or positive. Negative  $S$  means a limited spreading.

Also adhesion can be described by the energy characteristics of e.g. a substrate and the adhesive. Understanding adhesion is very important in many industrial applications, e.g. medical applications or for any kind of adhesives. To describe adhesion on a fundamental level different concepts have been created and include interfacial concepts looking at intermolecular forces and chemical bonds.

### **3.2. The contact angle**

The contact angle is a very useful value to describe the wetting ability of a liquid on a solid surface. A drop put on a solid will either spread and form a thin film or remain on it as a discrete drop. Angle  $\theta$  is formed between the planes tangent to the solid and liquid surfaces at the 3-phase wetting line. For complete wetting the contact angle becomes zero, contact angles of  $90^\circ$  and higher mean that there is no wetting and the drop will roll off the solid surface if this is tilted. Mostly the contact angle is accompanied by hysteresis due to the movement of the wetting line [77]. Those advancing angles  $\theta_A$  and receding angles  $\theta_R$  strongly depend on the prior processing of the surface, which e.g. could have led to a certain roughness of the surface. The advancing contact angle is always bigger than the receding contact angle and the static contact angle value can take any value between those limits (Figure 3-2). This topic will be described more in detail later.

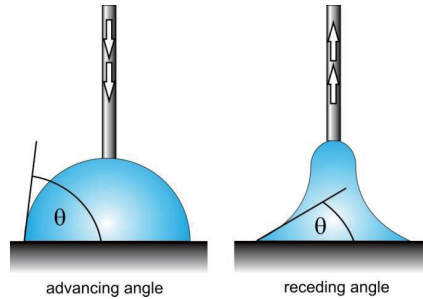


**Figure 3-2:** Advancing and receding contact angles. Depending on the direction the wetting line of the liquid moves different contact angles can be measured resulting e.g. from roughness of the solid surface.

### 3.2.1. Thermodynamics – Young's equation

A drop on a solid will take the shape that minimizes the free energy of the whole system. In equilibrium three interfaces are formed, each with a certain free energy per unit area  $\gamma_{SL}$ ,  $\gamma_{SV}$  and  $\gamma_{LV}$  (see Figure 3-1). The sum of all three energies should be a minimum at equilibrium. This leads to Young's equation:

$$\gamma_{SV} = \gamma_{SL} + \gamma_{LV} \cdot \cos \theta \quad (3-1)$$

The contact angle results from the balance between cohesive force within the liquid and the adhesive force between solid and liquid [77]:

$$\cos \theta = \frac{\gamma_{SV} - \gamma_{SL}}{\gamma_{LV}} \quad (3-2)$$

### 3.2.2. Contact angle hysteresis

#### 3.2.2.1. *Influence of surface roughness*

The ideal case of a liquid wetting a solid is when the solid is uniform and nondeformable. In this case only one contact angle appears. For real surfaces a hysteresis of the contact angle can be measured, resulting in two angles: the advancing  $\theta_A$  and the receding angle  $\theta_R$ . Reasons for contact angle hysteresis can be the penetration of the liquid into pores or surface roughness [79]. On a rough surface the front and rear side of the drop form the same angle, where they meet the solid surface (intrinsic angle  $\theta_0$ ), but the macroscopic contact angles  $\theta_A$  and  $\theta_R$  differ clearly. The influence of roughness on the contact angle was described by Wenzel, who considered the true area  $A$  of a rough surface (including all topographical phenomena) and of a projected area  $A'$  (macroscopic visible area). Wenzel defined a roughness factor  $r$ :

$$r = \frac{A}{A'} \quad (3-3)$$

which is  $> 1$  and becomes larger with increasing surface roughness.

The macroscopic contact angle is related to the intrinsic angle by the roughness factor  $r$ :

$$\cos \theta = r \cdot \cos \theta_0 \quad (3-4)$$

In combination for Young's equation one gets:



$$\cos \theta = r \cdot \left( \frac{\gamma_{SV} - \gamma_{SL}}{\gamma_{LV}} \right) \quad (3-5)$$

Two cases can be distinguished regarding the influence of roughness on the contact angle:

- 1)  $\cos \theta < 0$  ( $\theta > 90^\circ$ ) on a smooth surface: if the surface is roughened  $\cos \theta$  becomes even more negative and  $\theta$  increases. In this case surface roughness reduces wetting.
- 2)  $\cos \theta \geq 0$  ( $\theta \leq 90^\circ$ ) on a smooth surface:  $\cos \theta$  becomes more positive if roughness is introduced and  $\theta$  decreases. This means that roughness supports wetting.

#### 3.2.2.2. *Heterogeneity of the surface*

Most of the real surfaces consist of areas owning different wetting behavior. The wetting line of a drop put onto a heterogeneous surface mostly stops at the boundary of the different islands and an advancing and receding contact angle is formed. The high contact angle region is associated to the advancing and the low contact angle region to the receding angle. For heterogeneity much smaller than the liquid drop a composite angle can be defined. Cassie defined this angle as a measure of the area fractions of the regions with different wetting behavior  $Q_1$  and  $Q_2$  [79]:

$$\cos \theta = Q_1 \cdot \cos \theta_1 + Q_2 \cdot \cos \theta_2 \quad (3-6)$$

where  $\theta_1$  is the maximum and  $\theta_2$  is the minimum contact angle.

The higher the roughness or heterogeneity of the surface, the less contact angle measurements can be correlated to the chemical condition of the surface. Anyway, the calculation of the energy of such kind of surfaces is not worthless. Using the model of Owens, Wendt, Rabel and Kaelble [80] the energy value still describes the behavior of liquids to this surface. It should be kept in mind that this goes beyond the limits of this model and the measured values are only empirical [75].

### 3.3. The role of surface energies in wetting

#### 3.3.1. The origin of surface energies

For the liquid the origin of the surface energy can be described easily: the tension at the surface of a liquid results from different energetic condition of molecules within the phase and such directly located at the surface. The molecule at the surface has less contact to others than a molecule within the liquid (Figure 3-3). Due to this it cannot elaborate as much interaction as bulk molecules and this status is energetically unfavorable [81].

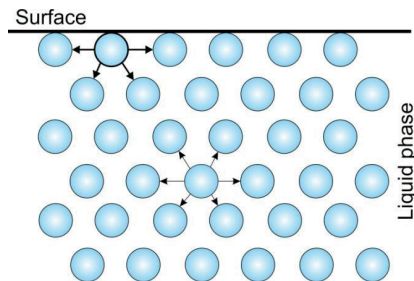


**Figure 3-3:** The origin of the surface energy of a liquid; Within the liquid all molecular forces can be compensated, but at the surface the energetic situation of the molecule is less favorable; due to this the system tries to keep the surface as small as possible to reduce its energy.

That is why the liquid tends to minimize its surface area and thereby tries to minimize the surface energy. If the surface area shall become larger, molecules have to be brought from an energetically favorable position within the liquid to this less favorable one at the surface. The

energy necessary to achieve this can be comprehended as the surface energy. For solids the principle of surface energy is the same as for liquids, but it is hardly possible to directly determine the energy necessary to enlarge the surface area. This due to the fact this energy is difficult to discriminate from deformation energies within the bulk. The surface energy of the solid can only be measured indirectly by determination of contact angles.

The value of the contact angle depends on the molecular interaction possible between solid and liquid. The higher the interaction at the phase boundary, the lower is the interfacial energy. If there is no interaction the contact angle  $\theta$  becomes  $180^\circ$  and Young's equation changes to:

$$\gamma_{SL} = \gamma_{SV} + \gamma_{LV}$$

For strong interaction the contact angle becomes zero and the liquid spreads spontaneously on the surface solid surface. In this case Young's equation changes to:

$$\gamma_{LV} = \gamma_{SV} - \gamma_{SL}$$

Young's equation provides a precise thermodynamic definition of the contact angle. Fowkes and Owens et al. extended the interpretation of the molecular interactions occurring between the liquid and the solid phase [75, 80]. They considered two different types of interactions, which add to the total value: a polar

and a dispersive type. This also results in a polar and dispersive part of the total surface energy of liquid and solid. Dispersive forces are present in all materials and result from van der Waals forces. The polar energy contribution is due to induced or permanent dipoles or hydrogen bonds. A prominent example for high polarity is water due to its dipole character, which also results in a high surface energy of around 72 mN/m.

To achieve a good wetting it must be energetically favorable for the whole system to replace the vapor/solid interface by a liquid/solid interface. This means that a reduction of the total surface energy must be achieved by forming the new interface. This is only possible if the liquid's surface energy is comparable or lower than that of the solid surface. The distinction between polar and dispersive energy contribution introduces an additional requirement for low contact angles. Due to the fact that only interactions between similar energy types are possible (polar/polar and dispersive/dispersive), solid and liquid must have a comparable energetic character regarding polar and dispersive energy contributions. A prominent example where no comparable energetic characteristics occur is the wetting behavior of water on a PTFE surface. PTFE has a very low surface energy of around 20 mN/m with almost no polar energy contribution. In contrast to this water is high energetic and has a strong polar energy part. Contact angles higher than  $100^\circ$  are formed by this system, which means that there is no wetting. The difference in total surface energy between both media is too big and the formation of a solid/liquid interface is not favorable. Due to this the contact area between water and PTFE is minimized, which results in a very high contact angle. Additionally the difference in dispersive/polar character between both materials is very high, so the polar energy part of water cannot interact with the PTFE because this does not own a polar energy contribution itself. Both factors lead to the nonwetting of PTFE by water.

### 3.3.2. Model considerations concerning surface energies

Surface energy values of a solid determined by contact angle measurement are the result of an interpretation of their behavior within the model used for the calculation, but not a fixed physical value of the analyzed surface. They strongly depend on measurement conditions like humidity and temperature and should only be understood as an approximation of the surface condition in the moment of measurement.

The models used for surface energy determination of a solid by contact angle measurement have developed from rough estimations starting with the work of Dupré in the 19<sup>th</sup> century [82] to more and more complex and accurate procedures considering polarity or the acid-base-model of Lewis. This section will give a brief introduction to the development of the models. A more detailed description can be found in chapter 5. The surface energy of a liquid can be measured directly by methods like pendant drop, ring or plate method (the experimental procedure is described in chapter 5). On the contrary the energy value of a solid surface can only be determined in an indirect way by measuring contact angles of test liquids on it.

The work of cohesion  $W_{ii}$  within a homogeneous liquid was described by Dupré as the work done by separating the medium forming 2 new surfaces  $2A$ . From the surface energy  $\sigma$   $W_{ii}$  can be calculated:

$$W_{ii} = 2 \cdot \sigma \quad (3-9)$$

If two different media are separated, the two newly formed surfaces have the energies  $\sigma_i$  and  $\sigma_j$ , and the formerly existing interfacial energy  $\gamma_{ij}$  disappears. The work of adhesion can therefore be described as:

$$W_{ij} = \sigma_i + \sigma_j - \gamma_{ij} \quad (3-10)$$

This interfacial energy was calculated by Antonow [83] from the difference of the surface energies of the two different media  $\sigma_1$  and  $\sigma_2$ :

$$\gamma_{12} = |\sigma_1 - \sigma_2| \quad (3-11)$$

The method of Antonow later has been shown to be an approximation, which is not accurate enough.

Further development of the calculation models has been done by Good and Girifalco [75], who described the work of cohesion to be dependent of the geometric mean of the energies which interact between the particles of the two phases:

$$W_{12} = 2 \cdot \Phi \cdot \sqrt{\sigma_1 \cdot \sigma_2} \quad (3-12)$$

The combination of equation 3-10 and 3-12 finally lead to:

$$\gamma_{12} = \sigma_1 + \sigma_2 - 2 \cdot \Phi \cdot \sqrt{\sigma_1 \cdot \sigma_2} \quad (3-13)$$

where  $\Phi$  is a parameter depending on molecular quantities, which cannot be determined empirically.

Today surface energy calculations of solids are done using known surface energy values of test liquids. Fowkes was the first who applied this method [84]. He

assumed that only interactions of the same type can appear between the phases and assigned this to the parameter  $\Phi$ . This means that only interactions of the type polar/polar and dispersive/dispersive can occur.

$$\gamma_{12} = \sigma_1 + \sigma_2 - 2 \cdot \sqrt{\sigma_1^D \cdot \sigma_2^D} \quad (3-14)$$

Owens, Wendt, Rabel and Kaelble [80] extended the method of Fowkes to polar energy contributions, assuming that polar and dispersive energy parts add to the total surface energy:

$$\sigma = \sigma^D + \sigma^P \quad (3-15)$$

which lead to the following equation:

$$\gamma_{12} = \sigma_1 + \sigma_2 - 2 \cdot \left( \sqrt{\sigma_1^D \cdot \sigma_2^D} + \sqrt{\sigma_1^P \cdot \sigma_2^P} \right) \quad (3-16)$$

Further development lead to the extended Fowkes method, which additionally includes interactions caused by hydrogen bonds [85]:

$$\sigma = \sigma^D + \sigma^P + \sigma^H \quad (3-17)$$

Equation 3-16 is thereby extended by an additional square root term:

$$\gamma_{12} = \sigma_1 + \sigma_2 - 2 \cdot \left( \sqrt{\sigma_1^D \cdot \sigma_2^D} + \sqrt{\sigma_1^P \cdot \sigma_2^P} + \sqrt{\sigma_1^H \cdot \sigma_2^H} \right) \quad (3-18)$$

Oss and Good made another approach considering the acid-base model of Lewis to describe the polar energy contribution [86]. The acid part  $\sigma^+$  and the base part  $\sigma^-$  add to the polar fraction:

$$\gamma_{12} = \sigma_S + \sigma_L - 2 \cdot \left( \sqrt{\sigma_S^D \cdot \sigma_L^D} + \sqrt{\sigma_S^+ \cdot \sigma_L^-} + \sqrt{\sigma_S^- \cdot \sigma_L^+} \right) \quad (3-19)$$

The model of Wu is an alternative to Oss and Good for low energy surfaces  $< 35$  mN/m [87]. This method makes use of the harmonic mean for dispersive and polar energy parts, which does not work for high energetic surfaces:

$$\gamma_{12} = \sigma_1 + \sigma_2 - 4 \cdot \left( \frac{\sigma_1^D \cdot \sigma_2^D}{\sigma_1^D + \sigma_2^D} + \frac{\sigma_1^P \cdot \sigma_2^P}{\sigma_1^P + \sigma_2^P} \right) \quad (3-20)$$

All described models can be used to calculate the interfacial energy of two phases, and with the help of contact angle measurements the energetic character a solid surface. The experimental application of the models is described in chapter 6.

### 3.4. Wetting concerns in wet chemical PERR for 32/22 nm technology

As features become smaller, effects like pattern and pore collapse or nonwetting of very small structures are complicating wet chemical PERR. Especially for structures beyond 100 nm those effects can cause feature destruction or prevent residue removal. In this section pattern collapse and nonwetting of sub-100 nm structures due to the surface energy of the cleaning liquid are discussed.



### 3.4.1. Pattern collapse of low-k dielectric features

Pattern collapse is well known for resist structures in photolithography. The features begin to topple over and can become deformed or stick together when a high energetic liquid is driven out during drying. This effect will not be restricted to resist patterns, but can also occur during wet cleaning of very small dielectric features as recently reported [108-110] (**Figure 3-4**). Especially porous materials are known to have low mechanical strength and can therefore easily be distorted or destroyed due to pattern collapse effects [73, 88, 89]. This will especially be critical for trench structures.

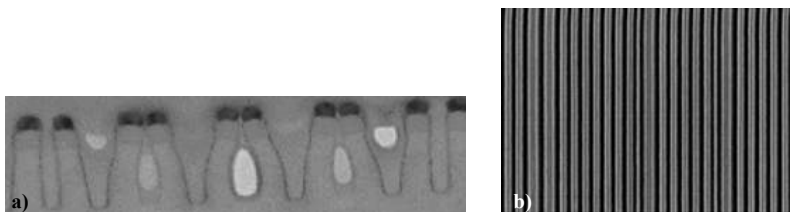


**Figure 3-4:** Collapse of ultra low-k dielectric trench structures after drying. This effect well known for photoresist patterns can also occur for porous dielectric features as shown by TSMC (Figure 3-4a) [108] and Hynix (Figure 3-4b) [110].

The contributors to pattern collapse are at least three forces: capillary forces acting on the structures, adhesion between the features and the underlying film and the mechanical properties of the structure material. In wet cleaning the capillary force will be the main driver of pattern collapse, so this section will focus on this. When the liquid remains between the trench walls, the largest force is acting on the features. If the liquid level is lower than the feature height, a meniscus is formed due to the surface energy of the liquid (**Figure 3-5**).

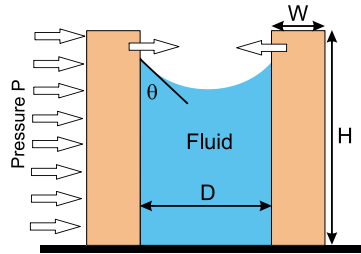


**Figure 3-5:** The forces acting on the sidewalls of a small trench filled with a liquid result from strong capillary forces directly depending on the surface energy of the liquid and can cause pattern collapse. [88, 89].

Stress is built up on the trench walls, which directly depends on the surface energy of the liquid (equation 3-21):

$$\sigma = \frac{6 \cdot \gamma \cdot \cos \theta}{D} \cdot \left(\frac{H}{W}\right)^2 \quad (3-21)$$

The force produced by the surface energy of the liquid can also be described by the pressure acting on the feature walls:

$$p = \frac{\gamma}{R} \quad (3-22)$$

where  $R$  is the radius of curvature of the liquid meniscus.

$$R = \frac{D}{2 \cdot \cos \theta} \quad (3-23)$$

with  $D$  describing the distance of the sidewalls.

Finally the pressure acting on a sidewall can be determined by

$$p = \frac{2 \cdot \gamma \cdot \cos \theta}{d} \quad (3-24)$$

In all cases a high surface energy of the cleaning liquid is responsible for larger stress or pressure on the sidewalls, which can lead to the destruction of the features (Figure 3-6).

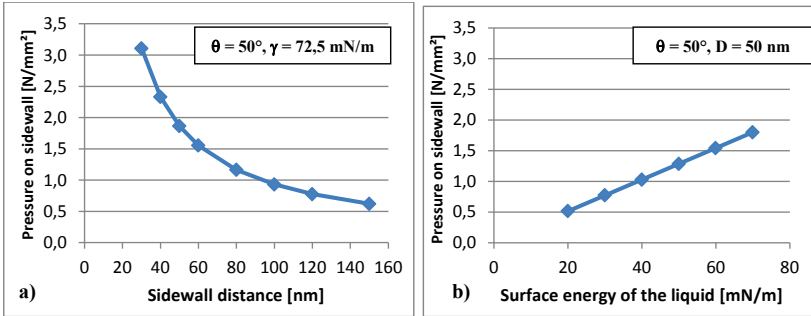


**Figure 3-6:** The pressure on a trench sidewall depending on the sidewall distance (a) and the surface energy of the liquid filling the trench (b). With decreasing feature sizes the pressure rapidly increases and can lead to a collapse of the structure; by decreasing the liquid's surface tension the pressure can be reduced.

### 3.4.2. Non-wetting of small structures

In the situation of a liquid penetrating into a structure, the liquid has to fully replace the gas within the feature [90, 91]. Considering a rough surface, pinning of the wetting line at edges can occur. This situation can be extended to also happen if the topography is not a surface roughness, but small high aspect ratio features. The

pinning of the wetting line then leads to an entrapment of air within the feature. For interconnect structures this effect is especially critical for vias. The formation of a gas cavity only occurs in structures of a certain depth. A critical aspect ratio can be calculated, above which the gas is entrapped (Figure 3-7).

The contact line of the liquid penetrating into the feature can be approximated by a straight line. For complete wetting this line gets in contact to the feature bottom before contacting the opposite sidewall. If the line contacts the opposite sidewall before the bottom, a gas cavity is formed.

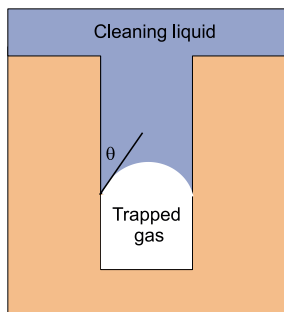


**Figure 3-7:** Nonwetting of small structures; a gas cavity can form in the structure and surfaces to be cleaned cannot be reached by the solution; this effect is critical especially for via structures

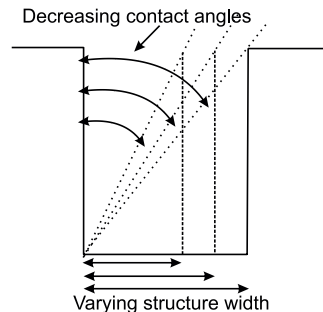


**Figure 3-8:** Model for a rough estimation of contact angles required for complete liquid filling of a small structure. For complete filling the wetting line has to reach the bottom before contacting the opposite sidewall [90]

In Figure 3-8 the borderline case is illustrated, where the wetting line is just able to contact the bottom and the critical aspect ratio defined for this case is equivalent to  $\cot \theta$ . Although this calculation is only a rough approximation, one can get an impression of the contact angles necessary to avoid gas entrapment when structures become smaller and the aspect ratio increases (Table 3-1). High aspect ratio

features can therefore only be wetted if the contact angle at the sidewall is small enough, which means that a decrease of the surface energy of the liquid is necessary.

**Table 3-1:** Calculated contact angles necessary to completely fill a small via structure. Although this is only a rough estimation, the values give a hint what to overcome in future technology nodes (note that the contact angle of a water based cleaning solution on a polymeric residue surface is about 60-70°)

Aspect ratio	Contact angle
1	45°
2	26°
3	18°
4	14°
5	11°

### 3.5. Strategies to optimize the wetting behavior

To avoid pattern collapse or nonwetting of small structures, the wetting behavior of the system solid/liquid has to be optimized. This can be done in different ways by modification of the solid or the liquid. To increase the wettability of a low-energy solid surface it can be treated with plasma processes or corona discharges to allow the formation of polar species on the surface. This method is applied to improve the wettability of PTFE surfaces [92], but looking at the sensible materials within the interconnect system this treatment may be too aggressive and damaging.

By decreasing the surface energy of the liquid, the wetting of low-energetic surfaces can be clearly improved. Surface energy decrease can be achieved by adjusting the solvent system of the cleaning solution. For instance mixing water

with a low energetic organic solvent will rapidly decrease the surface tension of the system (Figure 3-9). But this method would be in contrast to the efforts of IC industry to use wet cleaning solutions with low amounts of organic solvents. Another approach can be the application of surface active agents, so called surfactants, which also are able to decrease the surface energy of a liquid.

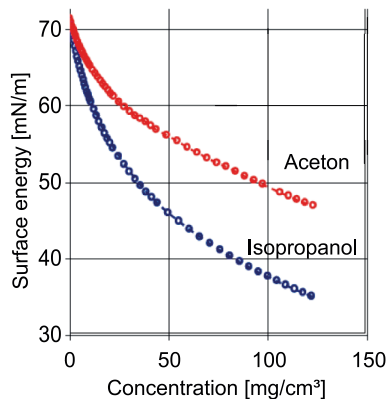


**Figure 3-9:** Reduction of the surface energy of water by adding organic solvents like acetone or Isopropanol. This approach of surface energy reduction stands in contrast to the trend in microelectronic production to use water based cleaning solutions. (Source: Imeter Ober- und Grenzflächenspannung, Beispiel Prüfbericht Isopropanol-Wasser, <http://www.unimeter.net/Download/OFS-GFS/IsopropanolWasser.pdf>)

In photolithography surfactants are already in use to reduce pattern collapse of resist structures [93], but there are only few studies dealing with surfactant solutions applied on interconnect materials like porous low-k dielectrics or copper [94, 95]. The following chapter will give a general introduction on the effects of surfactants on the surface energy of a liquid.



## **4. Application of surfactants for liquid surface energy decrease**

### **4.1. General introduction**

Surfactants are low molecular compounds with an amphiphilic character. They consist of a hydrophilic or polar head group and a hydrophobic or nonpolar tail (Figure 4-1 a) [96-98].

Due to this composition surfactants are surface active in several solvents, especially in water. They adsorb on an interface in an aqueous media, no matter what kind of phase builds up the interface to the water. By adsorbing the surfactants form a monomolecular film at the interface, which can strongly influence the character of the whole system. Based on this many applications of surfactants have developed:

- Reduction of the interfacial energy between water and an adjacent phase.
- Change of the wetting properties between water and solid surfaces.
- Formation of electrical double layers at interfaces.

By exceeding a characteristic concentration, surfactants are aggregating to large molecular compounds called micelles (Figure 4-1 b and c). Between monomers and micelles a thermodynamic equilibrium is established. Within micelles the hydrophobic groups are aligned towards the center, away from the aqueous phase, and the hydrophilic groups are in contact to the polar phase. Micelles can have different sizes and appearances, which especially affect the rheological behavior of the solution. For very high concentrations strong steric, electrostatic and van-der-Waals interactions occur between the agglomerates. This results in the formation of a short-range and long-range order, which can lead to the appearance of liquid crystal phases (Figure 4-2).



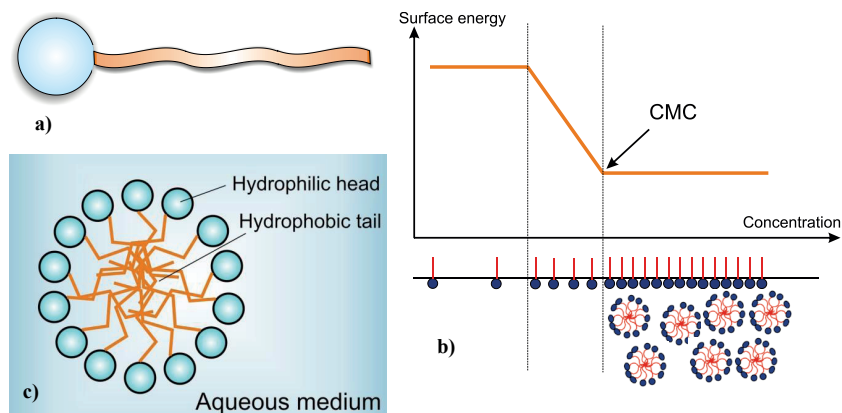


**Figure 4-1:** Basic construction of surfactant molecules and micelles. a) simple surfactant molecule consisting of hydrophilic head and hydrophobic tail. b) surfactants adsorb at the interface of a polar and nonpolar medium until all available places are captured. At this point described by the critical micelle concentration (cmc) the molecules form conglomerates within the polar phase [111]. c) Within those micelles the hydrophobic tails of the molecules are aligned towards the center and the hydrophilic groups are aligned towards the polar phase.

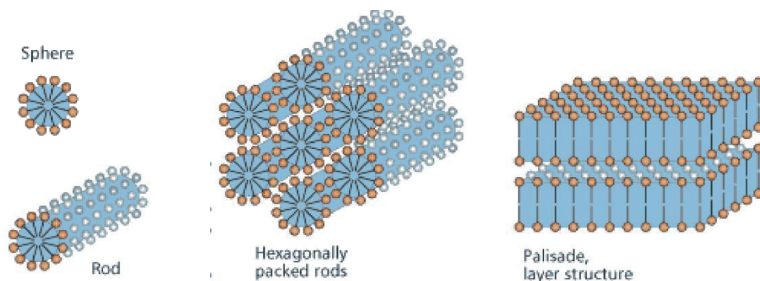


**Figure 4-2:** Micellar conglomerates are able to form a variety of 3-D structures. With increasing surfactant concentration the conglomerates become more complex from a simple sphere to rods, packed rods or layer structures [112].

## **4.2. Classification of surfactants by the hydrophilic group**

### **4.2.1. Ionic surfactants**

This type of surfactant's hydrophilic group is able to dissociate into ions in a polar solvent. An ionic group stays at the hydrophobic part of the molecule (surfactant ion) while the other ion, called counter ion, leaves the compound. The surfactant ion keeps the surfactant's characteristics. Counter ions can be of any kind reversely charged. Depending on the charge of the surfactant ion anionic and cationic surfactants can be distinguished.

### **4.2.2. Amphoteric surfactants**

In the contrary to ionic surfactants amphoteric surfactants contain a cation and an anion covalently bonded to each other, so they are not able to dissociate. Not necessarily the ions have to be directly connected to each other, but can contain spacer groups. In macroscopic view amphoteric surfactants are not charged, but charge can be built up by adding cations, especially protons, which bond to the anionic molecule part and thereby become cationic surfactants. The same can be done by adding hydroxyl ions which bond to the cationic part and form anionic surfactants. Examples for this class of surfactants are amino acid surfactants and betaines.

### **4.2.3. Nonionic surfactants**

The hydrophilic group of a nonionic surfactant is not able to dissociate into ions. Anyway the hydrophilic group has a polar character to ensure water solubility of the surfactant molecule. Those polar groups can be hydroxyl-, amino-, carboxyl-, ether- or amidic groups. By containing only one of those polar groups the water

**Table 4-1:** Surfactants classified by type of polar head group, typical examples and applications.

	<b>Anionic</b>	<b>Cationic</b>	<b>Nonionic</b>	<b>Amphoteric</b>
<b>Functional group</b>	R-SO <sub>3</sub> <sup>-</sup> sulfonates R-O-SO <sub>3</sub> <sup>-</sup> sulfates R-COO- carboxylates	R <sub>4</sub> N <sup>+</sup> quaternary ammonium compounds R <sub>4</sub> P <sup>+</sup> quaternary phosphonium compounds R <sub>3</sub> S <sup>+</sup> tertiary sulfonium compounds	R-O-(CH <sub>2</sub> -CH <sub>2</sub> -O)- H ethoxylates HO-(CH <sub>2</sub> -CH <sub>2</sub> -O)- H polyethylene glycols	R <sub>3</sub> N <sup>+</sup> -COO- Betaines and Ampholytes
<b>Typical examples</b>	Natrium dodecyl benzolsulfonate Coconut fatty alcohol polyglycoether carboxylates	N-cetyl-N-N-N-trimethyl ammonium umbromid (CTAB)	Polysorbates (Tween) Alkyl phenyl ethoxylates (Triton)	Coconut fatty acid amidopropyl betaines
<b>Application</b>	Universally applied in detergent, rinsing and cleaning solutions, shampoos, wetting agent, personal care products	Antistatic (softeners and conditioners), corrosion inhibitors, flotation agent	Universally applied as detergent, wetting agent, degreasing agents, emulsifiers, shampoos, personal care	Wetting agent, foaming agent, emulsifier, shampoos
<b>Industry</b>	Textile industry, metalworking industry, paper industry and Cosmetics	Textile industry, pharma industry	Textile industry, metalworking industry, food industry, paper industry, cosmetics	Cosmetics

solubility of the molecule is too low in most cases. To be surface active the molecule therefore has to contain more than one hydrophilic group. Typical surfactants of this type are polyglycolic ether surfactants, polyalcoholic surfactants and sorbitans. Table 4-1 shows typical fields of surfactant applications.

### **4.3. Classification of the surfactants by the hydrophobic group**

#### **4.3.1. Hydrocarbon surfactants**

The hydrophobic group of those surfactants is in general a hydrocarbon chain, which is connected to the hydrophilic group. Different structures are possible: n-alkyl, branched alkyl and aromatic alkyl surfactants. N-alkyl surfactants contain an unbranched alkylic group and the hydrophilic group is placed at the end of the chain. The alkylic group can contain 6 – 22 carbon atoms. In Gemini surfactants, which are branched molecules with two hydrophobic chains, the hydrophilic groups are situated more in the center of the molecule. Multichained surfactants can show very complex branched molecular structures.

#### **4.3.2. Perfluorinated surfactants**

Perfluorinated surfactants in principle have the same structure as common hydrocarbon surfactants with the difference that all hydrogen atoms are replaced by fluorine atoms. For practical application especially n-perfluoralkyl surfactants are important due to their temperature stability and compatibility to aggressive media. The main drawback of those surfactants is that they are not biodegradable. Unstable perfluorinated surfactants can be modified by adding CH<sub>2</sub>-spacer groups to increase stability. Perfluorinated surfactants can be ionic, amphoteric or nonionic.

#### 4.3.3. Silicon containing surfactants

The basic structure of those kinds of surfactants contains siloxanes  $-\text{Si}-\text{O}-$ , where hydrophobic methyl groups are bonded to the silicon atom. Monofunctional trimethylsiloxane groups  $(\text{CH}_3)_3\text{-Si-O}$  (signed M) are situated at the end of the siloxane chains, bifunctional dimethylsiloxanes (signed D) are the nonterminating chain groups. Hydrophilic groups (ionic, amphoteric or nonionic) are bonded directly or by  $\text{CH}_3$  spacer groups to the M or D groups. The shortest kinds of silicon containing surfactants have the structure M-D-M and do contain only one hydrophilic group. Besides this also polymeric Si-surfactants are applied, which have the structure  $\text{M-D}_x\text{-M}$ , with  $x > 3$ . They mostly contain more than one hydrophilic group to increase water solubility. Silicon containing surfactants are highly stable at increased temperature. Their biggest drawback is that they are sensible to hydrolysis and are very fast destroyed in aqueous media.

#### 4.3.4. Block-copolymers

Block-copolymeric surfactants are built up by molecular blocks with hydrophilic or hydrophobic character. Two types of block-copolymers, which are surface active, have been found. Tri-block-copolymers containing a central hydrophobic polyoxypropylen block (POP) with a hydrophilic polyoxyethylen block (POE) at each side and 2-alkyl-oxazilone based surfactants which depending on the length of the alkyl chain are built up by hydrophilic blocks A and by hydrophobic blocks B. Block-copolymers are nonionic surfactants, which can be solid, crystalline or liquid, depending on the content of hydrophobic blocks.

#### **4.4. Surfactants in aqueous media**

##### **4.4.1. Solubility of surfactants**

Water molecules have a strong dipole moment due to their bended structure, which means that water is highly polar and strong cohesive forces are acting between the molecules. Hydrogen bonds are additionally enhancing this character. All together this leads to the high surface energy of water of around 72 mN/m. To form a gap within water is therefore only possible by investing a lot of energy to overcome the cohesive forces. Nevertheless water is a very good solvent for other polar media, because the adhesion of polar molecules to water overcompensates the necessary energy.

The situation is different for nonpolar molecules, e.g. hydrocarbons. Energetic benefit is very low by adhesion of those molecules on water and energy necessary to form a gap cannot be compensated. Additionally water is highly regular structured at the phase boundary to hydrocarbons like to any other phases to where only weak interactions are possible. If a hydrocarbon is dispersed in water, the water molecules tend to reorganize to get an energy benefit and the hydrocarbon molecules are pushed away to form a hydrocarbon phase within the water. The solubility of surfactants in water depends on the length of the hydrophobic chain. For short chains only small gaps within the water have to be formed, while energy expense for long chain surfactants becomes very high. This means that with increasing chain length the solubility of the surfactant in water decreases.

For surfactant molecules solvated in water the situation is as follows: due to the strong adhesion of the water molecules connected with the energetically benefit a solvation of a short chain surfactant is possible. The hydrophobic part is forced into the polar phase and the hydrophilic part prohibits the formation of a hydrocarbon

phase within the water. But after all, the system contains a lot of high energetic interfaces between water molecules and the hydrocarbon surfactant chains. As a result the system tries to minimize the contact area of water to the hydrophobic surfactant part and to maximize the contact to the hydrophilic head groups. There are two ways to achieve this. The surfactant molecules get shifted to the phase boundary with their hydrophobic chain towards the surrounding nonpolar phase and the hydrophilic groups in contact to water. This effect is described as adsorption of surfactant molecules at a phase boundary. The surrounding phase can be air, but also any other kind of immiscible nonpolar liquid or solid phase.

Due to the contact of the polar headgroups to water, the adsorbed film is monomolecular. An equilibrium between adsorbed surfactants and water is built up and an increasing of the surfactant concentration results in an increased amount of molecules adsorbed at the phase boundary. At the saturation point the interface is fully occupied by surfactant molecules. The second way to minimize contact between water and hydrophobic chains is a reversible agglomeration of surfactant molecules within the water phase. The hydrophobic chains are aligned away from the polar phase, the hydrophilic parts align towards water. This effect is called micellation.

Micelle formation starts if a critical surfactant concentration is reached, the critical micelle concentration cmc. By diluting the solution the micelles dissolve. The surface activity of surfactants and their adsorption at a highly energetic interface, e.g. water/air, partly compensates the energetically unfavorable situation. Water molecules are in contact with polar surfactant parts and the nonpolar medium is in contact to the hydrophobic part of the surfactant. The aqueous phase is no longer forced to minimize its surface as much as before, which means that the surface energy decreases.

#### 4.4.2. Surface activity at liquid/vapor interface

The easiest case to describe the phases of concentration depending surface activity of an amphiphilic molecule is that of water insoluble surfactants. This section describes the way surfactants align and interact if their concentration is increased from step to step (Figure 4-3).

- 1) The spreading molecules have a large distance to each other. They lay on the liquid surface and show no interaction to each other [Figure 4-3a].
- 2) More molecules adsorb and they begin to interact with each other [Figure 4-3b].
- 3) The interface gets more and more occupied by the surfactant molecules. Most of them are still laying on the surface, but the first start to set upright and their hydrophobic chains stick out of the liquid towards the surrounding phase. Finally all hydrophobic chains stand upright, but the hydrophilic groups are statistically distributed at the surface [Figure 4-3c].
- 4) The hydrophobic chains stand upright and the hydrophilic groups have organized to form a two dimensional crystal like lattice. The space occupied by each surfactant molecule is equivalent to the cross section of the hydrophobic groups and the molecular film is incompressible [Figure 4-3d].
- 5) By further increasing the concentration of the surfactant at the interface the film collapses. The hydrophilic groups get partly lifted off the liquid, sliding onto the hydrophobic species remaining at the interface and a multilayered structure forms [Figure 4-3e].

In the case of water soluble surfactants the regime is mostly the same, but a film collapse is improbable. If the interface is completely occupied, the surplus



surfactant molecules move into the liquid. This means that for water soluble surfactants not only a surface concentration, but also a certain surfactant concentration within the liquid exists.

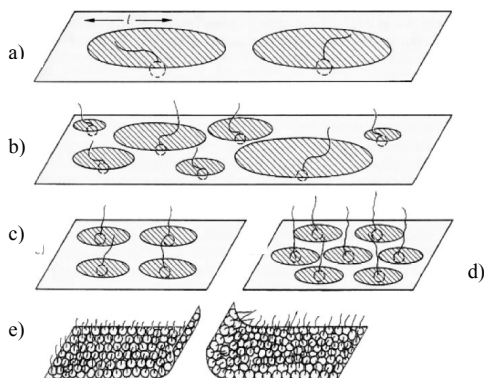


**Figure 4-3:** Surfactant molecules adsorbed at a polar / nonpolar interface. At low concentrations the molecules have a large distance to each other (a). With increasing concentration the molecules begin to interact (b) and a short range and long range order appears (c, d), until the film finally collapses (e) [98].

For surfactant application two values are important: the maximum decrease in surface energy and the quantitative surface activity of the species. The lowest reachable surface energy depends on the cohesive forces between the hydrophobic groups at the surface and is limited by the amount of surfactant molecules able to adsorb at the interface without going into film collapse. This means that the minimum surface energy is equal for surfactants which have the same type of hydrophobic chain. Hydrocarbon-based surfactants are able to decrease the surface energy of water to about 30 mN/m. The hydrophilic group has only a low influence on the lowest reachable surface energy, but nonionic surfactants were found to decrease the surface energy more than ionic species. The structure of the

hydrophobic chain strongly influences the surface energy value. Block-copolymers of the poly (oxyethylene) - poly (oxypropylene) - poly (oxyethylene) (POE-POP-POE) type can reach the same values as other hydrocarbon based surfactants, because the hydrophobic chains are comparable. Silicon containing and perfluorinated surfactants reach the lowest surface energies of 25 mN/m and 20-25 mN/m, respectively.

#### **4.4.3. Interfaces between liquids and solids**

Surfactant adsorption at solid surfaces in principle works like described for liquid/vapor, but can show some special issues. Solid surfaces normally are not homogeneous, but can have pores, edges or unsaturated bonding states. Additionally solid surfaces can be charged, which strongly influences the adsorption behavior of a surfactant. This means that the hydrophobic effect may be not the only reason for a surfactant molecule to adsorb at the interface. At hydrophobic surfaces the surfactant will turn its hydrophobic chain towards this surface, where van-der-Waals forces between both occur. The hydrophilic groups are aligned towards the polar liquid and the solid surface becomes hydrophilic. On a hydrophilic surface the situation is the other way round: the solid surface becomes hydrophobic. For higher surfactant concentrations a second molecular layer can form, returning the solid surface to a hydrophilic character.

## **4.5. Surfactants in nonaqueous media**

### **4.5.1. Surfactants in polar solvents**

The formation of micelles is only possible here, if the solvent is as strongly polar as water. In solvents like alcohols, ethers or amines with very low surface energy no adsorption of surfactants at interfaces occurs. For high energetic solvents like glycerin or formamid micelle formation follows the same mechanisms as observed in water.

### **4.5.2. Surfactants in nonpolar solvents**

Many surfactants are also soluble in nonpolar solvents. Here the situation for the polar headgroup is comparable to that of the hydrophobic group in water: the nonpolar solvent tries to have little contact to them, which can result in the formation of inversed micelles. The hydrophilic head aligns to the center of the micelle and the hydrophobic chain is turned towards the solvent (Figure 4-4). A formation of inversed micelles has been proved for all kinds of nonpolar hydrocarbon-based solvents. One special effect of inversed micellation is their ability to trap water. Most solvents contain traces of water. The hydrophilic head groups of the surfactant molecules get strongly bonded to the water and the inversed micelle forms around the water. For some solvents the presence of water was found to be necessary to form inversed micelles.

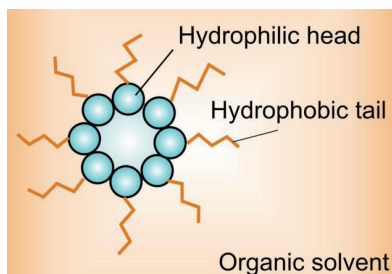


**Figure 4-4.** Structure of an inversed micelle. In nonpolar media the hydrophobic tails of the surfactant molecules align towards the nonpolar phase and the head groups to the micelle's center. If water remnants are present they can be trapped inside the inversed micelle.

#### **4.6. Dynamic behavior of surfactant molecules – diffusion and adsorption**

The surface of a liquid is not a distinct separation line, but a thin layer, only few molecules thick. Inside this layer the solution's properties are not homogeneous. They depend on the height position inside the layer. With lower distance to the phase boundary the surfactant concentration increases. To describe the processes at the surface mathematically an interface boundary with no height was defined by Gibbs (Figure 4-5). By placing this line at the level of highest surfactant concentration, the inhomogeneous region below the line can be described as a subsurface and allows a differentiation of diffusion and adsorption. The diffusion describes the movement of the molecules from the bulk solution to the subsurface and the adsorption describes the movement from the subsurface to the surface. Both processes occur with different rates and strongly influence the total rate of the decrease in surface energy. The rate of surface energy lowering can be more influenced by diffusion or adsorption, which depends on the surface age, surfactant

concentration, solvent characteristics and type of surfactant. The slower process of both dominates the total rate in surface energy reduction by surfactants.

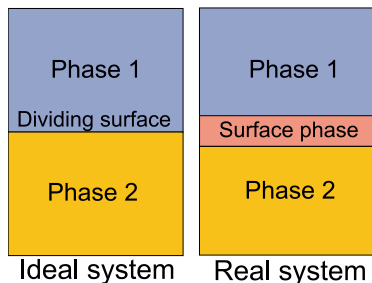


**Figure 4-5:** Surface model of Gibbs. While in the ideal system the dividing surface of two phases is a single line, a real system can be described by a surface phase of a certain thickness.

#### 4.7. Surfactants in PERR

Only few studies have been published which are dealing with the application of surfactants to wet chemical cleaning solutions. Le et al. studied the effects of nonionic surfactants out of the Triton series provided by Dow Chemicals in a diluted HF solution applied to porous dielectrics. It was found that the surfactant diffused into the porous structure of the low-k material [94]. Using an alcohol for rinsing the surfactant could be removed. Keagy et al. applied a hydrocarbon-based surfactant as an emulsifier in supercritical CO<sub>2</sub>-PERR processing to keep the system water/CO<sub>2</sub> stable [95].

In this work a broad range of surfactants, including nonionic, anionic, perfluorinated, silicon containing and block-copolymers are going to be evaluated regarding their applicability to low-k dielectrics, metals and barrier materials.

The selected surfactants will be combined with SAC or water based wet PERR solutions. The description of the surfactants selected can be found in chapter 7.



## **5. Analytical methods**

### **5.1. Determination of surface energies and wetting behavior**

#### **5.1.1. The surface energy of the solid**

All methods described in this section are based on contact angle measurements of testing liquids with a known energetic character on the substrate studied.

##### *5.1.1.1. The method of Zisman*

The Zisman method uses critical surface energies of liquids to determine the energy characteristics of a solid surface. This formerly widely used calculation based on the method of Antonow, which has been revised. Due to this the Zisman method is not in use anymore and will not be discussed further in this work [99].

##### *5.1.1.2. Equation of state*

The efforts to determine the surface energy of a solid by a single contact angle measurement using a liquid with known surface energy led to the development of the equation of state method [75, 100]. Starting with Young's equation a relation between the surface energy of a liquid and the interfacial energy of the liquid-solid system was found by empirical methods. The influences of polar and dispersive interactions are not taken into account by this method. So the equation of state is only suitable for systems where only dispersive contributions are present.



#### 5.1.1.3. *The method of Fowkes*

Fowkes was the first who determined the dispersive and polar energy contributions of a solid surface [75, 101]. The dispersive fraction of the solid is determined by contact angle measurement with at least one purely dispersive liquid. Fowkes combined Young's equation with the term for dispersive interactions and got:

$$\cos \theta = 2 \cdot \sqrt{\sigma_s^D} \cdot \frac{1}{\sqrt{\sigma_L^D}} - 1 \quad (5-1)$$

Based on the equation of a straight line

$$y = m \cdot x + b \quad (5-2)$$

$\cos \theta$  is plotted versus  $\frac{1}{\sqrt{\sigma_L^D}}$  and the dispersive energy contribution can be calculated from the slope of the line  $m = 2 \cdot \sqrt{\sigma_s^D}$ .

#### 5.1.1.4. *The method of Owens, Wendt, Rabel and Kaelble (OWRK)*

The method of Fowkes and OWRK are comparable with the difference that Fowkes needed two calculation steps to determine dispersive and polar energy contributions of the solid surface. Owens et al. stated that the surface energy of each phase can be split up into a polar and a dispersive part [80]. They used the Fowkes method and were able to determine polar and dispersive energy contributions in one step using the contact angle values of two known testing liquids. The equation of the interactions of solid and liquid was transposed by application of the term for a straight line. Finally they got:

$$\frac{(1 + \cos \theta) \cdot \sigma_L}{2 \cdot \sqrt{\sigma_L^D}} = \sqrt{\sigma_s^P} \cdot \sqrt{\frac{\sigma_L^P}{\sigma_L^D}} + \sqrt{\sigma_s^D} \quad (5-3)$$

$$y = m \cdot x + b$$

Y and x are plotted and the dispersive part of the surface energy can be obtained from the intercept b and the polar part from the slope of the line (Figure 5-1). The OWRK method has been used to calculate the surface energies of solid surfaces in this work.

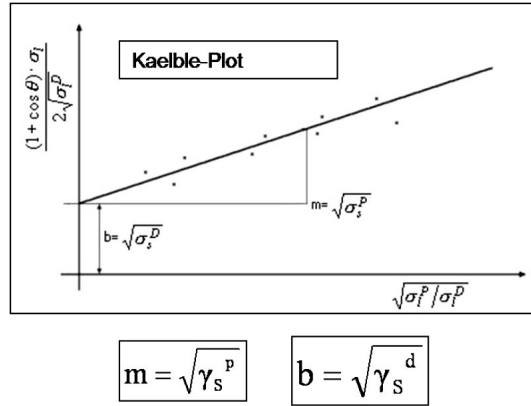


**Figure 5-1:** Kaelble plot as a result of contact angle measurements to determine the surface energy of a solid. By linear regression of the contact angle values a straight line can be found. The slope of this line gives the polar and the intercept gives the dispersive energy part of the studied solid surface. (Source: Kruss DSA-100 user manual, <http://www.kruss.de>)

### 5.1.2. The surface energy of the liquid

#### 5.1.2.1. *The ring method*

The ring method is one of the oldest to determine surface energies of liquids and mostly the values found in tables have been calculated using this method [102]. A ring is brought in contact with the surface of the liquid, lifted up so a liquid lamella forms and the force applied just in the moment before the lamella is destroyed is measured (Figure 5-2 a). Additionally the length of the lamella  $L$ , the weight force of the lifted liquid and the contact angle at the ring are needed to determine the liquid's surface energy:

$$\sigma = \frac{F_{max} - F_V}{L \cdot \cos \theta} \quad (5-4)$$

At the force maximum the contact angle become zero, so  $\cos \theta = 1$ .

Correction calculations are necessary to patch inaccuracies, e.g. different maximum forces are measured for the lamella at the inner and outer side of the ring. The correction factors can be found in tables, drawn by Harkine and Jordan.

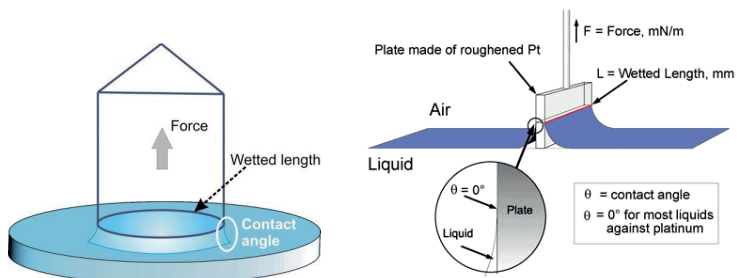


**Figure 5-2:** Ring method (a) and plate method (b) to determine the total surface energy of a liquid. In both methods the force needed to pull the ring / plate out of the studied liquid, the wetted length of the liquid lamella formed and the contact angle are used for calculation. (Source: KRUSS Newsletter archive, issue 06/2004, application, online edition: <http://www.kruss.de/en/newsletter/newsletter-archives/2004/issue-06/application/application-01.html>)

#### 5.1.2.2. The plate method

A plate made of roughened platinum is dipped into the liquid and lifted [103]. The contact angle of the liquid wetting the plate and the according force necessary to lift the plate are measured (Figure 5-2 b). By determining the wetted length the surface energy of the liquid can be calculated:

$$\sigma = \frac{F}{L \cdot \cos \theta} \quad (5-5)$$

Due to the fact that the wetting of roughened platinum is nearly perfect, the contact angle mostly becomes zero and  $\cos \theta = 1$  can be applied.

### 5.1.2.3. The pendant drop method

A drop of the investigated liquid is formed at a dosing needle with a relatively large diameter. According to Laplace the pressure difference between the inner and outer side of the drop is in inverse proportion to the main radii of curvature of the interfacial segments of the drop (Figure 5-3). By iterative calculation of the force equilibrium of the surface energy holding the drop together and the weight force the surface energy of the liquid can be calculated by drop shape analysis [104]. The digital picture analysis determines the shape of the drop and by including the scale of magnification on the screen and the density of the liquid its surface energy is calculated. The drop neck can be excluded from the picture analysis to minimize inaccuracies. All total surface energy values of liquids in this work have been determined by using the pendant drop method.

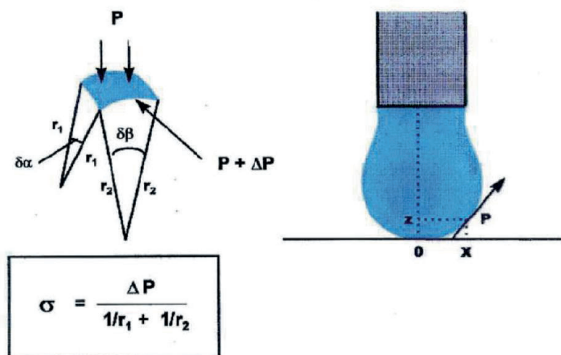


**Figure 5-3:** The pendant drop method is a simple and accurate method to determine the surface energy of a liquid by a software aided drop shape analysis. The only value necessary to be known is the density of the studied liquid. (Source: Oberflächenspannung von Flüssigkeiten – Eine Einführung, KRUSS GmbH, DSA-100 Manual Attachment (2003))

#### 5.1.2.4. Polar and dispersive energy contributions of the liquid

The methods described before provides the total value of the liquids surface energy only. To determine the polar and dispersive surface energy part of the liquid an additional contact angle measurement is necessary [38]. Starting from the equation of the OWRK method at first the dispersive energy contribution is determined. The equation is modified and one gets:

$$\sqrt{\sigma_L^D \cdot \sigma_S^D} + \sqrt{\sigma_L^P \cdot \sigma_S^P} = \frac{\sigma_L \cdot (\cos \theta + 1)}{2} \quad (5-6)$$

$\sigma_L$  is known from the pendant drop method and  $\sigma_L^D$  is the value that is going to be calculated, but the equation has too much unknown variables. This problem can be overcome by using a solid surface whose energy character is known and which is nearly completely dispersive. Such a solid can be PTFE, which does not have polar energy contributions. By using the OWRK method the surface energy of PTFE is determined, usually varying between 20-25 mN/m with less than 1% polar energy part, which can be neglected. The surface energy of PTFE is equal to  $\sigma_S^D$  within the equation and because there is no polar energy contribution the term containing  $\sigma_S^P$  becomes zero. The only unknown value left is  $\theta$ , which can be determined by contact angle measurement of the studied liquid on PTFE. Finally the dispersive energy contribution of the liquid can be obtained from:

$$\sigma_L^D = \frac{\sigma_L \cdot (\cos \theta + 1)^2}{4 \cdot \sigma_S^D} \quad (5-7)$$

and the polar energy contribution is afterwards calculated by

$$\sigma_L^P = \sigma_L - \sigma_L^D \quad (5-8)$$

## 5.2. Experimental setup

Contact angle measurements and the determination of the total surface energy of the liquids have been done using the Kruss DSA 100 contact angle measurement system. It is equipped with a semi-automatic dosing unit, a high speed CCD camera system and a freely adjustable x-y-z-table. The software “Drop shape analysis” allows contact angle measurement using different modes. For the contact angle measurement in this work the sessile drop mode was used. The testing liquid used for the calculation of the energetic character of the solid surfaces can be found in Table 5-1. They were chosen to cover a broad range of energetic characters. For the contact angle measurements five drops with a constant volume of 4  $\mu\text{L}$  have been dosed and the mean value has been used as result. The total surface energy of the liquid was determined by the pendant drop method using a rather large dosing needle with an inner diameter of 1.83 mm. A PTFE plate has been used for the contact angle measurements to determine polar and dispersive energy contribution of the liquid. Each time the energetic character of the PTFE plate was determined by the OWRK method before the experiments. The technical parameters like resolution and measurement failures of the Kruss DSA 100 are listed below.

Kruss DSA 100:

- Range of contact angle measurement:  $0 - 180^\circ$ ,  $\pm 0.1^\circ$  accuracy
- Range of surface energies (liquid):  $1\text{E-}2 - 1000 \text{ mN/m}$ ,  $0.01 \text{ mN/m}$  resolution
- Measurement failure for sessile drop:  $\theta \leq 15^\circ$ :  $2^\circ$ ;  $\theta > 15^\circ$ :  $1^\circ$
- Measurement failure for pendant drop:  $\pm 3 \text{ mN/m}$

**Table 5-1:** Energetic character of the testing liquids used for surface energy calculation of solid samples by contact angle measurement. The values are taken from the material database of the KRUSS DSA 100 system.

Testing liquid	Dispersive [mN/m]	Polar [mN/m]	Total [mN/m]
1-octanol	26.2	1.4	27.6
Ethylene glycol	29.0	18.7	47.7
Water	21.8	51.0	72.8

### 5.3. Dynamic surface energy of surfactant solutions

For dynamic processes, where new interfaces between liquid and the surrounding medium are formed and destroyed quickly, the dynamic behavior, especially the adsorption speed of a surfactant molecule to this interface is important. To reduce the surface energy of the cleaning liquid the surfactant molecules have to be present at the interface. This reduction in surface energy is not achieved instantly, but takes some time depending on the ability of the surfactant to diffuse to and adsorb at the interface. The dynamic behavior of a surfactant solution can be determined by the method of maximum bubble pressure [105]. The basic principle of this method is shown in Figure 5-4.

A PTFE capillary with a known radius is inserted into the liquid and gas bubbles are pressed into the liquid at an exactly defined frequency. The pressure needed to press the bubble into the liquid passes through a maximum value, which is recorded. When the bubble is pressed into the liquid the pressure is initially below the maximum pressure. In the moment the radii of the bubble and the capillary are the same, the maximum pressure is reached. The bubble forms an exact hemisphere and the following relationship between the maximum pressure  $P_{max}$ , the hydrostatic pressure  $P_0$  inside the capillary, the surface energy  $\sigma$  and the inner radius  $r$  exists:



$$\sigma = \frac{(P_{max} - P_0) \cdot r}{2} \quad (5-9)$$

After the maximum pressure point the “dead time” of the measurement starts, the bubble becomes larger and the pressure decreases. Finally the bubble detaches and the cycle starts again.

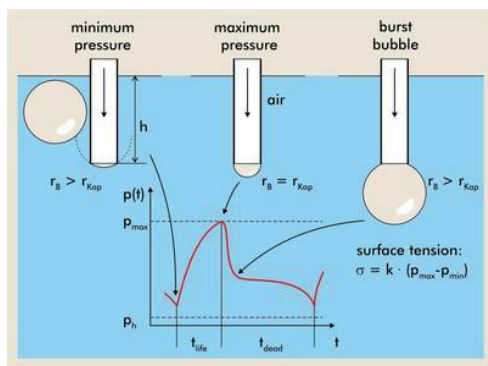


**Figure 5-4:** By the maximum bubble pressure method the dynamic behavior of a surfactant solution. Especially the adsorption speed of the molecules to a newly formed interface can be determined. The maximum bubble pressure is reached in the moment the bubble's diameter is the same as that the capillary. This value is used to calculate the dynamic surface energy of the solution at a certain surface age. (Source: SITA process solutions, <http://www.sita-process.com/theory/basics-about-sita-process-solutions/process-parameter-surface-tension/>))

Dynamic surface energy measurements of surfactant solutions have been performed using the Kruss PocketDyne, a mobile tensiometer applying the method of maximum bubble pressure. The tensiometer is calibrated before each measurement series to the surface energy of water at the actual liquid temperature. Surface ages

of 20 – 1000 ms in 11 steps have been used to determine the dynamics of a certain surfactant. To stabilize the calculated surface energy value the actual bubble frequency was kept for at least 20 seconds to get an accuracy of  $\pm 2$  mN/m.

## **5.4. Analytics for material compatibility**

### **5.4.1. Spectral ellipsometry**

Film thickness and refractive index of the low-k dielectric samples have been determined by spectral ellipsometry using the Sentech SE 850. This ellipsometer is able to work in a spectral range of 190 – 2550 nm at incident angles of 40 – 90°. For the low-k samples a spectral range of 350 – 830 nm was used. The fitting of the measured spectra was done using a simple film stack consisting of silicon / SiO<sub>2</sub> / air. The parameters of the SiO<sub>2</sub> layer were modified to fit a low-k material. Therefore its refractive index was reduced to approximately 1.35 as a starting parameter for the fitting using a Cauchy model. At least five measurements have been done per sample at different positions and at an incident angle of 70°. The mean square error (MSE) for dense dielectric samples was 0.5 – 1.5 and for porous samples 1.5 – 5.0.

### **5.4.2. CV – measurement**

Permittivity and leakage current density of dielectric samples have been determined by a mercury probe measurement using the SSM 490i system. At least 5 measurements have been done per sample. Leakage currents can be determined directly. The k-value has to be calculated from a measured capacitance of the

Si/low-k/Hg stack at a frequency of 100 kHz. By applying equation 5-10 the relative dielectric number  $\epsilon_{rel}$  can be determined.

$$C = \epsilon_0 \cdot \epsilon_{rel} \cdot \frac{A}{d} \quad (5-10)$$

The area A of the mercury probe is determined before each measurement series. To accurately calculate the k-value the thickness of the dielectric layer has to be determined before. Therefore the test points of the ellipsometric measurement were adjusted to the point of the CV measurement. The mean variation of the leakage current values can be up to 12%, for the k-value the mean variation usually is not higher than 3%.

#### 5.4.3. FTIR

The structural properties of dense and porous low-k samples have been determined by Fourier Transform Infrared Spectroscopy (FTIR) using the Bruker IFS 66 and Bruker Tensor 27 spectrometers in mid infrared spectral range (MIR). The sample chamber was rinsed with dried air (IFS 66) or nitrogen (Tensor 27) for 10 minutes before the scanning. A blanket silicon substrate was used for background measurement, whose spectrum gets subtracted from the spectra taken of the Si/low-k stack. For interpretation the transmission spectra were converted into adsorption mode with a correction of the baseline. Figure 5-5 shows a typical FTIR spectrum of a porous CVD SiCOH dielectric.

The spectrum can be divided into the fingerprint section from approximately 500 – 2000  $\text{cm}^{-1}$  which identifies the material and the section of the functional groups up to 4000  $\text{cm}^{-1}$ . In Table 5-2 the most important peaks to characterize a low-k dielectric are listed [106].

**Table 5-2:** Wavenumber regions describing the typical structure of SiCOH materials and the most probable origin of the vibration modes. The colored regions can also be seen in Figure 5-5.

Wavenumber [ $\text{cm}^{-1}$ ]	Vibration mode	Origin / Comments
440	Si – O – Si vibration	Network and ring opening vibrations
780	Stretching Si – C	SiMe <sub>1</sub>
800	Stretching Si – C	SiMe <sub>2</sub>
848	Bending H – Si – O, stretching Si – C	SiMe <sub>3</sub>
890	Bending H – Si – O	H – SiO <sub>3</sub>
1055	Stretching (asym.) Si – O – Si	Network Si-O-Si angle $\sim 144^\circ$
1135	Stretching (asym.) Si – O – Si	Cage Si-O-Si angle $\sim 150^\circ$
1275	Bending (symm.) C – H <sub>3</sub>	SiMe <sub>x</sub>
2880	Stretching (symm.) C – H <sub>2</sub>	CH <sub>2</sub>
2927	Stretching (asym.) C – H <sub>2</sub>	CH <sub>2</sub>
2971	Stretching (asym.) C – H <sub>3</sub>	CH <sub>3</sub>

All wavenumbers listed above have to be conceived as possible ranges of assignment of a peak to a special molecular structure. Each difference in the dielectric structure, e.g. caused by fluctuations of the deposition or curing process can affect minor shifting of peaks.

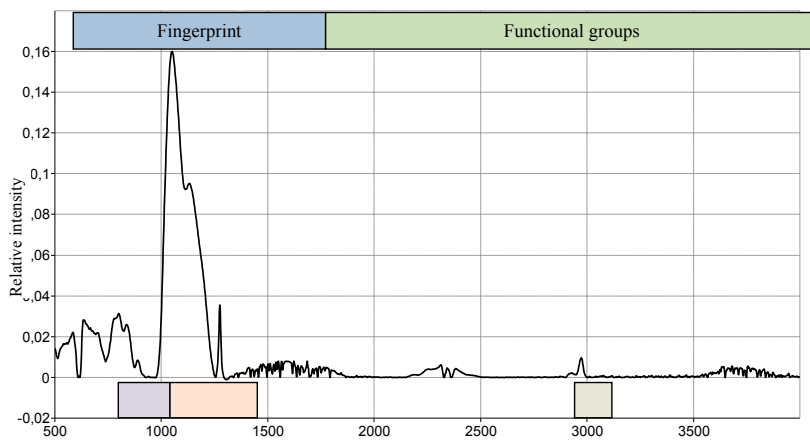


**Figure 5-5:** FTIR spectrum of a porous CVD-SiCOH dielectric in pristine condition.

#### 5.4.4. Sheet resistance

The sheet resistance of metallic and barrier materials has been determined by 4-point-probe measurements using the Tencor Omnimap RS 50 system. Sheet resistance data have been recorded at 49 or 81 points at the center of the sample and distributed over two radii. The standard deviation of the  $R_s$  values normally is not higher than 5%.

## **6. Experimental determination of surface energies and wetting behavior**

### **6.1. Sample and process description**

This chapter describes all solid samples and processes which have been used to determine and influence surface energies, wetting behavior and material compatibility. The samples were provided and processed by industrial partners (GLOBALFOUNDRIES, Air Products and Chemicals Inc.). Especially the etching processes introduced in this chapter are only described basically due to the fact that further processing parameters are protected by an NDA. In all cases the substrates have been cut into 10x10 cm or 4x4 cm samples.

#### **6.1.1. Description of the solid samples**

##### *6.1.1.1. Low-k and ultra low-k materials*

In this work 4 different CVD SiCOH low-k and ultra low-k materials of 500 nm film thickness have been studied, of which 2 are porous and 2 are dense dielectrics. The dielectrics have been produced by PECVD using a precursor containing the silicon source and organic species, which in case of the samples provided by Air Products was DEMS, followed by an UV curing process. For the porous samples a porogen like alpha-terpinene has been added to the deposition process. The properties of the dielectrics are listed in the following Table 6-1.

**Table 6-1:** Low-k and ultra low-k dielectrics studied in this work.

<b>Material</b>	<b>k-value</b>	<b>Substrate diameter</b>	<b>Referred to as</b>
Porous CVD SiCOH dielectric, provided by Global Foundries Inc.	2.5	300 mm	low-k 1
Porous CVD p-DEMS dielectric, provided by Air Products and Chemicals Inc.	2.2	200 mm	low-k 2
Dense CVD SiCOH dielectric, provided by Global Foundries Inc.	3.0	300 mm	low-k 3
Dense CVD SiCOH dielectric, fabricated at Fraunhofer ENAS	3.2	150 mm	low-k 4

#### 6.1.1.2. *Metals and barrier materials*

For compatibility studies and wetting tests Copper, CoWP and diffusion barrier Materials have been investigated. The sample properties can be found in Table 6-2.

**Table 6-2:** Metallic and barrier materials studied in this work.

<b>Material</b>	<b>Film thickness</b>	<b>Substrate diameter</b>	<b>Referred to as</b>
Electroplated Copper, provided by GLOBALFOUNDRIES Inc.	1000 nm	300 mm	Cu 1
Electroplated Copper, fabricated at Fraunhofer ENAS	1000 nm	150 mm	Cu 2
CoWP on electroplated Copper, provided by GLOBALFOUNDRIES Inc.	15 nm	300 mm	CoWP
Sputtered TiN, fabricated at TU Chemnitz / ZfM	40 nm	150 mm	TiN
Sputtered TaN, fabricated at TU Chemnitz / ZfM	40 nm	150 mm	TaN

#### 6.1.1.3. *Other solid samples*

For additional studies on surface energy and wetting behavior an OMCTS hardmask layer and a low-k 1 sample treated by a CMP process using Acuplane slurry have been investigated. Both types of samples have been provided by Global Foundries Inc. on 300 mm Si substrates. The samples will be referred to as OMCTSHM and CMP.

### 6.1.2. **Description of plasma processes**

This section describes the different plasma processes applied to the low-k samples listed above to determine their influence on the energetic character of the low-k surfaces and therefore on their ability to be wetted by cleaning solutions. The processes are divided into etching processes, stripping processes and processes expected to have a polymerizing character and therefore will produce a kind of polymeric model residue on the low-k surface.

#### 6.1.2.1. *Etching processes*

The etching processes applied to the low-k samples are mainly based on CF-containing chemistries. To develop less damaging plasma processes the influence of additional species, e.g. Argon or Nitrogen, within the plasma is studied. By increasing their gas flow in a common CF<sub>4</sub> etching process the effects on surface energy of the low-k samples is studied. Table 6-3 shows the process conditions.



**Table 6-3:** Description of the etching processes applied to dense and porous dielectric samples.

Process	Parameters	Referred to as
20 sec main etching process, performed at GLOBALFOUNDRIES	C-H-F-containing etching gas	ME
Via etching process, performed at Global Foundries Inc.	CF-containing etching gas	VE
CF <sub>4</sub> etching process with 12 sccm CF <sub>4</sub> gas flow performed at Fraunhofer ENAS: Oxford Instruments ICP reactor, ICP power 1000W at 7 mTorr process pressure; process time on dense low-k: 30 s, process time on porous low-k: 10 s		
CF <sub>4</sub>	No additives	CF <sub>4</sub>
CF <sub>4</sub> with Ar addition	Ar gas flow varied: 2, 4, 6 and 8 sccm	Ar2, Ar4, Ar6, Ar8
CF <sub>4</sub> with CO addition	CO gas flow varied: 2, 4, 6 and 8 sccm	CO2, CO4, CO6, CO8
CF <sub>4</sub> with N <sub>2</sub> addition	N <sub>2</sub> gas flow varied: 2, 4, 6 and 8 sccm	N22, N24, N26, N28
CF <sub>4</sub> with O <sub>2</sub> addition	O <sub>2</sub> gas flow varied: 2, 4, 6 and 8 sccm	O22, O24, O26, O28

#### 6.1.2.2. *Polymerizing etching processes*

To simulate the wetting behavior of a polymeric plasma etch residue etching processes have been applied which are known to support the formation of a CF-containing residue on a low-k surface. The processes are based on CF-containing chemistries with varied process parameters (process time and gas flow of additives expected to support polymerization). The process conditions can be found in Table 6-4.

**Table 6-4:** Description of the polymerizing plasma processes used to produce etch residue surfaces.

Process	Parameters	Referred to as
Polymerizing etching process using a CF-containing etching gas, performed at GLOBALFOUNDRIES	Varied process time: 10 s, 15 s and 30 s	Poly10, Poly15, Poly30
CF <sub>4</sub> etching process with 12 sccm CF <sub>4</sub> gas flow performed at Fraunhofer ENAS: Oxford Instruments ICP reactor, ICP power 1000W at 7 mTorr process pressure; process time on dense low-k: 30 s, process time on porous low-k: 10 s		
CF <sub>4</sub> with C <sub>4</sub> F <sub>8</sub> addition	C <sub>4</sub> F <sub>8</sub> gas flow varied: 2, 4, 6 and 8 sccm	C4F82, C4F84, C4F86, C4F88
CF <sub>4</sub> with H <sub>2</sub> addition	H <sub>2</sub> gas flow varied: 2, 4, 6 and 8 sccm	H22, H24, H26, H28

Additionally a CF-polymer layer deposited by PECVD using the Applied Materials P5000 at TU Chemnitz / ZfM was investigated to enable the comparison to a polymeric residue produced by an etching process. These samples will be referred to as CVDPoly.

#### 6.1.2.3. Plasma stripping processes

The influence of plasma stripping processes on the surface energy of a low-k material has been investigated by application of different stripping chemistries. Plasma strip 1 and 2 (referred to as PS1 and PS2, respectively) have been performed using a reducing chemistry and plasma strip 3 (PS3) was performed using an oxidizing chemistry. All stripping processes have been realized at Global Foundries Inc. Further process parameters are NDA protected.

### 6.1.3. Description of the liquid samples

The surface energy of four commercially available and two experimental cleaning liquids provided by Air Products and Chemicals Inc. has been determined. All liquids are designed to remove plasma etch residues from porous low-k materials and are described to be compatible to materials used within BEOL processing. The cleaning solutions are described in Table 6-5, classified by their water content. Further information about the composition of the solutions is protected by a NDA.

**Table 6-5:** Description of the wet cleaning solutions studied in this work

Cleaning solution	Water content	Referred to as
ACT EZ Strip 511	< 50 %	A1
ACT EZ Strip 520	< 50 %	A2
ACT NAC-1	< 50 %	A3
ACT EZ Strip 530	50 – 80 %	B1
87F (experimental solution)	50 – 80 %	B2
3L (experimental solution)	> 80 %	C1

## 6.2. Surface energies of the solid samples

### 6.2.1. Low-k and ultra low-k dielectrics after etching processes

In pristine condition the porous low-k dielectric has a low energetic surface with almost no polar contribution. All applied etching processes introduced a polar energy part, whose quantity strongly depends on the type of process and increases the total surface energy of the low-k surface (Figure 6-1). The low surface energy of the pristine low-k and especially the missing of a polar energy contribution will

lead to a very poor wetting behavior by water based cleaning solutions due to the fact that any polar energy part of the liquid cannot interact with this surface. The increase in surface energy by the etching processes and the introduction of a polar energy part will support the wetting of this surface by many liquids, but also shows that finding the appropriate cleaning solution depends on the process applied to the solid surface.

After the ME process the low-k dielectric's surface energy shows the smallest increase, keeping a more dispersive than polar character. All other etching processes changed the energetic character of the low-k surface from dispersive to polar with an energy increase up to 50 mN/m. The addition of Argon and the increase of its gas flow do not change the effect of the  $\text{CF}_4$  etching process on the low-k material surface. The introduction of a strong polar energy part can be due to the destruction of hydrophobic groups in the surface near area by the plasma process, supporting the formation of polar groups at dangling bonds, e.g. the saturation of free bonding places by  $-\text{OH}$ . The formation of silanols in the surface near area of the low-k dielectric is one part of a plasma damage occurring during etching. The calculation of the low-k's surface energy characteristics can therefore not only be used to determine its wetting properties but to give a hint whether an etching process produces a material damage or not.

In Figure 6-2 the dispersive and polar energy contributions of the dense low-k materials 3 and 4 are shown. In pristine condition both materials have nearly complete dispersive energy character, while the total surface energy of low-k 4 is slightly higher than that of low-k 3. In contrast to the porous low-k 1 the application of a  $\text{CF}_4$  etching process with argon addition does not increase the surface energy up to 50 mN/m but only to 38 mN/m and the polar energy contribution after this process is not as high as for the porous low-k. This can be

due to the dense structure of the material. The addition of oxygen to the etching process shows a strong increase of the polar energy part of the surface, which can be due to the strong depletion of carbon in the surface near areas of the material by oxygen species in an etching plasma. The surface energy of low-k 4 is also increased by the etching process with addition of  $\text{CO}_2$  or  $\text{N}_2$  with the change of the material's character from dispersive to polar, but the addition of  $\text{CO}_2$  produces a lower polar energy part than the addition of  $\text{N}_2$ .

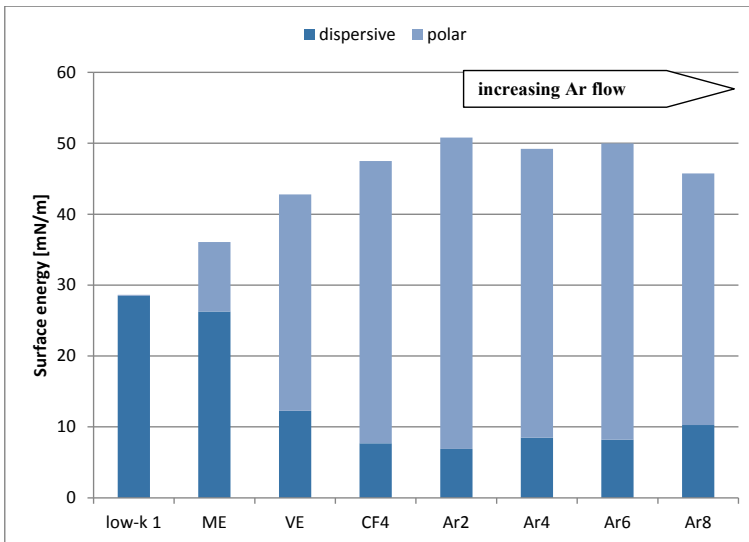


**Figure 6-1:** Dispersive and polar energy contributions of the porous low-k 1 in pristine condition and after several etching processes. All processes introduced a certain polar energy part, which lead to a strong increase in total surface energy.

The results show that it strongly depends on the process applied to a low-k material how its wetting behavior is affected and makes it difficult to find a universal cleaning solution to remove residues of the etching processes. Also the type of dielectric used for integration is one issue. In the case of the  $\text{CF}_4$  etching process

with addition of Argon the surface energy of the porous dielectric is obviously more affected than that of the dense dielectric. Also this means the dielectric could be damaged by an etching process, the increase of the surface energy of the liquid and especially the introduction of a polar energy part in all studied cases will support wetting of this surface.

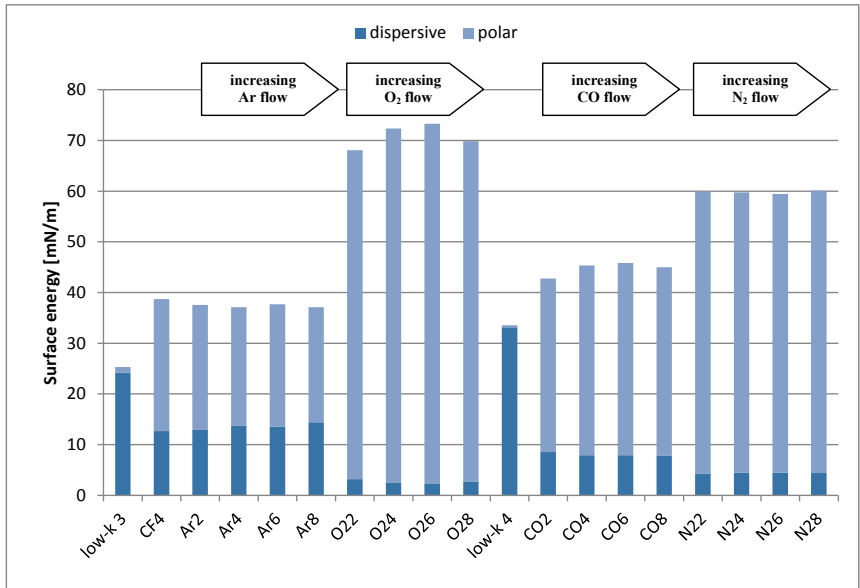


**Figure 6-2:** Dispersive and polar energy contributions of the dense low-k 3 and low-k 4 in pristine condition and after several etching processes. Especially the oxygen addition introduced a large polar energy part. In all cases the total surface energy of the samples was increased by plasma processing.

### 6.2.2. Surfaces after polymerizing processes

The polymerizing processes applied to the low-k material produce very low energetic surfaces with surface energies between 27 mN/m and 36 mN/m, which implies the formation of a polymeric surface layer. Compared to the CF-Polymer deposited by CVD the polymerized surfaces have a higher polar energy part and therefore a higher total surface energy (Figure 6-3).

The extension of the process time (Poly10, 15 and 30) leads to an increased dispersive energy contribution with a slight decrease in total surface energy. The same effect can be found by the  $C_4F_8$ - and  $H_2$  added processes, where an increased gas flow of the additive leads to a lower surface energy with a decreased polar energy contribution. This effect is more pronounced for the  $C_4F_8$ -added than for the  $H_2$ -added process. The results show clearly that the energetic character of polymeric etch residue surfaces strongly depends on process parameters applied to the material. Because the formation of a contact angle of a liquid on a solid is only influenced by the uppermost layers, the change in energetic character cannot be declared by an increased film thickness of the polymer but by a change in chemical composition of the surface. The results show that the calculation of the surface energy can be used as a very sensible method to detect whether a polymer has been formed or not and the influence of the variation of the process parameters applied to a surface.

Due to their low surface energy these polymerized surfaces will be difficult to wet by high energy cleaning solutions and the difference in their energetic character makes it hard to find an universal cleaning liquid for all surfaces.

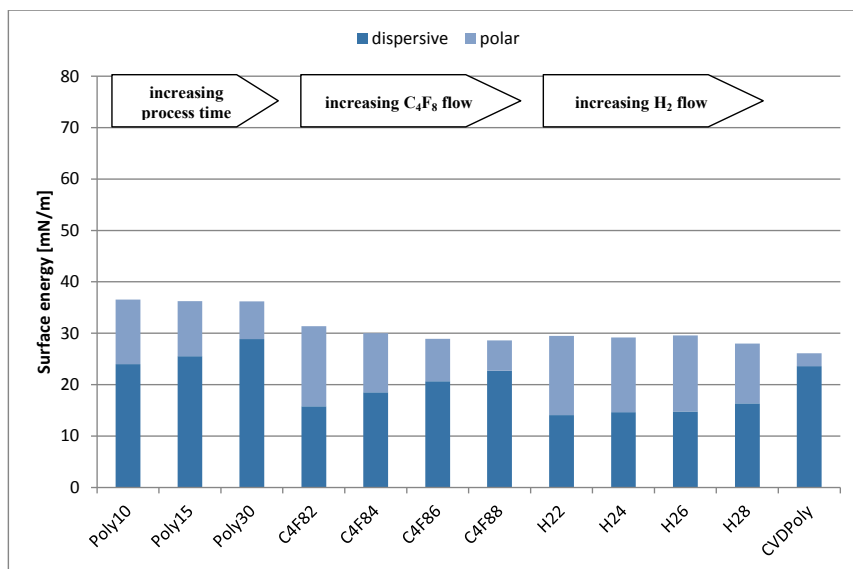


**Figure 6-3:** Dispersive and polar energy contribution of etch residue surfaces formed by different etching processes with varied process parameters. For comparison the energetic character of a CVD-formed CF-Polymer is shown. Surface energies of 30-40 mN/m have been determined for all studied residue surfaces. Although the polymeric residue owns a polar contribution, the low total surface energy may cause difficulties in wetting those kinds of surfaces.

### 6.2.3. Ultra low-k dielectrics after stripping processes

Two different reducing stripping processes (PS 1 and PS 2) and one oxidizing stripping process (PS 3) have been applied to low-k (Figure 6-4). Both reducing stripping processes introduce a polar energy part to the material, which is nearly completely dispersive in pristine condition. After PS 1 the material keeps its more dispersive than polar energy character and the total surface energy is increased to 35 mN/m. Even the type of stripping chemistry is comparable to PS 1, PS 2 leads to a much larger increase in surface energy, turning the energetic character of the



material from dispersive to polar. The surface energy increased up to 41 mN/m. The strongest effect on the low-k's surface can be found for PS 3, which introduces a large polar energy part and increases the surface energy of the dielectric up to 58 mN/m. Oxidizing stripping chemistries are known to lead to a reduction of the carbon content of the low-k and the formation of polar groups like silanols, which can declare the occurrence of this large polar energy part of the material after PS 3.

Even the formation of polar energy contributions and the increase in total surface energy implies a plasma damage of the dielectric, it is supporting the wetting behavior of the material by equalizing the energetic character of the solid to this of many liquids.

#### **6.2.4. Metallic surfaces and barriers**

The surface energy of metals and barrier materials used within the interconnect system of integrated circuits has been calculated to determine their wetting behavior (Figure 6-5). The copper layers (Cu 1 and Cu 2), both deposited by electroplating, show a very similar energetic character with a low surface energy of about 30 mN/m of which about 1/3 is polar. The copper, which can be in contact with a cleaning solution not only while etch residue removal but also while post-CMP cleaning, will be difficult to wet due to its low surface energy. The CoWP layer's surface energy is only slightly higher than that of the copper samples, also its polar energy part is larger. Both barrier materials (TiN and TaN) have a strong polar energy contribution, but differ in total surface energy, which is much higher for TaN with more than 50 mN/m. Therefore TaN will show the best wetting behavior.

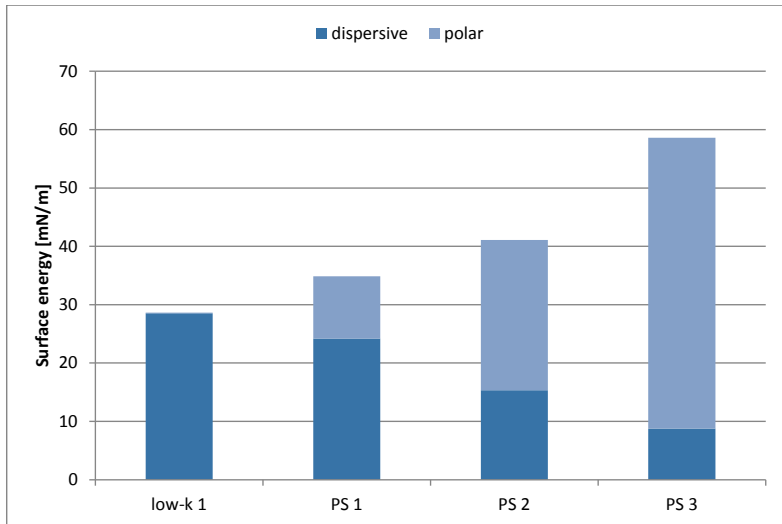


**Figure 6-4:** Dispersive and polar energy contributions of low-k 1 after reducing (PS 1 and PS 2) and oxidizing (PS 3) stripping processes. As shown for the plasma etching processes stripping introduces a polar energy part to the low-k material. Differences in energetic characters can not only be found for reducing and oxidizing processes, but also within reducing plasmas using different process conditions.

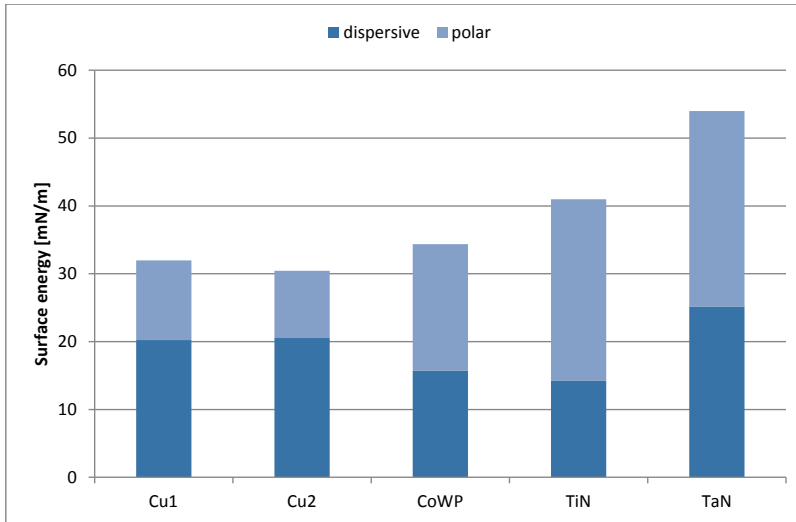


**Figure 6-5:** Dispersive and polar energy contributions of copper and barrier materials applied within the interconnect system. The copper samples show a very low surface energy comparable to the values found for etch residue surfaces. All other samples own a more or less higher polar energy contribution.

#### 6.2.5. Polished and hardmask surfaces

Wet cleaning processes are not only important for etch residue removal, but also after other processes within the fabrication of integrated circuits. Especially after chemical mechanical polishing (CMP) processes a cleaning step is necessary to remove slurry residues. After the CMP process the surface to be cleaned can for instance be copper or a hardmask layer, which acts as a stop-layer for the CMP process. To remove slurry residues by wet cleaning the wetting of the surface by the cleaning solution is essential. A CMP process using Acuplane slurry (Dow Chemical) was applied on low-k 1 and a hardmask layer based on

Octamethylcyclotetrasiloxane (OMCTS) has been studied. To determine the wetting behavior of both surfaces their surface energy has been calculated.

The CMP process introduced a strong polar energy contribution to the dielectric and increased its total surface energy from 28 mN/m up to more than 40 mN/m (Figure 6-6). Due to this energy increase this layer will show a better wetting behavior than the pristine low-k 1, but this also implies a damage of the surface near area and the formation of polar groups. The OMCTSHM layer has a completely dispersive character with a slightly higher total surface energy than the pristine low-k 1, which means that this surface will show a very poor wetting behavior due to its low energy and the missing of a polar energy part.

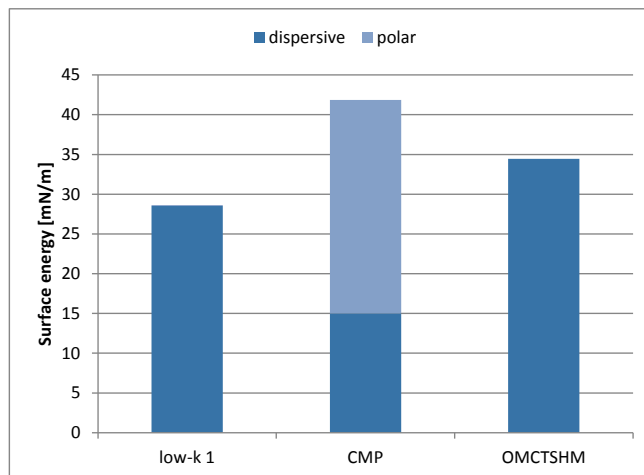


**Figure 6-6:** Dispersive and polar energy contribution of low-k 1 after a CMP process and of an OMCTS hardmask layer

### 6.3. Surface energies of the cleaning solutions

The studied cleaning solutions show a broad range of surface energies and all have a more or less strong polar energy part (Figure 6-7). The solvent based liquids A1 and A2 are low-energetic with surface energies below 40 mN/m and will therefore show the best wetting behavior on low energy solid surfaces. Solution A3, which also has a water content lower than 50%, shows a much higher surface energy of about 60 mN/m, which means that solvent based cleaning liquids are not low-energetic in any case and a determination of their surface energy is necessary. Solutions B1 and B2 differ in their surface energy by 11 mN/m, even they have a comparable content of water. B2 has a very high surface energy of about 66 mN/m and low energetic solids will difficultly be wetted by this solution.

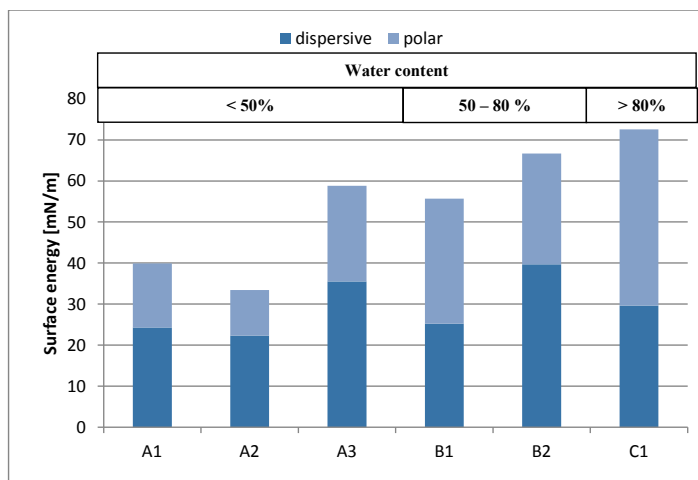


**Figure 6-7:** Dispersive and polar energy contribution of the cleaning solutions studied in this work. All studied liquids own a certain polar energy contribution and vary in total surface energies depending on their water content.

Solution C1 with the largest water content of more than 80% shows the highest surface energy with 72,6 mN/m, which is comparable to that of water (72,4 mN/m at room temperature). This solution will have the most critical wetting behavior on low energy solid surfaces.

#### 6.4. Contact angle analysis

The wetting behavior of a liquid on a solid surface can be determined by calculating the surface energies of both. A comparable energetic character of both, which includes the total surface energy value and the ratio of polar and dispersive energy contribution, should provide the best wetting behavior. A contact angle analysis of the studied cleaning liquids on a selection of the solid surfaces characterized in the previous sections is performed to test, if this type of prediction is reliable.

Figure 6-8 shows the contact angles of all studied cleaning solutions on low-k 1, the etch residue surfaces Poly10, Poly15, Poly30, low-k 1 after a main etching process (ME) and the stripping processes PS1-3. The low-energetic and dispersive low-k 1 surface shows the most critical wetting behavior. Due to the missing of any polar energy contribution the cleaning solutions are not able to form low contact angles. The high-energetic solutions B2 and C1 show contact angles higher than 90°, which means that no wetting occurred.

For all other surfaces the low-energetic cleaning solutions A1 und A2 show the best wetting behavior with contact angles lower than 26°. This can be declared by the comparable energy characteristics of liquids and solids. The more high energetic cleaning solutions are not able to form contact angles lower than 36°, depending on the difference between the energy values of the solid and the liquid. Dispersive and polar energy contributions of solid and liquid also show a clear connection to the

value of the contact angles, which become lower if the ratio of dispersive and polar energy part of both species is most comparable.

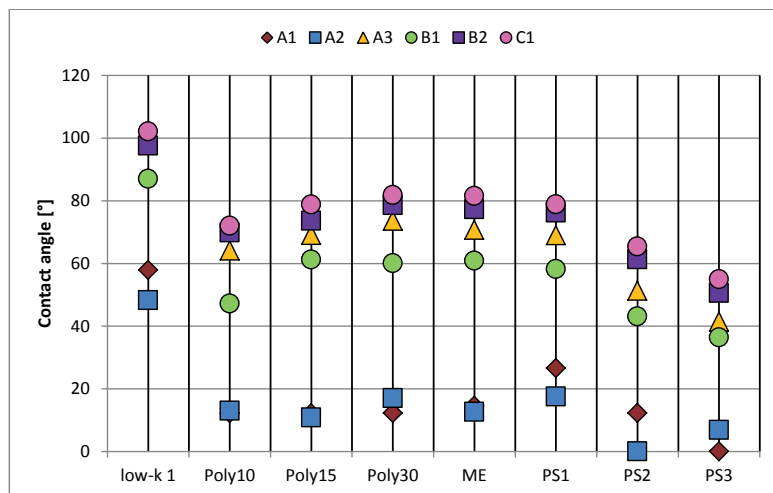


**Figure 6-8:** Contact angles of the studied cleaning solutions on selected surfaces. The solutions A1 and A2 with the lowest water content show the best wetting behavior. Due to its dispersive character the pristine low-k 1 is difficult to wet by all studied solutions.

### 6.5. Finding the appropriate cleaning solution with sufficient wetting behavior without additional contact angle measurements

In Table 6-6 the contact angles of the cleaning liquids and the differences between the surface energies of the solid surfaces and the liquids are shown, which clearly shows the context between both parameters. The best wetting behavior can be achieved by cleaning solutions, which have the same or less surface energy as the solid surface.

**Table 6-6:** The contact angles of the cleaning liquids on selected surfaces (CA, value on the left side) and the differences between the surface energies of liquids and solids (ED, value on the right side) are compared. A small difference between the surface energies will produce a small contact angle on this surface. The results confirm that calculating the energetic character of solid and liquid gives a sound appreciation of the wetting behavior to be expected.

	A1		A2		A3		B1		B2		C1	
	CA	ED	CA	ED	CA	ED	CA	ED	CA	ED	CA	ED
Poly10	12,2	3,36	13	-3,14	64,1	22,26	47,2	19,16	69,9	30,16	72	36,06
Poly15	12,2	3,64	10,8	-2,86	69,1	22,54	61,2	19,44	73,6	30,44	78,8	36,34
Poly30	12,3	3,69	17	-2,81	73,6	22,59	60,1	19,49	78,6	30,49	81,8	36,39
ME	14,6	3,81	12,6	-2,69	70,7	22,71	60,9	19,61	77,3	30,61	81,5	36,51
PS1	26,6	5,03	17,5	-1,47	69	23,93	58,2	20,83	76,2	31,83	78,9	37,73
PS2	12,3	-1,19	0	-7,69	51,3	17,71	43,1	14,61	61,3	25,61	65,4	31,51
PS3	0	-9,93	6,9	-16,43	41,4	8,97	36,4	5,87	50,6	16,87	55	22,77

Legend			
Contact angle			
< 20°	20 - 40°	40 - 60°	> 60°
Energy difference			
< 5 mN/m	5 - 15 mN/m	15 - 25 mN/m	> 25 mN/m

To find the appropriate cleaning solutions with the best wetting behavior on a special surface the first parameter to look at is the total surface energy of both media. If the difference is small or the cleaning liquid's surface energy is smaller than that of the solid, a good wetting can be achieved. The second step is to



determine the ratio of dispersive and polar energy contribution of both phases. As seen for instance for the pristine low-k 1 sample, a large difference in the ratio of dispersive and polar energy parts will prohibit good wetting. In this special case the missing of any polar energy part of the dielectric will complicate wetting due to the fact that all cleaning liquids studied have a polar energy contribution, which cannot interact with a totally dispersive surface.

The results show that the determination of the energetic character of solid and liquid can be applied to find the appropriate combination of both for best wetting. Additional wetting tests of any available cleaning solution on the surface are not necessary. If e.g. a surface has a very low energy, high energetic cleaning solutions can be excluded from testing or application.

This procedure to find the best combination of solid and liquid has to be reconsidered if for instance the solid is expected to have a high roughness. As described on chapter 3.2.2. surface roughness can strongly affect the wetting behavior of a solid surface and should be analyzed.

## **6.6. Selection of cleaning solution to be optimized in their wetting behavior**

The results of the surface energy calculations show that the majority of solid surfaces, whether they are CF containing polymers, surfaces after etching processes or copper, have a low surface energy of below 45 mN/m. The introduction of a polar energy contribution to the completely dispersive low-k dielectrics supports their wetting behavior due to the fact that all studied cleaning solutions also have a more or less large polar energy part. In most cases this change in energy characteristics of the solid is not enough to ensure a good wetting by water based cleaning solutions, because the difference of the surface energies of solid and liquid

is too big. In Table 6-7 the differences between total surface energy of the studied cleaning solutions and a selection of the analyzed solid surfaces are shown.

The low energetic cleaning solutions having a water content lower than 50 % will show a good wetting behavior on most solid surfaces due to a low difference in surface energy. Cleaning solutions with higher water content, especially solution C1 containing more than 80% water, will not be able to form small contact angles on the solids studied in this work and need to be optimized regarding their wetting behavior. One approach is to lower their surface energy by the application of surfactants and will be described in the following chapter for the high energetic cleaning solutions B1, B2 and C1.

**Table 6-7:** Differences in total surface energy of the cleaning solutions and a selection of solid surfaces studied in this work. Negative or very small values indicate the best wetting behavior of the system solid / liquid. For the solutions with high water content the wetting of most of the studied solid surfaces will be difficult due to the large energetic difference between both.

Water content →		< 50 %			50 - 80 %		> 80 %
Solid surfaces ↓		A1	A2	A3	B1	B2	C1
porous and dense low-k dielectrics before and after etching processes	low-k 1	11,27	4,77	30,17	27,07	38,07	43,97
	low-k 1 + ME	3,81	-2,69	22,71	19,61	30,61	36,51
	low-k 1 + VE	-2,88	-9,38	16,02	12,92	23,92	29,82
	low-k 1 + Ar8	-5,84	-12,34	13,06	9,96	20,96	26,86
	low-k 3	14,6	8,1	33,5	30,4	41,4	47,3
	low-k 3 + Ar8	2,8	-3,7	21,7	18,6	29,6	35,5
	low-k 3 + O28	-29,96	-36,46	-11,06	-14,16	-3,16	2,74
	low-k 4	6,37	-0,13	25,27	22,17	33,17	39,07
	low-k 4 + CO8	-5,08	-11,58	13,82	10,72	21,72	27,62
	low-k 4 + N28	-20,23	-26,73	-1,33	-4,43	6,57	12,47
Etch residues	Poly30	3,69	-2,81	22,59	19,49	30,49	36,39
	C4F88	11,28	4,78	30,18	27,08	38,08	43,98
	H28	11,92	5,42	30,82	27,72	38,72	44,62
stripping processes	PS1	5,03	-1,47	23,93	20,83	31,83	37,73
	PS2	-1,19	-7,69	17,71	14,61	25,61	31,51
	PS3	-18,71	-25,21	0,19	-2,91	8,09	13,99
Metals and barriers	Cu1	7,93	1,43	26,83	23,73	34,73	40,63
	CoWP	5,52	-0,98	24,42	21,32	32,32	38,22
	TiN	-1,1	-7,6	17,8	14,7	25,7	31,6
	TaN	-14,1	-20,6	4,8	1,7	12,7	18,6
Other	low-k 1 + CMP	-1,95	-8,45	16,95	13,85	24,85	30,75
	OMCTSHM	5,44	-1,06	24,34	21,24	32,24	38,14

Legend				
Surface energy difference	< 5 mN/m	5 - 15 mN/m	15 - 30 mN/m	> 30 mN/m

## **7. Optimized wetting of cleaning solutions by application of surfactants**

### **7.1. Process and sample description**

#### **7.1.1. Selection of surfactants**

The selection of surfactants for decreasing the surface energy of the cleaning solutions B1, B2 and C1 was performed under several points of view: the samples should cover a wide range of surfactant types, be easy and safe in handling (nontoxic), environmentally friendly with no or low foaming. One focus was on nonionic surfactants due to their good compatibility to many solvent systems. Additionally anionic, fluorinated and silicon-containing surfactants have been studied. Cationic surfactants have been excluded due to environmental issues. The surfactants used in this work are described below.

#### *Nonionic surfactants*

- 1) Envirogem™ 360 (EG360): Low-foam, nonionic Gemini-surfactant with HLB 3 - 4, highly biodegradable and environmentally friendly
- 2) Carbowet™ 100 (CW100): Low-foam surfactant with HLB 10 – 11, based on ethoxylated 2,4,7,9-Tetramethyldec-5-yne-4,7-diol (TMDD, chemical structure can be seen in Figure 7-1)

Surfynol™ series:

Acetylene diol based nonionic Gemini-surfactants with 2 hydrophilic and at least 2 hydrophobic parts in one molecule; highly surface active with low foaming.

- 3) Surfynol™ 104 E (S104E): Surfactant in ethylene glycol, HLB 4
- 4) Surfynol™ 2502 (S2502): Ethoxylated/propoxylated form of the surfactant base, HLB 7 – 8
- 5) Surfynol™ 465 (S465): Ethoxylated form of the surfactant base, HLB 13
- 6) Surfynol™ 485 (S485): Ethoxylated form of the surfactant base, HLB 17
- 7) Tetronic™ 701 (Tetra): Ethylenediamine tetrakis(propoxylate-block-ethoxylate) tetrol; low-foam tetra-functional block ethoxylate) tetrol; low-foam tetra-functional block copolymer with HLB 1 – 7 (chemical structure can be seen in Figure 7-2)

Anionic surfactants

- 1) Glycolic acid ethoxylate 4-nonylphenyl ether (GACnonyl): slightly foaming surfactant (chemical structure can be seen in Figure 7-3)
- 2) Glycolic acid ethoxylate lauryl ether (GAClauryl): slightly foaming surfactant (chemical structure can be seen in Figure 7-4)

Special surfactants:

- 1) Zonyl™ PFBE fluorotelomer (Fluoro): PFBE stands for perfluorobutylethylene, fluorocarbon based surfactant (chemical structure can be seen in Figure 7-5)
- 2) Tegotronic™ SC (Silox): polyether modified trisiloxane, “superspreader” surfactant (chemical structure can be seen in Figure 7-6)

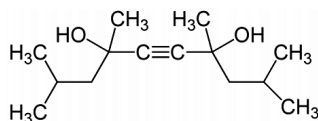


**Figure 7-1:** 2,4,7,9-Tetramethyldec-5-yne-4,7-diol

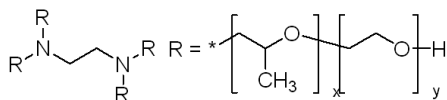


**Figure 7-2:** Ethylenediamine tetrakis(propoxylate-block-ethoxylate) tetrol

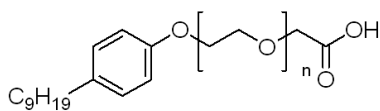


**Figure 7-3:** Glycolic acid ethoxylate 4-nonylphenyl ether

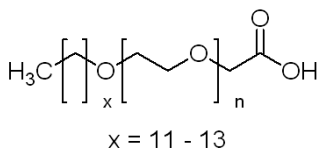


**Figure 7-4:** Glycolic acid ethoxylate lauryl ether



have been performed to determine the influence of surfactant solutions on metals and barrier materials.

## **7.2. Dynamic surface energy of DIW-mixed surfactants**

All surfactants have been mixed in deionized water (DIW) at several concentrations beginning from 0.02 % up to 0.1 % in steps of 0.02 % (all values are volume percent). The dynamic surface tension of each solution has been determined by maximum bubble pressure measurement at surface ages from 20 ms up to 1000 ms. In Figure 7-7 the dynamic behavior of the solutions at a concentration of 0.08 % is shown (all other data can be found in the appendix section E).

The lowest surface energy is reached by the silicon containing surfactant with 23.8 mN/m, but shows a strong slope of the dynamic surface energy at low surface ages. A fast adsorbing surfactant is S485 but does not reach a low surface energy. The fluorinated surfactant Zonyl did not show a dynamic surface energy reduction, which may be due to a very low adsorption speed.

Due to the broad range of dynamic behavior of the surfactant solutions the selection of species to be used for the following studies was done by the lowest surface energy reached at 1000 ms surface age and the slope of the curves, which stands for the dynamic behavior of the solutions. The slope has been determined by adding an exponential trendline to each curve, where a lower value stands for a higher adsorption speed.



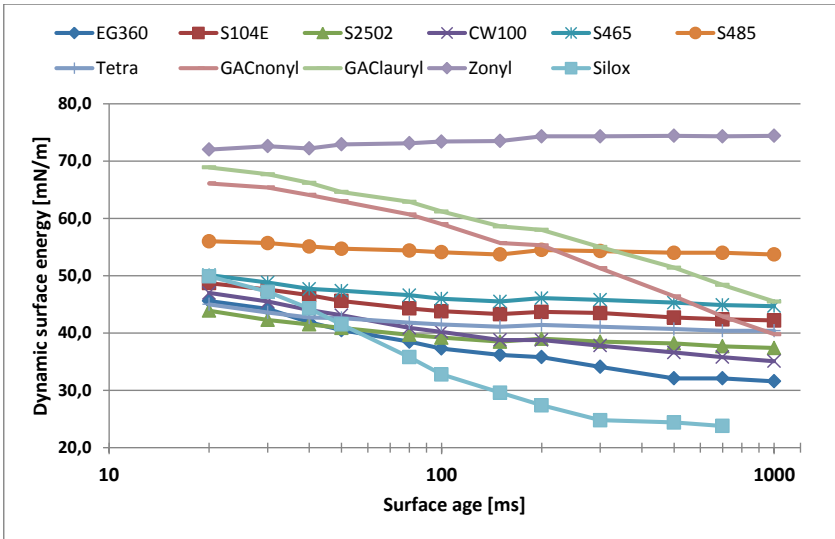


**Figure 7-7:** Dynamic behavior of the studied surfactants mixed in DIW at a concentration of 0.8%. The solutions show a broad range of adsorption speeds and lowest reachable surface energy. This gives rise to the assumption that a compromise between both attributes has to be made selecting appropriate surfactants.

The results in Table 7-1 show that in most cases a compromise between low surface energy and low adsorption speed has to be made, but surface energy was decided to have a higher priority. A limit at around 40 mN/m is set due to the fact that most of the solid surfaces analyzed in the previous chapter have a surface energy comparable to this. Four surfactants have been selected for further analysis: EG360 due to its low surface energy and a medium slope, S2502 due to a surface energy smaller than 40 mN/m and a small slope, Tetra due to its very small curve slope and a medium surface energy and Silox due to its very low surface energy. Also GACnonyl has a surface energy slightly below 40 mN/m, it was excluded due to its tendency to foaming.

**Table 7-1:** The minimal dynamic surface energy at 1000 ms surface age and the slope of the dynamic curves of all studied surfactants. For further studies the selection of surfactants was done by both values and is marked in this table.

	Minimal surface energy [mN/m]	Slope	Selected for further investigation
EG360	31.6	-3.7	X
S104E	42.2	-1.5	
S2502	37.4	-1.5	X
CW100	35.1	-3.0	
S465	44.7	-1.2	
S485	53.7	-0.5	
Tetra	40.4	-1.0	X
GACnonyl	39.8	-6.9	
GAClauryl	45.5	-5.9	
Zonyl	74.4	0.7	
Silox	23.8	-8.0	X

**Legend**

> 60 mN/m	< 60 mN/m	< 50 mN/m	< 40 mN/m	< 30 mN/m	Surface energy
> 7	< 7	< 5	< 3	< 1	Slope

### 7.3. Dynamic surface energy of surfactants mixed in cleaning solutions

#### 7.3.1. Analysis at room temperature

The four selected surfactants EG360, S2502, Tetra and Silox have been mixed in the cleaning solutions B1, B2 and C1 at concentrations of 0,1 %. Bath temperature was kept at room temperature for the dynamic surface energy analysis. The results are shown in Figure 7-8.

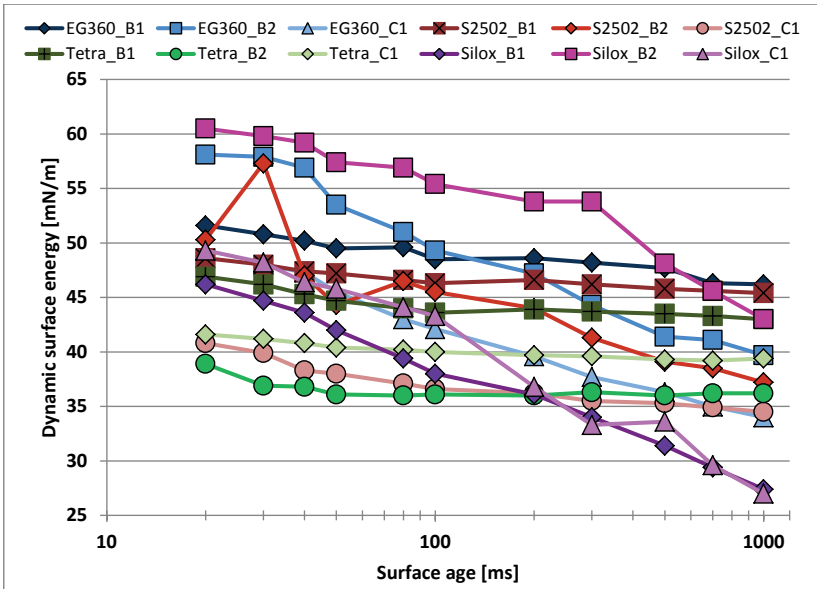


**Figure 7-8:** Dynamic behavior of the selected surfactants at room temperature mixed in cleaning solutions B1, B2 and C1 at a concentration of 0.1 %. In all cases the dynamic surface energy decreased, but only few solutions reached a dynamic equilibrium.

In all cases the total surface energy of the cleaning solution was reduced, but surfactant addition also changed the dynamic behavior of the liquids and only in a few cases a dynamic equilibrium could be reached. Figure 7-9 shows the change of total surface energy of the solutions using the lowest surface energy reached at a surface age of 1000 ms.

The highest reduction in total surface energy compared to the initial value was possible for solution C1 with the largest water content, where a reduction from 72 mN/m to less than 30 mN/m was possible using Silox. For solution B1 also Silox reached the lowest value in surface energy, but compared to initial surface energy

the reduction is much lower for all other surfactants. The results imply that cleaning solutions with high water content profiteer most by surfactant addition.

In Figure 7-10 the slopes of the curves are compared to the values the surfactant solutions reached when mixed in DIW. Using Tetra the changes of the slope only slightly changed compared to the initial conditions. When mixed in B1 the slope could be reduced for all surfactants while for other solutions no clear trend of dynamic behavior was found. This implies that the water content of the solutions does not directly impact on dynamic surface tension when applying surfactants.

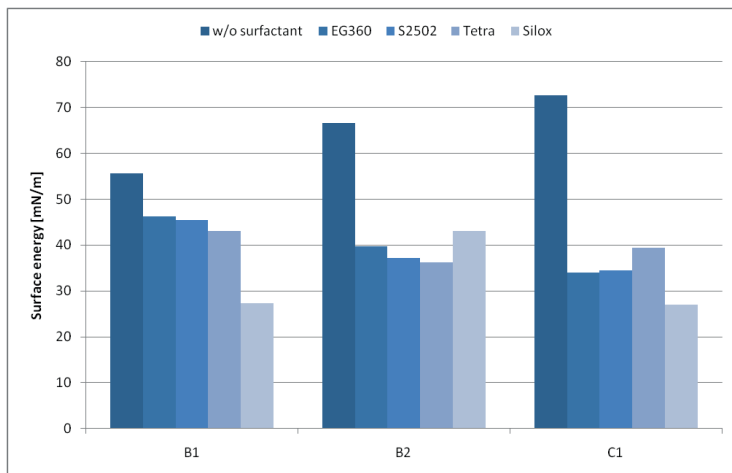


**Figure 7-9:** The lowest surface energy reached at a surface age of 1000 ms when applying surfactants to the cleaning solutions B1, B2 and C1. The largest effect was found for the solution with the highest water content.

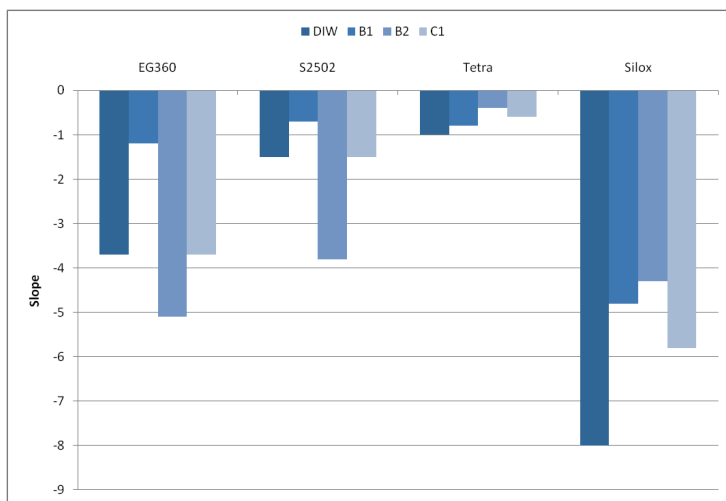


**Figure 7-10:** Slopes of the dynamic surface energy curves of surfactants mixed in cleaning solutions B1, B2 and C1. The dynamic behavior strongly differs for different surfactants and cleaning solutions. A general prediction of the surfactant's behavior added to a cleaning solution with a certain amount of water cannot be given.

### 7.3.2. Impact of surfactant addition on the static surface energy of the cleaning solutions

The cleaning solutions B2 and C1 additionally have been investigated regarding their static surface energy characteristic after adding 0.1 % of the surfactants EG360, S2502 and Tetra. By contact angle measurements the dispersive and polar surface energy contributions have been determined. In contrast to the dynamic behavior of the solutions, which is strongly affected by the addition of surfactant species, the static dispersive and polar energy characteristics only slightly change. The investigation showed that the main effect of surfactant addition is the lowering of the total surface energy values of the solutions (Figure 7-11). Solution B2 showed only slight changes of the percentages of the polar and dispersive energy contributions, which means that the besides the lowering of the total surface energy

value the energetic character of the liquid is only slightly affected by the surfactants (Figure 7-12). An addition of EG360 and S2502 to solution C1 showed a decrease of the polar energy part of about 10-20%, nearly equalizing the energetic character of this solution to the characteristics of solutions B2.

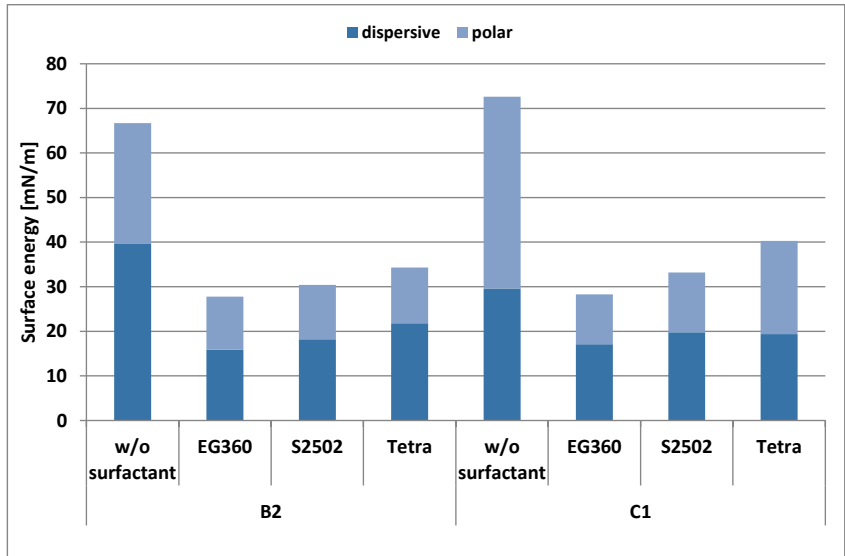


**Figure 7-11:** Static energy characteristics of solution B2 and C1 after adding the surfactants EG360, S2502 and Tetra. The investigation showed that the main effect of surfactant addition is the lowering of the total surface energy values of the solutions

### 7.3.3. Analysis at increased bath temperature

The cleaning solutions analyzed in this work are developed not only for processes at room temperature, but also for temperature ranges up to 50°C. In most cases the supplier of the solutions gives an advice in which range best cleaning results can be achieved. The liquids studied are suitable to be used at temperature ranges from room temperature up to 45°C and effects on the dynamic behavior of a surfactant at

higher temperatures are not known yet. To determine the influence of a higher bath temperature dynamic measurements at 35°C have been performed.

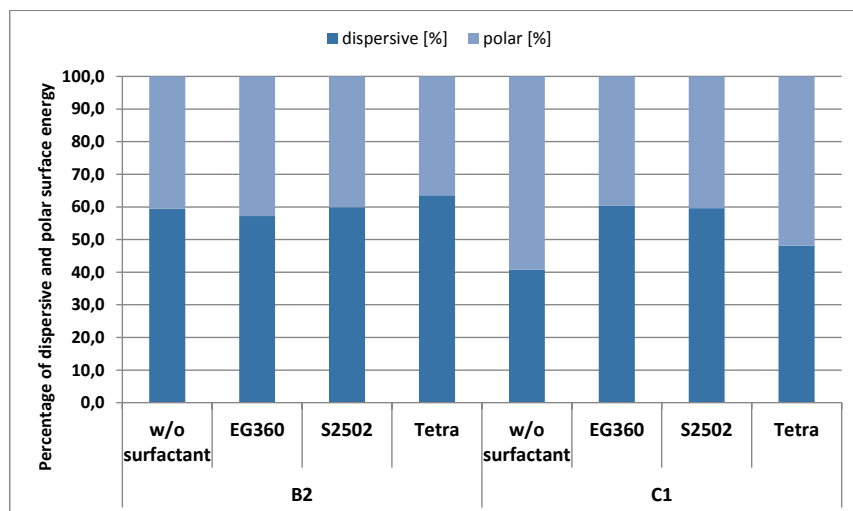


**Figure 7-12:** Percentages of dispersive and polar surface energy contributions of solutions B2 and C1 after adding the surfactants EG360, S2502 and Tetra.

Figure 7-13 compares the dynamic surface energy of S2502 mixed in B1, B2 and C1 at room temperature and at 35°C bath temperature. The dynamic behavior of the surfactant solutions only slightly changes at increased temperature, which can be seen for all 4 surfactants applied (see appendix section F). This implies that in a medium temperature range the dynamic surface energy of the surfactant solution is not affected.

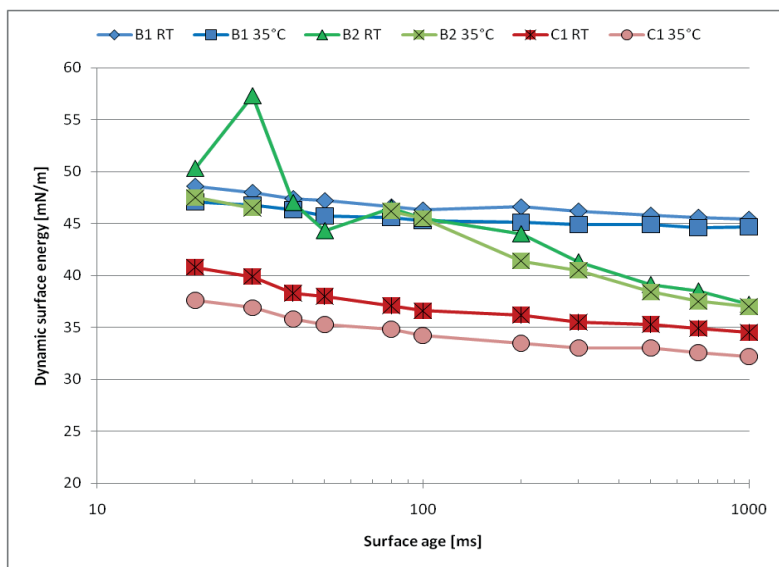


**Figure 7-13:** Comparison of the dynamic behavior of S2502 mixed in solution B1, B2 and C1 at room temperature and a bath temperature of 35°C. The results show that at medium bath temperature the dynamic behavior of the surfactant solutions is only slightly changed.

#### 7.3.4. Long term stability of surfactant solutions

A cleaning solution with optimized wetting behavior by adding a surfactant has to show stable dynamic parameters if the surfactant is mixed into the solution long before use. To determine whether a surfactant aided solution is stable over a long time all 4 studied surfactants have been mixed with the cleaning solutions B1, B2 and C1 at a concentration of 0,1 %. The dynamic surface tension has been measured just after mixing and 7 weeks after surfactant addition.

Table 7-2 shows the change in dynamic surface energy after 7 weeks. Only EG360 and S2502 seem to be stable after this time in all cleaning solutions. Tetra shows a large energy change in solution B2 at low surface ages and normalizes at high



surface ages. Most critical is the long term behavior of Silox. Mixed in B2 the changes are in a medium range, but mixed in B1 and C1 a large increase in surface energy can be seen. This may be due to the destruction of the surfactant and therefore to a decreased concentration of surfactant molecules within the liquid. If less molecules exist in the solution, the decrease in dynamic surface tension with increasing surface ages cannot be as large as for higher concentrations. The same was found for low surfactant concentrations in DIW. With increased concentration a lower surface energy could be reached at 1000 ms surface age. This implies that if Silox should be applied to a cleaning solution, it has to be added just before use of the liquid.

**Table 7-2:** Long term stability of surfactants mixed in the cleaning solutions B1, B2 and C1. After 7 weeks only EG360 and S2502 seem to be unchanged while especially Silox shows a large difference in dynamic surface energy. This may be due to the fact that silicon containing surfactants are known to be easily destroyed in aqueous media by hydrolysis.

Solution B1				
Surface age [ms]	EG360	S2502	Tetra	Silox
20	-0,3	-0,4	1,6	10,5
30	0	-0,3	1,4	12,1
40	-0,4	-0,2	1	12,6
50	0,1	-0,4	0,9	14,4
80	-0,7	-0,3	0,3	16,9
100	0	-0,3	0,6	18
200	-0,4	-0,6	0,2	20,1
300	-0,7	-0,5	-0,1	22,1
500	-0,6	-0,3	0	24,9
700	0	-0,2	0,1	26,8
1000	-1	-0,1	0,1	28,7

Solution B2				
Surface age [ms]	EG360	S2502	Tetra	Silox
20	3	-0,9	28,8	2,2
30	2	-10	30,2	1,9
40	1	-1,8	29,3	2,5
50	2,2	-1	29,2	4,2
80	1,2	-5,9	27	4,1
100	1,2	-6,3	25,4	4,7
200	-0,7	-6,5	19,5	6,4
300	-0,7	-5,2	15,2	6,1
500	-0,1	-3,7	12	11,2
700	-1,3	-3,9	9,7	13,5
1000	-2,1	-3,1	8,1	15,9

Solution C1				
Surface age [ms]	EG360	S2502	Tetra	Silox
20		0	8,8	13,2
30	2,7	-0,5	6,9	13,7
40	0,4	0,4	5,1	15,2
50	0,5	0	4,7	16
80	0	-0,1	3,5	17,7
100	-0,7	-0,1	3,4	18,1
200	-0,5	-0,1	2,9	24,5
300	-0,7	0,2	2,4	28,1
500	-1,5	-0,1	2,4	27,9
700	-0,8	-0,2	2,4	31,7
1000	-1,3	-0,2	1,7	34,1

**Legend****absolute deviation**

< 3 mN/m	< 8 mN/m	< 15 mN/m	≥ 15 mN/m
----------	----------	-----------	-----------

## 7.4. Compatibility of surfactant solutions to a porous low-k dielectric

### 7.4.1. Surfactants mixed in DIW

All studied cleaning solutions have been designed to be compatible to common materials used within BEOL processing. This especially includes their compatibility to porous low-k dielectrics and copper, which means that optical, electrical and structural properties of the materials are not affected by the solutions and there is no loss of material due to etching or corrosion in the case of copper. Solutions B1, B2 and C1 have been investigated regarding their effects on low-k 1 and Cu1 and were found to not degrade the properties of the materials. As reported in chapter 6 solutions B1, B2 and C1 need to be optimized regarding their wetting behavior, which can be done by application of surfactants.

**Table 7-3:** Refractive index, k-value and leakage current density of the porous low-k 2 treated by surfactants mixed in DIW. The results show that optical and electrical parameters of the material are degraded when applying a DIW rinse after the treatment. Using IPA for rinsing nearly recovers material properties.

		n	k	J [A/cm <sup>2</sup> ]
	Reference	1,3604	2,24	1,60E-10
	IPA only	1,3507	2,11	1,60E-10
Surfactant	Rinse			
EG360	DIW	1,5685	3,7	4,00E-06
S2502		1,5514	3,03	1,40E-06
Silox		1,429	2,86	1,60E-06
Tetra		1,389	2,42	1,10E-09
EG360	IPA	1,364	2,2	2,2E-10
S2502		1,3729	2,08	5,2E-10
Silox		1,397	2,06	4,50E-09
Tetra		1,373	2,34	9,1E-10

**Legend**

< 1,38	< 1,4	< 1,42	> 1,42	Refractive index
< 2,4	< 2,6	< 2,8	> 2,8	k-value
1E-10	1E-9 - 1E-8	1E-7 - 1E-6	> 1E-6	J (order of magnitude)

Besides the decrease in surface energy and proper dynamic parameters a surfactant aided cleaning solution has to be compatible the materials used within the interconnect system. To test the effects of a surfactant solution on a porous low-k material the low-k 2 samples have been treated with surfactants mixed in deionized water (DIW) at a surfactant concentration of 0,1% for 1 minute. After immersion the samples have been rinsed with DIW or isopropyl alcohol (IPA) for 3 minutes. Table 7-3 shows the results of optical and electrical analysis after surfactant treatment. Except the samples treated with Tetra all DIW rinsed samples show a strong increase in refractive index, k-value and leakage current density. For the

Tetra solution these values only slightly increased. Rinsing with IPA did not lead to a degradation of optical and electrical parameters of low-k 2. The k-values marked red in **Table 7-3** are much too low and may result from a failure in the CV-measurement, which could not be explained till now, and should not be considered. In Figure 7-14 the section of functional groups of the FTIR spectra recorded for all surfactant treated samples is shown. This section of the spectra turned out to give the best hint whether or not surfactant residues are present within the porous material. Within the fingerprint area of the spectra the peaks of the Si-O-Si skeleton of the low-k material and the peaks assigned to the surfactants overlap and are therefore not exactly detectable. In the spectra of Figure 1 the region of functional  $\text{CH}_x$  groups with the main  $\text{CH}_3$  peak at  $2975\text{ cm}^{-1}$  are shown.

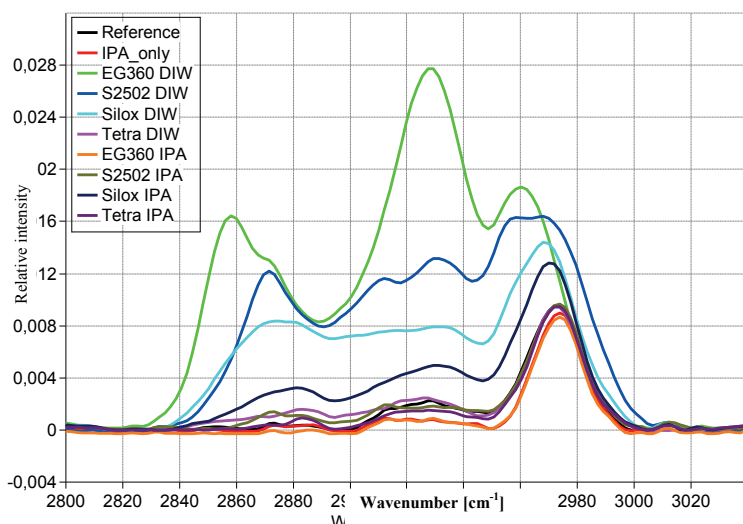
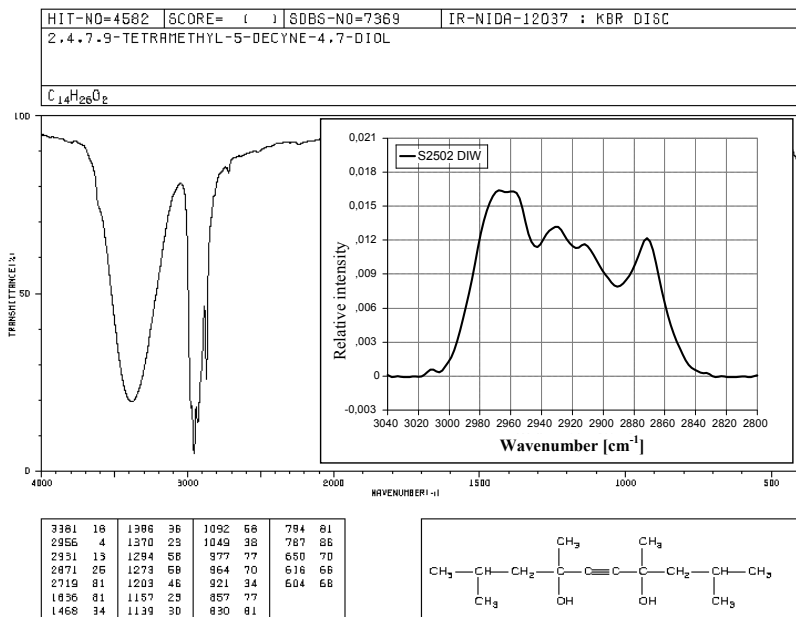


**Figure 7-14:** Functional group section of the FTIR spectra recorded for surfactant treated porous low-k 2 dielectric using DIW and IPA for rinsing. After DIW rinsing additional  $\text{CH}_x$  peaks occur, which cannot be assigned to the low-k material and are therefore thought to be caused by residual surfactant species within the dielectric. After IPA rinsing those peaks nearly vanished.

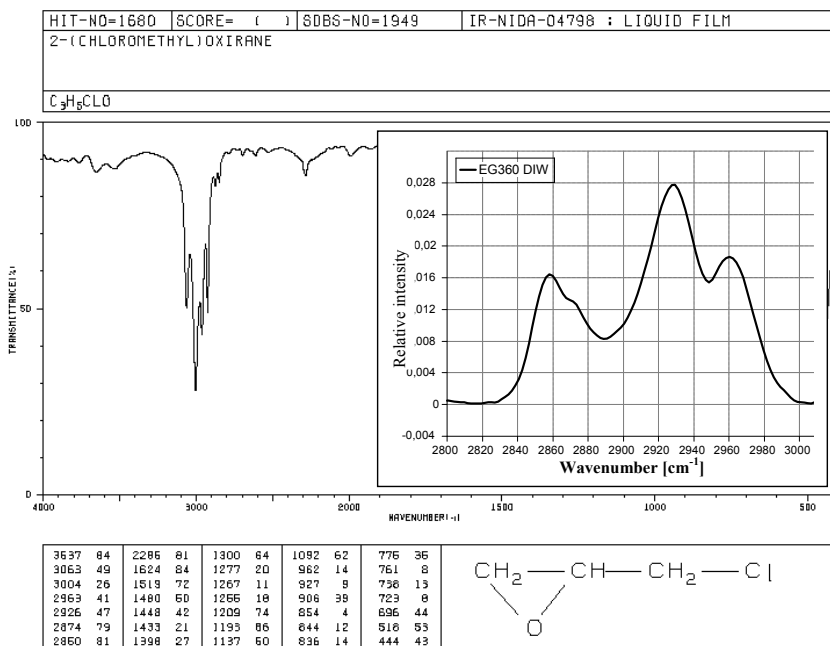
The DIW rinsed samples show a strong increase in  $\text{CH}_3$  and the introduction of additional  $\text{CH}_x$  peaks at lower wavenumbers. Those peaks vanish if the samples are rinsed with IPA. Peaks from  $2840\text{--}2870\text{ cm}^{-1}$  and from  $2915\text{--}2940\text{ cm}^{-1}$  belong to a medium to strong C-H stretching vibration (symmetrical and asymmetrical) of  $-\text{CH}_2-$  fragments. The ranges  $2865\text{--}2885\text{ cm}^{-1}$  and  $2950\text{--}2975\text{ cm}^{-1}$  can be assigned to a medium to strong C-H stretching (symmetrical and asymmetrical) of R- $\text{CH}_3$  components. This large amount of additional  $\text{CH}_x$  species cannot be declared by a change in the low-k composition but by the remaining of surfactant species within the porous material structure. The solution containing EG360, S2502 and Silox show the highest amount of residual surfactants within the low-k dielectric, while for Tetra this effect is not observed. DIW rinsing therefore is not able to remove all surfactant species. After IPA rinse the residual surfactants nearly vanished. Only for Silox a slight increase in  $\text{CH}_x$  species remained.

Figure 7-15 a shows the transmission spectrum of TMDD, which is the basic structure of S2502 and Figure 7-15 b shows the functional groups section of low-k 2 after treatment with S2502. Comparison of the section of functional groups in the FTIR spectra shows that strong peaks at  $2871\text{ cm}^{-1}$ ,  $2931\text{ cm}^{-1}$  and  $2956\text{ cm}^{-1}$  can be found in both spectra, which supports the assumption of residual surfactants species within the dielectric after DIW rinsing. The additional peaks occurring in the FTIR spectrum in Figure 7-15 b may be due to the fact that S2502 is an ethoxylated and propoxylated version of TMDD. Comparable results can be found looking at the transmission spectrum of 2-(chloromethyl)-oxirane shown in Figure 7-16 a, which is one of the basic compounds of EG360 (Figure 7-16 b). Peaks around  $2860\text{ cm}^{-1}$ ,  $2874\text{ cm}^{-1}$ ,  $2926\text{ cm}^{-1}$  and  $2963\text{ cm}^{-1}$  can be seen in both spectra and cannot be assigned to the low-k material, which gives rise to the assumption that those peaks

belong to residual surfactant species remaining within the porous structure of the dielectric after DIW rinsing.



**Figure 7-15:** Transmission spectrum of TMDD (section of functional groups) and the same spectral region of a S2502 treated porous low-k dielectric (inset). Typical peaks of the  $CH_x$  region occur in both spectra and give rise to the assumption that the additional peaks in the SiCOH-spectra are caused by residual surfactant species. (Source: Spectral Database for Organic Compounds, SDBS)



**Figure 7-16:** Transmission spectrum of 2-(chloromethyl) oxirane (functional groups) and the same spectral region of the EG360 treated low-k 2 material. 2-(chloromethyl) oxirane is one of the main components of EG360 and typical peaks of this substance can also be found in the SiCOH-spectrum after surfactant treatment. (Source: Spectral Database for Organic Compounds, SDDBS)

Additionally increase of DIW rinsing time from 3 minutes to 10 minutes was performed. Figure 7-17 shows the spectra of low-k 2 after treatment with Silox and Tetra at increased rinsing times. The additional CH<sub>x</sub> peaks for Silox can be seen with a comparable intensity for both rinsing times which means that residual surfactant species could not be removed. Increased rinsing times did not show an adversarial effects on Tetra treated samples.



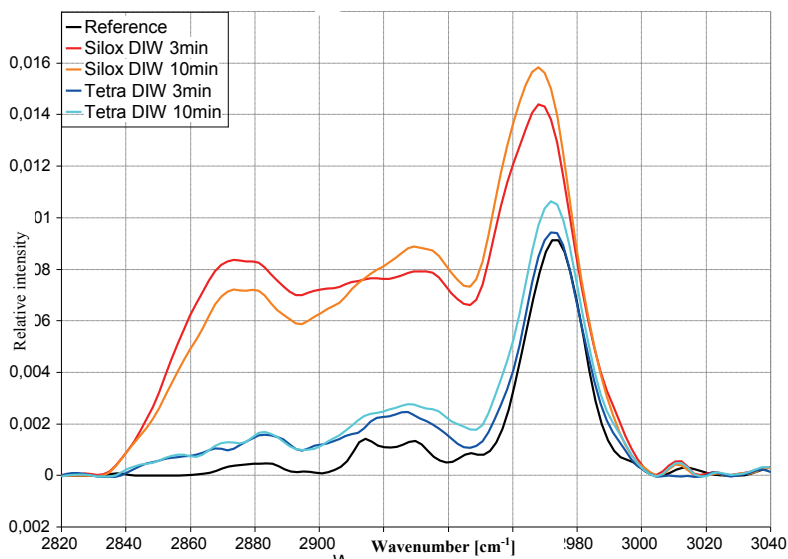


**Figure 7-17:** FTIR spectra of low-k 2 after treatment with Silox and Tetra with increased DIW rinsing time. An increase of the DIW rinsing time from 3 to 10 minutes has no effect and the peaks assigned to the residual surfactant species still occur with comparable intensity.

#### 7.4.2. Surfactants mixed in cleaning solutions at room temperature

The selected surfactants have been mixed with the cleaning solutions B1, B2 and C1 at a concentration of 0,1%. Low-k 2 samples have been immersed in these solutions for 3 minutes followed by a 3 minute rinse using DIW or IPA. Additionally for Silox and Tetra the rinsing time has been increased to 10 minutes. Optical, electrical and structural parameters of the low-k samples have been determined to test the compatibility of the surfactant aided solutions to this material.

**Table 7-4:** Refractive index, k-value and leakage current density of low-k 2 samples treated with the surfactant aided cleaning solutions B1, B2 and C1. As seen for the surfactants mixed in DIW an IPA rinse is necessary to recover the material's properties after surfactant treatment.

			n	k	J [A/cm²]
		Reference	1,3604	2,24	1,60E-10
Surfactant	Rinse	Cleaner			
EG360	DIW	B1	1,584	3,12	6,10E-05
		B2	1,555	3,64	4,40E-05
		C1	1,553	3,36	5,80E-05
	IPA	B1	1,386	2,63	6,00E-07
		B2	1,403	2,31	3,80E-05
		C1	1,388	2,34	4,40E-06
S2502	DIW	B1	1,426	5,06	2,00E-04
		B2	1,494	2,9	5,00E-06
		C1	1,521	2,92	4,30E-06
	IPA	B1	1,373	3,79	7,50E-05
		B2	1,403	2,47	1,20E-05
		C1	1,359	2,24	4,50E-08
Silox	DIW	B1	1,421	2,57	9,60E-08
		B2	1,429	2,46	1,60E-07
		C1	1,48	2,41	2,00E-07
	IPA	B1	1,368	2,33	6,20E-09
		B2	1,373	2,37	1,30E-06
		C1	1,377	2,37	4,50E-08
Tetra	DIW	B1	1,384	2,45	1,60E-08
		B2	1,389	2,23	2,60E-09
		C1	1,385	2,31	5,00E-08
	IPA	B1	1,366	2,29	1,50E-06
		B2	1,409	2,35	2,50E-07
		C1	1,378	2,33	7,90E-10

#### Legend

< 1,38	< 1,4	< 1,42	> 1,42	Refractive index
< 2,4	< 2,6	< 2,8	> 2,8	k-value
1E-10	1E-9 - 1E-8	1E-7 - 1E-6	> 1E-6	J (order of magnitude)

Table 7-4 shows the refractive index, k-value and leakage current density of the low-k samples after surfactant treatment. As seen for the surfactants mixed in DIW the samples rinsed with DIW show a strong increase in refractive index and k-value, except the Tetra aided solutions. In most of the cases an IPA rinse recovers the material parameters. Only for S2502 mixed in cleaner B1 the k-value could not be decreased to a value comparable to the reference.

The leakage current densities of almost all samples treated with the surfactant solutions are found to be 2-5 orders of magnitude higher than the reference value and the rinsing solutions do not seem to have a clear influence on this. Especially for EG360 and S2502 the increase in leakage current density is very high. It is not clear if this is due to the surfactant treatment, because the samples used for EG360 and S2502 originate from another low-k 2 wafer than those for Silox and Tetra. Figure 7-18 shows the section of functional  $\text{CH}_x$  groups of the surfactants mixed in cleaner B1 and compares the influence of the applied rinsing solutions. As seen for the surfactants mixed in DIW, residual surfactant species represented by additional  $\text{CH}_x$  peaks can only be found for the DIW rinsed samples, except samples treated with Tetra. Although cleaner B1 contains an organic solvent, an IPA rinse is necessary to recover the material properties of the low-k dielectric. The IPA rinsed samples do not show remnants of the surfactants. Comparable results have been found for the cleaning solutions B2 and C1, but the intensity of the additional  $\text{CH}_x$  peaks depends on the type of cleaner applied.

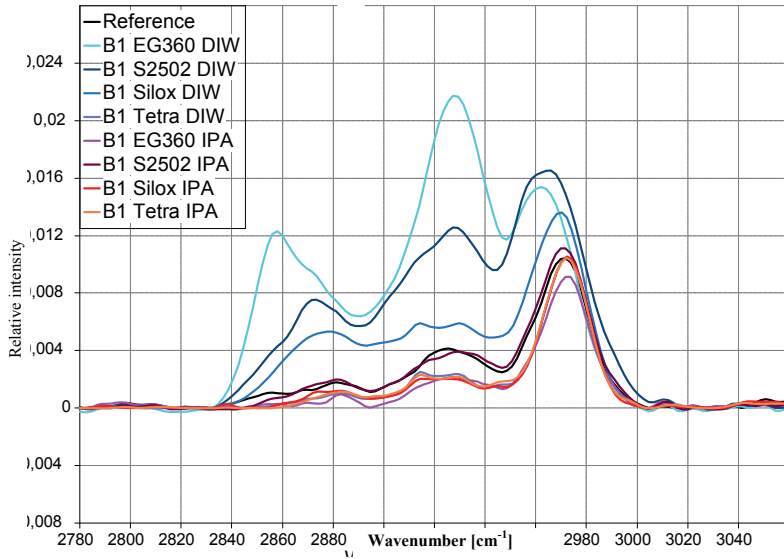


**Figure 7-18:** FTIR spectra of low-k 2 samples treated with the surfactant aided cleaning solution B1. Dispite for Tetra an IPA rinse is necessary to remove residual surfactant species.

In Figure 7-20a and b EG360 and S2502 are compared regarding their influence on the low-k material when mixed in different cleaning solutions. The spectra show that mixing in B1 results in the lowest peak intensity while surfactants mixed in B2 produce the highest intensity.

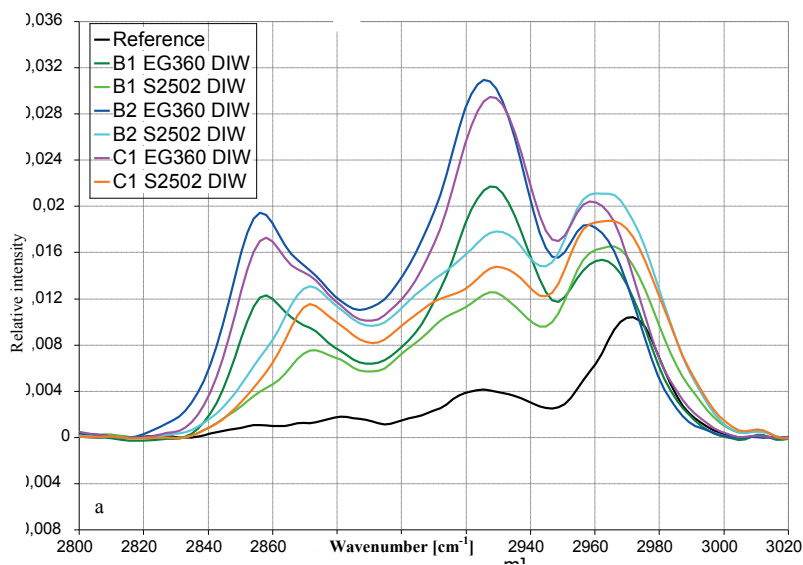


**Figure 7-19:** Comparison of EG360 and S2502 mixed in different cleaning solutions and their effect on low-k 2 samples. a) DIW rinsing, b) IPA rinsing. Peak intensities not only differ for the two surfactants but also for the solutions they are applied to. For solution B2 the highest peak intensities were found. The solutions also showed an influence on surfactant removal using an IPA rinse (b); S2502 mixed in B2 was not removed completely.

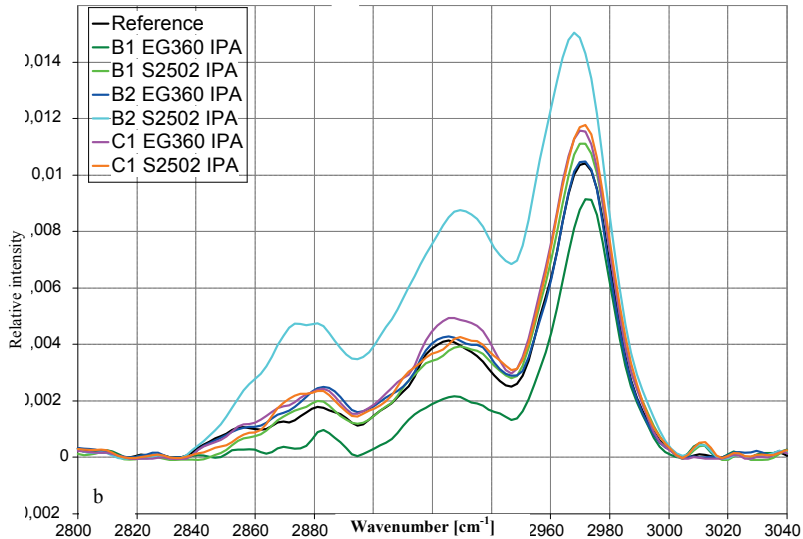


**Figure 7-20:** Comparison of EG360 and S2502 mixed in different cleaning solutions and their effect on low-k 2 samples. a) DIW rinsing, b) IPA rinsing. Peak intensities not only differ for the two surfactants but also for the solutions they are applied to. For solution B2 the highest peak intensities were found. The solutions also showed an influence on surfactant removal using an IPA rinse (b); S2502 mixed in B2 was not removed completely.

#### 7.4.3. Surfactants mixed in cleaning solutions at elevated bath temperature

The influence of bath temperature on the low-k 2 samples has been tested under the same conditions as before at a bath temperature of 35°C. Only a small influence on the refractive index can be seen with 6,5% as the highest change compared to samples treated at room temperature. The k-value shows a wide distribution with no clear trend regarding surfactant or rinsing solution. In most cases a small to medium increase has been detected. Only the samples treated with S2502 in B1 show a strong decrease in k-value. The leakage current density of the EG360 and S2502 treated samples clearly decreased by 1-5 orders of magnitude while J of the

Silox and Tetra treated samples only slightly changed (Table 7-5). It is not clear if the strong decrease in leakage current density for EG360 and S2502 is an effect of the bath temperature. The samples used in this study have been cut from the same wafer as the Silox and Tetra treated samples in the last experimental series at room temperature. So the changes of  $J$  can also be due to a contamination of the used low-k substrate.

The spectra in Figure 7-21 show the comparison of EG360 and S2502 mixed in cleaner B1 and C1 at room temperature and at 35°C. The rinsing solution in all cases was DIW. For EG360 mixed in B1 almost no influence of the bath temperature can be seen while the peak intensity of the S2502 treated samples decreases at 35°C. EG360 mixed in C1 shows a decrease and S2502 an increase in peak intensity of  $\text{CH}_x$  species. The results show that the effect of elevated bath temperatures strongly depends on the type of cleaning solution and surfactant used and no universal prediction is possible.

**Table 7-5:** Change of refractive index, k-value and leakage current density of low-k 2 samples treated with surfactant solutions at elevated bath temperature. While n is only slightly affected, the k-values show a broad distribution and no clear trend dedicated to elevated bath temperature can be found. The large changes in J can be due to a contamination of the substrates used for the studies at room temperature and cannot be clearly assigned to an effect of elevated bath temperature.

Surfactant	Rinse	Cleaner	n	k	J [A/cm <sup>2</sup> ]
EG360	DIW	B1	-1,5	2,9	-2
		B2	2,0	2,2	-2
		C1	1,8	18,5	-2
	IPA	B1	-0,5	4,6	-1
		B2	-1,4	28,1	-1
		C1	-1,7	-8,5	-4
S2502	DIW	B1	6,1	-50,2	-4
		B2	6,3	7,6	-2
		C1	2,9	6,2	-2
	IPA	B1	-0,1	-38,5	-5
		B2	-1,7	10,9	-2
		C1	2,3	-4,9	-2
Silox	DIW	B1	6,5	-1,9	0
		B2	-2,4	4,5	-1
		C1	-4,3	21,2	-1
	IPA	B1	0,4	0,9	1
		B2	-0,4	7,2	-2
		C1	-0,4	2,1	0
Tetra	DIW	B1	1,9	9,4	0
		B2	1,0	10,8	0
		C1	1,6	3,5	0
	IPA	B1	0,3	0,9	-3
		B2	-1,1	15,7	0
		C1	-0,6	-5,2	0

n, k decrease		no change		n, k increase	
> 10 %	2 - 10 %	± 2 %	2 - 10 %	> 10 %	
J decrease (orders of magnitude)			J increase (orders of magnitude)		
> 2	1 - 2	0	1 - 2	> 2	



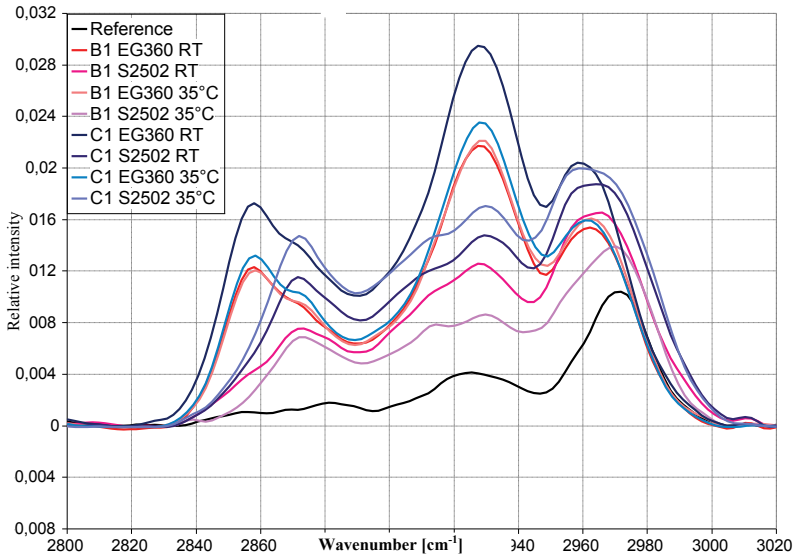


**Figure 7-21:** FTIR spectra of low-k 2 samples after surfactant treatment at elevated bath temperatures. The effects of the temperature strongly depend on the type of surfactant and cleaner used and no universal prediction is possible.

## 7.5. Compatibility to metals and barrier materials

### 7.5.1. Influence on sheet resistance

The compatibility of the surfactant aided cleaning solutions to Cu, TiN and TaN has been determined by sheet resistance measurement. DIW and IPA have been used as rinsing solutions.

Table 7-6 shows the total variation of the sheet resistance from the values measured for the untreated samples. The Cu<sub>2</sub> samples show a broad distribution of values with deviations from 0-27%. A clear influence of the rinsing solutions, the cleaner type or surfactant cannot be seen. Without surfactant the cleaning solutions B1, B2 and C1 did not alter the sheet resistance of copper so the variations can only be due to the surfactants. Except for Silox in C1 on TaN the surfactant solutions show a good compatibility to the barrier materials TiN and TaN with sheet resistance variation not bigger than 6%. Silox mixed in cleaning solution C1 produces a total variation of 10-13% for both rinsing solutions.

### 7.5.2. Surface condition after rinsing

While all low-k samples have a clean surface without visible particles or other contaminations after rinsing using DIW and IPA, the copper, TiN and TaN samples show discolorations when rinsed with IPA for nearly all surfactant solutions. An inspection by optical microscopy showed not only discolored regions, but also the formation of regular structures and in some cases a kind of crystal like surface contaminations (**Figure 7-22** a-f). A contamination of the IPA used for rinsing can be excluded. The liquid was taken from a new bottle of CMOS quality IPA by supplied by J.T. Baker. A possible explanation of the surface contaminations in the case of copper could be a chemical reaction of IPA with copper oxide, but is rather implausible due to the fact that a redox reaction between IPA and copper oxide occurs when copper-II-oxide is present, which is not the case here.

**Table 7-6:** Total variation of the sheet resistance of copper, TiN and TaN samples after surfactant treatment. Independent from the rinsing solution and cleaner used the copper samples show a broad distribution of sheet resistance variation from 0-27%. The TiN and TaN samples showed a good and very good compatibility to surfactant aided cleaning solutions.

Surfactant	Rinse	Cleaner	Cu2	TiN	TaN
EG360	DIW	B1	27,7	3,2	2,6
		B2	1,7	4,1	0,8
		C1	7,9	2,9	0,3
	IPA	B1	0,6	0,8	1,8
		B2	23,2	2,3	1,2
		C1	2,3	2,9	0,1
S2502	DIW	B1	21,5	1,7	2,6
		B2	13,0	1,4	6,4
		C1	8,5	0,8	1,3
	IPA	B1	10,7	1,7	4,3
		B2	2,8	2,9	3,4
		C1	6,2	4,7	1,8
Silox	DIW	B1	7,3	2,0	6,2
		B2	13,6	5,1	3,7
		C1	1,7	2,3	10,0
	IPA	B1	15,3	4,4	0,8
		B2	10,2	0,5	7,9
		C1	11,3	4,1	13,4
Tetra	DIW	B1	3,4	4,7	4,3
		B2	11,3	1,1	4,1
		C1	0,0	6,0	1,6
	IPA	B1	10,7	1,4	6,0
		B2	4,5	0,8	5,4
		C1	9,0	3,5	5,4

**Legend**

< 2 %	< 5 %	< 10 %	≥ 10 %
-------	-------	--------	--------

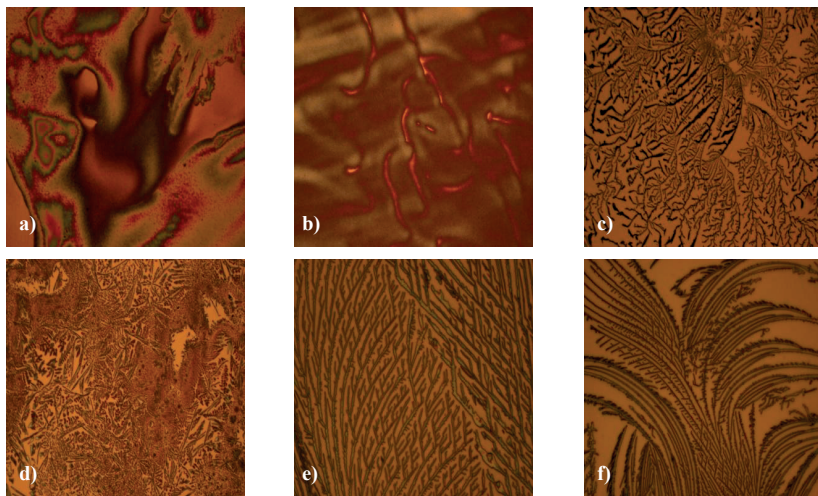


**Figure 7-22:** Surface condition of copper and TiN samples after surfactant treatment and IPA rinsing. a) Copper: Tetra in B2, b) Copper: Silox in C1, c) TiN: Silox in B2, d) TiN: EG360 in C1, e,f) Silox in C1

Another explanation could be the formation of inverted micelles and their agglomeration on the surface to regular structures. Inverted micelles can be formed in organic solutions with low water content. In this case the surfactant molecules arrange to micelles with the polar head group in the center of the micelle and the nonpolar tail towards the surrounding organic medium and small amounts of water can be enclosed. The IPA used for rinsing contains 0,05% water, which could support the assumption that inverted micelles have been formed. Like other micelles inverted micelles are able to form agglomerates and regular structures. The surface contaminations can also be due to the formation of gel like structures which have been observed for surfactant aided organic solvents. Especially Gemini

surfactants like EG360 and S2502 have been found to form gels [107], which could have been deposited on the metallic surfaces.

The origin of the contaminations on the metallic and barrier materials could not be declared and has to be analyzed in future studies. Also none of the possible explanations declares why there are no contaminations on the dielectric samples.

### **7.6. Influence of surfactant addition on the wetting behavior of the cleaning solutions and on pattern collapse forces**

Wetting behavior of surfactant solutions on low-energetic solid surfaces **Table 7-8** the contact angles of cleaning solutions B2 and C1 with and without surfactant addition on several surfaces are compared. The results show that by adding a surfactant, as examples EG360, S2502 and Tetra are listed, a distinct reduction in contact angle values was achieved. The largest decrease in contact angles occurred for cleaner C1 which has a water content higher than 80%. Especially for the etch residue surfaces Poly10, Poly15 and Poly30, which are difficult to wet due to their low surface energy, contact angles reduced from 70-80° to 20-25°. As expected the pristine low-k1 shows a poor wetting behavior due to its highly dispersive character. Contact angles could only be reduced to 46-64° using cleaner C1. This reduction of the contact angles is mainly due to the reduction of surface energy by surfactant application. The difference between surface energy of solid and liquid could be decreased and in most of the cases the total energy of the liquid is now lower than that of the solid. Table 7-7 shows those energy differences for several solids and cleaning solution B2 and C1 with and without surfactants.

**Table 7-7:** Surface energy difference of selected solids and liquids with and without use of surfactants. A large energy difference resulting from the high surface energy of water based cleaning solutions prohibits a good wetting of the solid. By application of surfactants this difference is strongly reduced, which will be favorable to the wetting behavior of the cleaning solutions on the low energetic solid surfaces.

	Water content →	50 - 80 % B2				> 80 ° C1			
Solid surfaces ↓	Surfactant →	w/o	EG360	S2502	Tetra	w/o	EG360	S2502	Tetra
porous and dense low-k dielectrics before and after etching processes	low-k 1	38,1	-0,8	1,8	5,7	44,0	-0,3	4,6	11,7
	low-k 1 + ME	30,6	-8,3	-5,7	-1,8	36,5	-7,8	-2,9	4,2
	low-k 1 + VE	23,9	-15,0	-12,4	-8,5	29,8	-14,5	-9,6	-2,5
	low-k 1 + Ar8	21,0	-17,9	-15,3	-11,4	26,9	-17,4	-12,5	-5,4
	low-k 3	41,4	2,5	5,1	9,0	47,3	3,0	7,9	15,0
	low-k 3 + Ar8	29,6	-9,3	-6,7	-2,8	35,5	-8,8	-3,9	3,2
	low-k 3 + O28	-3,2	-42,1	-39,5	-35,6	2,7	-41,6	-36,7	-29,6
	low-k 4	33,2	-5,7	-3,1	0,8	39,1	-5,2	-0,3	6,8
	low-k 4 + CO8	21,7	-17,2	-14,6	-10,7	27,6	-16,7	-11,8	-4,7
	low-k 4 + N28	6,6	-32,3	-29,7	-25,8	12,5	-31,8	-26,9	-19,8
Etch residues	Poly30	30,5	-8,4	-5,8	-1,9	36,4	-7,9	-3,0	4,1
	C4F88	38,1	-0,8	1,8	5,7	44,0	-0,3	4,6	11,7
	H28	38,7	-0,2	2,4	6,3	44,6	0,3	5,2	12,3
stripping processes	PS1	31,8	-7,1	-4,5	-0,6	37,7	-6,6	-1,7	5,4
	PS2	25,6	-13,3	-10,7	-6,8	31,5	-12,8	-7,9	-0,8
	PS3	8,1	-30,8	-28,2	-24,3	14,0	-30,3	-25,4	-18,3
Metals and barriers	Cu1	34,7	-4,2	-1,6	2,3	40,6	-3,7	1,2	8,3
	CoWP	32,3	-6,6	-4,0	-0,1	38,2	-6,1	-1,2	5,9
	TiN	25,7	-13,2	-10,6	-6,7	31,6	-12,7	-7,8	-0,7
	TaN	12,7	-26,2	-23,6	-19,7	18,6	-25,7	-20,8	-13,7
Other	low-k 1 + CMP	24,9	-14,1	-11,5	-7,6	30,8	-13,6	-8,7	-1,6
	OMCTSHM	32,2	-6,7	-4,1	-0,2	38,1	-6,2	-1,3	5,8

#### Legend

Surface energy difference	< 5 mN/m	5 - 15 mN/m	15 - 30 mN/m	> 30 mN/m
---------------------------	----------	-------------	--------------	-----------

**Table 7-8:** Contact angles of the cleaning solutions B2 and C1 on selected solid surfaces. The addition of surfactants resulted in a clear reduction of contact angles. In many cases contact angles larger than 80° have been reduced to 20-40°, depending on the surfactant applied.

Cleaner →		B2				C1			
Surfactant →		w/o	EG360	S2502	Tetra	w/o	EG360	S2502	Tetra
<b>Porous dielectric etching processes</b>									
low-k 1	pristine	95,6	59,2	55	51,6	99,9	46,7	57,7	64,3
	ME	77,3	26,7	32,3	36	81,5	22,1	23,8	37,7
	VE	67,5	28,3	32,6	35,2	72,9	16,2	31,2	40,7
	Ar8	65,6	31,7	34,7	35,2	59,1	21,2	28,4	36,8
<b>Dense dielectric etching processes</b>									
low-k 3	pristine	92,2	41,9	45,5	40,4	93,9	35,2	46	58,6
	Ar8	67,3	34,5	30,9	44,4	62,2	21,6	31,4	37
<b>Etch residue surfaces</b>									
low-k 1	Poly10	69,9	30,3	40,3	46,7	72	22,2	21,2	23,7
	Poly15	73,6	40,3	39,6	41,3	78,8	20,1	22,2	20,4
	Poly30	78,6	41,4	44,8	47,7	81,8	25,5	21,3	23,9
	C4F88	81,2	40,9	41,9	48,3	74	41,1	40,4	44,9
	H28	78,3	39,4	36,4	43,5	78,1	32,3	36	44,6
low-k 3	C4F88	78,4	42,4	45,8	55,1	71	28,8	38,2	43,1
<b>Porous dielectric stripping processes</b>									
low-k 1	PS1	76,2	28,6	33	29,6	78,9	21,9	27,6	36,5
	PS2	61,3	26,6	35,7	31,8	65,4	20,7	27,1	33,3
	PS3	50,6	31,8	41,6	37,3	55	19,7	29,5	37,4
<b>Metals and barriers</b>									
	Cu1	89,6	32,3	38	43,4	95	24,3	35,1	48,1
	Cu2	93,4	40,2	38,6	45,2	81,3	27,9	45,7	55,2
	CoWP	89,5	32,4	33,6	37,1	78,5	21	32,3	46,3
	TaN	66,6	25,5	0	17,8	14,9	0	0	0
	TiN	63,6	23,8	24,9	0	22,9	0	26,5	26,2
<b>Porous dielectric CMP</b>									

Cleaner →		B2				C1			
Surfactant →		w/o	EG360	S2502	Tetra	w/o	EG360	S2502	Tetra
and hardmask									
low-k 1	CMP	63	21,8	25,1	33,5	72,9	22,1	14,7	31,9
	OMCTSHM	96,9	58,1	54,4	60,5	98,7	44,6	60,7	69,1

**Legend**

< 20°	< 30°	< 50°	< 70°	< 90°	≥ 90°
-------	-------	-------	-------	-------	-------

### 7.6.1. Influence of wetting optimized cleaning solutions on pattern collapse forces

Figure x shows calculated values of the pressure acting on the sidewalls of a low-k dielectric trench structure. The calculation uses the surface energy values obtained for the cleaning solutions B2 and C1 with addition of the surfactants EG360, S2502 and Tetra compared to the values without surfactant addition for several sidewall distances. The analysis shows that by reducing the surface energy of the cleaning solutions the pressure acting on the sidewalls can be reduced by nearly 50% for critical feature sizes like 30 or 15 nm (Figure 7-23: Calculated pressure acting on the sidewalls of a low-k dielectric structure for cleaning solutions with optimized wetting behavior.).



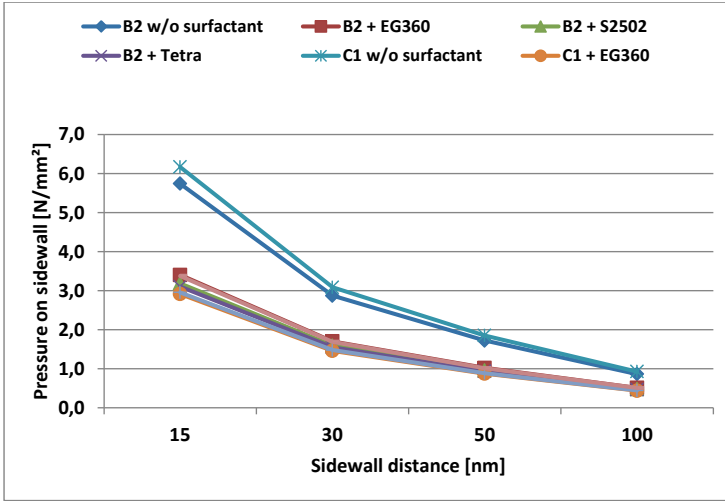


**Figure 7-23:** Calculated pressure acting on the sidewalls of a low-k dielectric structure for cleaning solutions with optimized wetting behavior. By reducing the surface energy of the liquid the pressure can be reduced by nearly 50% for the most critical dimensions.

### 7.7. Process advice for a wetting optimized and material compatible wet cleaning process for PERR

A reduction of the surface energy of a cleaning liquid has been found to be essential to enable a good wetting of low energetic solid surfaces. By the application of surfactants in water based cleaning solutions the difference between the total surface energy values of solid and liquid could be reduced. To apply surfactant aided cleaning solutions, e.g. within BEOL processing, they have to be compatible to any materials they will be in contact with. Additional attention has to be paid to the dynamic behavior of the surfactant, especially looking on highly dynamic single wafer processes like spin-on or spray cleaning. Long-term stability in aqueous media and at elevated temperatures should also be ensured.

The study showed that there have to be made some compromises, e.g. between low surface energy and fast adsorption or between the preference of water based solutions and the necessity of an IPA rinse in many cases. The properties of the surfactant aided solutions not only differ for each surfactant, but also for the content of water of the solutions. This makes it hard to give a general advice for processing of surfactant aides cleaners and new combinations of surfactant and cleaning solution has to be tested comprehensively.

In Table 7-9 the properties of the tested surfactant solutions have been rated regarding their general behavior of the liquid (dynamics, surface energy, long term stability) and their compatibility to materials used in BEOL processing. This includes all optical and electrical properties of a porous low-k dielectric and the change in sheet resistance of the metals and barrier materials. On a scale of 1 – 4, where 4 is the best value, the solutions have been rated. The summary of the rating can be seen in Table 7-9, the detailed rating (scale 1 – 12) can be found in the appendix section I. Regarding general surfactant behavior all surfactants except Silox show good to very good ratings. The low values of silox in this case are due to its low adsorption speed and its instability in aqueous media.

The choice of the rinsing solution turned out to be essential to provide compatibility to a porous low-k dielectric. Except for Tetra only the IPA rinsed samples achieved a good rating. In the case of Tetra the DIW rinsed samples have a slightly lower rating than the IPA rinsed at 35° bath temperature, but show a much better compatibility than all other surfactants. For the metallic and barrier samples no clear influence of the rinsing solution can be found. Except two values for Silox all solutions showed good compatibility to those materials.

**Table 7-9:** Rating of the cleaner / surfactant combinations studied in this work. This rating considers dynamic surfactant behavior and long term stability as well as compatibility issues. The copolymeric surfactant Tetra received the highest ratings

independent from the cleaning solution it is applied to. This is mainly due to the fact that using Tetra an IPA rinse is not necessary in any case.

Surfactant → Cleaner →	EG360			S2502			Silox			Tetra		
	B1	B2	C1	B1	B2	C1	B1	B2	C1	B1	B2	C1
<b>Surfactant behavior</b>	9	8	9	10	8	10	6	5	6	10	8	10
<b>Compatibility</b>												
<b>porous low-k room temperature</b>												
DIW	3	3	3	3	3	4	7	7	6	9	10	10
IPA	7	7	9	6	6	11	11	10	11	10	8	12
<b>porous low-k 35°C</b>												
DIW	4	4	5	7	5	5	7	9	6	7	8	9
IPA	9	6	12	12	8	11	11	10	10	11	7	12
<b>metals / barriers</b>												
DIW	7	11	9	8	7	10	8	5	8	9	8	10
IPA	11	8	10	8	9	9	8	7	5	7	9	7
<b>Total</b>	<b>50</b>	<b>47</b>	<b>57</b>	<b>54</b>	<b>46</b>	<b>60</b>	<b>58</b>	<b>53</b>	<b>52</b>	<b>63</b>	<b>58</b>	<b>70</b>

**Legend**

10 - 12	7 - 9	4 - 6	1 - 3
---------	-------	-------	-------

The contamination of the surface using IPA as rinsing solution of the copper and barrier samples has not been included tot hiss rating but should be kept in mind. As long as the origin of the contamination is not found, an IPA rinse for those materials could be critical, although it is necessary for removing surfactant residues from the porous dielectric.

The rating shows that for every cleaning solution studied Tetra achieved the highest rating. An application of Tetra in cleaning solution C1 with the highest content of water showed the best results:

- The higher the water content, the more effective is this surfactant.
- Tetra is long term stable and can be mixed in the solution long before application.
- An IPA rinse is not necessary.
- Tetra can also be applied at elevated bath temperatures.

- If rinsed with DIW Tetra can also be in contact with copper and barrier materials without degrading their parameters.

The best results have been achieved at the following process conditions: Tetra with a minimum concentration of 0,1% at bath temperatures from room temperature up to at least 35°C, followed by a DIW or IPA rinse for 3 minutes. Also S2502 can be applied at comparable process conditions, but needs an IPA rinse.



## **8. Summary and Outlook**

The combination of a plasma cleaning process and a wet cleaning step is a common method to remove plasma etch residues consisting of polymeric  $\text{CF}_x$  species and inorganic species like silicon and copper, which can be backspattered during the dry etching of the dielectric stack. With the integration of low-k dielectrics commonly applied plasma processes for PERR are critical due to their ability to degrade the low-k dielectric's electrical and structural properties. As an alternative wet chemical cleaning processes are considered. The wet cleaning solutions have to be able to efficiently remove organic and inorganic residue species without affecting underlying dielectrics or metals. With reaching the 32/22 nm technology node additional wetting based challenges like pattern collapse or the nonwetting of small structures will occur. Therefore the development of wet cleaning solutions for PERR will have to consider the wetting behavior of the solids to be cleaned and of the liquid solutions to ensure an efficient residue removal.

### **Determination of surface energies**

This work at first focuses on the fundamental understanding of the wetting properties of materials of the interconnect system like porous and dense dielectrics after several etching and stripping processes as well as barrier materials copper and of commercially available PERR solutions. The determination of the surface energies of solid and liquid as well as both's polar and dispersive energy contributions is used to analyze the wetting behavior. It was shown that the surface energetic character of the dielectrics reacts very sensible towards any variation of the plasma processes the low-k material is treated with. To the pristine and nearly

complexly dispersive low-k dielectric a more or less strong polar energy part is introduced which leads to an increase of the total surface energy of the solid. Both factors influence whether or not this solid is good wetted by the cleaning liquid.

The analysis showed that by determining the energetic character of solid and liquid the appropriate combination of both can be found. Once the energetic character of the cleaning liquid is known, it is possible to make a prediction, whether or not this solution will be able to wet a certain solid surface without additional wetting tests. Contact angle measurements of the studied cleaning solutions on several dielectric samples have proven this assumption. To achieve the best wetting behavior two factors have to be considered. The total surface energy of liquid and solid has to be within a comparable range to avoid large energy differences, which are not favorable to the system and wetting will be difficult or will not occur. Best wetting can be achieved if the surface energy of the liquid is smaller than that of the solid and the formation of a large interface lowers the energy of the whole system. Additionally the ratio of polar and dispersive energy contributions of both media has to be comparable. This can be clearly seen for the dispersive low-k 1 material, where no wetting with the highly polar liquid water was possible. This is due to the fact that the polar energy parts of water are not able to interact with the dispersive solid surface. For ideal wetting of low energy surfaces, which have not only been found for etch residue surfaces or pristine low-k dielectrics but also for electroplated copper, the cleaning liquid has to be low energetic with a comparable surface energetic character. The analysis showed that especially cleaning solutions with a large content of water are high energetic and the large energy difference to most of the studied solids hinders a good wetting. This effect is especially critical if small via holes are covered with low energetic surfaces like etch residues and copper.

One opportunity to overcome the wetting difficulties therefore is the reduction of the total surface energy of the cleaning liquids. The strategy to achieve this followed in this work is the application of surfactants, a method only occasionally studied in the recent years and not extended to a broad range of interconnect materials.

In addition to the evaluation of the wetting behavior the determination of the energetic character of the dielectrics turned out to be a fast and very sensible way to learn about the effects of plasma processes on the surface. The introduction of polar energy contributions to a formerly dispersive low-k dielectric can be assigned to the material alteration by plasma damage. Highly polar –OH groups saturating dangling bonds after plasma processing can cause the increase in polar surface energy. The analysis showed that the change in surface energy characteristics of the dielectrics strongly depends on the kind of plasma processes, plasma chemistries, additives and process durations or whether or not a polymeric surface layer has been deposited. That is why this method can be used as an additional analytic way to understand the process of plasma damage and can help to identify the species causing low-k degradation. But this also means that every change in plasma processing influences the wetting behavior of the dielectric surface which additionally to the mostly complex composition of an etch residue surface makes it even more hard to find a universal cleaning solution.

### **Application of surfactants**

The selection of surfactants for application in PERR solutions not only has to consider to which value the surface energy of the liquid can be lowered. Additionally the dynamic behavior, which means how fast the surfactant is able to



adsorb at an interface, the long term stability in aqueous media, the influence of the liquid's temperature and especially the compatibility to the materials the surfactant will be in contact with have to be analyzed. The surfactants chosen include nonionics, anionics as well as a fluorinated, a silicon containing and a block-copolymeric surfactant.

A first selection was done by evaluating the lowest reachable dynamic surface energy, the adsorption speed of the surfactants mixed in DIW and the formation of foam, which lead to the exclusion of the anionic and fluorinated surfactants. The measurements showed that a compromise between high adsorption speed and low surface energy has to be made. Two nonionic Gemini surfactants, the silicon containing and the block-copolymeric have been selected for further studies. Mixed in the cleaning solutions the surfactants showed the highest reduction in surface energy for solutions with very high water content. The increase in bath temperature only showed a small influence on the dynamic behavior of the solutions and the long term stability of the surfactant dynamics was found to be critical for the silicon containing surfactant. After 7 weeks the dynamic surface energy increased which can be due to the fact that silicon surfactants tend to be destructed by hydrolysis.

The compatibility tests including the evaluation of optical, electrical and structural parameters of a porous dielectric showed that choosing the appropriate rinsing solution after surfactant treatment is essential. Optical and electrical material properties have been strongly altered if DIW was chosen for rinsing. FTIR analysis showed that this may be due to the incorporation of residual surfactant species within the porous structure of the dielectric. An IPA rinse was able to remove those species and the material parameters could be nearly recovered. The block-copolymer is the only surfactant for which the IPA rinse was not necessary, which

may be due to the large size of the molecule. Increased bath temperature and variation of the DIW rinsing time did not bring any differences.

The compatibility of the surfactant aided cleaning solutions to copper and barrier materials has been determined by analyzing the change in sheet resistance of the solid samples. For copper a good compatibility with medium changes in sheet resistance was found, independent from the rinsing solution chosen. The barrier materials TiN and TaN showed a good to very good compatibility to the surfactant solutions with only minor changes in sheet resistance. Optical microscopy inspection of the copper and barrier samples showed a surface contamination after IPA rinsing, whose origin could not be declared till now but which seems not to have an influence on the sheet resistance. Possible explanations like the formation of inversed micellar conglomerates, gelation or a chemical reaction of IPA with the materials are considered.

Finally the determination of the surface energies of the surfactant aided cleaning solutions showed that the differences of the total surface energies of solids and liquids could be clearly reduced and in many cases the surface energy of the liquid now is lower than that of the solid. Contact angle analysis of the surfactant solutions on several low energetic solids showed much smaller values and an optimized wetting behavior. The most promising process scheme could be found for the block-copolymeric surfactant, for which no IPA rinse is necessary, and the nonionic surfactant S2502 in cleaning solutions with the highest water content.

## Outlook

In this work was shown that the application of surfactants in plasma etch residue removal is a promising way to ensure effective cleaning results in future technology nodes. As this is one of the first comprehensive studies on this topic, the processing has to be further optimized. The surfactant aided cleaning processes have to meet the requirements of the industry, e.g. the trend to use water based cleaning solutions. That's why especially the IPA rinsing solutions have to be replaced or modified, e.g. by dilution. Another or additional strategy could be the thermal destabilization of the residual surfactant within the porous low-k structure by heating up the substrate or by treatment with a high temperature rinse. Residual gas analysis while heating up the surfactant treated sample would be one approach to determine whether or not the surfactants have been removed. This could allow the application of surfactant species, which are actually not compatible to materials used in BEOL processing or the combination of surfactants to further improve the wetting behavior and the dynamics of cleaning solutions.

As reported the determination of the surface energetic character of a plasma processed low-k dielectric can help to evaluate the effects of the plasma on this surface. As the damage mechanisms of new etching and ashing processes is not completely understood till now, this analytical method can help to identify the damaging species within the plasma. This very sensible method will be further improved and can be extended to additional fields like post-CMP cleaning, the evaluation of adhesion properties or the effects of k-recovery processes.

## Appendix

### A Surface energy values of the studied solid surfaces and cleaning liquids

**Table A1:** Surface energy values of differently processed porous low-k dielectrics

	Surface energy [mN/m]		
	dispersive	polar	total
low-k 1	28.51	0.12	28.63
ME	26.28	9.81	36.09
VE	12.26	30.52	42.78
CF4	7.69	39.82	47.51
Ar2	6.91	43.91	50.82
Ar4	8.49	40.74	49.23
Ar6	8.21	41.77	49.98
Ar8	10.28	35.46	45.74

**Table A2:** Surface energy values of differently processed dense low-k dielectrics

	Surface energy [mN/M]		
	dispersive	polar	total
low-k 3	24.15	1.15	25.3
CF4	12.66	26.05	38.71
Ar2	12.87	24.68	37.55
Ar4	13.71	23.38	37.09
Ar6	13.54	24.16	37.7
Ar8	14.42	22.68	37.1
O22	3.18	64.92	68.1
O24	2.41	69.96	72.37
O26	2.36	70.92	73.28
O28	2.75	67.11	69.86
low-k 4	33.13	0.4	33.53
CO2	8.51	34.27	42.78
CO4	7.92	37.41	45.33
CO6	7.92	37.93	45.85
CO8	7.86	37.12	44.98
N22	4.31	55.62	59.93
N24	4.42	55.34	59.76
N26	4.48	54.96	59.44
N28	4.41	55.72	60.13

**Table A3:** Surface energy values of dielectric samples after polymerizing etch processes

	Surface energy [mN/m]		
	dispersive	polar	total
Poly10	24	12.54	36.54
Poly15	25.54	10.72	36.26
Poly30	28.89	7.32	36.21
C4F82	15.81	15.55	31.36
C4F84	18.53	11.5	30.03
C4F86	20.65	8.25	28.9
C4F88	22.74	5.88	28.62
H22	14.06	15.42	29.48
H24	14.66	14.54	29.2
H26	14.79	14.79	29.58
H28	16.38	11.6	27.98
CVDPoly	23.6	2.5	26.1

**Table A4:** Surface energy values of porous dielectric samples after different stripping processes

	Surface energy [mN/m]		
	dispersive	polar	total
low-k 1	28.51	0.12	28.63
PS 1	24.21	10.66	34.87
PS 2	15.33	25.76	41.09
PS 3	49.83	8.78	58.61

**Table A5:** Surface energy values of copper and barrier material samples

	Surface energy [mN/m]		
	dispersive	polar	total
Cu1	20.25	11.72	31.97
Cu2	20.53	9.93	30.46
CoWP	15.75	18.63	34.38
TiN	14.2	26.8	41
TaN	25.2	28.8	54

**Table A6:** Surface energy values of a porous dielectric after CMP and of a OMCTS hardmask layer

	Surface energy [mN/m]		
	dispersive	polar	total
low-k 1	28.51	0.12	28.63
CMP	15.02	26.83	41.85
OMCTSHM	34.46	0	34.46

**Table A7:** Surface energy values of the studied cleaning solutions

	Surface energy [mN/m]		
	dispersive	polar	total
A1	24.3	15.6	39.9
A2	22.3	11.1	33.4
A3	35.5	23.3	58.8
B1	25.2	30.5	55.7
B2	39.7	27	66.7
C1	29.6	43	72.6

## B Contact angle values and comparison of the energetic character of solids and liquids

**Table B1:** Contact angle values of the studied cleaning solutions on selected dielectric surfaces

	Contact angle values [°]					
	A1	A2	A3	B1	B2	C1
low-k 1	57.9	48.3	99.3	87	97.6	102.1
Poly10	12.2	13	64.1	47.2	69.9	72
Poly15	12.2	10.8	69.1	61.2	73.6	78.8
Poly30	12.3	17	73.6	60.1	78.6	81.8
ME	14.6	12.6	70.7	60.9	77.3	81.5
PS1	26.6	17.5	69	58.2	76.2	78.9
PS2	12.3	0	51.3	43.1	61.3	65.4
PS3	0	6.9	41.4	36.4	50.6	55

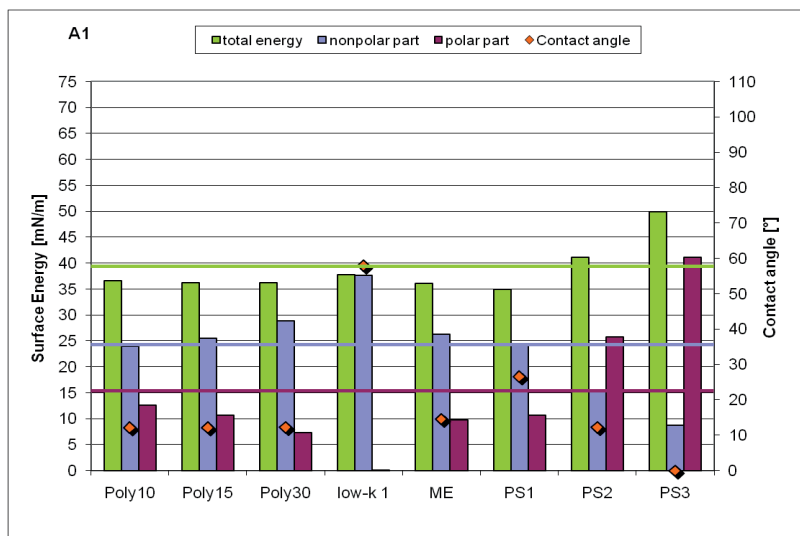


**Figure B1:** Energetic character of solution A1 compared with that of selected solid surfaces.

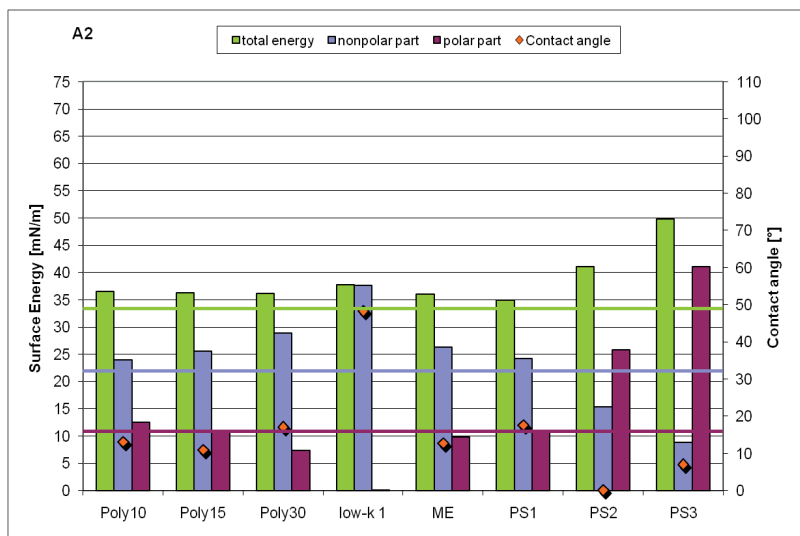


**Figure B2:** Energetic character of solution A2 compared with that of selected solid surfaces

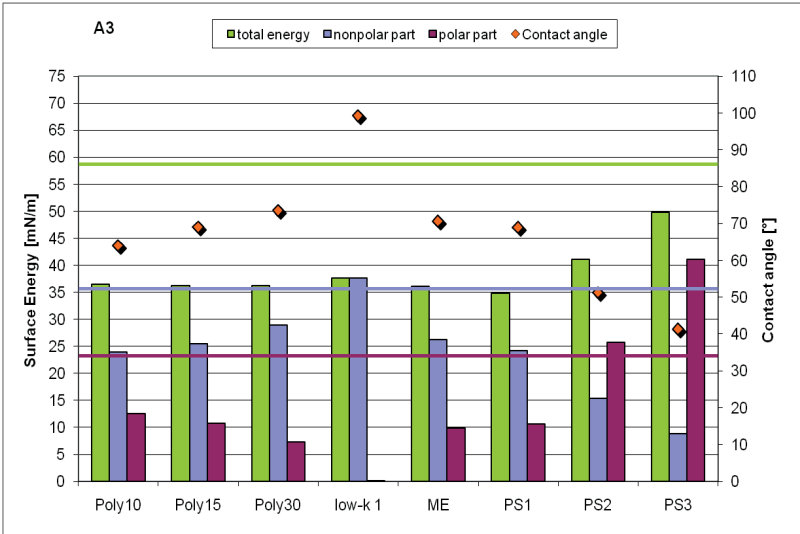


**Figure B3:** Energetic character of solution A3 compared with that of selected solid surfaces

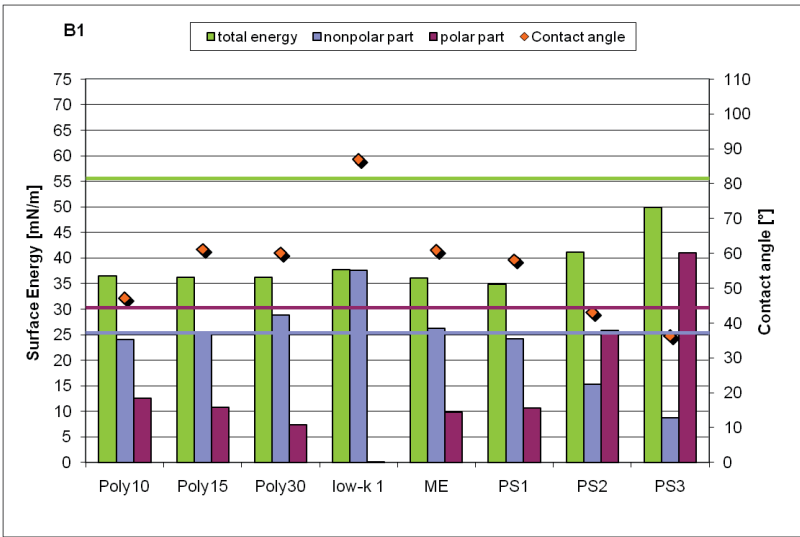


**Figure B4:** Energetic character of solution B1 compared with that of selected solid surfaces



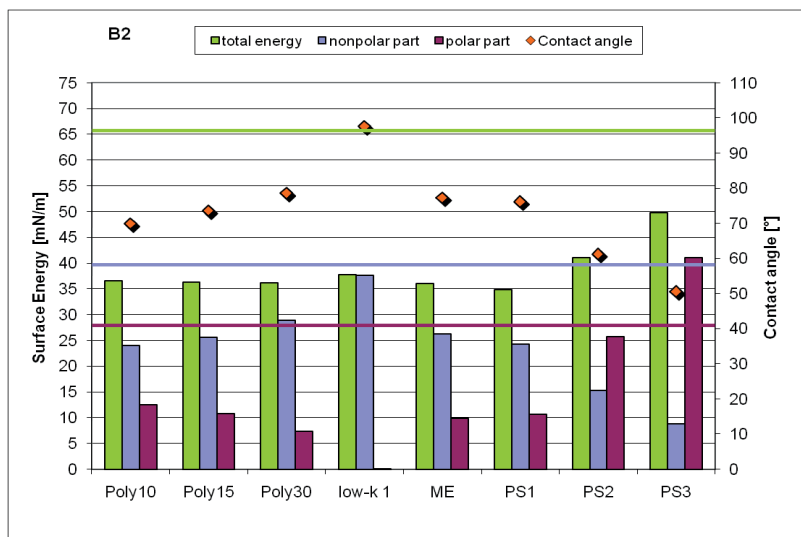


**Figure B5:** Energetic character of solution B2 compared with that of selected solid surfaces

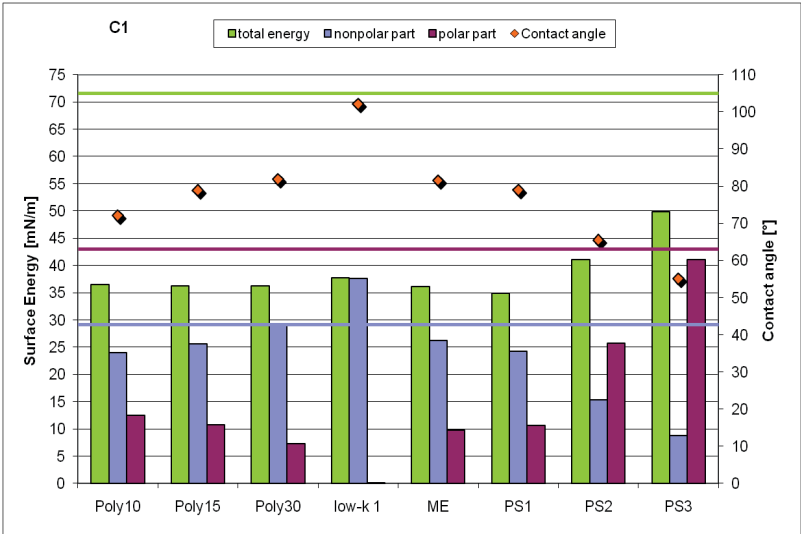


**Figure B6:** Energetic character of solution C1 compared with that of selected solid surfaces

### C. Surface energy calculation of the PTFE substrate

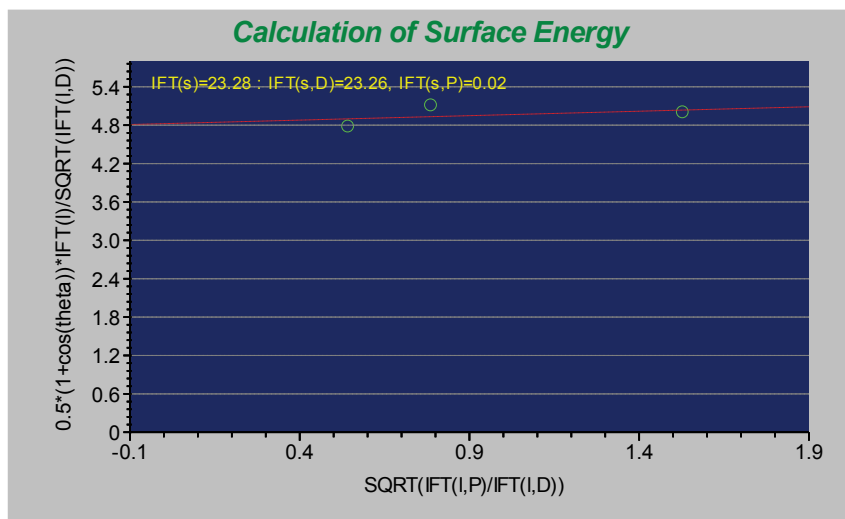


**Figure C1:** Plot of the contact angle measurement results on a PTFE substrate; This surface shows a polar energy part which can be neglected. The value of total surface energy (23.28 mN/m) was used to determine the dispersive surface energy contribution of the studied cleaning solutions.

**D Compatibility study of the solutions B1, B2 and C1 to a porous low-k dielectric and copper**

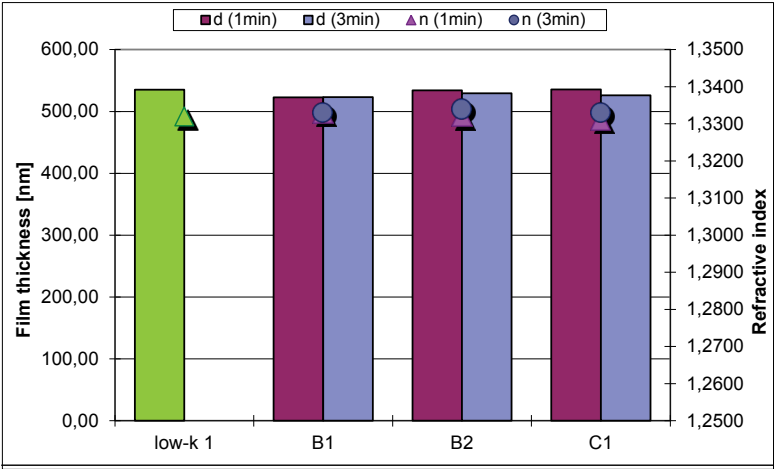


**Figure D1:** Film thickness and refractive index of the porous low-k before and after cleaning processes using solutions B1, B2 and C1. The changes in optical parameters have been determined by spectral ellipsometry and show only marginal changes. So the solutions were found to be compatible to this dielectric material.

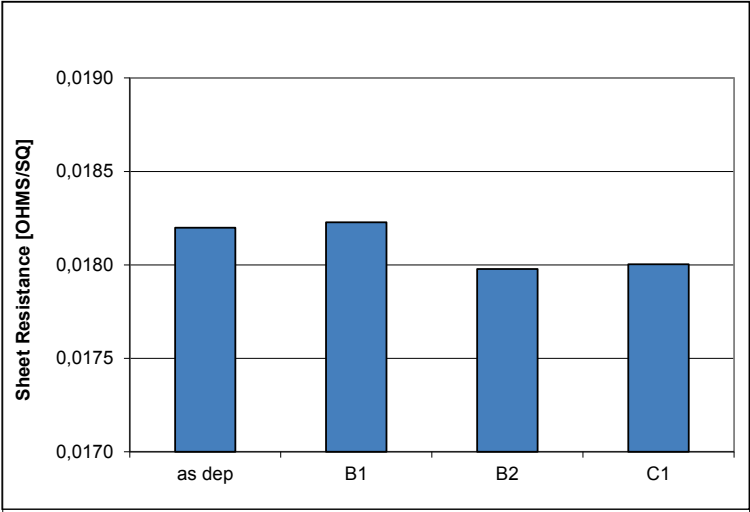
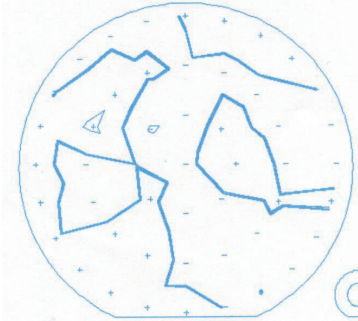
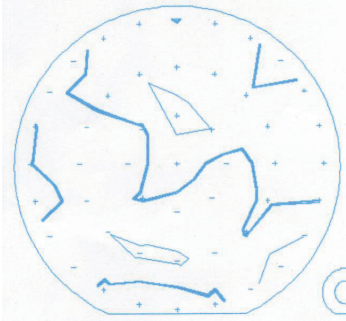


**Figure D2:** Sheet resistance values of copper before and after the cleaning process. Only slight changes in sheet resistance have been found. The cleaning solutions were found to be compatible to copper.



Copper as dep



B1

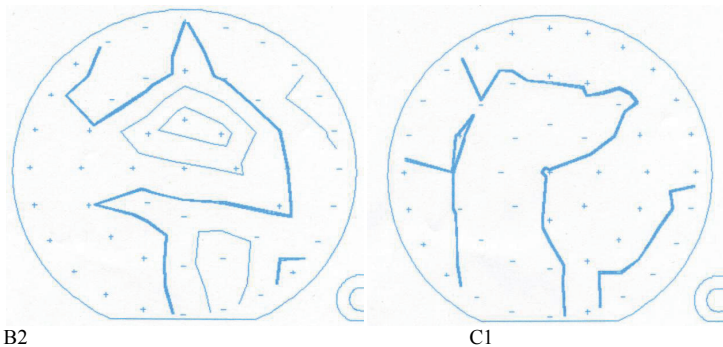


**Figure D3:** Sheet resistance profiles of copper before and after the cleaning processes. The mappings show a comparable character for each cleaning solution which implies that there is no decrease in film thickness.

**E Dynamic surface energy values of the studies surfactants mixed in DIW**

**Table E1:** Dynamic surface energy values of EG360 at different concentrations.

EG360	Concentration [%]					
Surface age [ms]	0.01	0.015	0.02	0.04	0.06	0.08
20	69.1	67.9	67.6	57.2	52.3	45.6
30	68.1	67.0	66.6	54.9	49.5	44.2
40	67.0	65.9	65.6	52.7	47.7	41.9
50	66.0	64.6	64.0	50.7	45.2	40.5
80	63.3	62.3	61.2	47.8	43.2	38.5
100	62.0	60.9	60.2	46.4	41.5	37.3
150	61.2	58.2	57.6	44.2	40.6	36.2
200	59.6	58.2	57.0	44.2	39.7	35.8
300	57.0	56.2	54.0	42.2	38.2	34.1
500	55.0	53.8	52.4	40.5	36.7	32.1
700	53.1	52.1	50.5	39.4	35.5	32.1
1000	51.8	50.7	48.8	38.4	34.9	31.6
1300	50.7	49.9	48.2	37.5	34.2	
1600	49.9	49.0		37.0		

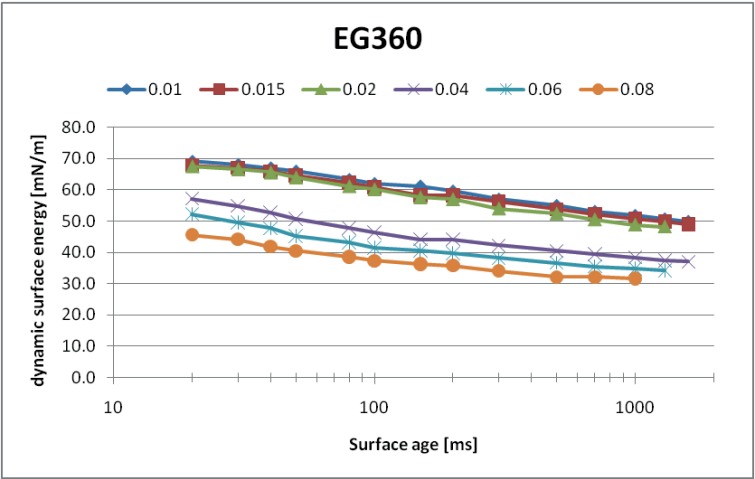


Figure E1: Dynamic behavior of EG360 at different concentrations.

Table E2: Dynamic surface energy values of S104E at different concentrations.

S104E	Concentration [%]					
Surface age [ms]	0.01	0.015	0.02	0.04	0.06	0.08
20	71.3	68.2	68.6	57.4	52.1	48.7
30	70.9	67.7	67.4	55.4	50.7	47.6
40	70.4	66.4	66.6	53.6	49.1	46.6
50	70.0	65.2	65.5	52.3	48.2	45.6
80	69.5	62.9	63.1	50.5	46.8	44.3
100	68.7	61.9	61.4	49.4	46.2	43.8
150	67.0	59.2	59.0	48.2	45.4	43.3
200	67.5	57.8	59.2	48.7	45.7	43.7
300	65.3	57.7	57.4	47.9	45.1	43.5
500	63.0	55.8	55.4	47.1	44.4	42.7
700	61.6	55.0	54.4	46.6	44.2	42.4
1000	59.9	54.2	53.6	46.5	43.7	42.2
1300	59.3	53.6	53.0	45.9	43.4	42.1
1600	58.7	53.3	52.7	45.7	43.6	

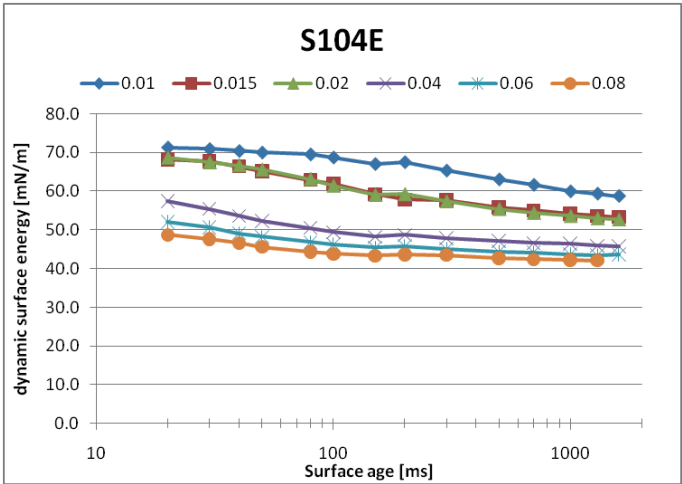


Figure E2: behavior of S104E at different concentrations.

Table E3: Dynamic surface energy values of S2502 at different concentrations.

S2502	Concentration [%]					
Surface age [ms]	0.01	0.015	0.02	0.04	0.06	0.08
20	70.2	66.9	63.1	54.4	50.0	43.9
30	70.2	65.8	61.7	52.6	48.5	42.3
40	69.9	64.4	60.2	50.8	46.9	41.5
50	69.5	63.2	58.6	49.8	45.8	40.9
80	68.8	60.8	56.4	47.5	44.2	39.7
100	67.9	59.3	55.2	46.7	43.0	39.2
150	66.5	56.9	52.6	45.0	42.3	38.5
200	66.0	56.8	52.9	45.3	42.7	39.0
300	63.8	54.8	51.2	44.4	42.1	38.5
500	60.9	52.5	49.4	43.3	41.3	38.2
700	59.1	51.5	48.7	42.9	40.5	37.7
1000	57.3	50.2	47.6	42.1	40.2	37.4
1300	56.2	49.6	47.0	42.1	40.1	37.4
1600	55.2	48.9	46.5	42.1	40.0	



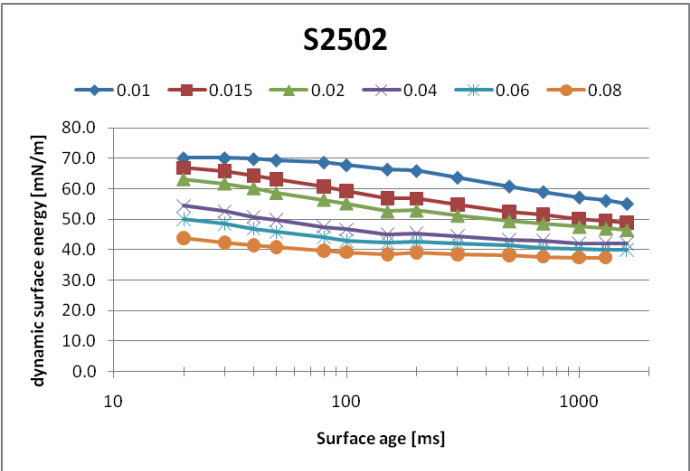
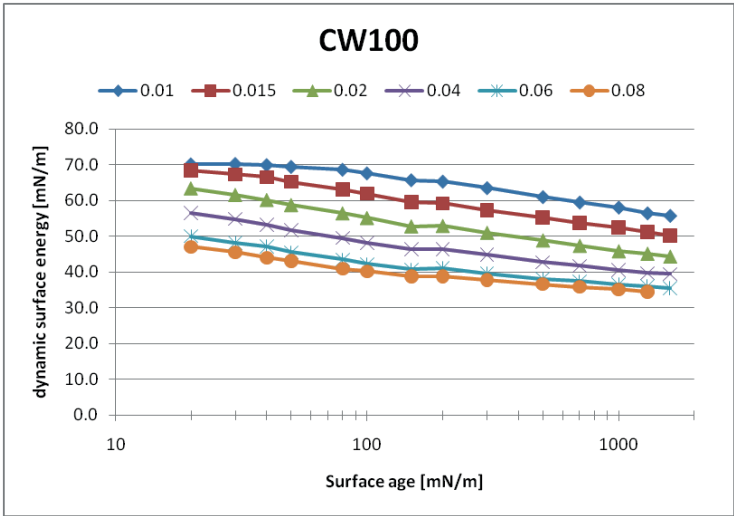


Figure E3: Dynamic behavior of S2502 at different concentrations.

Table E4: Dynamic surface energy values of CW100 at different concentrations.

CW100	Concentration [%]					
Surface age [ms]	0.01	0.015	0.02	0.04	0.06	0.08
20	70.1	68.4	63.3	56.5	50.0	47.0
30	70.2	67.3	61.5	54.8	48.1	45.5
40	69.9	66.5	60.1	53.2	47.1	44.0
50	69.4	65.2	58.7	51.7	45.5	43.1
80	68.6	63.1	56.4	49.5	43.5	40.9
100	67.6	61.9	55.1	48.2	42.2	40.2
150	65.7	59.6	52.8	46.3	40.7	38.8
200	65.3	59.2	52.9	46.3	41.0	38.8
300	63.5	57.3	51.0	44.8	39.6	37.8
500	61.0	55.2	48.9	42.7	38.1	36.6
700	59.5	53.7	47.4	41.7	37.4	35.8
1000	58.1	52.4	45.9	40.6	36.5	35.1
1300	56.5	51.2	45.2	39.7	36.0	34.5
1600	55.8	50.1	44.4	39.4	35.5	



**Figure E4:** Dynamic behavior of CW100 at different concentrations.

**Table E5:** Dynamic surface energy values of S465 at different concentrations.

S465 Surface age [ms]	Concentration [%]				
	0.01	0.015	0.04	0.06	0.08
20	64.6	61.0	53.2	52.6	50.1
30	63.4	59.5	51.8	51.2	48.8
40	62.1	58.4	50.3	50.3	47.7
50	61.1	57.2	49.7	49.5	47.4
80	59.2	55.5	48.5	48.3	46.6
100	58.2	54.6	48.2	47.8	46.0
150	56.6	53.2	47.3	47.1	45.5
200	57.1	53.7	47.7	47.7	46.1
300	55.9	52.8	47.2	47.2	45.8
500	54.4	51.7	46.8	46.6	45.3
700	53.8	51.2	46.5	46.2	44.9
1000	52.9	50.8	46.0	46.2	44.7
1300	52.4	50.3	45.8	46.0	44.6
1600	52.3	50.1	45.8		

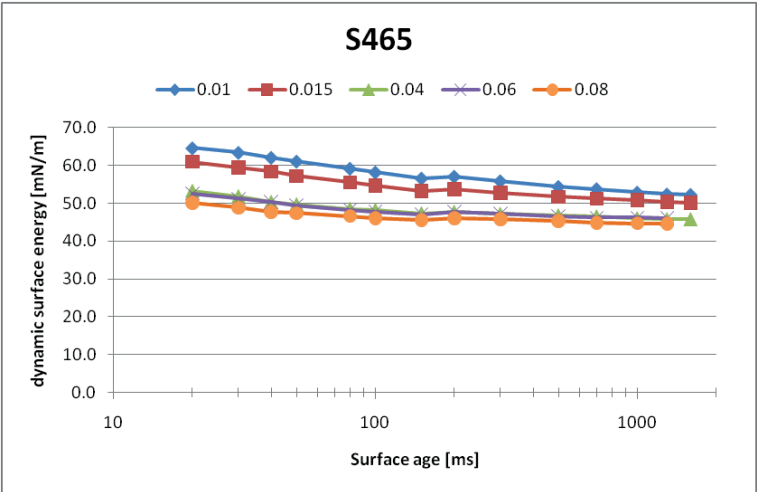
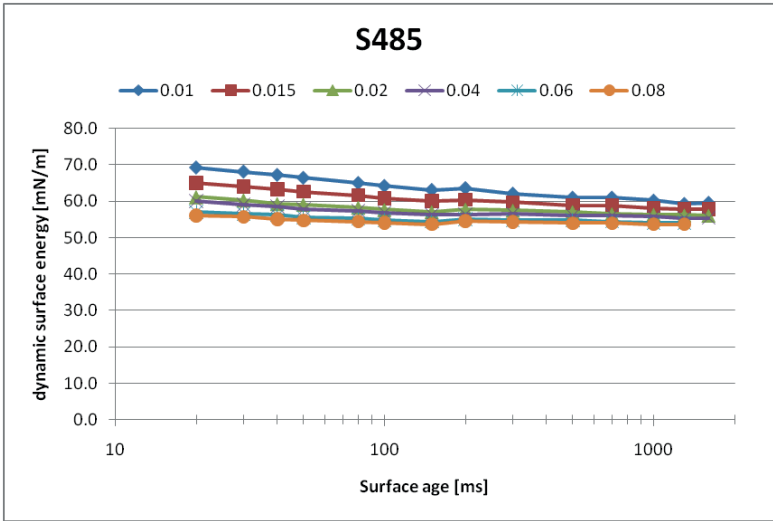


Figure E5: Dynamic behavior of S465 at different concentrations.

Table E6: Dynamic surface energy values of S485 at different concentrations.

S485	Concentration [%]					
Surface age [ms]	0.01	0.015	0.02	0.04	0.06	0.08
20	69.2	65.0	61.2	60.0	57.0	56.0
30	68.1	64.0	60.3	59.1	56.5	55.7
40	67.2	63.2	59.3	58.5	56.2	55.1
50	66.4	62.6	59.1	57.8	55.5	54.7
80	65.0	61.6	58.3	57.4	55.2	54.4
100	64.2	60.8	57.7	56.9	54.8	54.1
150	63.1	60.0	57.1	56.4	54.4	53.7
200	63.6	60.4	57.8	56.4	55.1	54.5
300	62.1	59.7	57.5	56.6	54.7	54.3
500	61.0	58.9	57.1	56.1	54.8	54.0
700	61.0	58.8	56.5	56.1	54.4	54.0
1000	60.2	58.0	56.4	55.7	54.0	53.7
1300	59.3	57.9	56.2	55.4	54.1	53.7
1600	59.6	57.8	56.1	55.4		



**Figure E6:** Dynamic behavior of S485 at different concentrations

**Table E7:** Dynamic surface energy values of GAClauryl at different concentrations.

GAClauryl	Concentration					
Surface age [ms]	0.02%	0.04%	0.08%	0.10%	0.15%	0.20%
20	69.8	69.7	68.9	69.5	70.5	69.6
30	68.6	68.9	67.7	68.7	70.2	68.3
40	67.4	67.7	66.2	67.2	69.5	67.2
50	66.1	66.9	64.6	65.8	68.7	66.2
80	64.2	64.0	62.9	63.8	67.1	63.8
100	62.8	63.0	61.2	62.4	66.0	62.5
150	60.2	60.4	58.6	60.0	63.7	59.7
200	59.3	59.3	58.0	59.0	62.5	58.8
300	56.5	56.5	55.0	56.1	59.8	56.1
500	52.8	53.3	51.4	52.3	56.4	52.1
700	50.0	50.3	48.4	49.8	53.7	49.2
1000	46.7	47.6	45.5	46.8	50.7	46.1
1300	44.8	45.5	43.4	44.4		

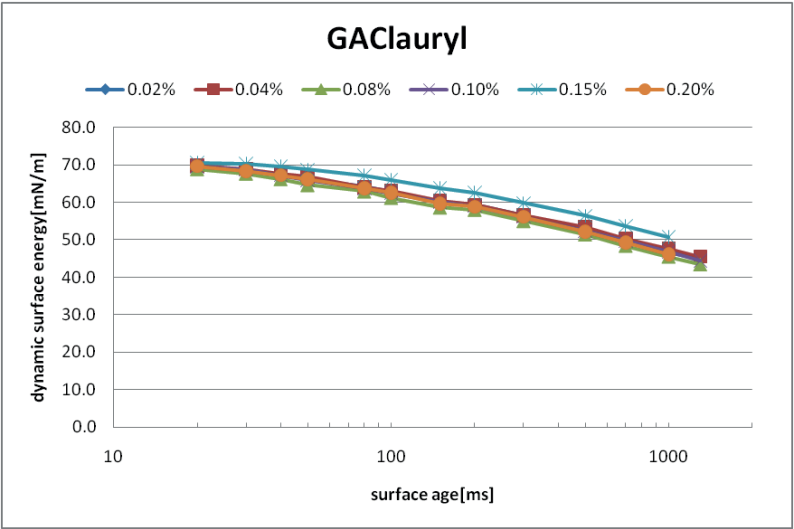
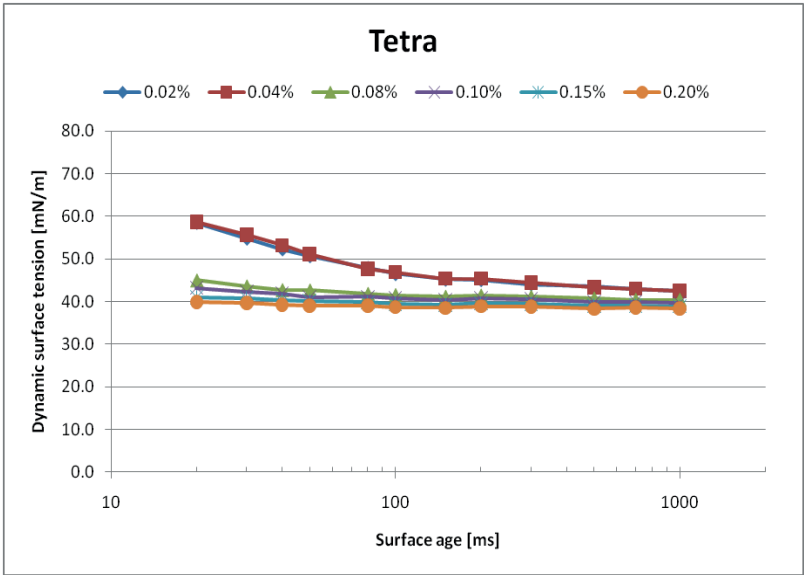


Figure E7: Dynamic behavior of GAClauryl at different concentrations.

Table E8: Dynamic surface energy values of Tetra at different concentrations

Tetra	Concentration					
Surface age [ms]	0.02%	0.04%	0.08%	0.10%	0.15%	0.20%
20	58.5	58.7	45.0	43.2	41.0	39.9
30	54.8	55.7	43.6	42.3	40.7	39.7
40	52.3	53.2	42.7	41.8	40.4	39.3
50	50.7	51.1	42.6	41.0	40.2	39.0
80	47.9	47.7	41.8	41.1	39.8	39.0
100	46.5	46.9	41.5	40.7	39.5	38.7
150	45.2	45.4	41.1	40.3	39.3	38.5
200	45.1	45.4	41.4	40.7	39.6	38.9
300	44.1	44.4	41.1	40.5	39.5	38.8
500	43.5	43.4	40.7	39.9	39.0	38.3
700	42.9	43.0	40.4	40.0	39.0	38.6
1000	42.5	42.5	40.4	39.7	38.9	38.4



**Figure E8:** Dynamic behavior of Tetra at different concentrations.

**Table E9:** Dynamic surface energy values of Zonyl at different concentrations

Zonyl	Concentration					
Surface age [ms]	0.02%	0.04%	0.08%	0.10%	0.15%	0.20%
20	71.4	71.6	72	72.5	72.6	72.7
30	71.6	72.1	72.6	72.8	72.8	72.9
40	71.4	72.2	72.2	73.2	72.9	72.9
50	71.7	72.8	72.9	73.4	73.2	73.1
80	72.5	73	73.1	73.6	73.5	73.4
100	72.4	73	73.4	73.8	73.5	73.4
150	72.6	73.1	73.5	73.6	73.7	73.6
200	73.6	74	74.3	74.6	74.7	74.6
300	73.8	74	74.3	74.5	74.6	74.6
500	73.9	74.1	74.4	74.5	74.8	74.7
700	73.8	74.2	74.3	74.7	74.8	74.7
1000	73.7	74.1	74.4	74.7	74.8	74.8

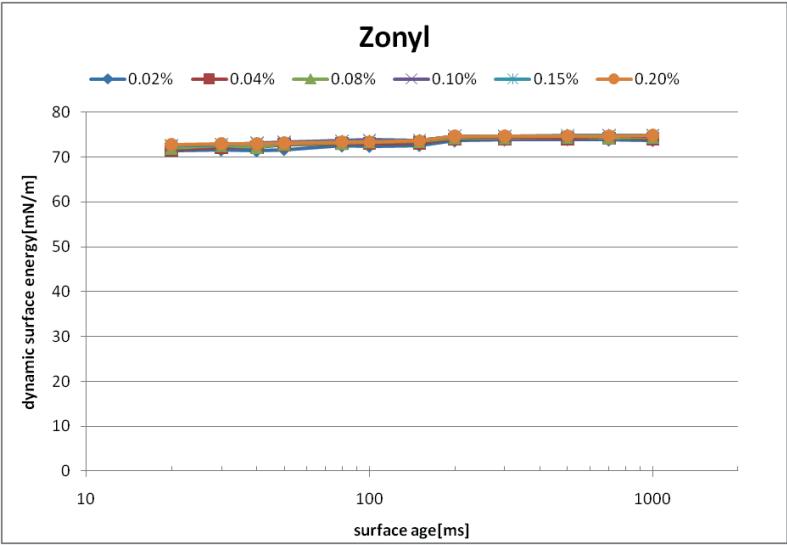
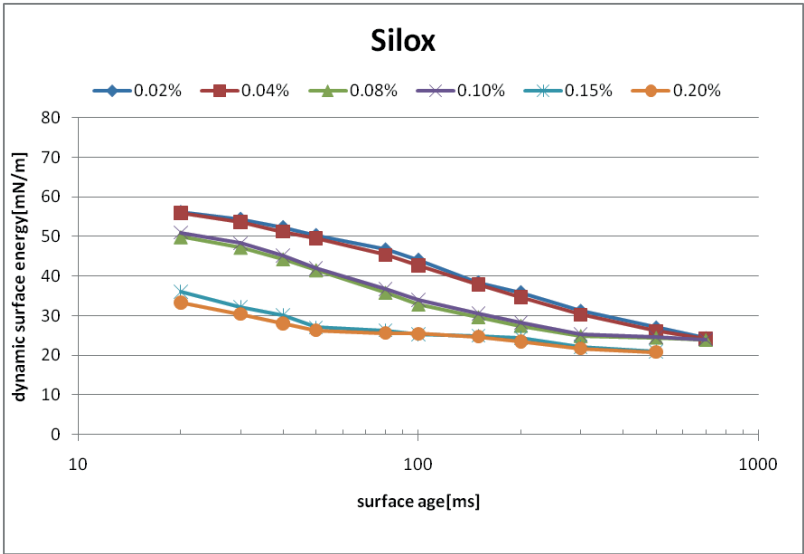


Figure E9: Dynamic behavior of Zonyl at different concentrations.

Table E10: Dynamic surface energy values of Silox at different concentrations.

Silox	Concentration					
Surface age [ms]	0.02%	0.04%	0.08%	0.10%	0.15%	0.20%
20	56.1	55.9	49.9	51	36	33.3
30	54.4	53.6	47.2	48.3	32.1	30.4
40	52.3	51.2	44.3	45.2	30.1	28
50	50.3	49.5	41.5	42	27	26.3
80	46.7	45.3	35.8	36.7	26.3	25.6
100	44.1	42.6	32.8	34	25.3	25.4
150	38.4	37.8	29.6	30.5	24.9	24.7
200	35.9	34.6	27.4	28.3	24.3	23.4
300	31.2	30.2	24.8	25.3	22.1	21.7
500	27	26.1	24.4	24.6	21	20.8
700	24.3	24.1	23.8	24		
1000						



**Figure E10:** Dynamic behavior of Silox at different concentrations.



## F Dynamic surface energy values and long term stability of the studied surfactants mixed in cleaning solutions

**Table F1:** Dynamic surface energy values of surfactants in the studied cleaning solutions.

Surface age [ms]	EG360			S2502			Tetra			Silox		
	B1	B2	C1	B1	B2	C1	B1	B2	C1	B1	B2	C1
20	51.6	58.1		48.6	50.3	40.8	46.9	38.9	41.6	46.2	60.5	49.3
30	50.8	57.9	48.0	48.0	57.3	39.9	46.2	36.9	41.2	44.7	59.8	48.2
40	50.2	56.9	47.3	47.4	47.0	38.3	45.3	36.8	40.8	43.6	59.2	46.4
50	49.5	53.5	45.5	47.2	44.3	38.0	44.7	36.1	40.4	42.0	57.4	45.8
80	49.6	51.0	43.0	46.6	46.5	37.1	44.0	36.0	40.2	39.4	56.9	44.1
100	48.5	49.3	42.1	46.3	45.5	36.6	43.6	36.1	40.0	38.0	55.4	43.3
200	48.6	47.2	39.6	46.6	44.0	36.2	43.9	36.0	39.7	36.1	53.8	36.8
300	48.2	44.3	37.7	46.2	41.3	35.5	43.7	36.3	39.6	34.0	53.8	33.3
500	47.7	41.4	36.3	45.8	39.1	35.3	43.5	36.0	39.3	31.4	48.1	33.6
700	46.3	41.1	35.0	45.6	38.5	34.9	43.3	36.2	39.2	29.4	45.6	29.6
1000	46.2	39.7	34.0	45.4	37.2	34.5	43.0	36.2	39.4	27.4	43.0	27.0

**Table F2:** Dynamic behavior of EG360 at elevated bath temperatures.

EG 360						
Surface age [ms]	B1 RT	B1 35°C	B2 RT	B2 35°C	C1 RT	C1 35°C
20	51.6	47.6	58.1	55.5		51.0
30	50.8	47.0	57.9	52.1	48.0	50.5
40	50.2	46.2	56.9	50.8	47.3	47.7
50	49.5	45.9	53.5	50.6	45.5	46.5
80	49.6	44.1	51.0	48.2	43.0	44.2
100	48.5	45.5	49.3	46.9	42.1	42.7
200	48.6	44.4	47.2	44.8	39.6	39.2
300	48.2	43.9	44.3	42.6	37.7	38.8
500	47.7	43.4	41.4	40.6	36.3	37.1
700	46.3	43.8	41.1	40.0	35.0	35.9
1000	46.2	42.4	39.7	39.8	34.0	34.0

**Table F3:** Dynamic behavior of S2502 at elevated bath temperatures.

<b>S2502</b>						
<b>Surface age [ms]</b>	<b>B1 RT</b>	<b>B1 35°C</b>	<b>B2 RT</b>	<b>B2 35°C</b>	<b>C1 RT</b>	<b>C1 35°C</b>
20	48.6	47.1	50.3	47.5	40.8	37.6
30	48.0	46.8	57.3	46.5	39.9	36.9
40	47.4	46.3	47.0		38.3	35.8
50	47.2	45.7	44.3		38.0	35.3
80	46.6	45.6	46.5	46.2	37.1	34.8
100	46.3	45.3	45.5	45.5	36.6	34.2
200	46.6	45.1	44.0	41.4	36.2	33.5
300	46.2	44.9	41.3	40.5	35.5	33.0
500	45.8	44.9	39.1	38.4	35.3	33.0
700	45.6	44.6	38.5	37.5	34.9	32.6
1000	45.4	44.7	37.2	37.0	34.5	32.2

**Table F4:** Long term stability of surfactants in cleaning solution B1.

<b>B1</b>	<b>EG 360</b>		<b>S2502</b>	
<b>Surface age [ms]</b>	<b>initial condition</b>	<b>after 7 weeks</b>	<b>initial condition</b>	<b>after 7 weeks</b>
20	51.6	51.3	48.6	48.2
30	50.8	50.8	48.0	47.7
40	50.2	49.8	47.4	47.2
50	49.5	49.6	47.2	46.8
80	49.6	48.9	46.6	46.3
100	48.5	48.5	46.3	46.0
200	48.6	48.2	46.6	46.0
300	48.2	47.5	46.2	45.7
500	47.7	47.1	45.8	45.5
700	46.3	46.3	45.6	45.4
1000	46.2	45.2	45.4	45.3

	<b>Tetra</b>		<b>Silox</b>	
<b>Surface age [ms]</b>	<b>initial condition</b>	<b>after 7 weeks</b>	<b>initial condition</b>	<b>after 7 weeks</b>
20	46.9	48.5	46.2	56.7
30	46.2	47.6	44.7	56.8
40	45.3	46.3	43.6	56.2
50	44.7	45.6	42.0	56.4
80	44.0	44.3	39.4	56.3
100	43.6	44.2	38.0	56.0
200	43.9	44.1	36.1	56.2
300	43.7	43.6	34.0	56.1
500	43.5	43.5	31.4	56.3
700	43.3	43.4	29.4	56.2
1000	43.0	43.1	27.4	56.1

**Table F5:** Long term stability of surfactants in cleaning solution B2.

<b>B2</b>	<b>EG 360</b>		<b>S2502</b>	
<b>Surface age [ms]</b>	<b>initial condition</b>	<b>after 7 weeks</b>	<b>initial condition</b>	<b>after 7 weeks</b>
20	58.1	61.1	50.3	49.4
30	57.9	59.9	57.3	47.3
40	56.9	57.9	47.0	45.2
50	53.5	55.7	44.3	43.3
80	51.0	52.2	46.5	40.6
100	49.3	50.5	45.5	39.2
200	47.2	46.5	44.0	37.5
300	44.3	43.6	41.3	36.1
500	41.4	41.3	39.1	35.4
700	41.1	39.8	38.5	34.6
1000	39.7	37.6	37.2	34.1

	<b>Tetra</b>		<b>Silox</b>	
<b>Surface age [ms]</b>	<b>initial condition</b>	<b>after 7 weeks</b>	<b>initial condition</b>	<b>after 7 weeks</b>
20	38.9	67.7	60.5	62.7
30	36.9	67.1	59.8	61.7
40	36.8	66.1	59.2	61.7
50	36.1	65.3	57.4	61.6
80	36.0	63.0	56.9	61.0
100	36.1	61.5	55.4	60.1
200	36.0	55.5	53.8	60.2
300	36.3	51.5	53.8	59.9
500	36.0	48.0	48.1	59.3
700	36.2	45.9	45.6	59.1
1000	36.2	44.3	43.0	58.9

**Table F6:** Long term stability of surfactants in cleaning solution C1.

<b>C1</b>	<b>EG 360</b>		<b>S2502</b>	
<b>Surface age [ms]</b>	<b>initial condition</b>	<b>after 7 weeks</b>	<b>initial condition</b>	<b>after 7 weeks</b>
20		53.6	40.8	40.8
30	48.0	50.7	39.9	39.4
40	47.3	47.7	38.3	38.7
50	45.5	46.0	38.0	38.0
80	43.0	43.0	37.1	37.0
100	42.1	41.4	36.6	36.5
200	39.6	39.1	36.2	36.1
300	37.7	37.0	35.5	35.7
500	36.3	34.8	35.3	35.2
700	35.0	34.2	34.9	34.7
1000	34.0	32.7	34.5	34.3

	<b>Tetra</b>		<b>Silox</b>	
<b>Surface age [ms]</b>	<b>initial condition</b>	<b>after 7 weeks</b>	<b>initial condition</b>	<b>after 7 weeks</b>
20	41.6	50.4	49.3	62.5
30	41.2	48.1	48.2	61.9
40	40.8	45.9	46.4	61.6
50	40.4	45.1	45.8	61.8
80	40.2	43.7	44.1	61.8
100	40.0	43.4	43.3	61.4
200	39.7	42.6	36.8	61.3
300	39.6	42.0	33.3	61.4
500	39.3	41.7	33.6	61.5
700	39.2	41.6	29.6	61.3
1000	39.4	41.1	27.0	61.1

## G Compatibility of surfactant solutions to copper and diffusion barrier materials

**Table G1:** Sheet resistance values of copper, TiN and TaN after surfactant treatment using different rinsing solutions

	Cleaner / Rinse	Cu1	TiN	TaN
<b>Reference</b>		1.77E-02	3.26E+01	2.38E+01
<b>Tetra</b>	B1 DIW	1.83E-02	3.42E+01	2.48E+01
	B1 IPA	1.96E-02	3.31E+01	2.28E+01
	B2 DIW	1.97E-02	3.22E+01	2.34E+01
	B2 IPA	1.85E-02	3.24E+01	2.52E+01
	C1 DIW	1.77E-02	3.46E+01	2.25E+01
	C1 IPA	1.93E-02	3.39E+01	2.25E+01
<b>Silox</b>	B1 DIW	1.90E-02	3.20E+01	2.23E+01
	B1 IPA	2.04E-02	3.12E+01	2.29E+01
	B2 DIW	2.01E-02	3.10E+01	2.14E+01
	B2 IPA	1.95E-02	3.25E+01	2.36E+01
	C1 DIW	1.80E-02	3.19E+01	2.19E+01
	C1 IPA	1.97E-02	3.13E+01	2.06E+01
<b>EG360</b>	B1 DIW	2.26E-02	3.37E+01	2.44E+01
	B1 IPA	1.78E-02	3.24E+01	2.36E+01
	B2 DIW	1.80E-02	3.13E+01	2.37E+01
	B2 IPA	2.03E-01	3.19E+01	2.42E+01
	C1 DIW	1.91E-02	3.17E+01	2.35E+01
	C1 IPA	1.79E-02	3.36E+01	2.38E+01
<b>S2502</b>	B1 DIW	2.15E-02	3.32E+01	2.44E+01
	B1 IPA	1.96E-02	3.21E+01	2.53E+01
	B2 DIW	2.01E-02	3.22E+01	2.41E+01
	B2 IPA	3.51E+02	3.17E+01	2.48E+01
	C1 DIW	1.92E-02	3.29E+01	2.46E+01
	C1 IPA	1.88E-02	3.11E+01	2.42E+01

## H Compatibility study of surfactant aided cleaning solutions on porous low-k dielectrics – FTIR data

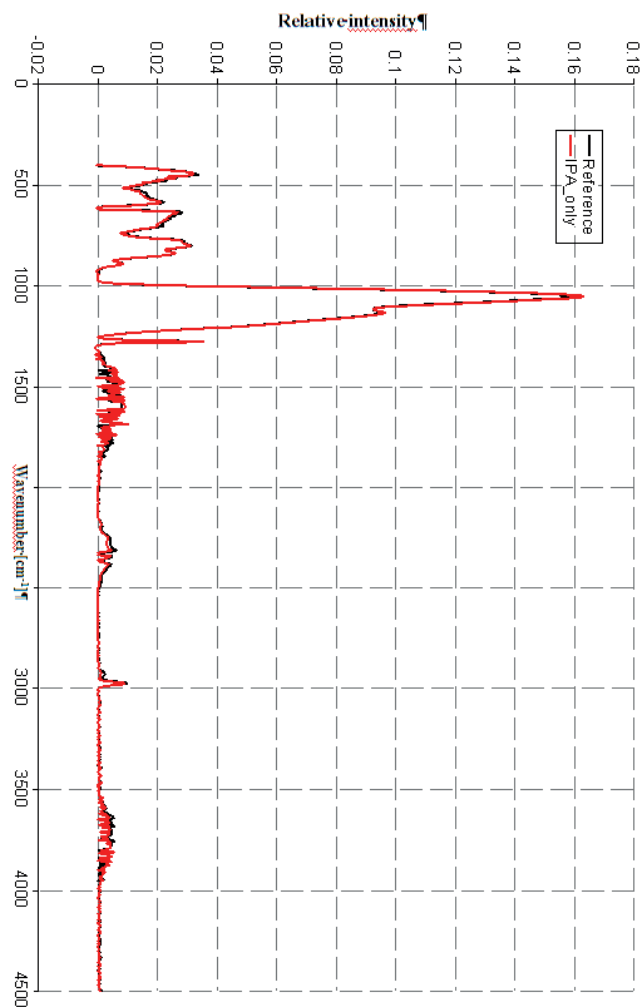


**Figure H1:** FTIR spectra of the porous low-k dielectric in pristine condition and after treatment with IPA.

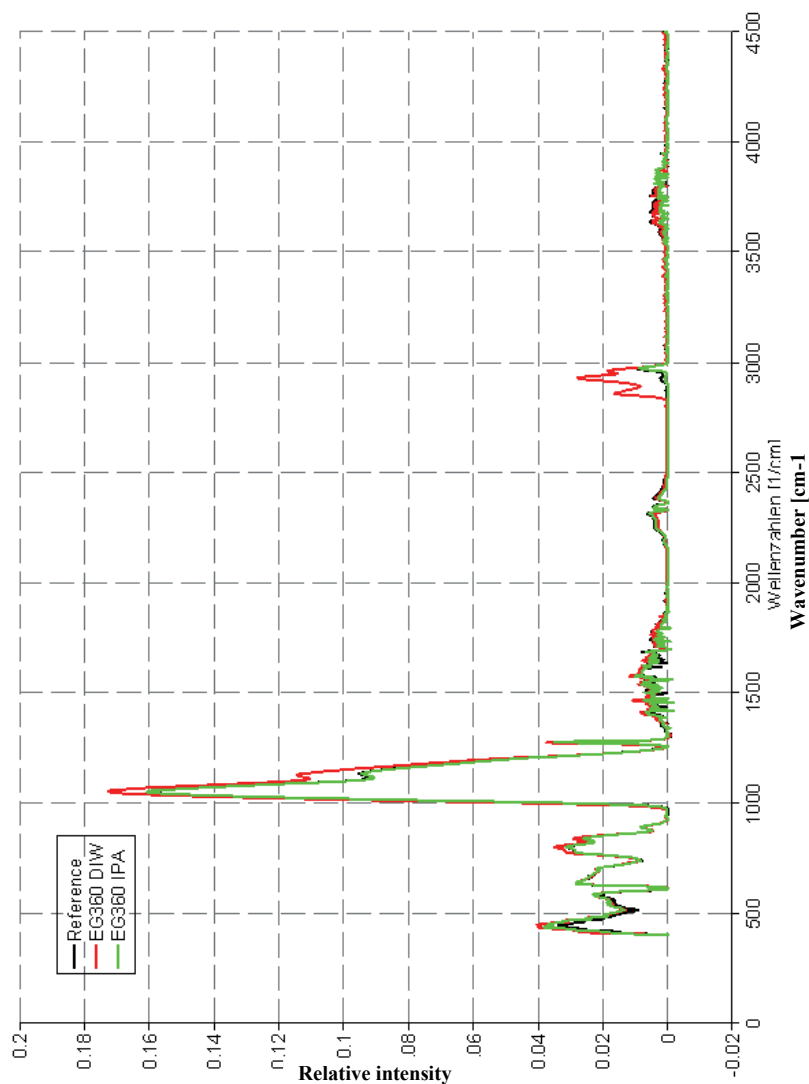


**Figure H2:** FTIR spectra of the porous low-k dielectric before and after treatment with EG360 and different rinsing solutions.



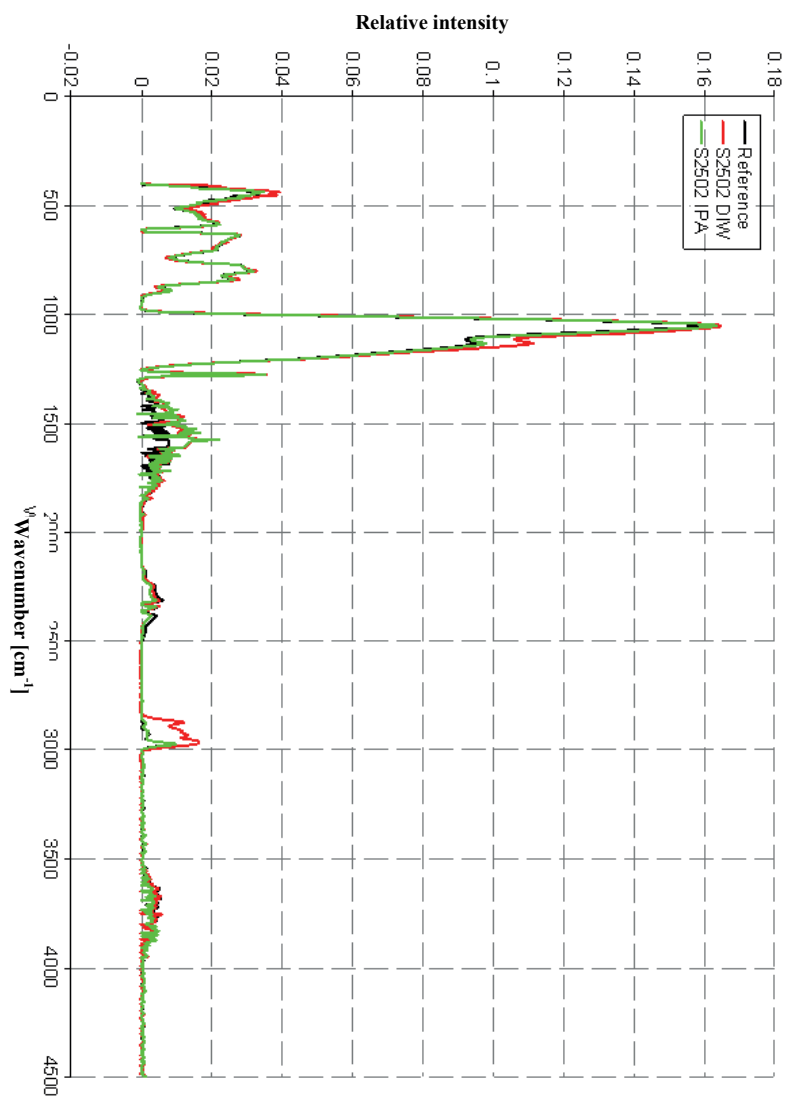


**Figure H3:** FTIR spectra of the porous low-k dielectric before and after treatment with S2505 and different rinsing solutions.

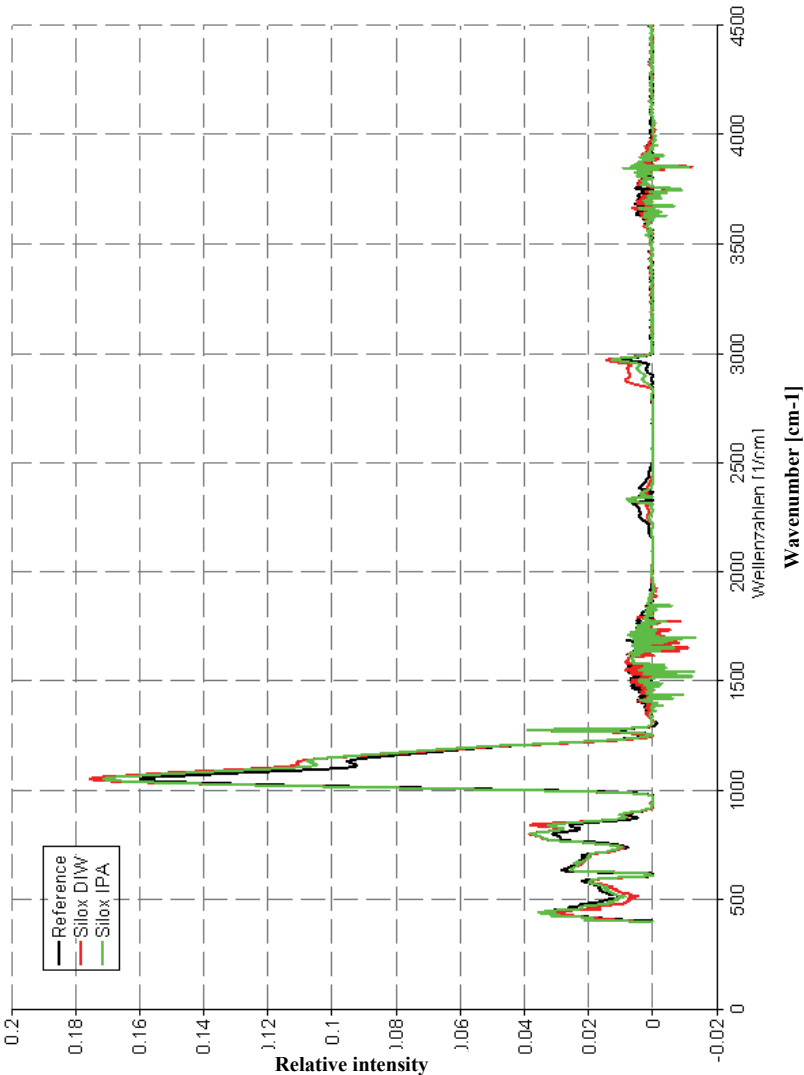


**Figure H4:** FTIR spectra of the porous low-k dielectric before and after treatment with Silox and different rinsing solutions.

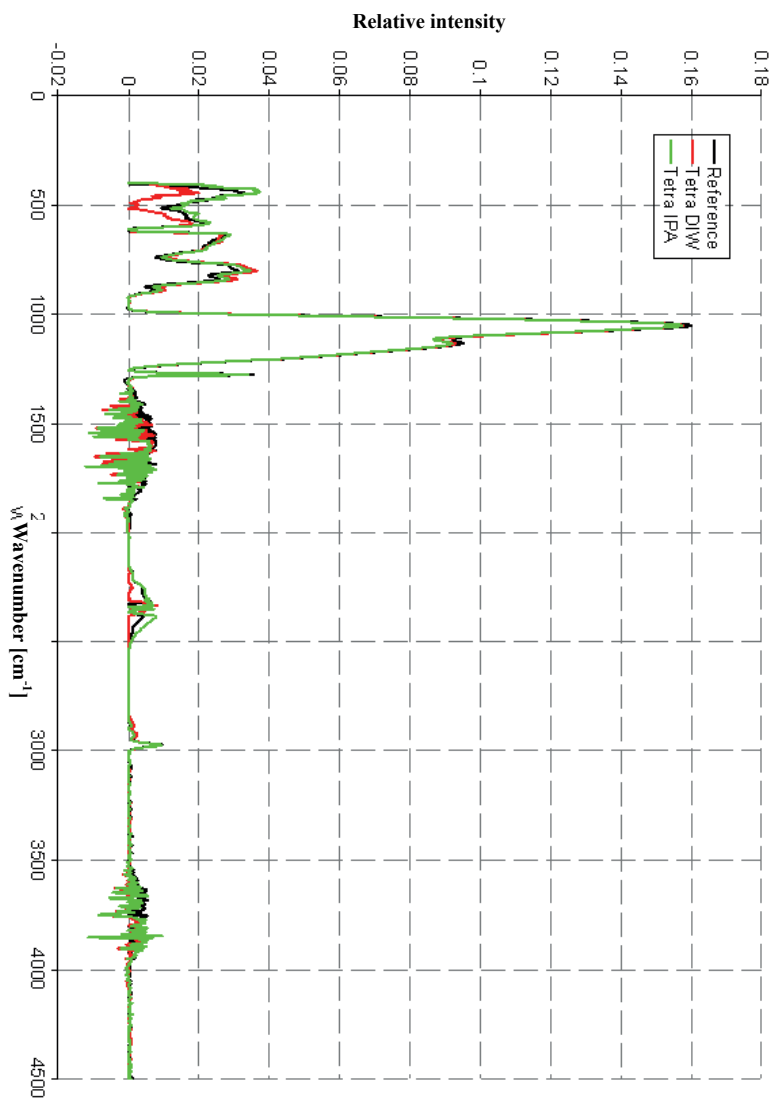


**Figure H5:** FTIR spectra of the porous low-k dielectric before and after treatment with Tetra and different rinsing solutions.

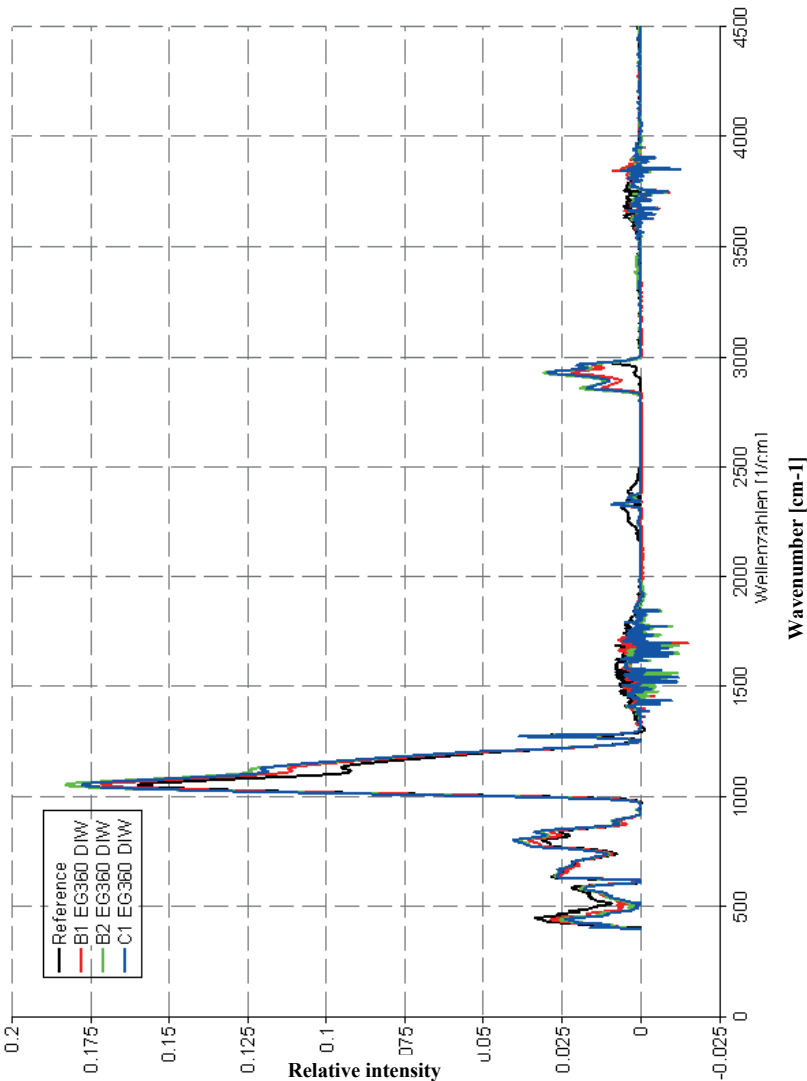


**Figure H6:** FTIR spectra of the porous dielectric before and after treatment with EG360 mixed in the studied cleaning liquids and DIW as rinsing solution.

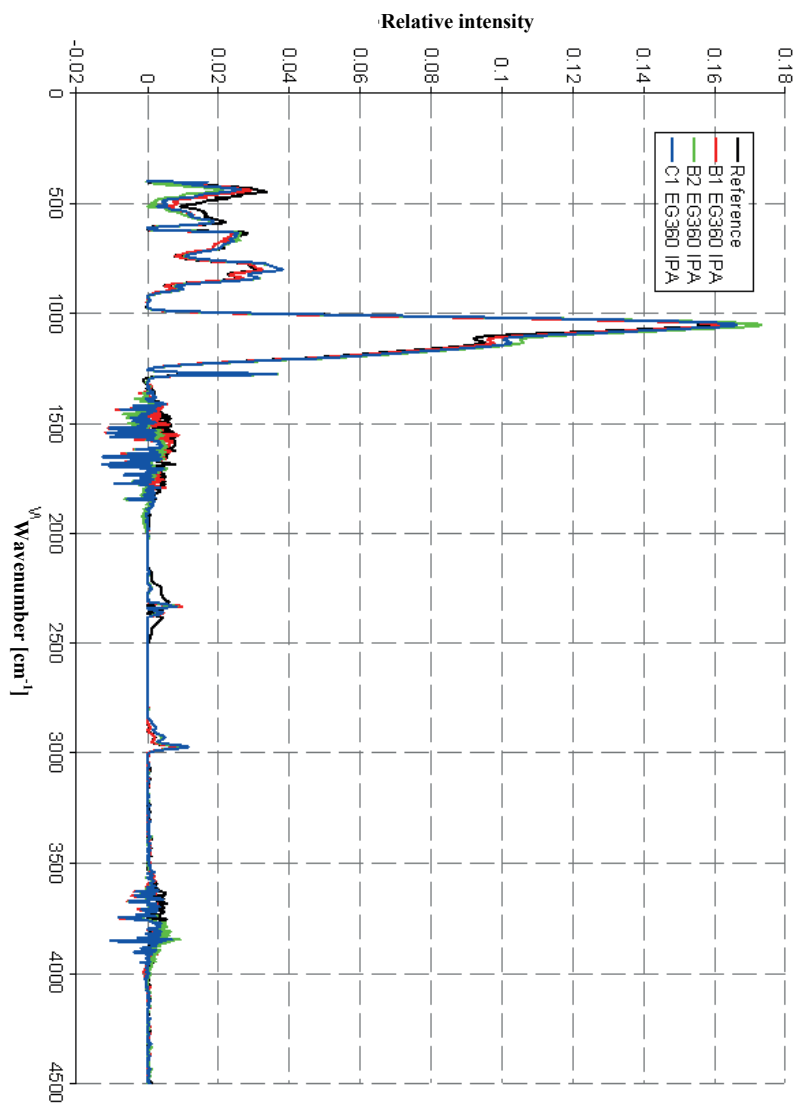


**Figure H7:** FTIR spectra of the porous dielectric before and after treatment with EG360 mixed in the studied cleaning liquids and IPA as rinsing solution.

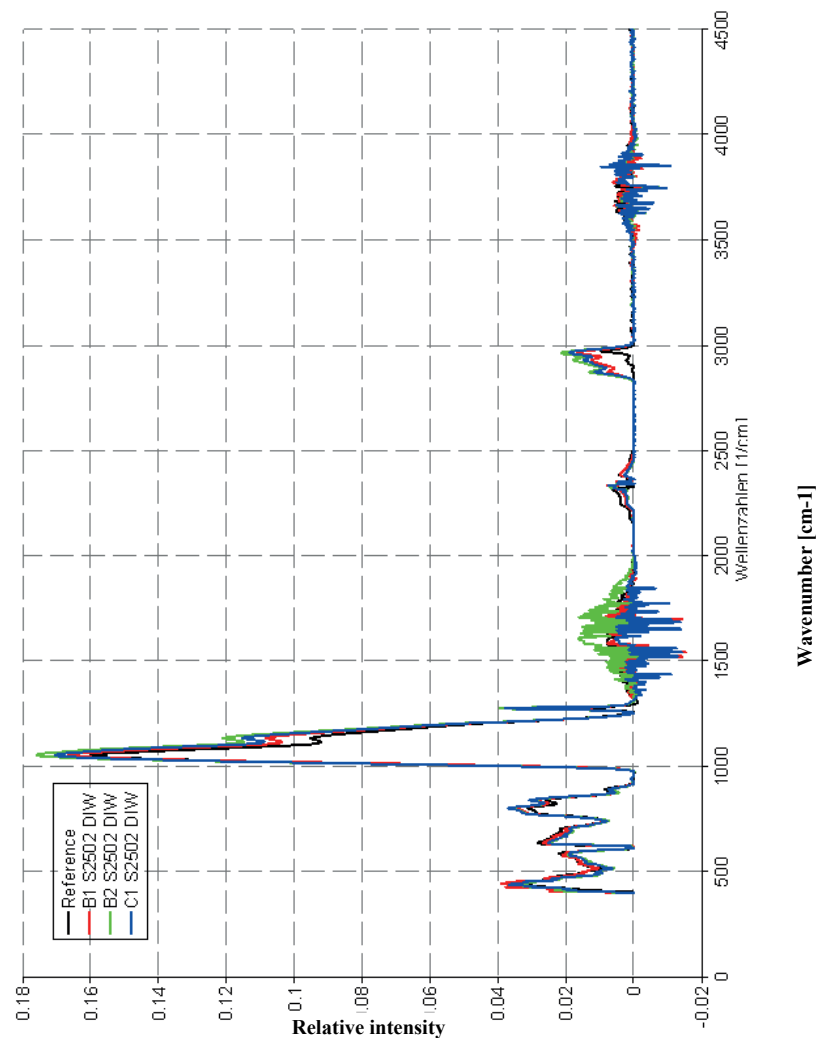


**Figure H8:** FTIR spectra of the porous dielectric before and after treatment with S2502 mixed in the studied cleaning liquids and DIW as rinsing solution.

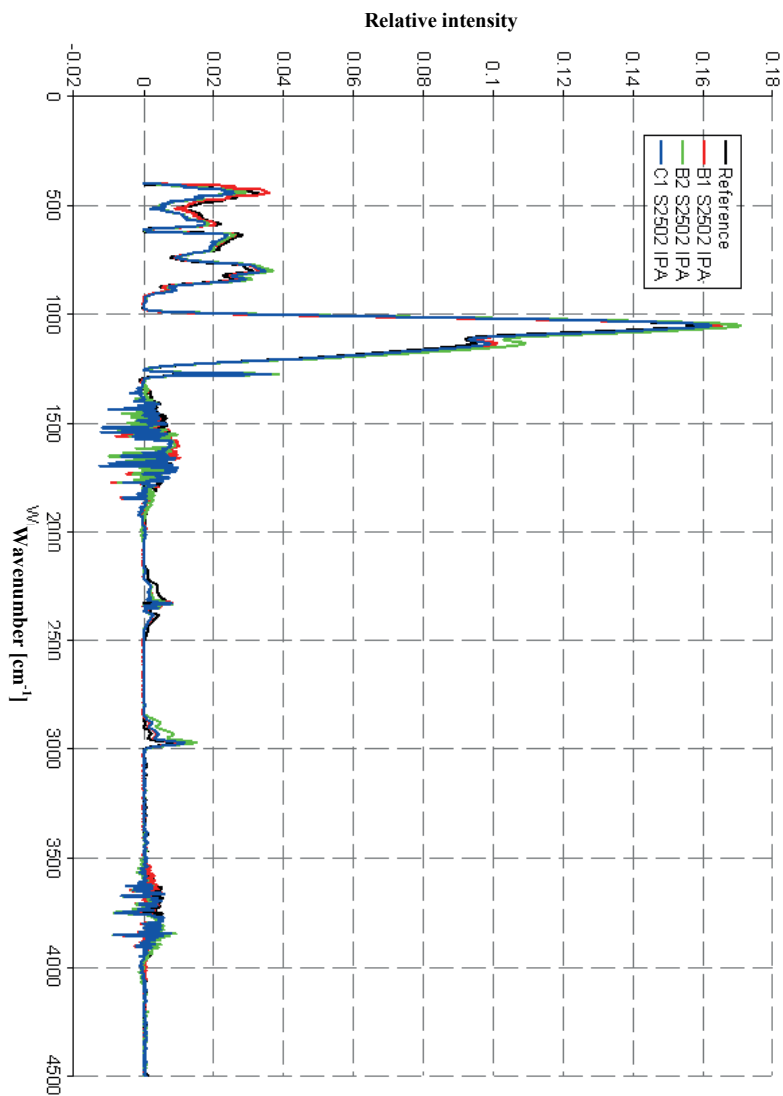


**Figure H9:** FTIR spectra of the porous dielectric before and after treatment with S2502 mixed in the studied cleaning liquids and IPA as rinsing solution.

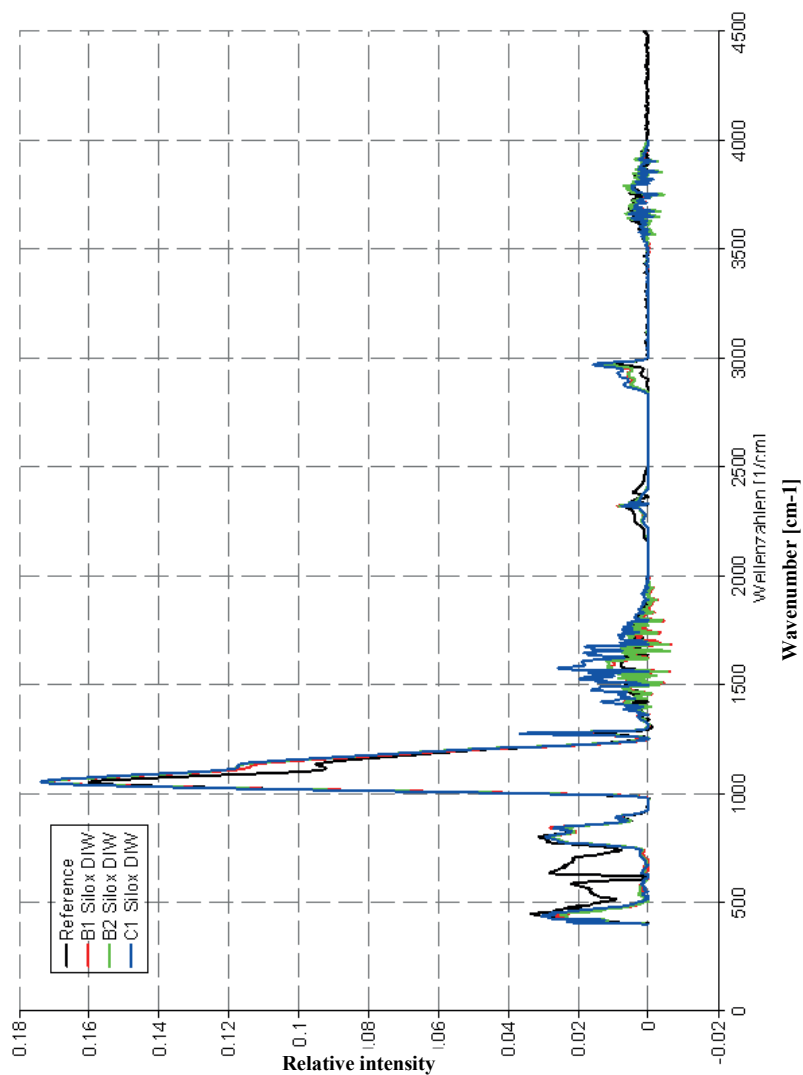


**Figure H10:** FTIR spectra of the porous dielectric before and after treatment with Silox mixed in the studied cleaning liquids and DIW as rinsing solution.



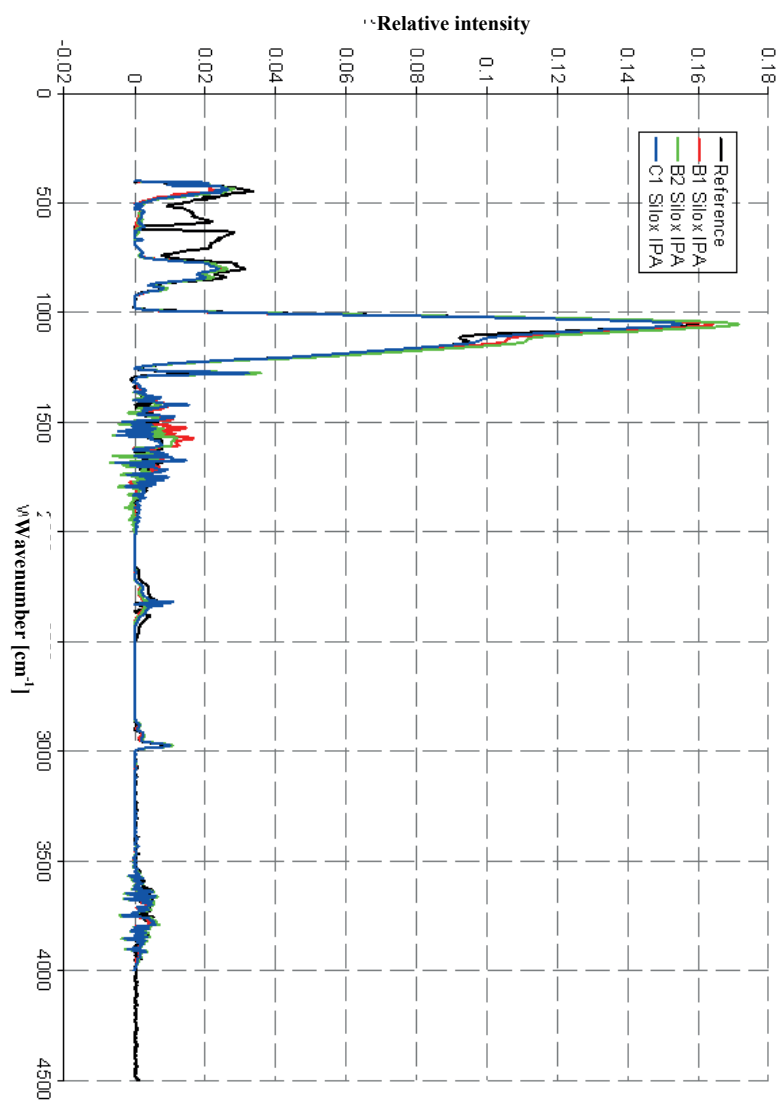


**Figure H11:** FTIR spectra of the porous dielectric before and after treatment with Silox mixed in the studied cleaning liquids and IPA as rinsing solution.

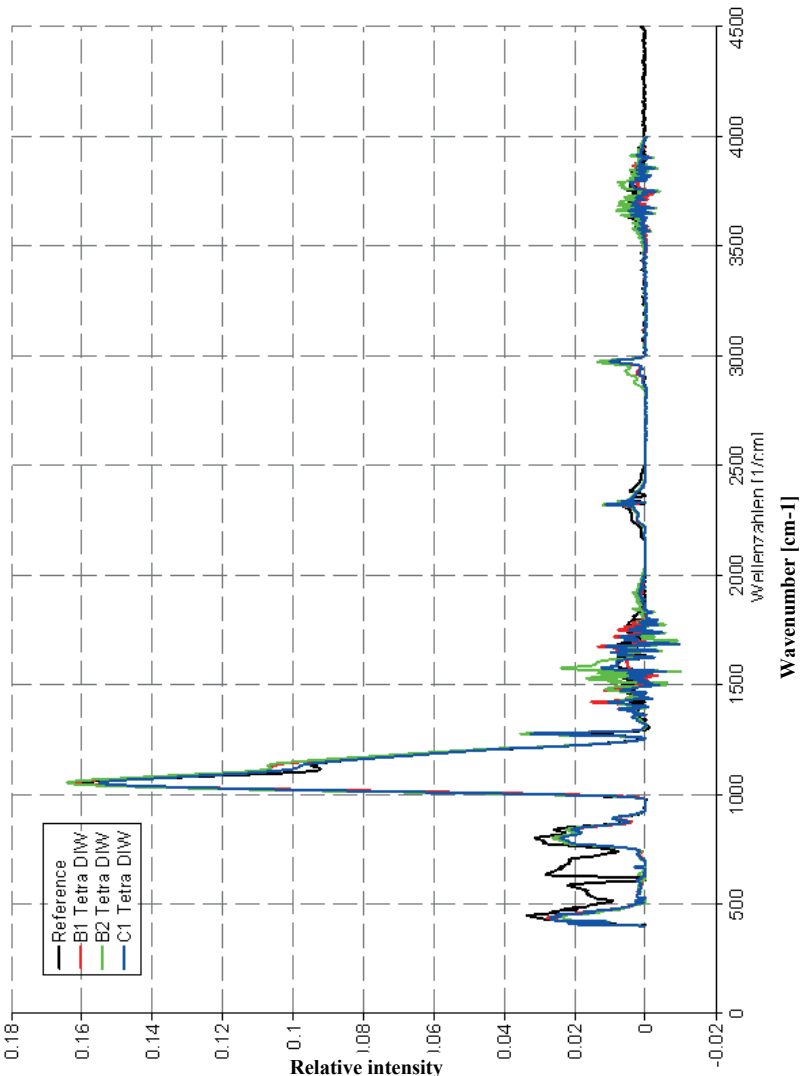


**Figure H12:** FTIR spectra of the porous dielectric before and after treatment with Tetra mixed in the studied cleaning liquids and DIW as rinsing solution.

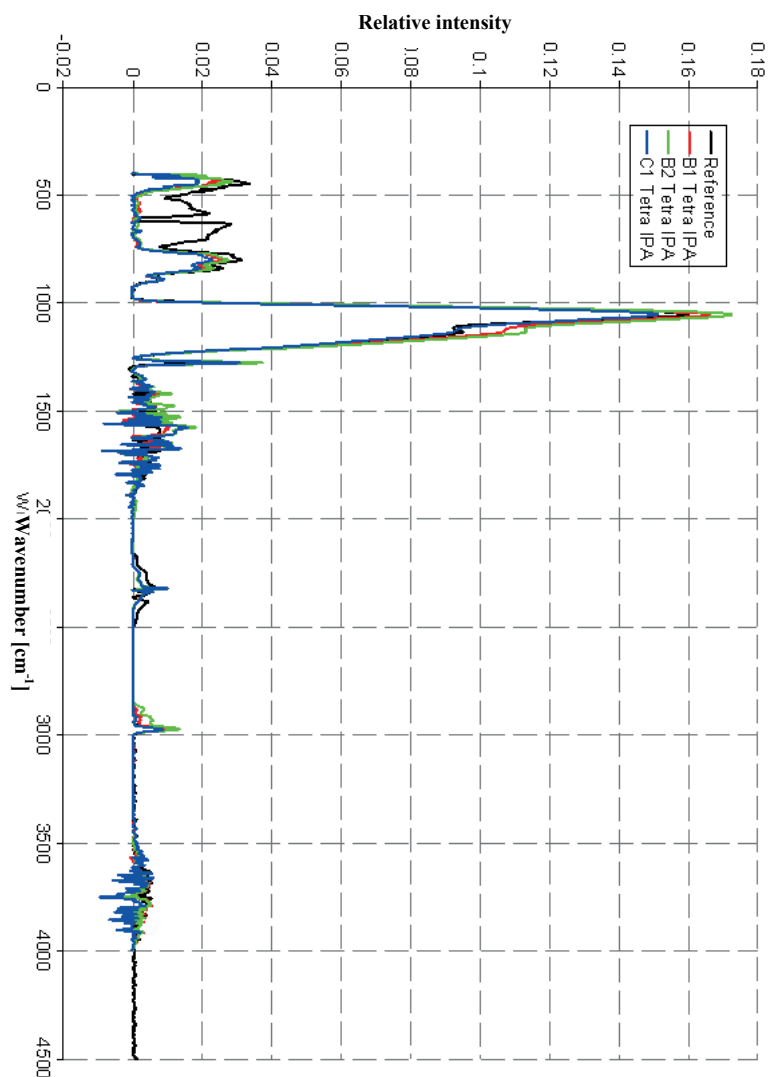


**Figure H13:** FTIR spectra of the porous dielectric before and after treatment with Tetra mixed in the studied cleaning liquids and IPA as rinsing solution.

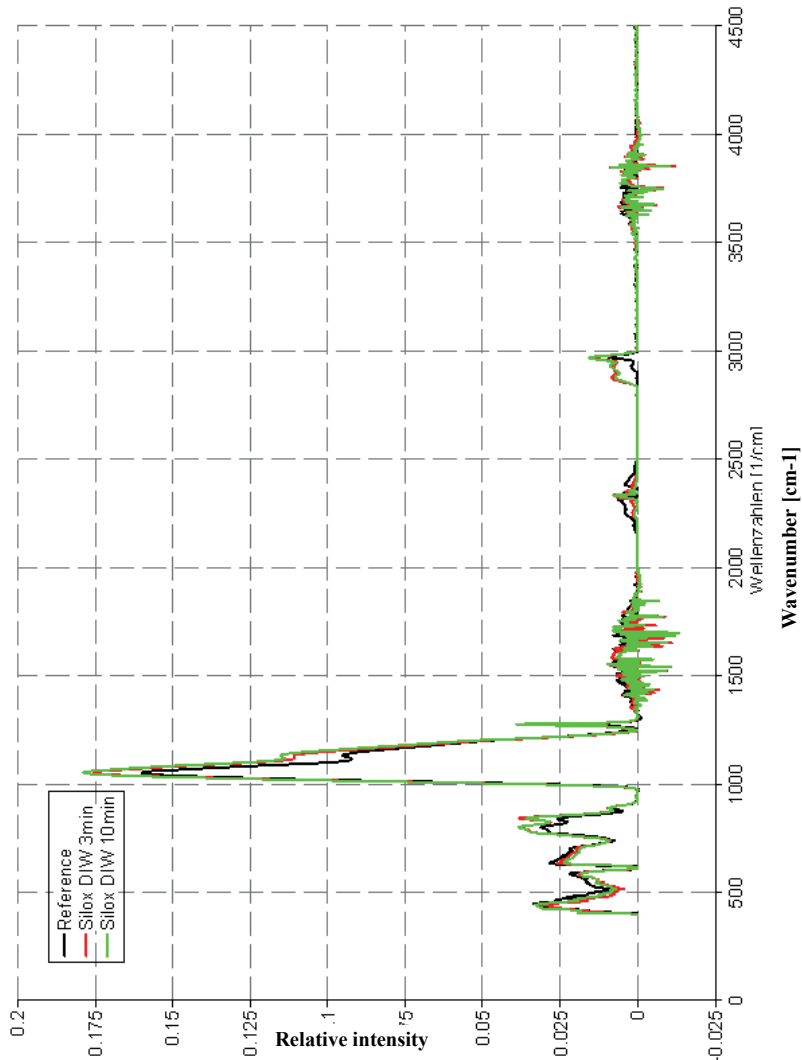


**Figure H14:** FTIR spectra of the porous low-k dielectric after treatment with Silox and different DIW rinsing times.

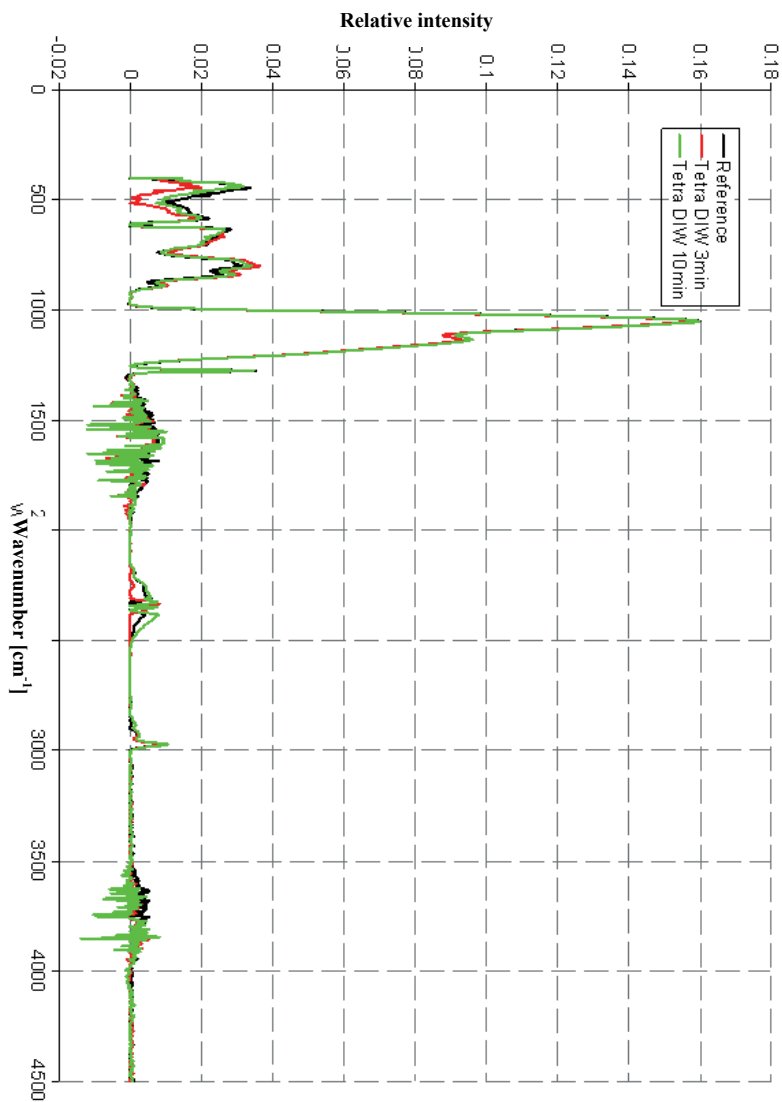


**Figure H15:** FTIR spectra of the porous low-k dielectric after treatment with Tetra and different DIW rinsing times.

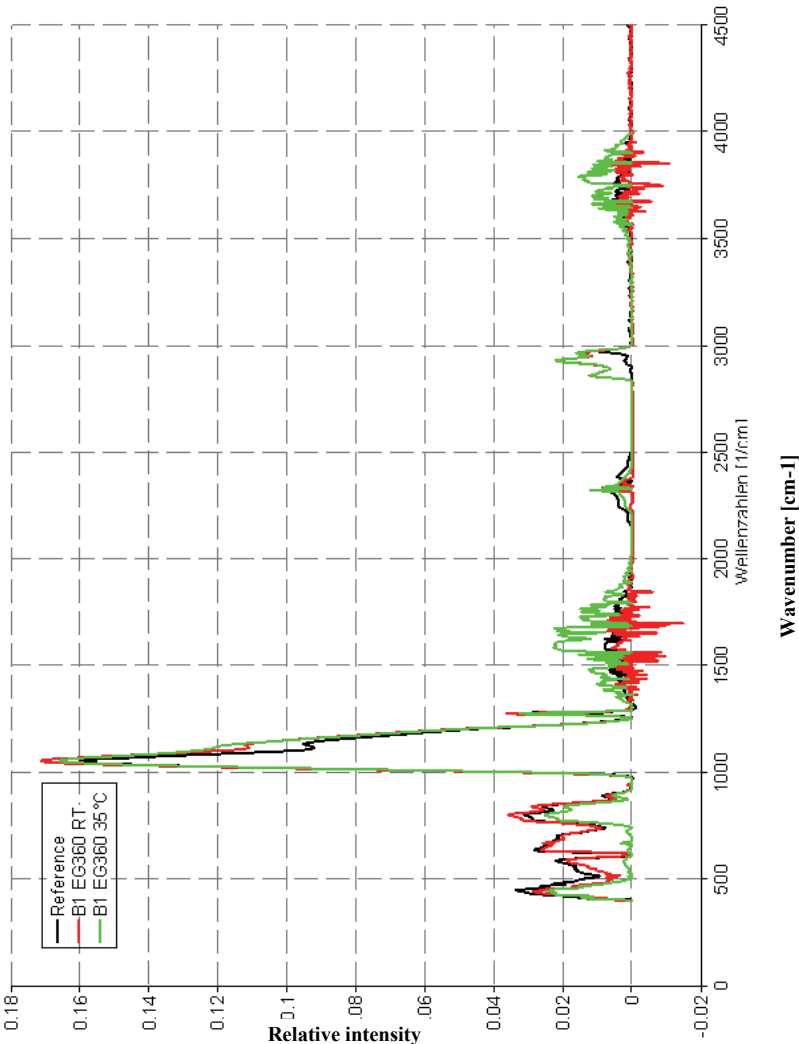


**Figure H16:** FTIR spectra of the porous low-k dielectric after treatment with EG360 mixed in solution B1 at elevated bath temperature.

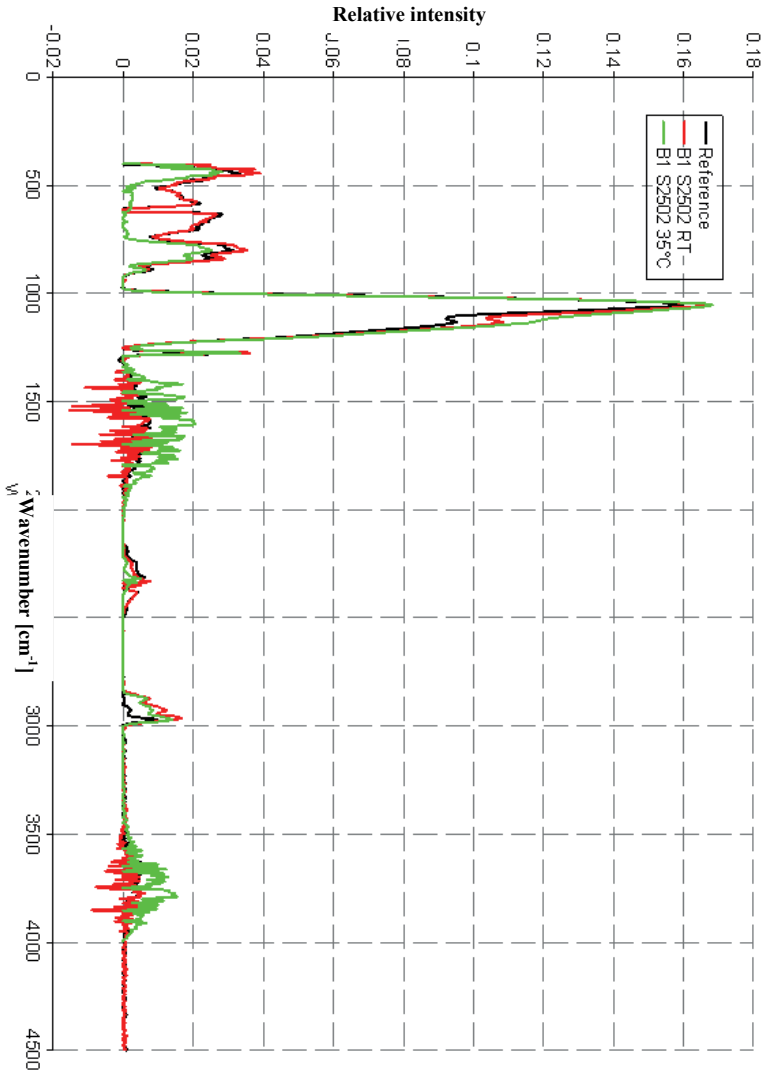


**Figure H17:** spectra of the porous low-k dielectric after treatment with S2502 mixed in solution B1 at elevated bath temperature.

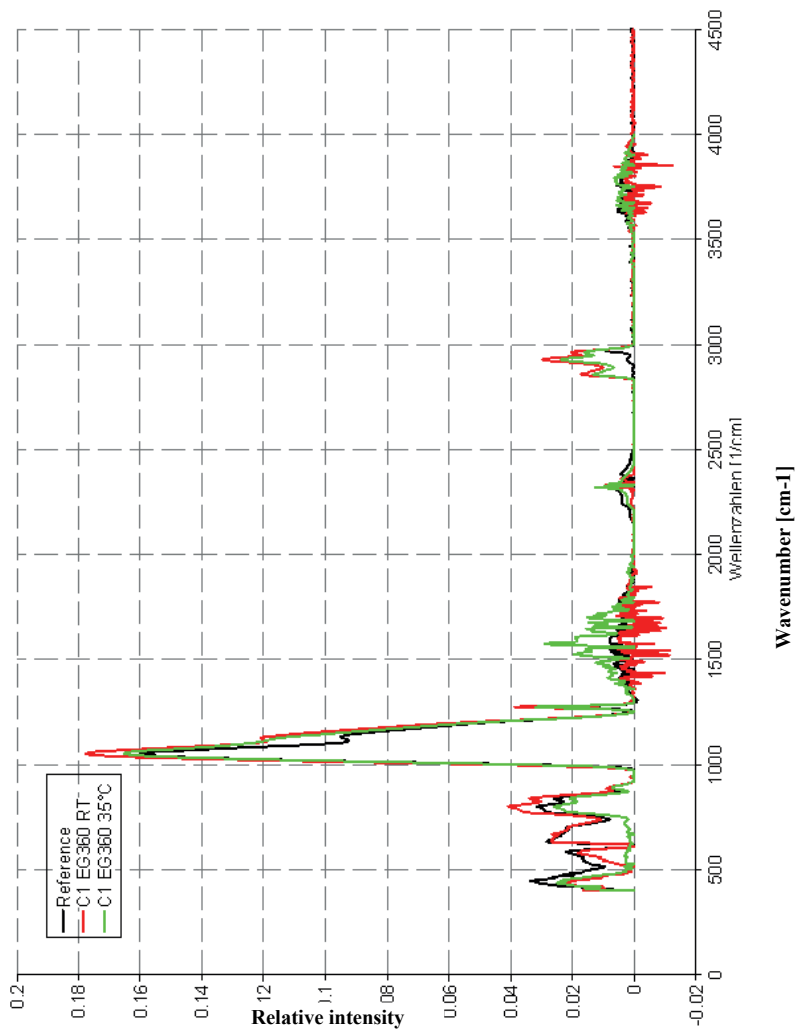


**Figure H18:** FTIR spectra of the porous low-k dielectric after treatment with EG360 mixed in solution C1 at elevated bath temperature.



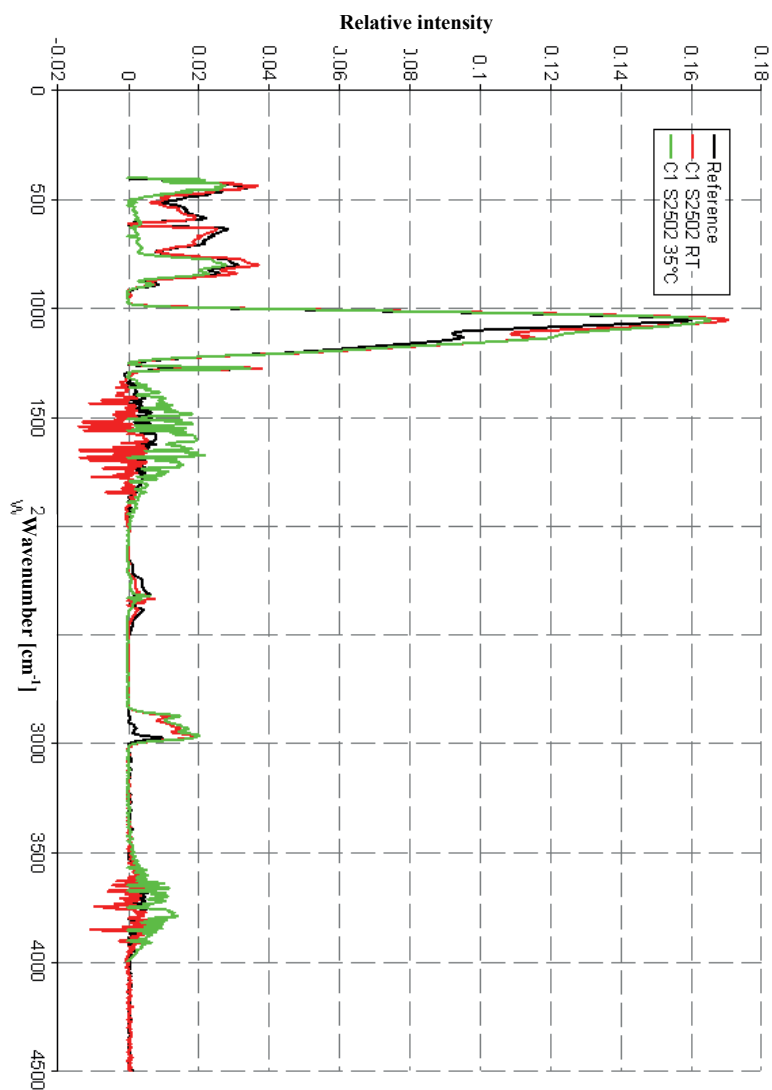


**Figure H19:** FTIR spectra of the porous low-k dielectric after treatment with S2502 mixed in solution C1 at elevated bath temperature.

## I Rating of the surfactant aided solutions regarding wetting behavior and material compatibility

**Table II:** Rating of the surfactant aided solutions including dynamics, surface energy, stability and material compatibility.

Surfactant → Cleaner →	EG360			S2502		
	B1	B2	C1	B1	B2	C1
Surface energy	2	3	3	2	3	3
Dynamics	3	1	2	4	2	3
Long term stability	4	4	4	4	3	4
Total	9	8	9	10	8	10
Compatibility to porous low-k	DIW / IPA					
Room temperature						
n	1 / 3	1 / 2	1 / 3	1 / 4	1 / 2	1 / 4
k	1 / 2	1 / 4	1 / 4	1 / 1	1 / 3	1 / 4
J	1 / 2	1 / 1	1 / 2	1 / 1	1 / 1	2 / 3
Total	3 / 7	3 / 7	3 / 9	3 / 6	3 / 6	4 / 11
35°C						
n	1 / 4	1 / 3	1 / 4	1 / 4	1 / 4	1 / 3
k	1 / 2	1 / 1	2 / 4	3 / 4	1 / 2	1 / 4
J	2 / 3	2 / 2	2 / 4	3 / 4	3 / 2	3 / 4
Total	4 / 9	4 / 6	5 / 12	7 / 12	5 / 8	5 / 11
Compatibility to metals / barriers						
Cu	1 / 4	4 / 1	2 / 3	1 / 1	1 / 3	2 / 2
TiN	3 / 3	3 / 3	3 / 3	4 / 4	4 / 3	4 / 3
TaN	3 / 4	4 / 4	4 / 4	3 / 3	2 / 3	4 / 4
Total	7 / 11	11 / 8	9 / 10	8 / 8	7 / 9	10 / 9

Surfactant →	S2502	Silox			Tetra		
Cleaner →	C1	B1	B2	C1	B1	B2	C1
Surface energy	3	4	2	4	2	3	3
Dynamics	3	1	1	1	4	4	4
Long term stability	4	1	2	1	4	1	3
Total	10	6	5	6	10	8	10
Compatibility to porous low-k	DIW / IPA	DIW / IPA					
Room temperature							
n	1 / 4	1 / 4	1 / 4	1 / 4	3 / 4	3 / 2	3 / 4
k	1 / 4	3 / 4	3 / 4	3 / 4	3 / 4	4 / 4	4 / 4
J	2 / 3	3 / 3	2 / 2	2 / 3	3 / 2	3 / 2	3 / 4
Total	4 / 11	7 / 11	7 / 10	6 / 11	9 / 10	10 / 8	10 / 12
35°C							
n	1 / 3	1 / 4	3 / 4	2 / 4	2 / 4	2 / 3	2 / 4
k	1 / 4	3 / 4	3 / 3	1 / 3	2 / 4	3 / 2	4 / 4
J	3 / 4	3 / 3	3 / 3	3 / 3	3 / 3	3 / 2	3 / 4
Total	5 / 11	7 / 11	9 / 10	6 / 10	7 / 11	8 / 7	9 / 12
Compatibility to metals / barriers							
Cu	2 / 2	2 / 1	1 / 1	4 / 1	3 / 1	1 / 3	4 / 2
TiN	4 / 3	4 / 3	2 / 4	3 / 3	3 / 4	4 / 4	2 / 3
TaN	4 / 4	2 / 4	3 / 2	1 / 1	3 / 2	3 / 2	4 / 2
Total	10 / 9	8 / 8	5 / 7	8 / 5	9 / 7	8 / 9	10 / 7

## References

- [1] J. Bardeen, W.H. Brattain, Phys. Rev. **74** 2 (1948), pp. 230-231
- [2] J. Bardeen, W. Brattain, W. Shockley: Three-Electrode Circuit Element utilizing Semiconductive Material, US Patent No. 2.524.035, Received June 27<sup>th</sup> 1948, Published October 3<sup>rd</sup> 1950
- [3] G.K. Teal, IEEE Transactions on Electron Devices ED **23** 7 (1976), pp. 621-639
- [4] B. Stoffels, Kilby, Noyce and the Integrated Circuit, OSP Magazine, <http://www.ospmag.com/issue/article/012009-Stoffels> (2009)
- [5] D. Khang, M.M. Atalla, IRE Solid State Device Res. Conf. Pittsburgh (1960)
- [6] G.E. Moore, Electronics 38 8 (1965)
- [7] ITRS Interconnect Working Group, 2009 Revision, [http://public.itrs.net/links/2009/inter/Presentations/Conference/3New Interconnect Presentation Hsinchu 16 Dec. 2009\\_v5.pdf](http://public.itrs.net/links/2009/inter/Presentations/Conference/3New%20Interconnect%20Presentation%20Hsinchu%2016%20Dec.%202009_v5.pdf)
- [8] Wikimedia Commons, [http://commons.wikipedia.org/wiki/File:Transistor\\_Count\\_and\\_Moore's\\_Law\\_-\\_2008\\_1024.png](http://commons.wikipedia.org/wiki/File:Transistor_Count_and_Moore's_Law_-_2008_1024.png), (2008)
- [9] R.R. Tummala, IEEE Spectrum, [http://spectrum.ieee.org/computing/hardware/moores\\_law-meets-its-match](http://spectrum.ieee.org/computing/hardware/moores_law-meets-its-match), (2006)
- [10] L. Favenne, V. Jousseau, G. Gerbaud, J. Appl. Phys. 102 (2007), 064107-1-9
- [11] A. Majumdar, G. Das, N. Patel, J. Electrochem. Soc. 155 1 (2008), pp. D22-D26
- [12] K. Maex, M.R. Baklanov, D. Shamiryan, J. Appl. Phys. 93 11 (2003), pp. 8793-8841
- [13] S. Verhaverbeke, S. Kuppurao, C. Beaudry, Semi. Intl. 25 91 (2002)
- [14] S. Sameer, K. Ajmera, P.D. Matz, Future Fab Intl. 17 (2004)
- [15] M.A. Fury, International Semiconductor Technology Conference ISTC, Shanghai (2004)
- [16] The International Technology Roadmap for Semiconductors, 2009 Edition, <http://www.itrs.net>
- [17] S. Jeng, R. Havemann, M. Chang, Mat. Res. Soc. Proc. 337 25 (1996)
- [18] P.J. Wolf, Overview of Dual Damascene Cu/Low-k Interconnect, ERC Retreat Stanford Aug. 14<sup>th</sup> 2003
- [19] V. Pavlidis, Technion Electrical Engineering,

- <http://webee.technion.ac.il/courses/048864/rochester/spring 2004 presentations/ inter-cap.pdf>, (2004)
- [20] A. Sonanane, B.N. Joshi, A.M. Mahajan, Progress in Electromagnetics Research Lett. 1 (2008), pp. 189-196
- [21] D.C. Edelstein, G.A. Aai-Halasz, Y.J. Mii, IBM J. Res. Dev. 39 (1995), pp. 383
- [22] S. Aksu, Interconnect of new millenium: Copper, <http://www.mse.berkeley.edu/groups/serdar/RESEARCH/copper.pdf>, (1999)
- [23] E.T. Ogawa, J. Kim, G.S. Haase, IEEE 41<sup>st</sup> Annual International Reliability Physics Symposium, Dallas, Texas (2003), pp. 166-172
- [24] P. Laube, Low-k technology, [http://www.halbleiter.org/en/metallization/copper/#Low-k\\_technology](http://www.halbleiter.org/en/metallization/copper/#Low-k_technology), (2010)
- [25] S. Fruehauf, I. Streiter, R. Puschmann, ULSI XVIII, Proceedings (2003), pp. 507-512
- [26] V. Antochshuk, M. Jaroniec, Chem. Mater. 12 8 (2000), pp. 2496-2501
- [27] A.T. Kohl, R. Mimna, R. Shick, Electrochem. Solid State Lett. 2 2 (1999), pp. 77-79
- [28] M. Ikeda, J. Nakahira, Y. Iba, IEEE (2003), pp. 71-73
- [29] S.M. Gates, D.A. Neumayer, M.H. Sherwood, J. Appl. Phys. 101 (2007), pp. 094103-1-8
- [30] A. Grill, V. Patel, K.P. Rodbell, J. Appl. Phys. 94 5 (2003), pp. 3427-3435
- [31] R.N. Vrtis, M.L. O'Neill, J.L. Vincent, Porogens, porogenated precursors and methods for using the same to provide porous organosilica glass films with low dielectric constants, US Patent 7384471, Received July 4<sup>th</sup> 2003, Published June 10<sup>th</sup> 2008
- [32] A. Zenasni, V. Jousseau, P. Holliger, J. Appl. Phys. 102 (2007), pp. 094107-1-8
- [33] K. Schulze, S.E. Schulz, M. Rennau, MRS Conf. Proc. AMC XXI, Mater. Res. Soc. (2006), pp. 309-316
- [34] P. Laube, Copper technology, [http://halbleiter.org/en/metallization/copper/#copper\\_technology](http://halbleiter.org/en/metallization/copper/#copper_technology) (2010)
- [35] A. Sankaran, M.J. Kushner, Appl. Phys. Lett. 82 12 (2003), pp. 1824-1826
- [36] Q.T. Le, C.M. Whelan, H. Struyf, Electrochem. Solid-State Lett. 7 9 (2004), pp. F49-F53
- [37] D. Eon, M. Darnon, T. Chevolleau, J. Vac. Sci. Technol. B 25 3 (2007), pp. 715-720
- [38] C.L. Timmons, Fluorocarbon Post-Etch Residue Removal Using Radical Anion Chemistry, Thesis at Georgia Institute of Technology November 2004

- [39] X. Li, X. Hua, L. Ling, J. Vac. Sci. Technol. A 20 (2002), pp. 2052
- [40] N. Posseme, T. Chevolleau, O. Joubert, J. Vac. Sci. Technol. B 21 (2003), pp. 2432
- [41] H. Cui, S.J. Kirk, D. Maloney, IEEE/SEMI Advanced Semiconductor Manufacturing Conference (2007), pp. 366-370
- [42] A. Somashekar, H. Ying, P.B. Smith, J. Electrochem. Soc. 146 6 (1999), pp. 2318-2321
- [43] A. Sankaran, M. Kushner, Appl. Phys. Lett. 82 12 (2003), pp. 1825-1826
- [44] G. Potter, G. Morrison, J. Vac. Sci. Technol. B 20 (1992), pp. 2398
- [45] F. Fonash, J. Electrochem. Soc. 137 (1990), pp. 3885
- [46] J. Simko, G. Oehrlein, J. Electrochem. Soc. 138 (1991), pp. 277
- [47] S. Verhaverbeke, S. Kuppurao, Semiconductor Intl. 25 (2002), pp. 91
- [48] D. Louis, C. Peyne, Microelectronic Eng. 46 (1999), pp. 307
- [49] K. Ueno, V.M. Donnelly, T. Kikkawa, J. Electrochem. Soc. 144 7 (1997), pp. 2665-2572
- [50] D. Shamiryan, M. Baklanov, J. Vac. Sci. Technol. B 20 (2002), pp. 1923
- [51] Y. Wang, R. Kumar, J. Electrochem. Soc. 151 (2004), pp. F73
- [52] J. Bao, H. Shi, J. Liu, J. Vac. Sci. Technol. B 26 (2008), pp. 219-226
- [53] B. Jinnai, T. Nozawa, S. Samukawa, J. Vac. Sci. Technol. B 26 6 (2008), pp. 1926-1932
- [54] O. Louveau, C. Bourlett, Microelectronic Eng. 73 (2004), pp. 351
- [55] A. Matsushita, IITC Proc. 147 (2003)
- [56] T. Mourier, IITC Proc. 245 (2003)
- [57] E. Ryan, Mater. Res. Soc. Symp. Proc. 766 (2003)
- [58] G. Beyer, A. Satta, Microelectronic Eng. 64 (2002), pp. 233
- [59] K. Yonekura, S. Skamori, J. Vac. Sci. Technol. B 22 (2004), pp. 548
- [60] S. Hwang, G. Lee, Surf. Coat. Technol. 174 (2003), pp. 835
- [61] M. Worsley, S. Brent, J. Vac. Sci. Technol. B 23 (2005), pp. 395
- [62] A. Grill, V. Sternhagen, J. Appl. Phys. 98 (2005), pp. 074502
- [63] X. Hua, J. Vac. Sci. Technol. B 24 (2006), pp. 1238

- [64] A. Humbert, L. Mage, *Microelectronic Eng.* 82 (2005), pp. 399
- [65] S. Xu, *J. Vac. Sci Technol. B* 25 (2007), pp. 156
- [66] M.A. Fury, *International Semiconductor Technology Conference ISTC*, Shanghai (2004)
- [67] S. Myneni, D.W. Hess, *J. Electrochem. Soc.* 150 12 (2003), pp. G744-G750
- [68] G. Levitin, S. Myneni, D.W. Hess, *J. Electrochem. Soc.* 151 6 (2004), G380-G386
- [69] W. Kern, *J. Electrochem. Soc.* 137 (1990), pp. 1887
- [70] C.L. Timmons, D.W. Hess, *J. Electrochem. Soc.* 155 10 (2008), H771-H777
- [71] I. Song, M. Spuller, G. Levitin, *J. Electrochem. Soc.* 153 4 (2006), G314-G318
- [72] G. Levitin, C. Timmons, D.W. Hess, *J. Electrochem. Soc.* 153 7 (2006), G712-G720
- [73] H.J. Lee, J.T. Park, J.Y. Yoo, *J. Korean Phys. Soc.* 42 (2003), pp. S202-S206
- [74] S.W. Ip, J.M. Toguri, *J. Mater. Sci.* 29 (1994), pp. 688-692
- [75] F. Thomsen, *Praxis der Kontaktwinkelmessung (5): Modelle nach Maß – vom Kontaktwinkel zur Oberflächenenergie*, KRÜSS GmbH, Applikationsberichte (2008)
- [76] U. Zorll, *Adhäsion* 9 (1974)
- [77] P.G. de Gennes, *Review of Modern Physics* 57 3 I (1985), pp. 827-863
- [78] M.J. Rosen, *Surfactants and Interfacial Phenomena* 3<sup>rd</sup> Edition, Hoboken, New Jersey, Wiley-Interscience (2004), pp. 244
- [79] Y.J. Sheng, S. Jiang, H.K. Tsao, *J. Chem. Phys.* 127 (2007), pp. 234704-1-7
- [80] D.K. Owens, R.C. Wendt, *J. Appl. Polymer Sci.* 13 (1969), pp. 1741-1747
- [81] H.J. Butt, K. Graf, M. Kappl, *Physics and Chemistry of Interfaces*, Wiley-VCH Verlag GmbH & Co. KGaA, Weinheim (2003), Chapter 2
- [82] A.M. Dupré, P. Dupré, *Théorie mécanique de la chaleur* (1869), Gauthier-Villars
- [83] R. Loman, N.P. Zwikker, *Physica* 7-12 (1934), pp. 1181-1201
- [84] T.F. Tadros, *Applied Surfactants – Principles and Applications*, Wiley-VCH Verlag GmbH & Co. KGaA (2005), Chapter 11
- [85] F.K. Hansen, *Surface Energy of Polymers*, [http://folk.uio.no/fhansen/surface\\_energy.pdf](http://folk.uio.no/fhansen/surface_energy.pdf), (2004)
- [86] C.J. van Oss, R.J. Good, M.K. Chaudhury, *Adv. Colloid Interface Sci.* 28 (1987), pp. 35

- [87] S. Wu, *Polymer Interface and Adhesion*, M. Dekker New York (1982)
- [88] J. Reese, 24<sup>th</sup> Annual Microelectronic Engineering Conference, May 2006, pp. 25-29
- [89] H. Namatsu, K. Kurihara, M. Nagase, *Appl. Phys. Lett* 66 20, (1995), pp. 2655-2657
- [90] M.T. Spuller, D.W. Hess, *J. Electrochem. Soc.* 150 8 (2003), pp. G476-G480
- [91] M. Olim, *J. Electrochem. Soc.* 144 12 (1997), pp. 4331-4335
- [92] B. Leclercq, M. Sotona, A. Baszkinb, *Polymer* 18 7 (1977), pp. 675-680
- [93] A. Drechsler, N. Petong, C. Bellmann, *Progress in Colloid and Polymer Science* 132 (2006), pp. 82-94
- [94] Q.T. Le, V. Jeannot, M.R. Baklanov, *Electrochem. Solid-State Lett.* 9 4 (2006), pp. F17-F21
- [95] J.A. Keagy, X. Zhang, K.P. Jonston, *J. of Supercritical Fluids* 39 (2006), pp. 277-285
- [96] G. Gawalek, *Tenside*, Akademie-Verlag Berlin 1975, Chapter 1
- [97] K. Kosswig, H. Stache [Hrsg.], *Die Tenside*, Carl Hanser Verlag München 1993, Chapter 1
- [98] T.F. Tadros, *Applied Surfactants – Principles and Applications*, Wiley-VCH Verlag GmbH & Co. KGaA 2005, Chapter 1
- [99] W. Preusser, C. Gierl, A. Rainer, *JOT* 10 (2002), pp. 106-108
- [100] A.W. Neumann, R.J. Good, C.J. Hope, *J. of Colloid and Interface Sci.* 49 2 (1974), pp. 291-304
- [101] K. Tamai, *Progress in Colloid and Polymer Science* 61 (1976), pp. 93-96
- [102] W.D. Harkins, H.F. Jordan, *J. Am. Chem. Soc.* 52 5 (1930), pp. 1751-1772
- [103] N. Wu, J. Dai, F.J. Micale, *J. of Colloid and Interface Sci.* 215 2 (1999), pp. 258-269
- [104] B. Song, J. Springer, *J. of Colloid and Interface Sci.* 184 1 (1996), pp. 77-91
- [105] V.B. Fainerman, R. Miller, P. Joos, *Colloid and Polymer Science* 272 6 (1994), pp. 731-739
- [106] A. Grill, D.A. Neumayer, *J. Appl. Phys.* 94 10 (2003), pp. 6697-6707
- [107] S.K. Hait, S.P. Moulik, *Current Science* 82 9 (2002), pp. 1101-1111
- [108] G.H. Kim, J.H. Han, 10th International Symposium on Ultra Clean Processing of Semiconductor Surfaces, Ostende (Belgium), 2010 Sep 20-22; Proceedings, pp. 34-35



- [109] A. Mallet, M. Prat, 10th International Symposium on Ultra Clean Processing of Semiconductor Surfaces, Ostende (Belgium), 2010 Sep 20-22; Proceedings, pp. 36-37
- [110] C.C. Yang, C.C. Ko, 10th International Symposium on Ultra Clean Processing of Semiconductor Surfaces, Ostende (Belgium), 2010 Sep 20-22; Proceedings, pp. 38-39
- [111] J.T. Kunjappu, "Ink Chemistry", Chemistry World 3 (2003), online edition: <http://www.rsc.org/chemistryworld/Issues/2003/March/>
- [112] T. Hargraves, "Surfactants: the ubiquitous amphiphiles" Chemistry World 7 (2003), online editions: <http://www.rsc.org/chemistryworld/Issues/2003/July>

## List of Figures

<b>Figure 1-1:</b> Moore's Law showing the transistor count doubling approximately every two years [8].....	2
<b>Figure 1-2:</b> Packing density of transistors on an IC and production cost per device. ....	3
<b>Figure 1-3:</b> Chemical elements applied in semiconductor technology. ....	5
<b>Figure 2-1:</b> Expected interconnect delay for copper and low-k devices. ....	12
<b>Figure 2-2:</b> Parasitic capacitances occurring within the interconnect system of an integrated circuit. ....	13
<b>Figure 2-3:</b> Typical precursor (a-d) and porogen (e-f) molecules used to fabricate dense and porous low-k dielectrics by PECVD. ....	18
<b>Figure 2-4:</b> Network structure of a porous low-k dielectric fabricated with TMCTS precursor without porogen addition (a) and with porogen (b). ....	19
<b>Figure 2-5:</b> Air gaps partially replacing low-k dielectrics within the interconnect system.....	19
<b>Figure 2-6:</b> Trench first – via last processing sequence. ....	21
<b>Figure 2-7:</b> Via first – trench last processing sequence.....	22
<b>Figure 2-8:</b> After patterning trench and via the diffusion barrier is deposited (a), the structure is filled with copper (b) and the excess copper is removed by CMP (c).....	22
<b>Figure 2-9:</b> Copper / low-k integration schemes. ....	24
<b>Figure 2-10:</b> Low-k damaging species occurring during plasma processing. ....	29
<b>Figure 3-1:</b> A liquid drop on a solid substrate forming the contact angle $\theta$ at the contact point of the phases solid / liquid / vapor. ....	40
<b>Figure 3-2:</b> Advancing and receding contact angles. ....	42
<b>Figure 3-3:</b> The origin of the surface energy of a liquid; .....	45
<b>Figure 3-4:</b> Collapse of ultra low-k dielectric trench structures after drying. This effect well known for photoresist patterns can also occur for porous dielectric features as shown by TSMC (Figure 3-4a) [108] and Hynix (Figure 3-4b) [110]. ....	52
<b>Figure 3-5:</b> The forces acting on the sidewalls of a small trench filled with a liquid result from strong capillary forces directly depending on the surface energy of the liquid and can cause pattern collapse.....	53
<b>Figure 3-6:</b> The pressure on a trench sidewall depending on the sidewall distance (a) and the surface energy of the liquid filling the trench (b).....	54
<b>Figure 3-7:</b> Nonwetting of small structures; a gas cavity can form in the structure and surfaces to be cleaned cannot be reached by the solution; this effect is critical especially for via structures.....	55
<b>Figure 3-8:</b> Model for a rough estimation of contact angles required for complete liquid filling of a small structure. For complete filling the wetting line has to reach the bottom before contacting the opposite sidewall [90] .....	55
<b>Figure 3-9:</b> Reduction of the surface energy of water by adding organic solvents like acetone or Isopropanol. This approach of surface energy reduction stands in contrast to the trend in	

microelectronic production to use water based cleaning solutions. (Source: Imeter Ober- und Grenzflächenspannung, Beispiel Prüfbericht Isopropanol-Wasser, <a href="http://www.unimeter.net/Download/OFS-GFS/IsopropanolWasser.pdf">http://www.unimeter.net/Download/OFS-GFS/IsopropanolWasser.pdf</a> ) .....	57
<b>Figure 4-1:</b> Basic construction of surfactant molecules and micelles. ....	60
<b>Figure 4-2:</b> Micellar conglomerates are able to form a variety of 3-D structures. ....	60
<b>Figure 4-3:</b> Surfactant molecules adsorbed at a polar / nonpolar interface. ....	68
<b>Figure 4-4:</b> Structure of an inversed micelle. ....	71
<b>Figure 4-5:</b> Surface model of Gibbs. ....	72
<b>Figure 5-1:</b> Kaelble plot as a result of contact angle measurements to determine the surface energy of a solid. ....	77
<b>Figure 5-2:</b> Ring method (a) and plate method (b) to determine the total surface energy of a liquid. .	79
<b>Figure 5-3:</b> The pendant drop method is a simple and accurate method to determine the surface energy of a liquid by a software aided drop shape analysis. ....	80
<b>Figure 5-4:</b> By the maximum bubble pressure method the dynamic behavior of a surfactant solution. ....	84
<b>Figure 5-5:</b> FTIR spectrum of a porous CVD-SiCOH dielectric in pristine condition. ....	88
<b>Figure 6-1:</b> Dispersive and polar energy contributions of the porous low-k 1 in pristine condition and after several etching processes. ....	96
<b>Figure 6-2:</b> Dispersive and polar energy contributions of the dense low-k 3 and low-k 4 in pristine condition and after several etching processes. ....	97
<b>Figure 6-3:</b> Dispersive and polar energy contribution of etch residue surfaces formed by different etching processes with variated process parameters. ....	99
<b>Figure 6-4:</b> Dispersive and polar energy contributions of low-k 1 after reducing (PS 1 and PS 2) and oxidizing (PS 3) stripping processes. ....	101
<b>Figure 6-5:</b> Dispersive and polar energy contributions of copper and barrier materials applied within the interconnect system. ....	102
<b>Figure 6-6:</b> Dispersive and polar energy contribution of low-k 1 after a CMP process and of an OMCTS hardmask layer. ....	103
<b>Figure 6-7:</b> Dispersive and polar energy contribution of the cleaning solutions studied in this work. ....	104
<b>Figure 6-8:</b> Contact angles of the studied cleaning solutions on selected surfaces. ....	106
<b>Figure 7-1:</b> 2,4,7,9-Tetramethyldec-5-yne-4,7-diol. ....	113
<b>Figure 7-2:</b> Ethylenediamine tetrakis(propoxylate-block-ethoxylate) tetrol. ....	113
<b>Figure 7-3:</b> Glycolic acid ethoxylate 4-nonylphenyl ether. ....	113
<b>Figure 7-4:</b> Glycolic acid ethoxylate lauryl ether. ....	113
<b>Figure 7-5:</b> Zonyl PFBE fluorotelomer. ....	114
<b>Figure 7-6:</b> Polyether modified trisiloxane. ....	114

<b>Figure 7-7:</b> Dynamic behavior of the studied surfactants mixed in DIW at a concentration of 0.8%.	116
<b>Figure 7-8:</b> Dynamic behavior of the selected surfactants at room temperature mixed in cleaning solutions B1, B2 and C1 at a concentration of 0.1 %.	118
<b>Figure 7-9:</b> The lowest surface energy reached at a surface age of 1000 ms when applying surfactants to the cleaning solutions B1, B2 and C1.	119
<b>Figure 7-10:</b> Slopes of the dynamic surface energy curves of surfactants mixed in cleaning solutions B1, B2 and C1.	120
<b>Figure 7-11:</b> Static energy characteristics of solution B2 and C1 after adding the surfactants EG360, S2502 and Tetra.	121
<b>Figure 7-12:</b> Percentages of dispersive and polar surface energy contributions of solutions B2 and C1 after adding the surfactants EG360, S2502 and Tetra.	122
<b>Figure 7-13:</b> Comparison of the dynamic behavior of S2502 mixed in solution B1, B2 and C1 at room temperature and a bath temperature of 35°C.	123
<b>Figure 7-14:</b> Functional group section of the FTIR spectra recorded for surfactant treated porous low-k 2 dielectric using DIW and IPA for rinsing.	128
<b>Figure 7-15:</b> Transmission spectrum of TMDD (section of functional groups) and the same spectral region of a S2502 treated porous low-k dielectric (inset).	130
<b>Figure 7-16:</b> Transmission spectrum of 2-(chloromethyl) oxirane (functional groups) and the same spectral region of the EG360 treated low-k 2 material.	131
<b>Figure 7-17:</b> FTIR spectra of low-k 2 after treatment with Silox and Tetra with increased DIW rinsing time.	132
<b>Figure 7-18:</b> FTIR spectra of low-k 2 samples treated with the surfactant aided cleaning solution B1.	135
<b>Figure 7-19:</b> Comparison of EG360 and S2502 mixed in different cleaning solutions and their effect on low-k 2 samples.	137
<b>Figure 7-20:</b> FTIR spectra of low-k 2 samples after surfactant treatment at elevated bath temperatures.	140
<b>Figure 7-22:</b> Calculated pressure acting on the sidewalls of a low-k dielectric structure for cleaning solutions with optimized wetting behavior.	148
<b>Figure B1:</b> Energetic character of solution A1 compared with that of selected solid surfaces.	162
<b>Figure B2:</b> Energetic character of solution A2 compared with that of selected solid surfaces.	162
<b>Figure B3:</b> Energetic character of solution A3 compared with that of selected solid surfaces.	163
<b>Figure B4:</b> Energetic character of solution B1 compared with that of selected solid surfaces.	163
<b>Figure B5:</b> Energetic character of solution B2 compared with that of selected solid surfaces.	164
<b>Figure B6:</b> Energetic character of solution C1 compared with that of selected solid surfaces.	165
<b>Figure C1:</b> Plot of the contact angle measurement results on a PTFE substrate; This surface shows a polar energy part which can be neglected. The value of total surface energy (23.28 mN/m) was used to determine the dispersive surface energy contribution of the studied cleaning solutions.	166

<b>Figure D1:</b> Film thickness and refractive index of the porous low-k before and after cleaning processes using solutions B1, B2 and C1 .....	167
<b>Figure D2:</b> Sheet resistance values of copper before and after the cleaning process. Only slight changes in sheet resistance have been found. ....	168
<b>Figure D3:</b> Sheet resistance profiles of copper before and after the cleaning processes. ....	169
<b>Figure E1:</b> Dynamic behavior of EG360 at different concentrations. ....	170
<b>Figure E2:</b> behavior of S104E at different concentrations. ....	171
<b>Figure E3:</b> Dynamic behavior of S2502 at different concentrations. ....	172
<b>Figure E4:</b> Dynamic behavior of CW100 at different concentrations. ....	173
<b>Figure E5:</b> Dynamic behavior of S465 at different concentrations. ....	174
<b>Figure E6:</b> Dynamic behavior of S485 at different concentrations. ....	175
<b>Figure E7:</b> Dynamic behavior of GAClauryl at different concentrations. ....	176
<b>Figure E8:</b> Dynamic behavior of Tetra at different concentrations. ....	177
<b>Figure E9:</b> Dynamic behavior of Zonyl at different concentrations. ....	178
<b>Figure E10:</b> Dynamic behavior of Silox at different concentrations. ....	179
<b>Figure H1:</b> FTIR spectra of the porous low-k dielectric in pristine condition and after treatment with IPA. ....	186
<b>Figure H2:</b> FTIR spectra of the porous low-k dielectric before and after treatment with EG360 and different rinsing solutions. ....	187
<b>Figure H3:</b> FTIR spectra of the porous low-k dielectric before and after treatment with S2505 and different rinsing solutions. ....	188
<b>Figure H4:</b> FTIR spectra of the porous low-k dielectric before and after treatment with Silox and different rinsing solutions. ....	189
<b>Figure H5:</b> FTIR spectra of the porous low-k dielectric before and after treatment with Tetra and different rinsing solutions. ....	190
<b>Figure H6:</b> FTIR spectra of the porous dielectric before and after treatment with EG360 mixed in the studied cleaning liquids and DIW as rinsing solution. ....	191
<b>Figure H7:</b> FTIR spectra of the porous dielectric before and after treatment with EG360 mixed in the studied cleaning liquids and IPA as rinsing solution. ....	192
<b>Figure H8:</b> FTIR spectra of the porous dielectric before and after treatment with S2502 mixed in the studied cleaning liquids and DIW as rinsing solution. ....	193
<b>Figure H9:</b> FTIR spectra of the porous dielectric before and after treatment with S2502 mixed in the studied cleaning liquids and IPA as rinsing solution. ....	194
<b>Figure H10:</b> FTIR spectra of the porous dielectric before and after treatment with Silox mixed in the studied cleaning liquids and DIW as rinsing solution. ....	195
<b>Figure H11:</b> FTIR spectra of the porous dielectric before and after treatment with Silox mixed in the studied cleaning liquids and IPA as rinsing solution. ....	196

<b>Figure H12:</b> FTIR spectra of the porous dielectric before and after treatment with Tetra mixed in the studied cleaning liquids and DIW as rinsing solution. ....	197
<b>Figure H13:</b> FTIR spectra of the porous dielectric before and after treatment with Tetra mixed in the studied cleaning liquids and IPA as rinsing solution. ....	198
<b>Figure H14:</b> FTIR spectra of the porous low-k dielectric after treatment with Silox and different DIW rinsing times. ....	199
<b>Figure H15:</b> FTIR spectra of the porous low-k dielectric after treatment with Tetra and different DIW rinsing times. ....	200
<b>Figure H16:</b> FTIR spectra of the porous low-k dielectric after treatment with EG360 mixed in solution B1 at elevated bath temperature. ....	201
<b>Figure H17:</b> spectra of the porous low-k dielectric after treatment with S2502 mixed in solution B1 at elevated bath temperature. ....	202
<b>Figure H18:</b> FTIR spectra of the porous low-k dielectric after treatment with EG360 mixed in solution C1 at elevated bath temperature. ....	203
<b>Figure H19:</b> FTIR spectra of the porous low-k dielectric after treatment with S2502 mixed in solution C1 at elevated bath temperature. ....	204



## List of Tables

<b>Table 1-1:</b> Guidelines for interconnect technology actually listed in the ITRS for short and long term development.....	4
<b>Table 3-1:</b> Calculated contact angles necessary to completely fill a small via structure.....	56
<b>Table 5-1:</b> Energetic character of the testing liquids used for surface energy calculation of solid samples by contact angle measurement. ....	83
<b>Table 5-2:</b> Wavenumber regions describing the typical structure of SiCOH materials and the most probable origin of the vibration modes. ....	87
<b>Table 6-1:</b> Low-k and ultra low-k dielectrics studied in this work.....	90
<b>Table 6-2:</b> Metallic and barrier materials studied in this work.....	90
<b>Table 6-3:</b> Description of the etching processes applied to dense and porous dielectric samples. ....	92
<b>Table 6-4:</b> Description of the polymerizing plasma processes used to produce etch residue surfaces.....	93
<b>Table 6-5:</b> Description of the wet cleaning solutions studied in this work .....	94
<b>Table 6-6:</b> The contact angles of the cleaning liquids on selected surfaces and the differences between the surface energies of liquids and solids are compared. ....	107
<b>Table 6-7:</b> Differences in total surface energy of the cleaning solutions and a selection of solid surfaces studied in this work. ....	110
<b>Table 7-1:</b> The minimal dynamic surface energy at 1000 ms surface age and the slope of the dynamic curves of all studied surfactants. ....	117
<b>Table 7-2:</b> Long term stability of surfactants mixed in the cleaning solutions B1, B2 and C1.....	125
<b>Table 7-3:</b> Refractive index, k-value and leakage current density of the porous low-k 2 treated by surfactants mixed in DIW. ....	127
<b>Table 7-4:</b> Refractive index, k-value and leakage current density of low-k 2 samples treated with the surfactant aided cleaning solutions B1, B2 and C1.....	133
<b>Table 7-5:</b> Change of refractive index, k-value and leakage current density of low-k 2 samples treated with surfactant solutions at elevated bath temperature. ....	139
<b>Table 7-6:</b> Total variation of the sheet resistance of copper, TiN and TaN samples after surfactant treatment.....	142
<b>Table 7-7:</b> Surface energy difference of selected solids and liquids with and without use of surfactants. ....	145
<b>Table 7-8:</b> Contact angles of the cleaning solutions B2 and C1 on selected solid surfaces. ....	146
<b>Table 7-9:</b> Rating of the cleaner / surfactant combinations studied in this work. ....	149



<b>Table A1:</b> Surface energy values of differently processed porous low-k dielectrics.....	138
<b>Table A2:</b> Surface energy values of differently processed dense low-k dielectrics.....	138
<b>Table A3:</b> Surface energy values of dielectric samples after polymerizing etch process .....	139
<b>Table A4:</b> Surface energy values of porous dielectric samples after different stripping processes .....	139
<b>Table A5:</b> Surface energy values of copper and barrier material samples.....	139
<b>Table A6:</b> Surface energy values of a porous dielectric after CMP and of a OMCTS hardmask layer.....	139
<b>Table A7:</b> Surface energy values of the studied cleaning solutions.....	140
<b>Table B1:</b> Contact angle values of the studied cleaning solutions on selected dielectric surfaces.....	140
<b>Table E1:</b> Dynamic surface energy values of EG360 at different concentrations.....	147
<b>Table E2:</b> Dynamic surface energy values of S104E at different concentrations.....	148
<b>Table E3:</b> Dynamic surface energy values of S2502 at different concentrations.....	149
<b>Table E4:</b> Dynamic surface energy values of CW100 at different concentrations.....	150
<b>Table E5:</b> Dynamic surface energy values of S465 at different concentrations.....	151
<b>Table E6:</b> Dynamic surface energy values of S485 at different concentrations.....	152
<b>Table E7:</b> Dynamic surface energy values of GAClauryl at different concentrations.....	153
<b>Table E8:</b> Dynamic surface energy values of Tetra at different concentrations.....	154
<b>Table E9:</b> Dynamic surface energy values of Zonyl at different concentrations.....	155
<b>Table E10:</b> Dynamic surface energy values of Silox at different concentrations.....	156
<b>Table F1:</b> Dynamic surface energy values of surfactants in the studied cleaning solutions.....	157
<b>Table F2:</b> Dynamic behavior of EG360 at elevated bath temperatures.....	157
<b>Table F3:</b> Dynamic behavior of S2502 at elevated bath temperatures.....	158
<b>Table F4:</b> Long term stability of surfactants in cleaning solution B1.....	159
<b>Table F5:</b> Long term stability of surfactants in cleaning solution B2.....	160
<b>Table F6:</b> Long term stability of surfactants in cleaning solution C1.....	161
<b>Table G1:</b> Sheet resistance values of copper, TiN and TaN after surfactant treatment using different rinsing solutions.....	162
<b>Table I1:</b> Rating of the surfactant aided solutions including dynamics, surface energy, stability and material compatibility.....	182

## List of equations

2-1	RC-product describing the signal delay of an interconnect system.....	10
2-2	Capacitance between metal wires and metallization levels.....	10
2-3	Power consumption of an integrated circuit.....	10
2-4	Equation of Debye describing the context of k-value and polarizability.....	11
2-5	Possible reaction mechanism responsible for carbon depletion in oxidizing plasmas.....	22
2-6	Possible reaction mechanism of Si-O-Si network formation.....	22
2-7	Possible reaction mechanism responsible for carbon depletion in reducing plasmas.....	23
2-8	Possible reaction mechanism leading to formation of silanols in reducing plasmas.....	23
2-9	Possible reaction mechanism resulting in the formation of Si-H bondings in reducing plasmas.....	23
3-1	Young's equation describing the interfacial energies and the contact angle of a three phase system.....	30
3-2	Modified Young's equation to determine the contact angle.....	30
3-3	Roughness factor described by Wenzel.....	31
3-4	Macroscopic contact angle.....	31
3-5	Young's equation combined with the roughness model of Wenzel.....	31
3-6	Contact angle of a heterogeneous surface described by Cassie.....	31
3-7	Young's equation in the case of no molecular interaction at the phase boundary....	33
3-8	Young's equation in the case of strong interactions at the phase boundary.....	33
3-9	Work of cohesion described by Dupré.....	34
3-10	Work of cohesion for a two phase system.....	34
3-11	Interfacial energy for a two phase system described by Antonow.....	35
3-12	Work of cohesion described by Good and Girifalco.....	35
3-13	Interfacial energy of a two phase system described by Good and Girifalco.....	35
3-14	Interfacial energy described by Fowkes considering dispersive energies.....	35
3-15	Polar and dispersive energy contributions adding to the total surface energy.....	35

3-16	Interfacial energy considering polar and dispersive energies described by Owens, Wendt, Rabel and Kaelble.....	36
3-17	Extendes Fowkes method considering hydrogen bonds.....	36
3-18	Interfacial energy described by the extended method of Fowkes.....	36
3-19	Interfacial energy considering acid-base model of Lewis.....	36
3-20	Interfacial energy described by Wu applying the harmonic mean of dispersive and polar energy contributions.....	36
3-21	Maximum stress on a sidewall of a liquid filled trench feature.....	38
3-22	Pressure acting on a trench wall of a liquid filled feature.....	38
3-23	Radius of the meniscus formed by the liquid surface within a feature.....	38
3-24	Pressure acting on a trench wall of a liquid filled feature considering the sidewall distance.....	38
5-1	Experimental version of Fowkes' method to determine dispersive energies.....	52
5-2	Equation of a straight line.....	53
5-3	Equation of the OWRK method modified to own the form of a straight line.....	53
5-4	Determination of the surface energy of a liquid by the ring method.....	54
5-5	Determination of the surface energy of a liquid by the plate method.....	55
5-6	Equation of the OWRK method modified for the determination energetic character of a liquid.....	56
5-7	Equation of the OWRK method after elimination of the polar contributions.....	57
5-8	Calculation of the polar energy contribution of a liquid.....	57
5-9	Dynamic surface energy calculated by the maximum bubble pressure method.....	58
5-10	Equation used to determine the k-value of a dielectric by CV measurement.....	60

## Theses

- 1) The removal of plasma etch residues after dielectric patterning is necessary to avoid high contact resistivities, to keep the critical dimensions of the interconnect system, to provide good adhesion of subsequent layers and to inhibit copper diffusion into the insulator.
- 2) Plasma based cleaning processes are critical towards dielectrics with a low k-value containing organic species. Carbon depletion and the densification of the surface near areas alter the dielectric's properties and lead to moisture uptake.
- 3) The substitution of plasma cleaning processes by wet chemical cleaning could be an alternative to avoid dielectric plasma damage.
- 4) With reaching the 32/22 nm technology nodes trench and via dimensions will decrease to  $< 50$  nm. This leads to new wetting based effects in BEOL wet cleaning like nonwetting of small features, pattern collapse and limited mass transport.
- 5) By determining the surface energetic character of solid and liquid the appropriate combination can be found to provide the best wetting. The more equal the energetic characters of both media are, the better will be their wetting behavior.
- 6) SiCOH type low-k dielectrics in pristine conditions are low energetic with a negligible polar energy contribution. Plasma processes alter this energetic character and introduce a polar energy part to the surface. The value of this

energy part strongly depends on the kind of plasma process, it's duration and the chemical composition of the plasma.

- 7)  $\text{CF}_4$  etching processes with addition of oxidizing species as well as oxidizing ashing processes introduce the largest polar energy contribution and lead to a strong increase in total surface energy of the dielectric from around 30 mN/m to more than 70 mN/m. A medium polar energy part is introduced by adding  $\text{N}_2$ , Ar or CO to the etching process. The impact of the additives on the energetic character of the dielectric is independent from their gas flow.
- 8) The addition of  $\text{C}_4\text{F}_8$  and  $\text{H}_2$  to the  $\text{CF}_4$  plasma also resulted in the introduction of small polar energy contributions, which have only slight effects on the total surface energy. The polar energy part decreases and the dispersive energy part increases with increasing gas flow or process duration. This is declared by the formation of a polymeric surface layer, whose chemical composition changes with gas flow and process duration.
- 9) Due to the fact that the dielectric surface reacts very sensible to any modification of the plasma process they are treated with, the determination of the surface energies of the solid can be used as an analytical method to indentify whether or not the dielectric was altered by the plasma process. This method is an easy and fast way to help to identify damaging species or the formation of a polymeric layer at the dielectric's surface.
- 10) Polymeric etch residues were found to be low energetic and therefore difficult to wet by high energetic liquids. The introduction of polar energy contributions by plasma processing enhances the ability of such a liquid to wet this solid surface, although this means that the dielectric has been

degraded by the process. Low surface energies have also been found for copper, TiN and OMCTS hardmask layers.

- 11) An appropriate cleaning solution for a certain solid surface in BEOL processing can be found without additional wetting tests by knowing the surface energetic character of both media.
- 12) Cleaning solutions with a high content of water are high energetic and have to be optimized in their wetting behavior to be applicable to the low energetic surfaces in trenches and vias after etching. The lowering of the surface energy of the cleaning liquids will improve their wetting behavior.
- 13) The lowering of the cleaning liquid's surface energy can be achieved by the application of surfactants. This approach has been studied only occasionally in the field of plasma etch residue removal. It's advantage compared to other wetting optimized processes like the application of supercritical fluids is the ability to use standard wet cleaning equipment and processing sequences.
- 14) Besides the lowest reachable surface energy of the liquid the dynamic behavior of the surfactant solutions is considered to make an appropriate selection. It was found that a compromise between high adsorption speed and low surface energy has to be made. Nonionic Gemini type surfactants with a low or medium HLB value as well as a siloxane based surfactant and a copolymeric molecule have been selected. The studied anionic surfactants have been excluded due to their tendency to produce foam in dynamic cleaning processes. A fluorinated surfactant has been excluded due to its very low adsorption speed.

- 15) The surface energy lowering effect of the surfactants depends on the water content of the cleaning solution. A higher water content results in a more effective decrease of surface energy.
- 16) The surfactant solutions can also be applied at elevated bath temperatures up to at least 35°C without modification of their dynamic behavior or surface energy value. Long term stability of at least 7 weeks in a cleaning solution was proven for the nonionic surfactants and for the copolymeric species in two of three cleaning solutions. The silicon containing surfactant is not long term stable and showed a much lower effectiveness after 7 weeks.
- 17) By choosing IPA as rinsing solution the surfactant aided cleaning liquids show a good compatibility to porous low-k dielectrics. Rinsing using DIW was not able to remove surfactant residues from the porous dielectric structure. This lead to the degradation of the electrical parameters of the dielectric and was shown by FTIR analysis. DIW rinsing was only effective for the copolymeric surfactant which could be due to its large molecule size.
- 18) The surfactant aided cleaning solutions showed a good compatibility to copper and barrier materials independent from the rinsing solution chosen. A surface contamination on copper and barrier materials after IPA rinsing could not be declared till now.
- 19) By application of surfactants the difference of the energetic character of the solids in BEOL after plasma processing and the cleaning liquids was lowered which lead to a clear decrease in contact angle values and therefore provides an optimized wetting behavior. A promising and compatible

processing scheme was found for the copolymeric surfactant: minimum concentration of 0,1% at bath temperatures from room temperature up to at least 35%, followed by a DIW or IPA rinse for 3 minutes. Calculations have shown, that the decreased surface energies of the liquids are also able to reduce the pressure acting on trench sidewalls and may therefore help to overcome pattern collapse of low-k dielectric features.

- 20) Optimized wetting behavior and material compatibility of surfactant aided cleaning solutions was found to be achievable and helps to overcome wetting issues occurring in 32/22 nm technology. Future studies have to include further development of suitable rinsing solutions to meet the requirements of industry to avoid the usage of organic solvents. New rinsing solutions could also prohibit the surface contamination found for copper and barrier materials after IPA rinsing.





## Curriculum Vitae

---

Name:	Ahner, Nicole Peggy		
Date of birth:	September 23rd 1975	Marital status:	Single, no children
Place of birth:	Stollberg / Erzgeb.	Nationality:	German

---

### Professional Experience

---

Since 01/2010	Research Associate at Center for Microtechnologies, Chemnitz University of Technology, Chemnitz (Germany)
04/2009 - 12/2009	Research Associate at Fraunhofer ENAS, Chemnitz (Germany)
04/2006 – 03/2009	PhD student in the International Research Training Group 1215 “Materials and Concepts for Advanced Interconnects” at Chemnitz University of Technology
01/1999-12/1999	Administration and logistics secretary at “Projekt Zukunft e.V.”, charitable non-profit organization, Oelsnitz / Erzgeb. and Chemnitz (Germany)

---

### Study

---

10/2000 – 03/2006	Studies in Electrical Engineering, specialization Electronics / Microelectronics at Chemnitz University of Technology Graduation degree: Dipl.-Ing. (1.7 “good”), Title of the Diploma thesis (in German): Development of a gap-fill process for application of spin-coating materials”
09/1994-11/1997	Studies in General Administration and Public Law at University of Applied Sciences of the Free State of Saxony Meißen (Germany), Graduation degree: State Examination as Public Administration Specialist

---

**School Education**

---

07/1994	Abitur (German university entrance qualification) at Gymnasium Thalheim / Erzgeb.
---------	--

---

Chemnitz, May 22<sup>nd</sup> 2011

## Own Publications and Conference Contributions

- 1) Ahner,N.; Fischer,T.; Zimmermann,S.; Schaller,M.; Prager,L.; Schulz,S.E.: UV assisted curing of plasma damaged porous ultralow-k materials for a k-recovery process: influence of curing-cycle modifications (Poster). Advanced Metallization Conference, Baltimore, Maryland (USA), 2009 Oct 13-15
- 2) Ahner,N.; Schaller,M.; Bartsch,C.; Baryschpolec,E.; Schulz,S.E.: Surface energy and wetting behaviour of plasma etched porous SiCOH surfaces and plasma etch residue cleaning solutions. 9th International Symposium on Ultra Clean Processing of Semiconductor Surfaces, Bruges (Belgium), 2008 Sep 21-24; Proceedings, pp 119-120
- 3) Ahner,N.; Schaller,M.; Bartsch,C.; Baryschpolec,E.; Schulz,S.E.: Surface energy and wetting behaviour of plasma etched porous SiCOH surfaces and plasma etch residue cleaning solutions. Solid State Phenomena, 145-146 (2009) pp 319-322
- 4) Ahner,N.; Schulz,S.E.; Blaschta,F.; Rennau,M.: Optical, electrical and structural properties of spin-on MSQ low-k dielectrics over a wide temperature range. Materials for Advanced Metallization - MAM, Dresden (Germany), 2008 Mar 2-5; Microelectronic Engineering, 85 (2008) pp 2111-2113 (ISSN 0167-9317)
- 5) Ahner,N.; Schulz,S.E.; Blaschta,F.; Rennau,M.: Thermal stability and gap-fill properties of spin-on MSQ low-k dielectrics. Materials for Advanced Metallization - MAM, Brugge (Belgium), 2007 Mar 4-7; Microelectronic Engineering, 84 (2007) pp 2606-2609 (ISSN 0167-9317)
- 6) Ahner,N.; Schulz,S.E.; Prager,L.; Schaller,M.: UV assisted curing of plasma damaged porous ultralow-k material after a k-restore process: influence of UV-wavelength and curing ambient. Advanced Metallization Conference - AMC 2008, San Diego, CA (USA), 2008 Sep 23-25
- 7) Ahner,N.; Schulz,S.E.; Zacher,M.: Surfactants as an Additive to Wet Cleaning Solutions for Plasma Etch Residue Removal: Compatibility to a Porous CVD-SiCOH Ultra Low-k Dielectric Material . 216th ECS Meeting , Vienna, Austria, October 4 - October 9 2009; ECS Transactions, Volume 25 Issue 5 (2009) pp 87-94

- 8) Ahner,N.; Zimmermann,S.; Schaller,M.; Schulz,S.E.: Optimized wetting behavior of water-based cleaning solutions for plasma etch residue removal by application of surfactants. 10th International Symposium on Ultra Clean Processing of Semiconductor Surfaces, Ostende (Belgium), 2010 Sep 20-22; Proceedings, pp 48-49
  
- 9) Fischer,T.; Ahner,N.; Zimmermann,S.; Schaller,M.; Schulz,S.E.: Influence of thermal cycles on the silylation process for recovering k-value and chemical structure of plasma damaged ultra-low-k materials (Talk). Advanced Metallization Conference, Albany, NY (USA), 2010 Oct 5-7
  
- 10) Schulz,S.E.; Ahner,N.: Deposition and properties of porous ultra-low-k dielectric films (Invited Talk). 8th Seminar Porous Glasses - Special Glasses, Wroclaw, 2007 Sept 4-8
  
- 11) Zimmermann,S.; Ahner,N.; Blaschta,F.; Schaller,M.; Ruelke,H.; Schulz,S.E.; Gessner,T.: Analysis of the impact of different additives during etch processes of dense and porous low-k with OES and QMS. Materials for Advanced Metallization MAM 2009, Grenoble (France), 2009 Mar 9-11
  
- 12) Zimmermann,S.; Ahner,N.; Blaschta,F.; Schaller,M.; Ruelke,H.; Schulz,S.E.; Gessner,T.: Analysis of the impact of different additives during etch processes of dense and porous low-k with OES and QMS. MAM 2009, Grenoble (France), 2009 Mar 9-11; Microelectronic Engineering, 87 (2010) pp 337-342 (ISBN 0167-9317 (ISSN))
  
- 13) Zimmermann,S.; Ahner,N.; Blaschta,F.; Schaller,M.; Zimmermann,H.; Ruelke,H.; Lang,N.; Roepcke,J.; Schulz,S.E.; Gessner,T.: Improvement of etch processes for SiCOH materials with novel in situ diagnostic and evaluation methods. AMC, Baltimore (USA), October 13-15, 2009; Proceeding of the Advanced Metallization Conference 2009, pp 101-110 (ISBN 987-1-60511-218-3)
  
- 14) Zimmermann,S.; Ahner,N.; Blaschta,F.; Schaller,M.; Zimmermann,H.; Ruelke,H.; Lang,N.; Roepcke,J.; Schulz,S.E.; Gessner,T.: Influence of the additives argon, O<sub>2</sub>, C<sub>4</sub>F<sub>8</sub>, H<sub>2</sub>, N<sub>2</sub> and CO on plasma conditions and process results during the etch of SiCOH in CF<sub>4</sub> plasma. Materials for Advanced Metallization MAM 2010, Mechelen (Belgium), 2010 Mar 7-10

- 15) Zimmermann,S.; Ahner,N.; Blaschta,F.; Schaller,M.; Zimmermann,H.; Ruelke,H.; Lang,N.; Roepcke,J.; Schulz,S.E.; Gessner,T.: Etch processes for dense and porous SiCOH materials: plasma states and process results. 3rd International Workshop Plasma Etch and Strip in Microelectronics, PESM 2010, Grenoble (France), 4-5 March 2010
- 16) Zimmermann,S.; Ahner,N.; Blaschta,F.; Schaller,M.; Zimmermann,H.; Ruelke,H.; Lang,N.; Roepcke,J.; Schulz,S.E.; Gessner,T.: Talk: Improvement of etch processes for SiCOH materials with novel in situ diagnostic and evaluation methods. AMC 2009, Baltimore (USA), October 13-15, 2009; Advanced Metallization Conference
- 17) Zimmermann,S.; Ahner,N.; Fischer,T.; Schaller,M.; Schulz,S.E.; Gessner,T.: Talk: A less damage patterning regime for a successful integration of ultra low-k materials in modern nanoelectronic devices . MRS Spring Meeting 2011, San Francisco (USA), April 25 - 29, 2011
- 18) Zimmermann,S.; Ahner,N.; Fischer,T.; Schulz,S.E.; Gessner,T.: Talk: A combined Etch, Cleaning and k-restore Process for less damage integration of ultra low-k materials. SEMICON 2010, Dresden (Germany), October 19-21, 2010